GEOLOGY AND GEOCHEMISTRY OF THE HEMBRILLO CANYON SUCCESSION, SAN ANDRES MOUNTAINS, SIERRA AND DONA ANA COUNTIES, NEW MEXICO

by
Dean E. Alford

Submitted in partial fulfillment
of the requirements for the degree of
Master of Science in Geology

New Mexico Institute of Mining and Technology
Socorro, New Mexico

May, 1987

"Your hearts know in silence the secrets of the days and nights.

But your ears thirst for the sound of your heart's knowledge.

You would know in words that which you have always known in thought.

You would touch with your fingers the naked body of your dreams."

Kalil Gibran

The Prophet, 1923

ABSTRACT

Proterozoic supracrustal rocks in the central San Andres Mountains, New Mexico are dominated by a large volume of metasediments, with associated diabase and minor felsic volcanic rocks. These rocks are collectively referred to as the Hembrillo Canyon succession. Metasediments are an important part of the succession. Felsic metavolcanic rocks are of local importance in the Hembrillo Canyon area only. The diabases of the area are common throughout the succession and have incompatible element distributions characteristic of basalts erupted in modern volcanic arcs. Mafic rocks exhibit tholeiitic trends and have undergone olivine plus or minus clinopyroxene fractionation. Incompatible element distributions in felsic metavolcanic rocks are similar to those in rhyolites from continental margin arcs and associated back-arc basins. Depletion of Ta and Nb relative to REE and Th in diabases indicate a subduction-zone component in the source. Felsic volcanics have relatively high contents of heavy REE and high field strength elements, a feature characteristic of felsic volcanics from continental rifts and from back-arc basins formed in or near continental crust.

The metasedimentary rocks of the area are comprised of quartzites, feldspathic quartzites, arkosites, meta-quartz wackes, and metagraywackes with minor metaconglomerates. These rocks contain low concentrations of Fe, Mg, Ti and Co, a feature characteristic of clastic sediments deposited on or near continental crust. Chemical and petrographic studies of the sediments indicate a dominantly felsic plutonic-volcanic provenance with minor mafic and andesitic input. Sedimentary structures (e.g. cross-bedding and imbricated pellets) indicate two source directions: one dominant source to the north contributing major amounts

of felsic igneous detritus, and a second, less important source contributing much finer grained volcanic material from a southerly direction. Sedimentary textures and structures suggest that the rocks were deposited in a series of submarine fans by turbidity currents in a proximal environment. Coarse grained arkoses, conglomerates and quartzites may represent channel fill deposits associated with the fans.

Overall, data suggest that the Hembrillo Canyon succession formed in a continental margin back-arc basin. Continental and arc detritus was rapidly fed into a tectonically active basin. Interbedded with the sediments are intrusive volcanic rocks and felsic tuffs. The mafic rocks in the area are derived from a mantle source with a significant subduction-zone component.

ACKNOWLEDGMENTS

Many people helped me during the preparation of this thesis, too many to thank here, but I do thank them all. In addition, the following people have gone beyond their daily lives to support me in this effort:

K.C. Condie for his guidance; the remainder of the committee: Dr. A.J. Budding and Dr. J. MacMillan; Gladys and Kelly Alford for their support; Mary Donohoe for her typing skills and continued support. Also, many thanks to the Geochemical Abuse Center (particularly G.P. Bowling) for support in the form of discussion and computer assistance; Theresa Wallace, public liaison at the White Sands Missile Range for her help in range access. Also, thanks to M. Knoper, D. Wronkiawicz and M. Bowie for editorial comments.

Table of Contents

List of Figures

List of Tables

INTRODUCTION

Supracrustal rocks of Proterozoic age are well exposed in southern New Mexico. They are present in the study area of this report (Fig. 1). These rocks, herein collectively called the Hembrillo Canyon succession, include a lithologically diverse suite of rocks dominated by quartz-rich metasediments and felsic and mafic metaigneous rocks (Plate 1). The metaigneous rocks occur as mafic subvolcanic dikes and sills and as felsic tuffs. Quartz-rich and quartz-intermediate sediments dominate the succession.

The objectives of this study are as follows:

1) Map, describe, and chemically classify the major Proterozoic rock types;
2) Determine stratigraphic relationships of the metaigneous and metasedimentary rocks;
3) Ascertain the regional metamorphic grade of the Proterozoic rocks; and,
4) Interpret the depositional and tectonic environments under which the Proterozoic rocks were deposited and metamorphosed.

The Hembrillo Canyon succession of the central San Andres Mountains belongs to the 1680-1700 Ma terrane as defined by Condie (1986; Fig. 2). The basement to this supracrustal section has not yet been recognized. Early work in the area (Bachman and Harbour, 1970; Lasky, 1932; Kelley, 1955; Kottlowski, 1955, 1959; and Kottlowski and others, 1956) established its similarity to other Precambrian terranes in southern New Mexico, but no further interpretations were made until recently.

Condie and Budding (1979), using geochemical and petrographic analyses, established the importance of this area to the overall interpretation of Proterozoic terranes in both southern New Mexico and the southwestern United States. Their tectonic interpretation of these rocks and similar rocks in Arizona and other parts

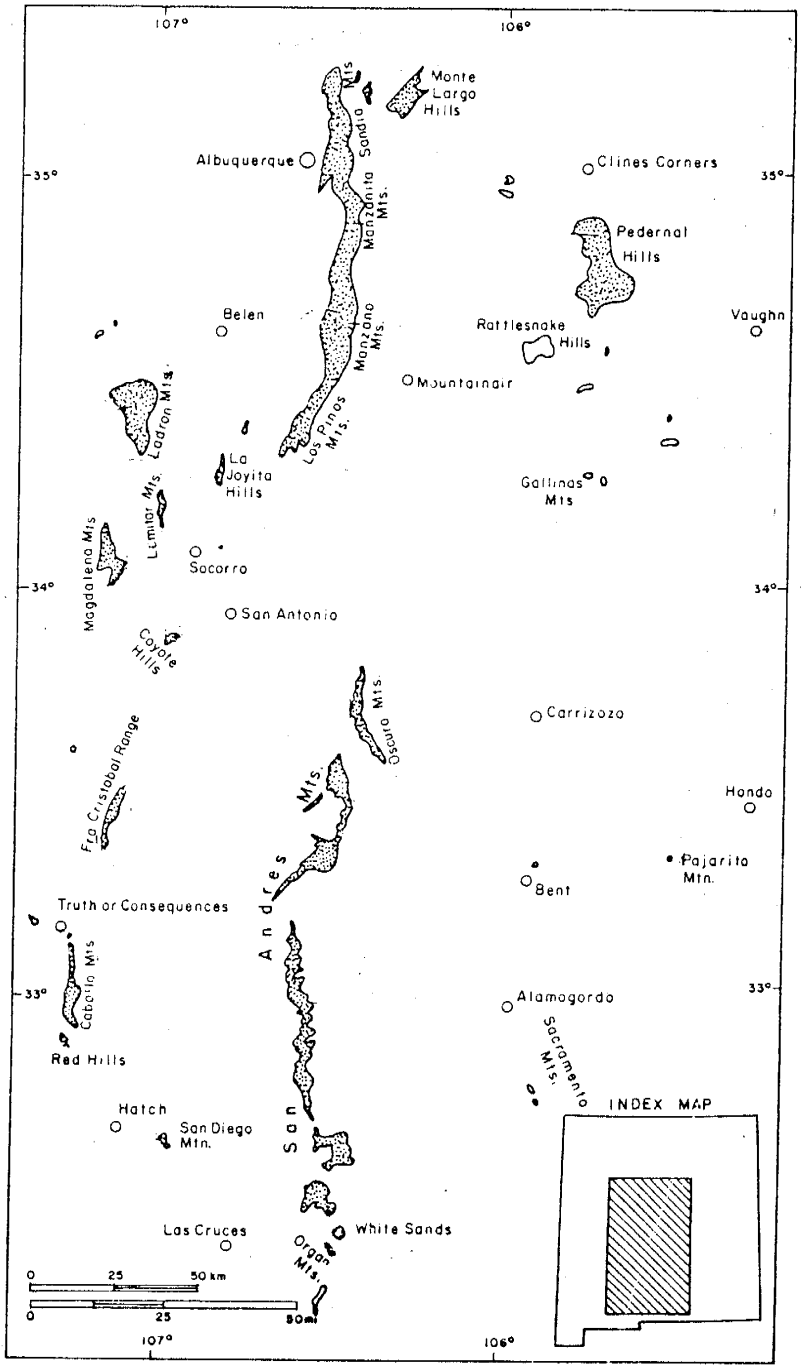

Figure 1
Precambrian rocks of southern New Mexico, including the central San Andres Mountains (after Condie and Budding, 1979).

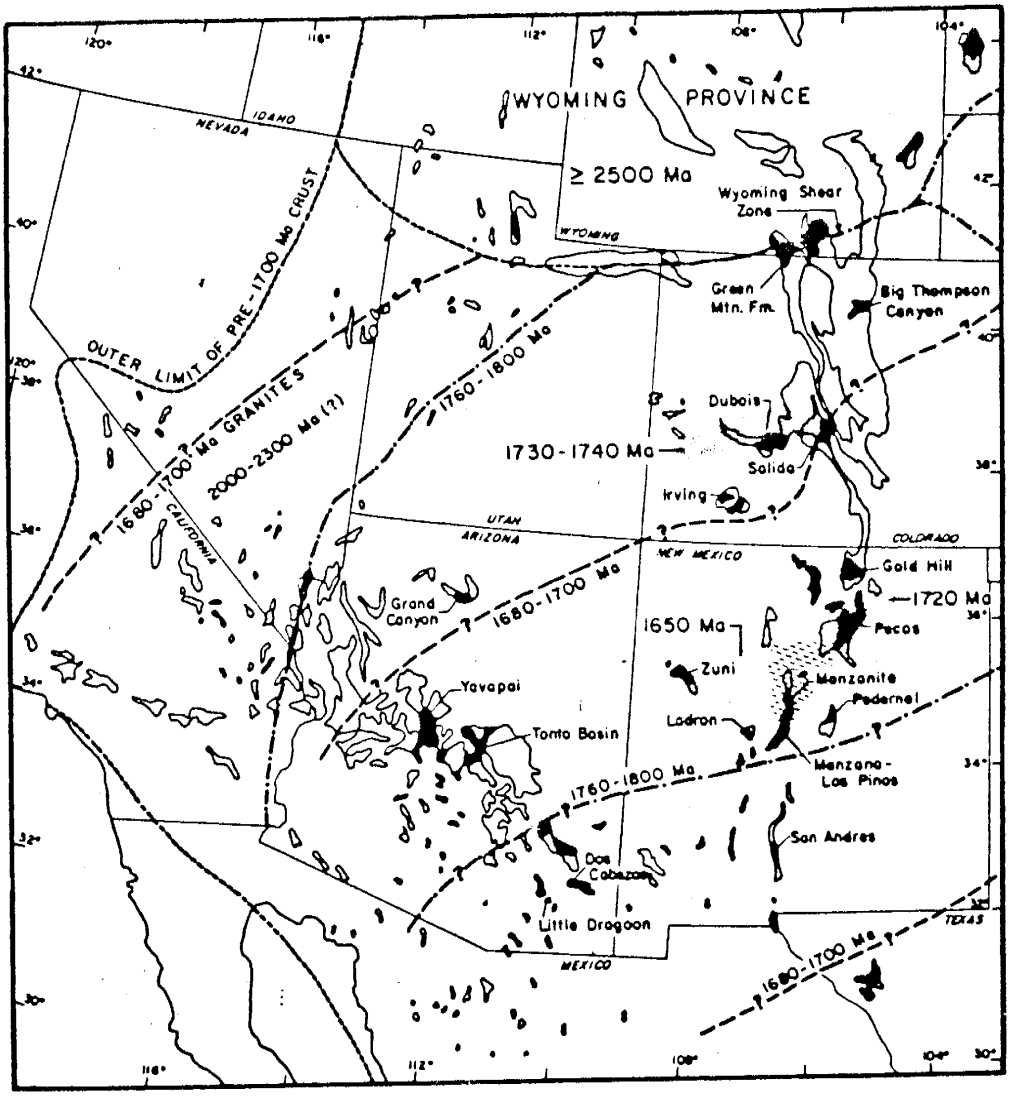

Figure 2
Distribution of Proterozoic supracrustal terranes
in the southwest U.S. (from Condie, 1986).

of New Mexico, was a multiple rift system. New data and reinterpretation of older data suggest that the Hembrillo Canyon succession is instead part of a series of arc-related basins (Condie, 1986). Data provided herein apparently supports this scheme and compares favorably with data from other areas (Copeland, 1986; Copeland and Condie, 1986; Bowling, 1987).

The coarsest sediments of the Hembrillo Canyon succession are conglomerate, arkosite, pebbly mudstone, feldspathic quartzite, and quartzites (Plate 1). Schists are important locally, and are the principal sedimentary type north of Hell Canyon. Metabasic rocks comprise approximately 15-20 percent of the succession and are widespread throughout the study area. Felsic volcanic rocks are generally restricted to the Hembrillo Canyon - Little Dry Canyon areas and comprise a small (five percent) part of the total lithologic package. One minor talc unit, originally described by Lasky (1932), occurs in Hembrillo Canyon and was interpreted by Condie and Budding (1979) as the derivative of devitrification and hydration of a volcanic ash. This conclusion is further supported by evidence from this study.

Metamorphic grade ranges from greenschist to the lower amphibolite facies. Throughout most of the study area, the succession shows the effects of at least two Proterozoic metamorphic events. One event is related to burial of the area, the other is related to contact metamorphism associated with the two anorogenic granitic plutons exposed in the area. A third deformational event is exhibited both in the Proterozoic rocks and the younger (Cambro-Ordovician to Permian) sediments lying unconformably on the Proterozoic rocks. This event was evidently caused by Cenozoic normal faulting associated with the Rio Grande rift com-

plex (Cape and others, 1983). Despite metamorphism, original sedimentary and igneous textures are preserved at many localities. Well-preserved cross-beds, graded beds, imbricated clasts, and other original structures are exposed in many parts of the section, particularly in the Hembrillo Canyon area.

The age of the Hembrillo Canyon succession is not well constrained, although recently, zircons have been removed from felsic tuff LD-1 in Little Dry Canyon and may provide a U-Pb zircon date (K.C. Condie, pers. comm., 1987). The succession probably belongs to the 1680-1700 Ma terrane in Figure 2. It is similar to successions in the Dos Cabezas Mountains, the Little Dragoon Mountains and other areas in southeastern Arizona, the Burro Mountains, the Caballo Mountains, and similar rocks in central and southern New Mexico (Condie, 1986; Copeland, 1986). Copeland (1986) reports the similarity of ages of the Pinal Schist to those of the Tonto Basin-Mazatzal Mountains of central Arizona, both of which may be part of the 1680-1700 Ma terrane. The two anorogenic plutons in the study area have been dated at 1.27 Ga (Condie and Budding, 1979).

Two previous tectonic settings have been proposed for the Hembrillo Canyon succession. Condie and Budding (1979) proposed a complex multiple rift system with associated eugeosynclinal assemblages. Condie (1986) reinterpreted the terrane to be part of a continental back-arc basin developed within an older 1760-1800 Ma terrane in central Colorado.

This study reports the results of a geochemical and sedimentological study of the Hembrillo Canyon succession in the central San Andres Mountains, Sierra and Dona Ana counties, New Mexico. Sample locations and access to the study area are outlined in Appendix A. New data presented in this paper, characterizing

the rock sequence in the study area is supplemented by that of Condie and Budding (1979).

Over 200 samples were collected, of which 26 metaigneous and 21 metasedimentary rocks are selected for detailed chemical analysis. Analyses were performed using both X-ray flourescence (XRF) and instrumental neutron activation analysis (INAA) techniques using methods established by Norrish and Hutton (1969) and Norrish and Chappell (1977) for XRF, and Gibson and Jagam (1980) for INAA. Analytical procedures are summarized in Appendix D. Accuracy and precision of these procedures are discussed in Appendix E. Chemical compositions and CIPW norms are given in Appendix B. Fifty-five samples were chosen for petrographic thin section studies and results of these analyses are given in Appendix C.

VOLCANIC ROCKS

Field Relationships

Amphibolites represent a small percentage (<20%) of the total lithologic package in the Hembrillo Canyon succession, but are generally widespread throughout the area. Most units occur as hypabyssal dikes or sills, and exhibit typical cross-cutting relationships with the surrounding sediments. Large sills occur north of Mayberry Canyon and in Hembrillo Canyon, causing small scale local deformation and shearing in adjacent sediments. In the southern part of the area, the amphibolites are fine to medium grained and massive, exhibiting no internal structure. In Sulfur Canyon, the amphibolites take on a more concordant nature and exhibit ophitic to sub-ophitic textures consisting of plagioclase laths (< 1 to 5 mm in length). Textures reminiscent of amygdules occur in one amphibolite on the south side of Hembrillo Canyon, and textures similar to small scale columns common in basalt flows occur in a narrow (1 to 2 m) amphibolite unit in Grandview Canyon.

Amphibolite units south of Sulfur Canyon are tholeiites with evolved compositions (Mg numbers of 36 to 50). Amphibolite units north of Sulfur Canyon are less evolved (Mg numbers of 55 to 65). It is apparent that most mafic units in the area are intrusive tholeiites.

Mafic units weather easily and form saddles or slopes. Their weathered color is commonly light green to grey, and they are dark green to black on fresh surfaces. Most units occur as thin dikes too small to map (< 1 to 2 m). A few units occur in the 5 to 10 m range, with two sills that are > 200m in length.

Contacts between these felsic units are very sharp. The Hembrillo Canyon felsic volcanics weather orange to red and are cliff formers. The Little Dry Canyon tuff weathers grey to white with finer grained portions weathering black. It commonly forms rubbly slopes.

Felsic igneous rocks are generally restricted to Hembrillo Canyon near the unconformity, although one ash-flow tuff occurs in Little Dry Canyon. These units make up $< 5\%$ of the total lithologic package. Three units (HEC 7, 8, and 38) of virtually identical nature occur as concordant layers (1 to 2 m thick) within the adjacent sediments and lie within 10 to 15 m of one another. Apparently rhyolitic tuffs, they exhibit relict quartz phenocrysts and relict fiammé. Thin layering occurs within these rhyolites as grain size banding, a feature common in both air-fall and ash-flow tuffs (Fisher and Schmincke, 1984). Many distinguishing features in these tuffs have been obscured by metamorphism. One unit occurring at the unconformity with the overlying Cambrian units cross-cuts adjacent units. It contains large K-feldspar phenocrysts (1 to 5 cm) in a matrix of fine-grained quartz and muscovite. Its chemical composition is similar to the nearby rhyolitic tuffs, suggesting a genetic association.

The rhyolitic tuff unit (LD-1) in Little Dry Canyon is thick (5 to 15 m) and contains better preserved original textures than its counterparts in Hembrillo Canyon. An example of well-preserved textures is reversed grading. Adjacent sediments indicate a younging direction to the northeast, and applying these data to the tuff, finer grained material occurs at the lower contact with grain size increasing towards the upper contact. Quartz and plagioclase phenocrysts occur in a fine grained matrix of K-feldspar, plagioclase, and quartz. Coarser material at

the top of the tuff consists of apparent pumice fragments with shard pseudomorphs and large fiammé (1 to 5 cm in length, 1 to 2 cm in width). The grading of the tuff, coupled with large fiammé, indicate that this unit is an ash-flow deposit. The fine grained material in the tuff results from abrasion and rounding of glass shards during pyroclastic flow (Fisher and Schmincke, 1984). Chemical analyses of fine grained matrix and coarse grained pumice fragments are virtually identical, supporting the idea of an ash-flow tuff.

Petrography

Twenty-seven volcanic rocks were studied in thin section: 18 amphibolites, 4 felsic volcanics, and 5 metagabbros. All have been metamorphosed from upper greenschist to lower amphibolite facies, as discussed in the metamorphism section. The mineral assemblage of metabasalts is hornblende + plagioclase + chlorite + epidote/clinozoisite ± quartz ± magnetite. Plagioclase content is commonly 5 to 25% with plagioclase laths ranging up to approximately 5 mm in length. Most epidote and quartz occur as veins and fracture fillings, although some occur in apparently relict amygdules and along rinds of possible columnar structures. Chlorite occurs as a retrograde replacement of hornblende.

Felsic volcanic rocks exhibit assemblages dominated by K-feldspar. Other minerals found in these rocks include quartz (as relict phenocrysts and/or pumice fragments) + plagioclase ± zircon ± sericite. Sericite occurs as an alteration product of plagioclase and K-feldspar. Hematite is rarely found in these rocks.

Metagabbros, although chemically and mineralogically similar to the metabasalts, are coarser grained and contain well-developed crystals of hornblende and

plagioclase with plagioclase laths reaching a maximum length of approximately 2.5 mm.

A more detailed petrographic description of individiual samples can be found in Appendix D.

Geochemistry

The volcanic rocks of the study area represent a biomodal suite that is characteristic of many other Proterozoic terranes. This bimodality is prevalent throughout much of the Proterozoic, although it may be due to a lack of preservation of intermediate material or to a sampling bias (Condie, 1986).

Classification with the SiO_2 - Nb/Y diagram of Winchester and Floyd (1976; Fig. 3) illustrates the bimodality of the Hembrillo rocks, with data points falling into two distinct groups: sub-alkaline basalts and rhyolites. The SiO_2-Zr/TiO_2 diagram (Winchester and Floyd, 1976; Fig. 4) further illustrates this bimodality. Major element compositions of these rocks show calc-alkaline trends with some tholeiitic characteristics on the Jensen cation diagram (Jensen, 1976; Fig. 5) and the AFM diagram (Irvine and Baragar, 1971; Fig. 6). These diagrams also indicate that iron fractionation has occurred in Hembrillo basalts. The data for these rocks suggest a discontinuous calc-alkaline series typical of many Proterozoic bimodal suites. A compositional gap between basalts (SiO_2 = 43 to 52%) and rhyolites ($SiO_2 \geq 72\%$) is readily apparent.

Mafic Rocks

The basalts in the area show significant ranges in Rb, Sr, and Ba (Table B-1, Appendix B). Chondrite normalized rare earth element (REE) patterns for

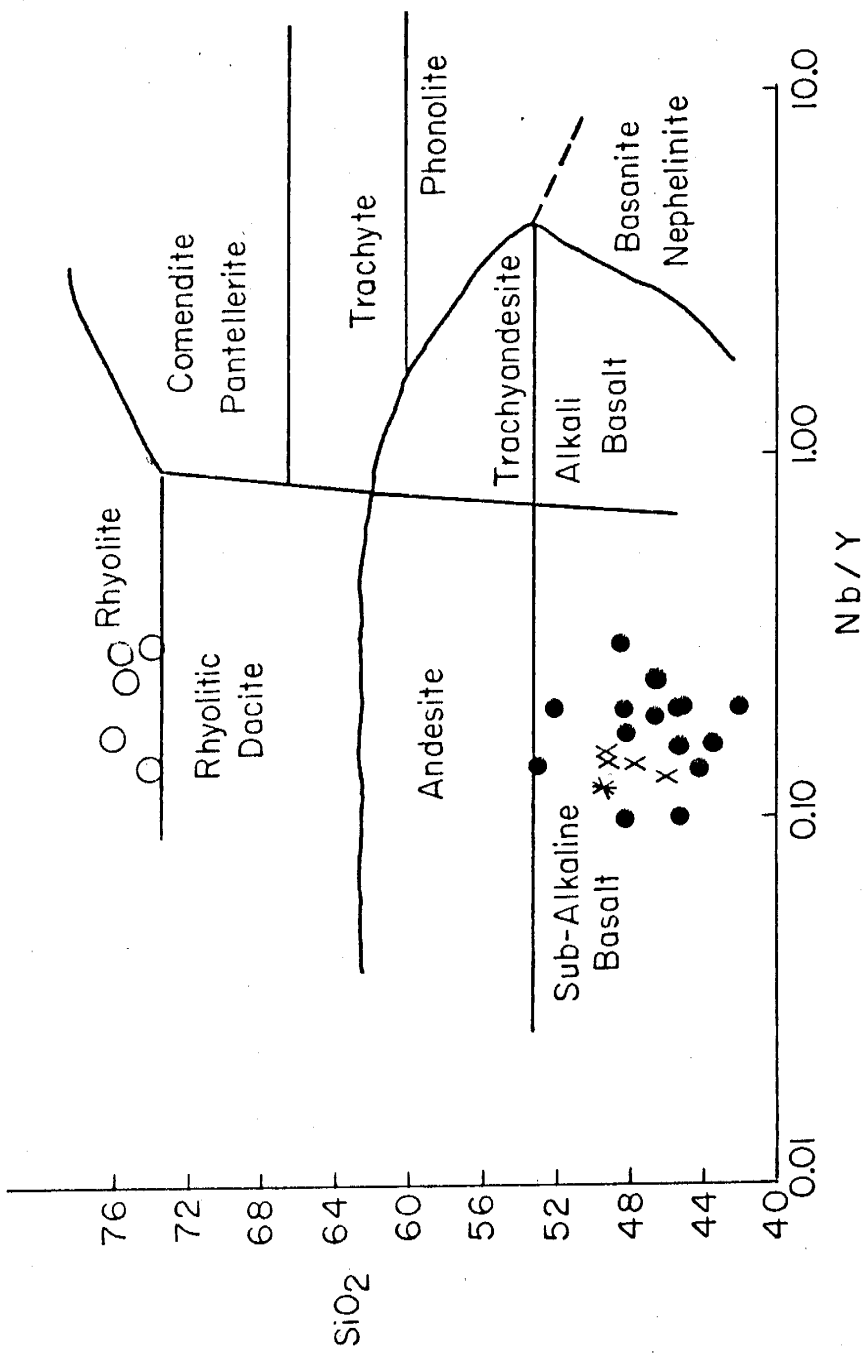

Figure 3
Classification of volcanic and subvolcanic rocks of the Hembrillo Canyon area, south-central New Mexico. Fields from Winchester and Floyd (1976). Filled circles, basalt data from this study; crosses, basalt data from Condie and Budding (1979); open circles, rhyolite data from this study.

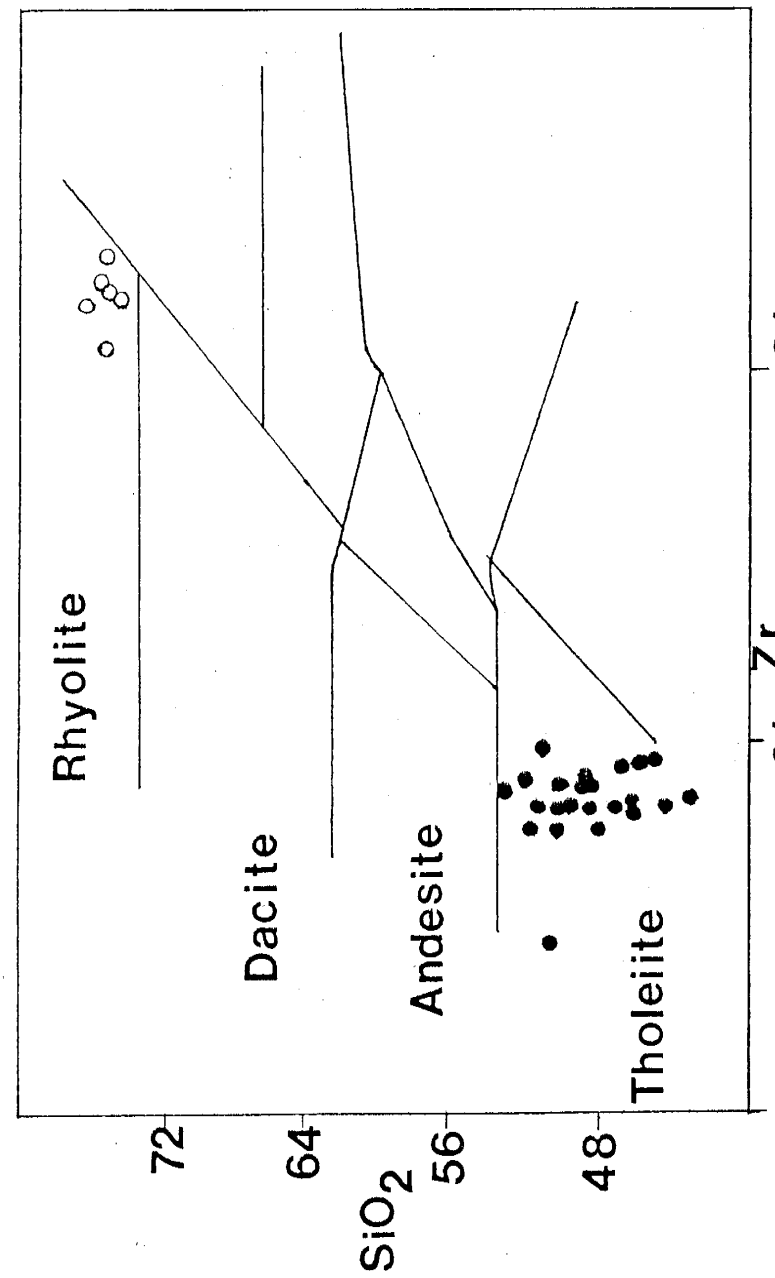

Figure 4
SiO_2-Zr/TiO_2 classification diagram
(Winchester and Floyd, 1967) for Hembrillo volcanics.

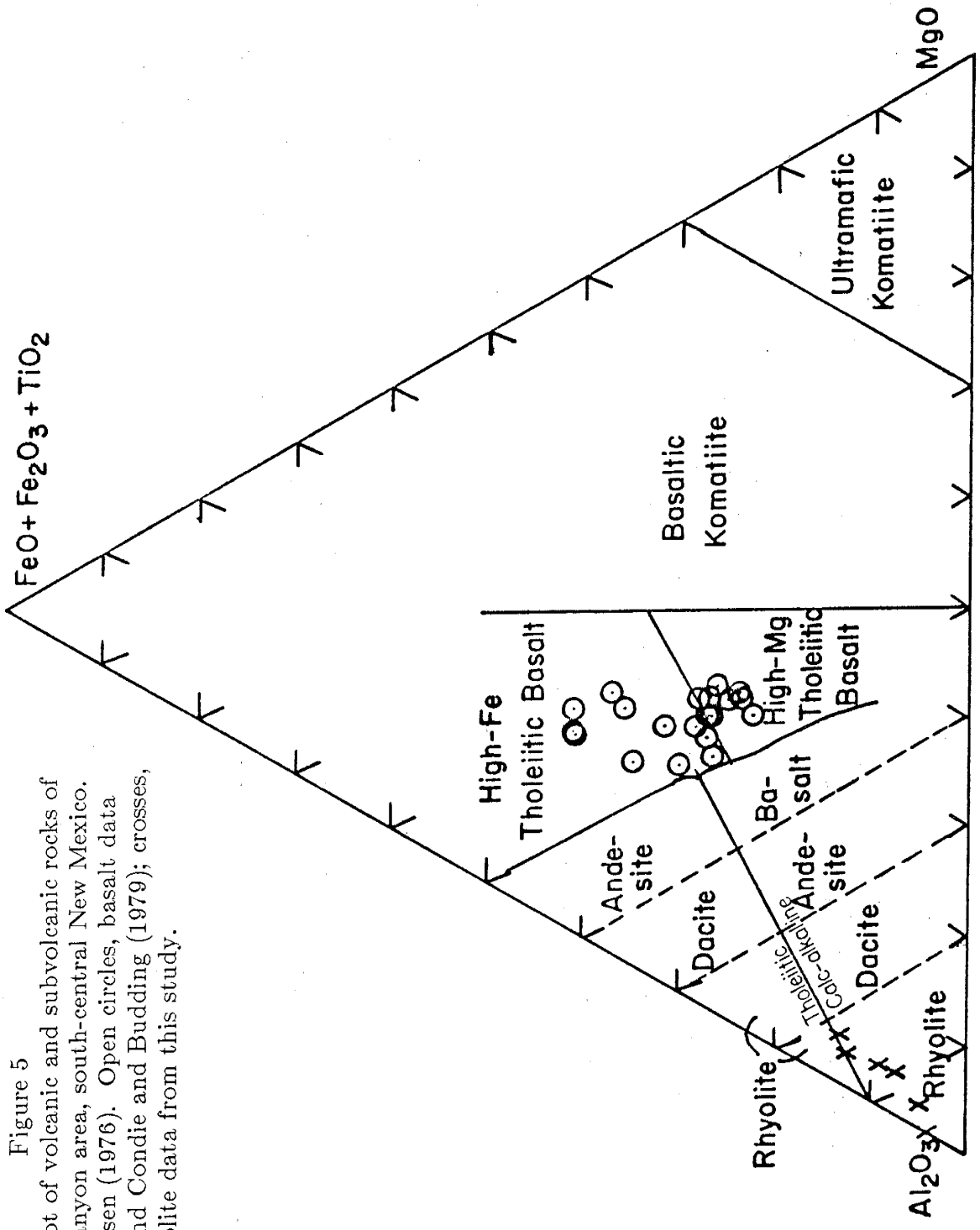

Figure 5
Jensen Cation plot of volcanic and subvolcanic rocks of the Hembrillo Canyon area, south-central New Mexico. Fields from Jensen (1976). Open circles, basalt data from this study and Condie and Budding (1979); crosses, rhyolite data from this study.

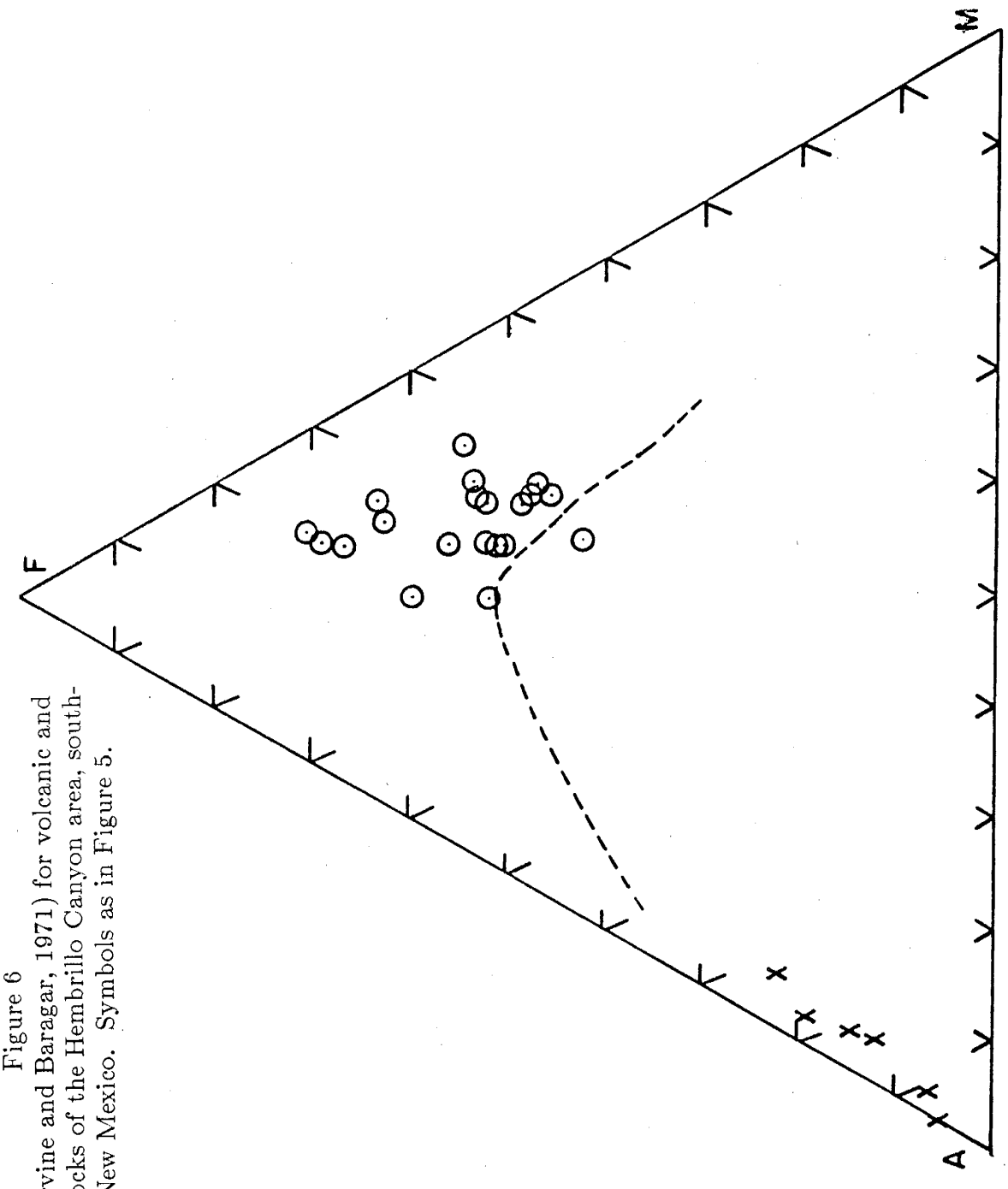

Figure 6
AFM plot (Irvine and Baragar, 1971) for volcanic and subvolcanic rocks of the Hembrillo Canyon area, south-central New Mexico. Symbols as in Figure 5.

the basalts are flat to slightly light REE enriched (Figs. 7 and 8). Flat REE patterns are typical of the tholeiitic series and indicate that fractionation of garnet from the melt was not important (Dostal, 1977).

Incompatible trace elements, when plotted on mid-ocean ridge basalt (MORB) normalized multi-element diagrams, characterize basalts from different tectonic settings. The patterns are dependent on sample composition and/or on contamination during crustal ascent, but not on fractional crystallization or partial melting (Pearce, 1983). Comparison of ancient basalts to those of modern settings are made possible with the MORB-normalized diagrams because the effects of partial melting or fractional crystallization change pattern levels, not pattern shapes (Pharaoh and Pearce, 1984). Saunders and Tarney (1984) indicate that enrichment of large-ion lithophile (LIL) elements (Sr, K, Rb, Ba, Th) versus high-field strength (HFS) elements (Ta, Nb, Ce, P, Zr, Hf, Sm, Ti, Y, Yb) is common in volcanic rocks formed in volcanic arcs. High LIL/HFS ratios are characteristic of basalts from narrow, juvenile basins (Saunders and Tarney, 1984), whereas low LIL/HFS ratios are characteristic of basalts from broad, mature basins.

Ta-Nb anomalies relative to REE and Th observed in Figures 9 and 10 indicate a significant subduction zone component in the source of these basalts (K.C. Condie, pers. comm.). Figure 10 also compares the Hembrillo Canyon basalts to average compositions of basalts from various tectonic settings. The Hembrillo Canyon basalts best compare with continental arc basalts (CAB) in both pattern shape and magnitude. Dehydration of a descending slab enriches the overlying mantle wedge in H_2O and decouples the LIL elements from the HFS elements. H_2O lowers the solidus of the mantle wedge and LIL elements ascend with

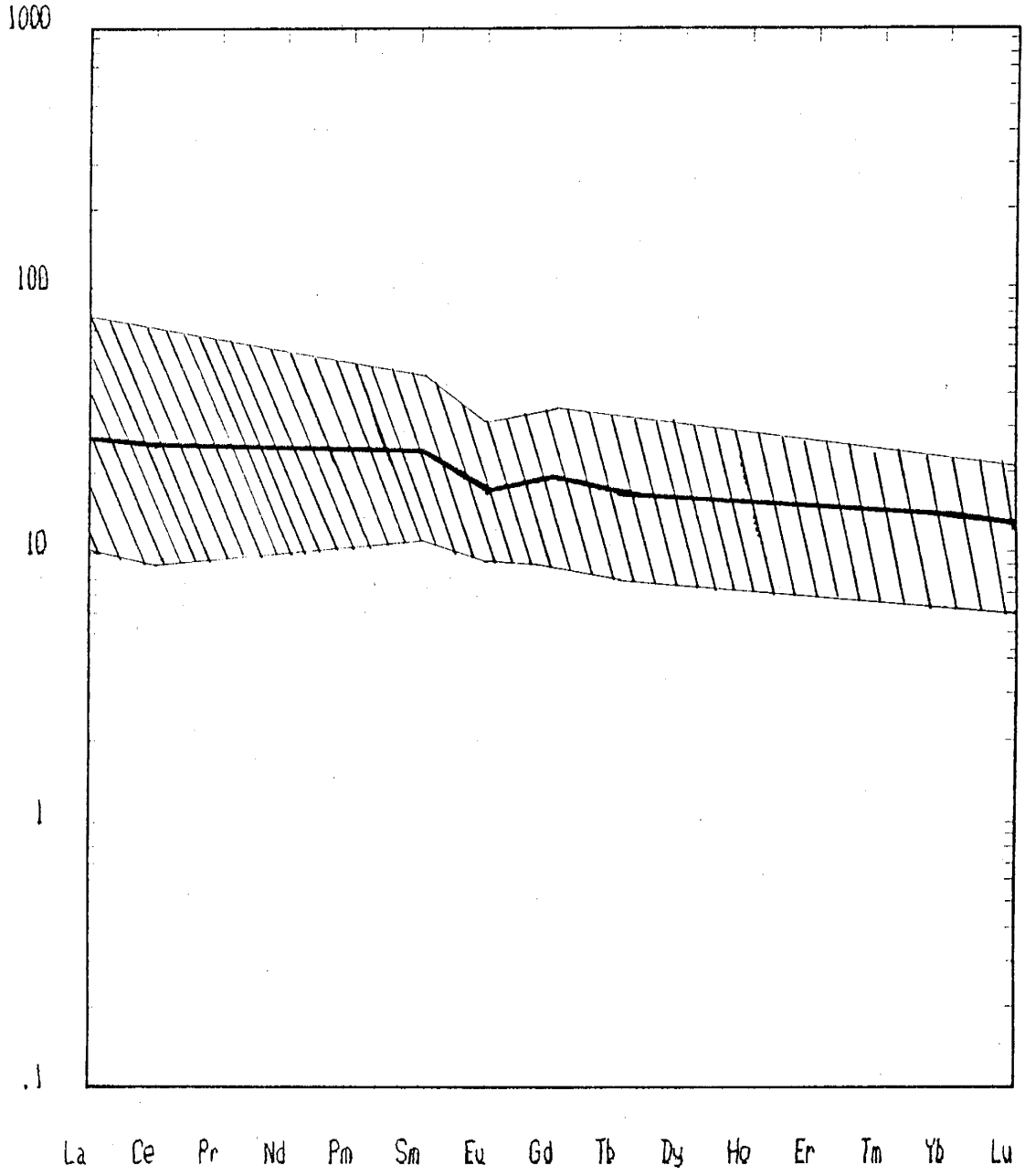

Figure 7
Chondrite normalized rare earth element distributions of Hembrillo Canyon basalts. Heavy line is average composition (n=18), hatchured area indicates range of values.

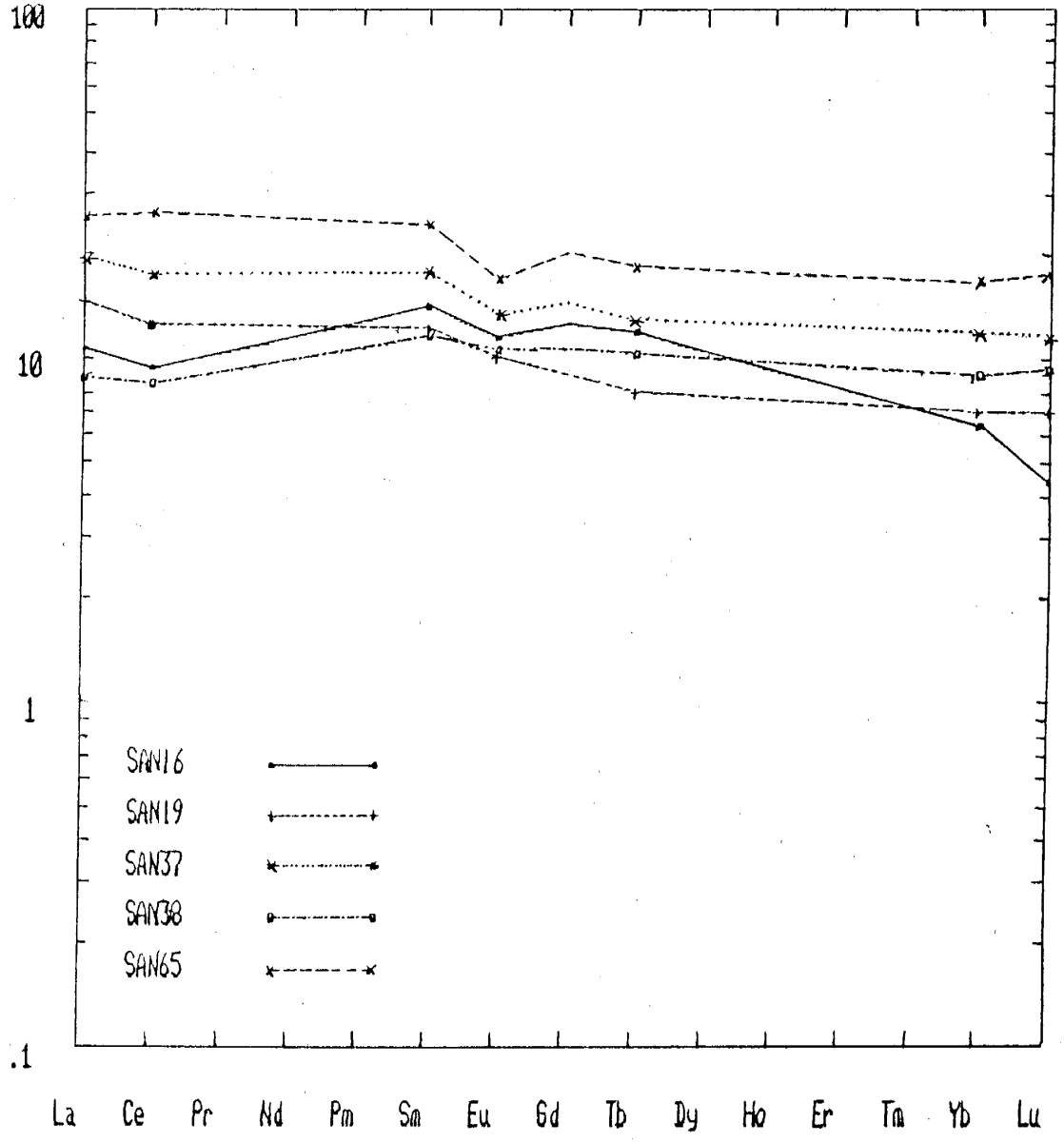

Figure 8
Chondrite normalized REE distributions in
Hembrillo Canyon basalts.

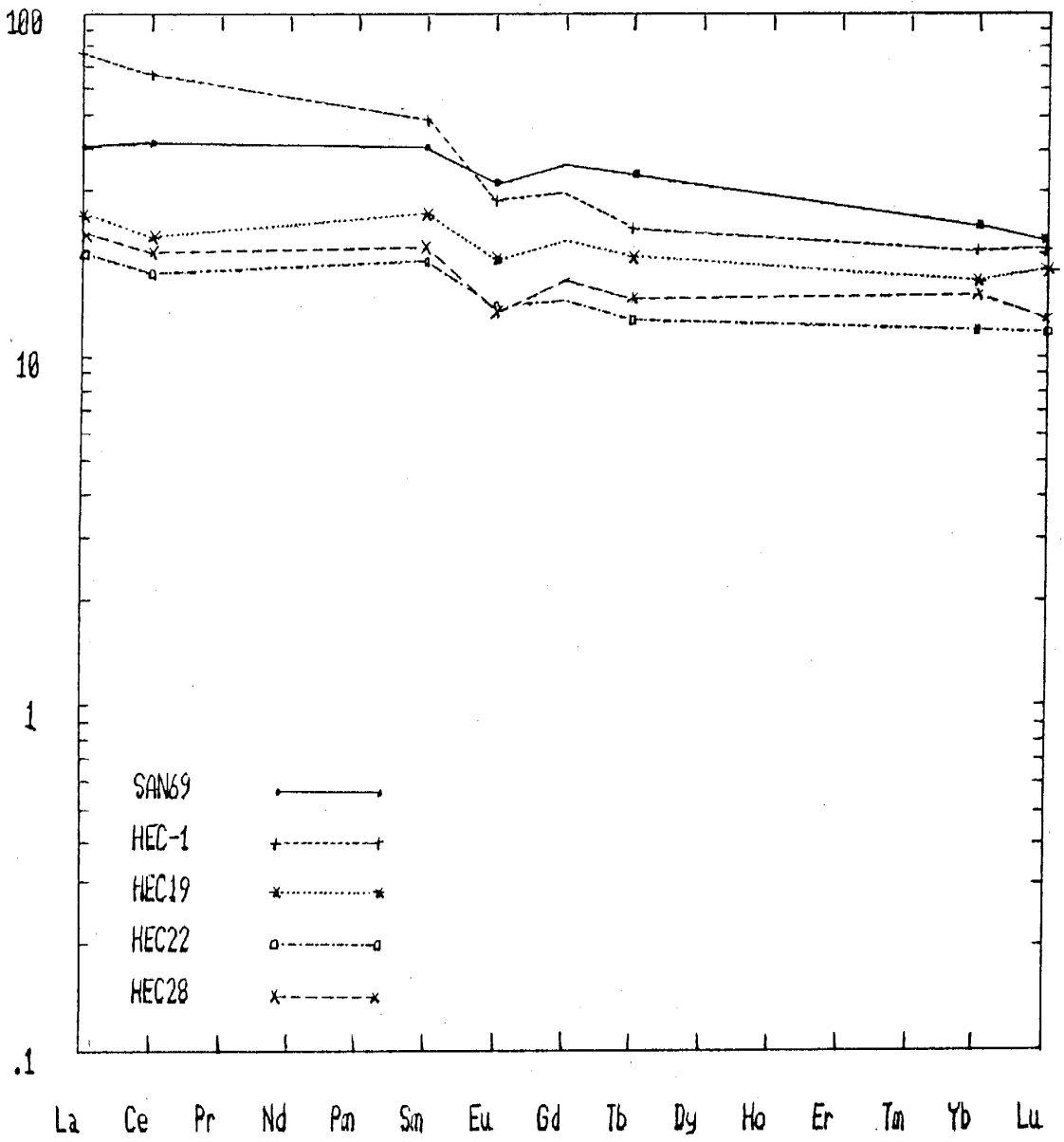

Figure 8 (continued)
Chondrite normalized REE distributions in
Hembrillo Canyon basalts.

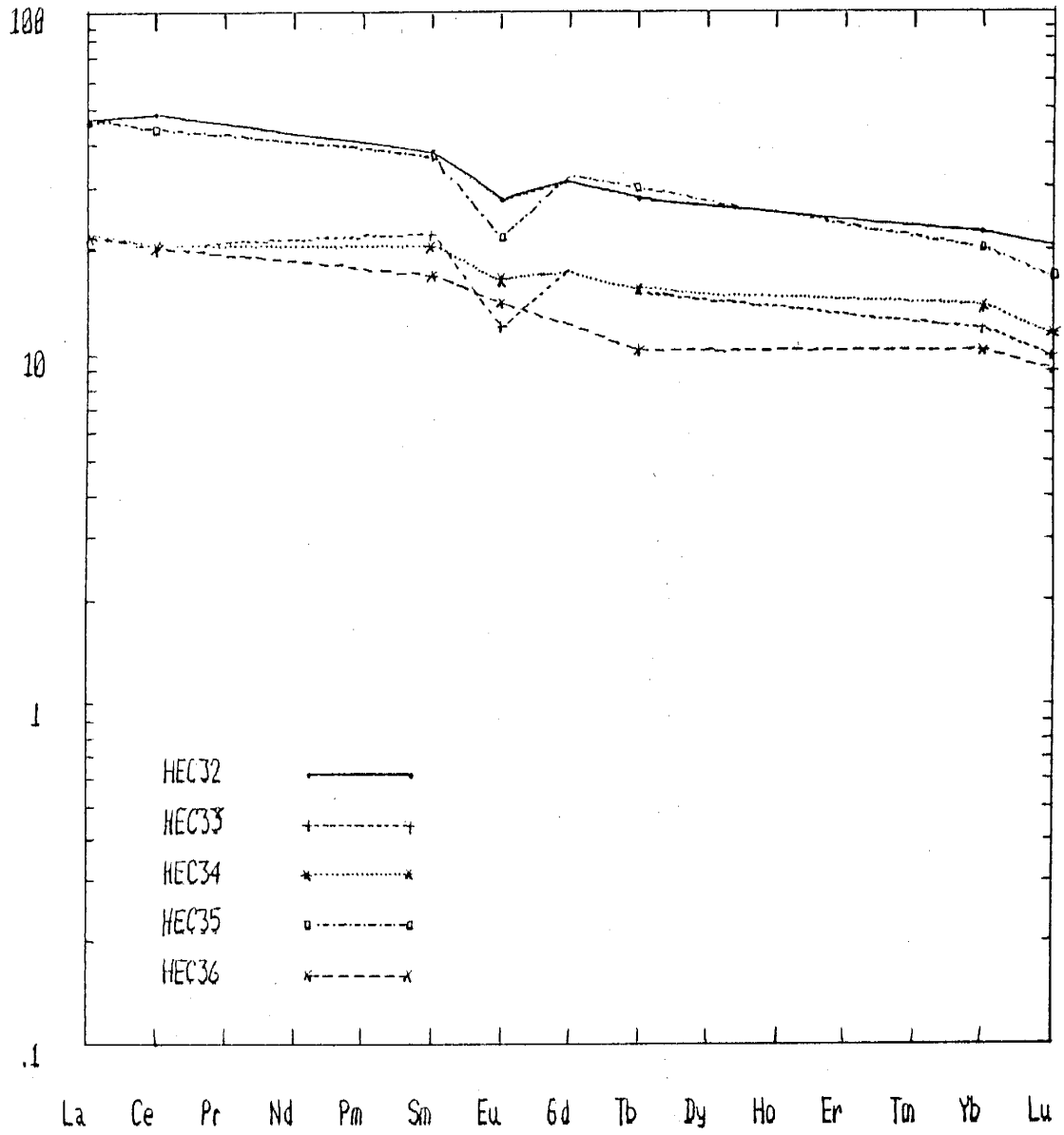

Figure 8 (continued)
Chondrite normalized REE distributions in
Hembrillo Canyon basalts.

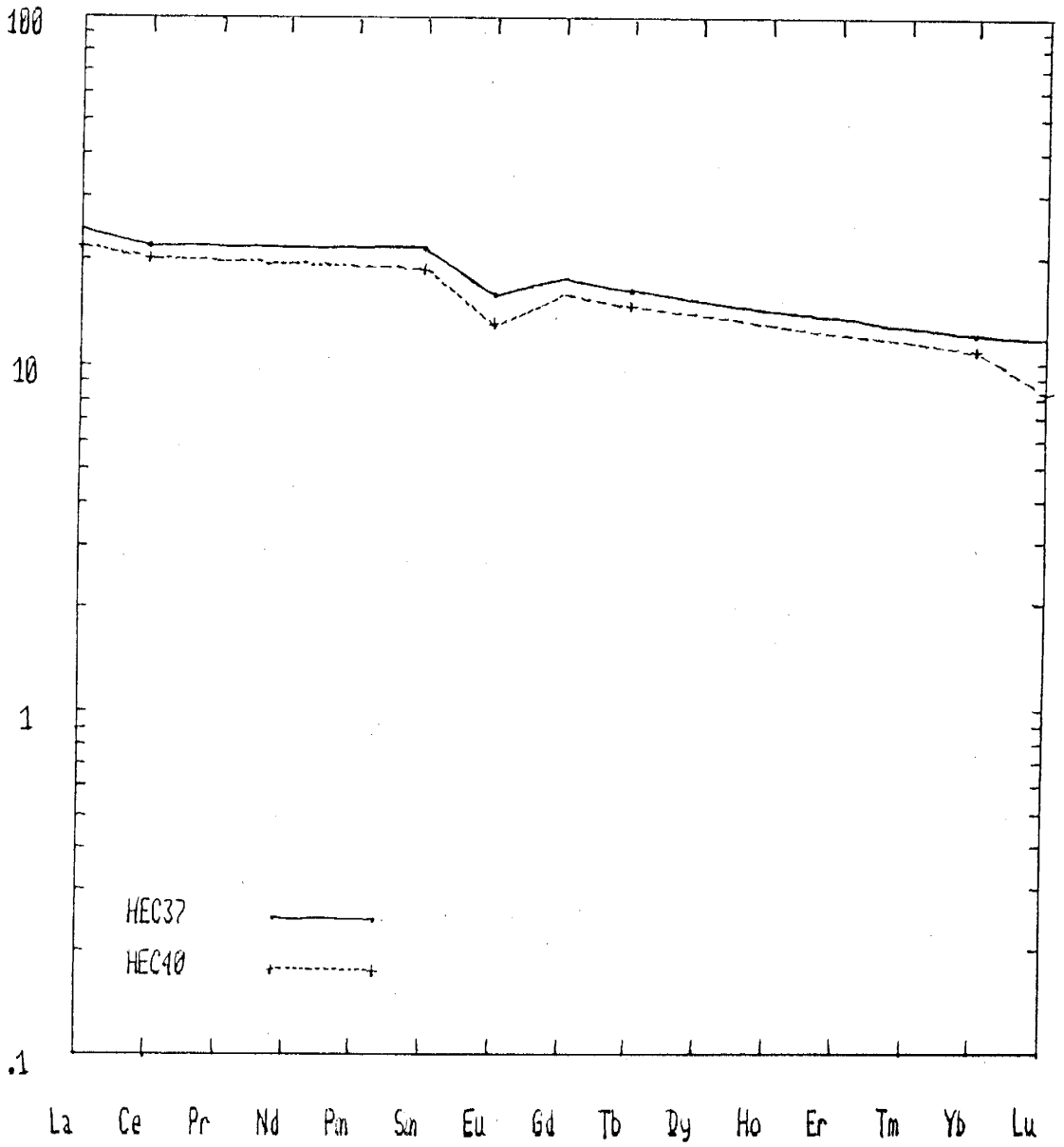

Figure 8 (continued)
Chondrite normalized REE distributions in
Hembrillo Canyon basalts.

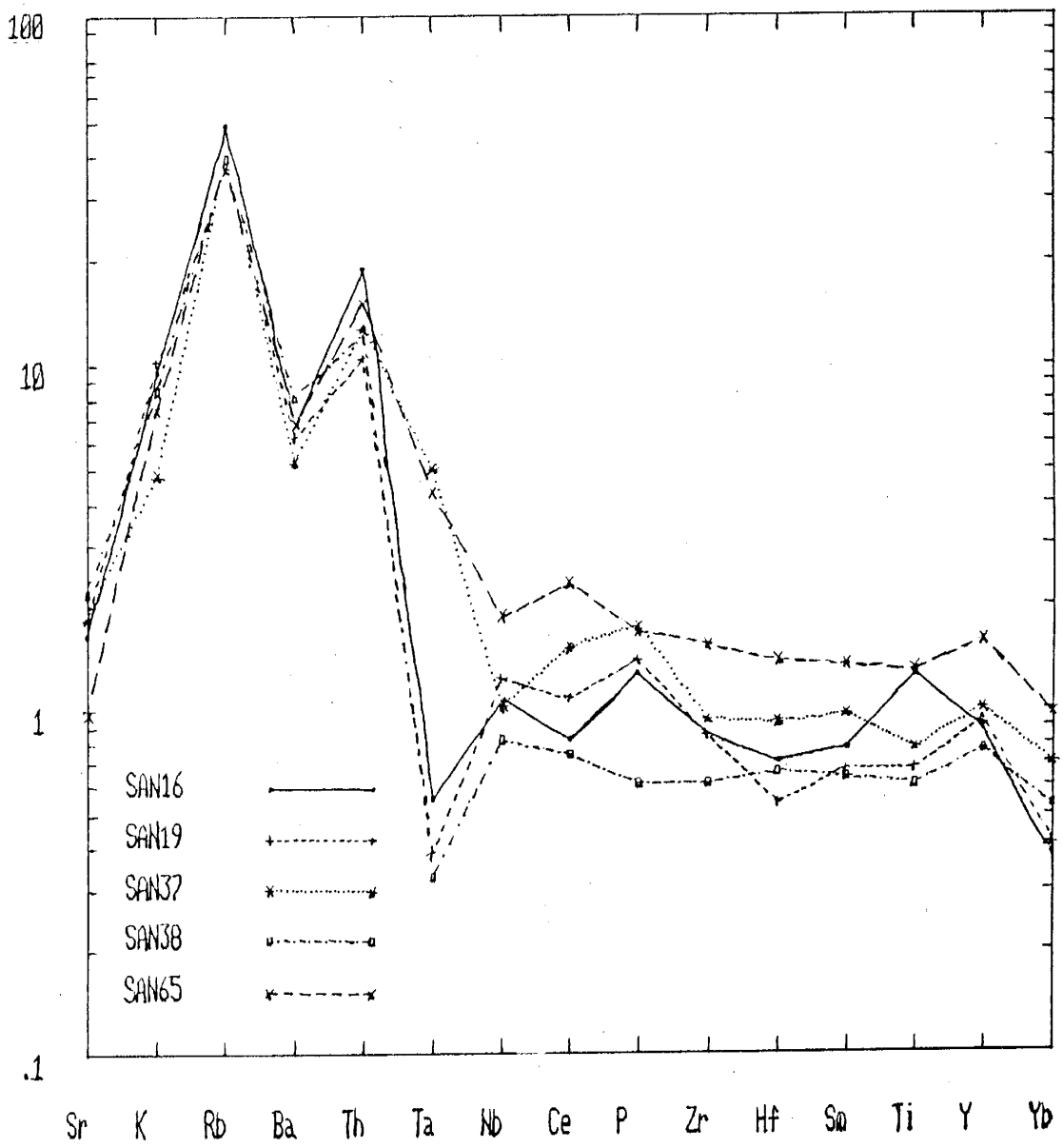

Figure 9
MORB normalized distributions for
all Hembrillo basalts.

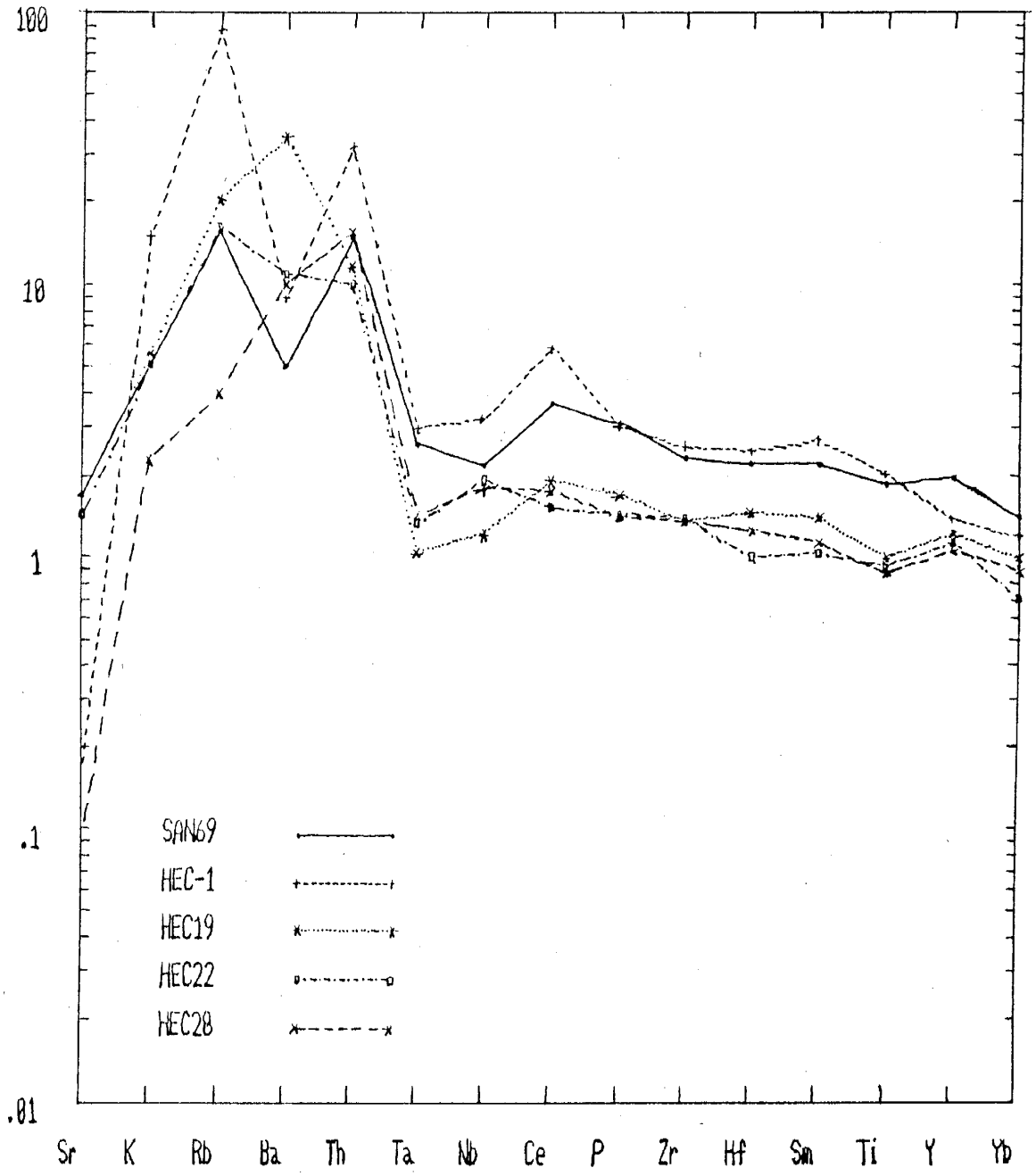

Figure 9 (continued)
MORB normalized distributions for
all Hembrillo basalts.

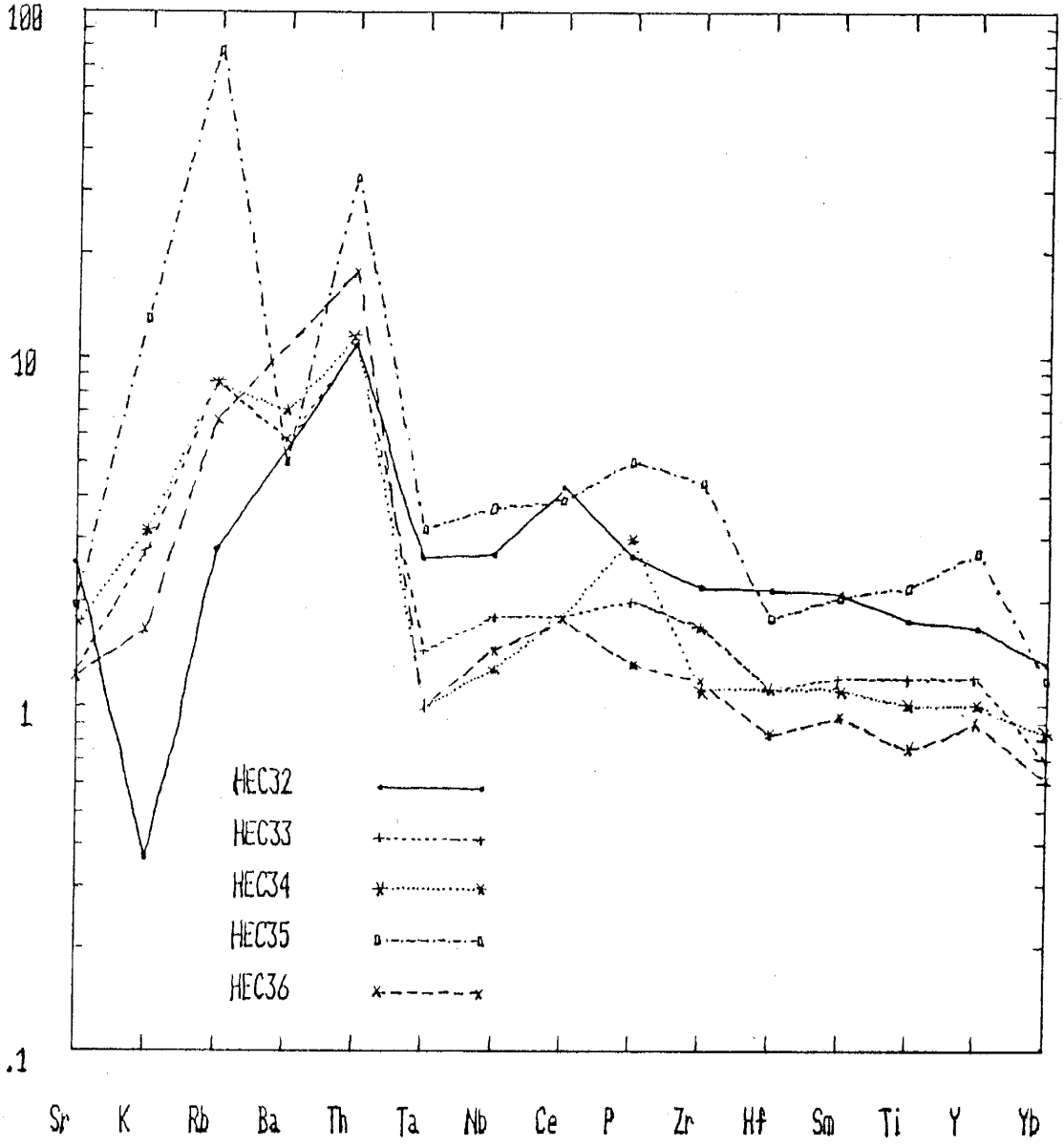

Figure 9 (continued)
MORB normalized distributions for
all Hembrillo basalts.

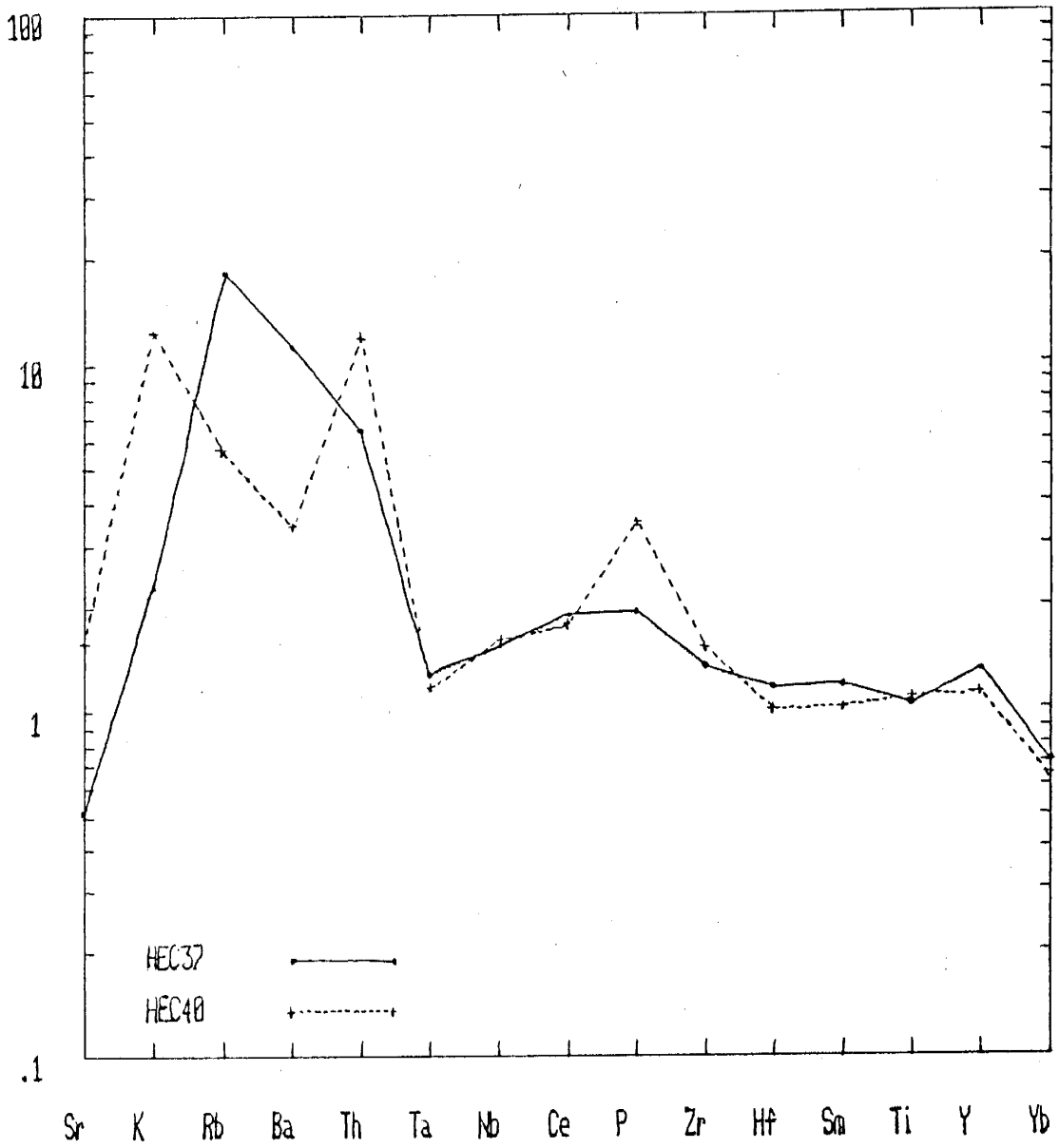

Figure 9 (continued)
MORB normalized distributions for
all Hembrillo basalts.

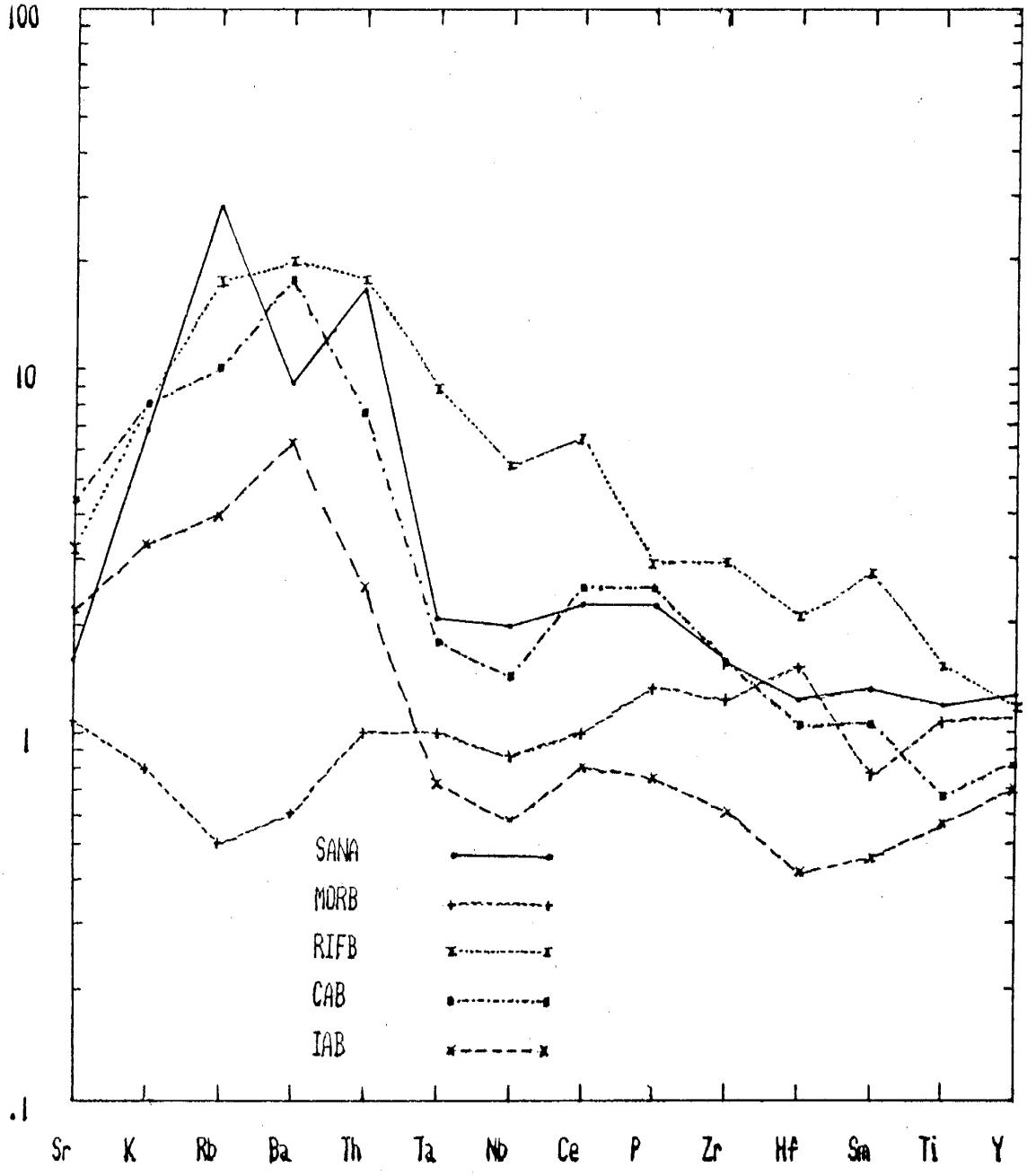

Figure 10
MORB normalized diagram comparing Hembrillo Canyon basalts to basalts from other tectonic settings. SANA = average of Hembrillo Canyon basalts; MORB = Mid-Oceanic Ridge Basalt average; RIFB = rift basalts; CAB = continental arc basalts; IAB = island arc basalts.

volatiles derived from the subducting slab. The lowered solidus allows melting to occur at lower temperatures. Enrichment of LIL elements with respect to HFS elements occurs due to the relative mobility of LIL versus HFS elements. HFS elements are not easily mobilized by ascending volatiles and remain in heavy mineral phases in the mantle wedge or the subducted slab.

Figure 11 illustrates a comparison of average Hembrillo Canyon basalts to the average compositions of basalts from the Calupuy and Casma groups of the central Chilean Andes (Dostal, 1977; Lopez-Escobar and others, 1977) and the average compositions of basalts from the Sarmiento and Tortuga complexes of the southern Chilean Andes (Saunders and others, 1979; Stern, 1980). Both the Calupuy-Casma group and Sarmiento-Tortuga complex data sets have been interpreted as remnants of continental marginal basins formed by back-arc spreading behind the Cretaceous Andean arc (Dott and others, 1982). The Hembrillo Canyon average falls within the ranges of these data sets, with similar overall pattern shapes and magnitudes.

Further distinctions of tectonic settings can be made by plotting the chemical data for the Hembrillo Canyon basalts on various tectonomagmatic diagrams. The Ti/Y versus Nb/Y diagram (Fig. 12; Pearce, 1983) allows separation of basalts into three categories: within plate basalts (WPB), MORB, and arc basalts (IAB). The Hembrillo Canyon basalts fall into the overlap in the arc and MORB fields. Earlier comparisons indicate that Hembrillo basalts are dissimilar to MORB, and must therefore be of arc origin.

Another discrimination diagram for basalts is the Zr-Y-Ti diagram (Fig. 13; Pearce and Cann, 1973). This diagram separates arc basalts from calc-

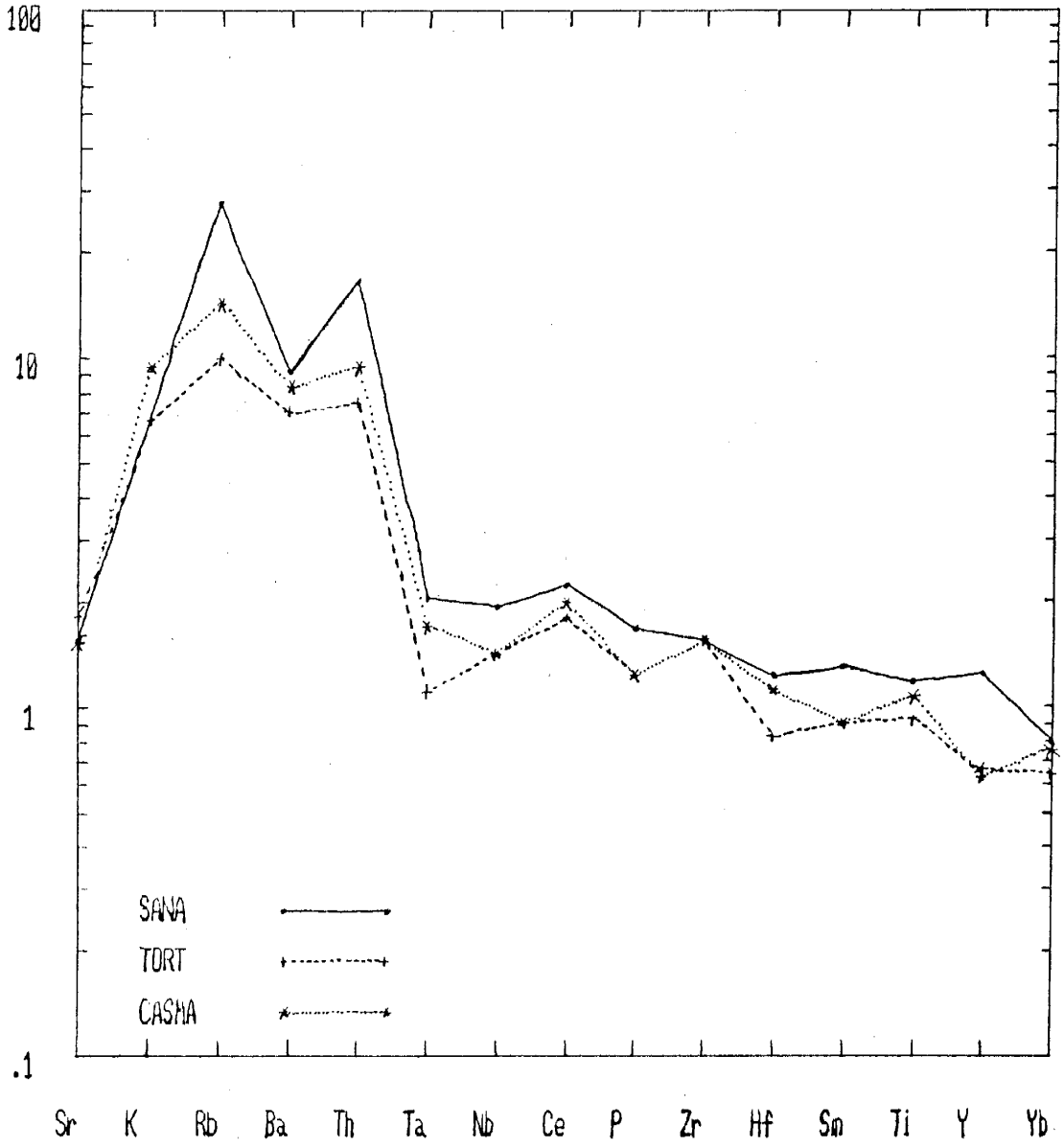

Figure 11
MORB normalized diagram comparing Hembrillo Canyon average basalts to basalts from the Calupuy-Casma groups of central Chile (Dostal, 1977; Lopez-Escobar, 1977) and the Tortuga-Sarmiento complexes of southern Chile (Saunders and others, 1979; Stern, 1980).

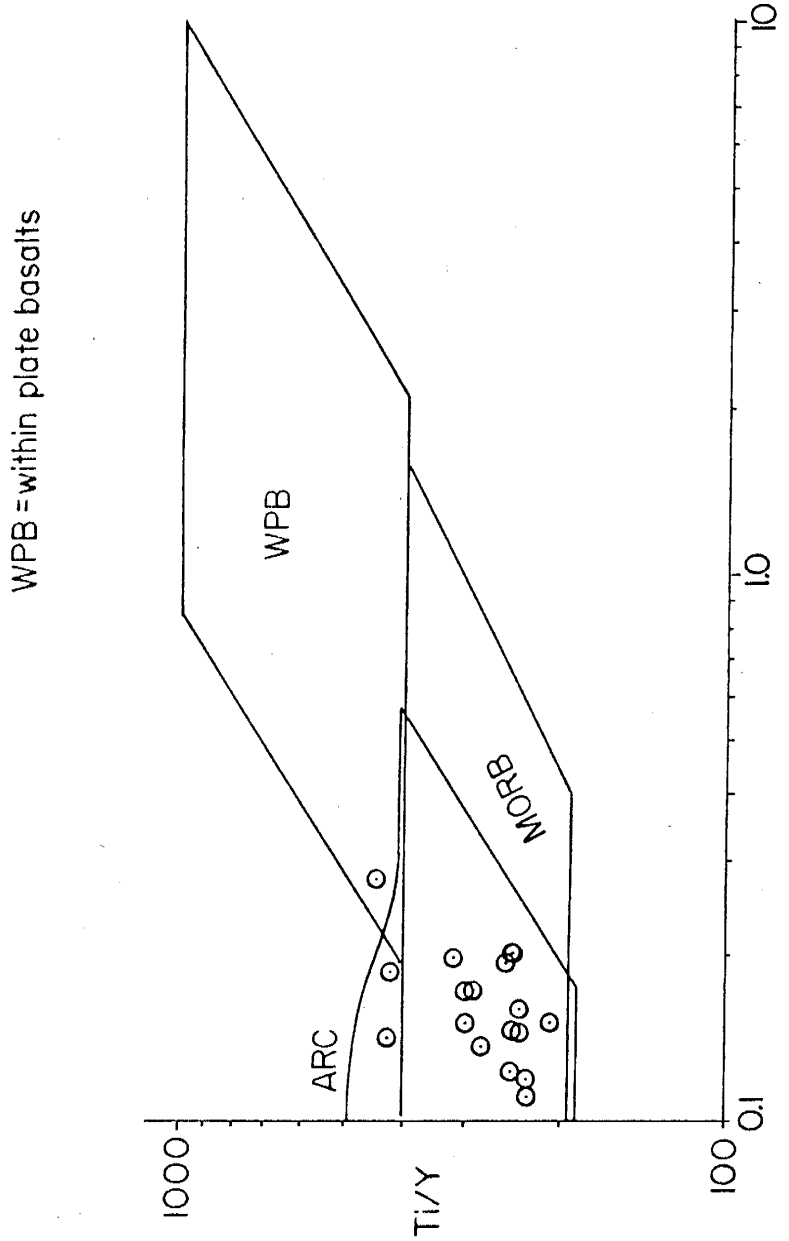

Figure 12
Ti/Y versus Nb/Y discrimination diagram (Pearce, 1983).
Open circles: Hembrillo Canyon basalts.

Figure 13
Hembrillo basalts plotted on the Zr-Y-Ti discrimination diagram of Pearce and Cann (1973). A: Island arc tholeiites; B: Island arc tholeiites and MORB; C: calc-alkaline basalts; W: within plate basalts (continental and oceanic island).

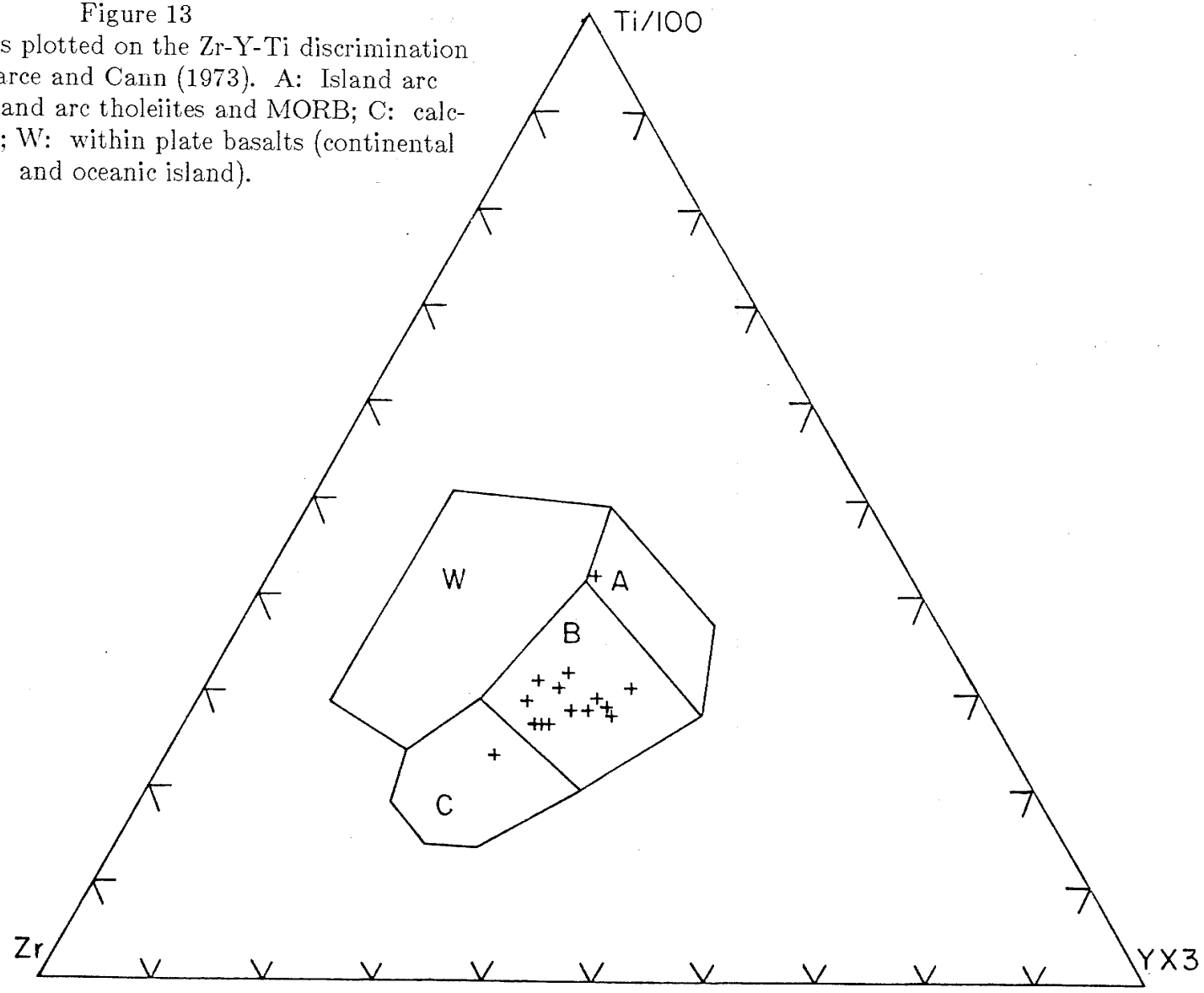

alkaline basalts and WPB. The data for the Hembrillo basalts all fall in the MORB and arc fields (A, B, and C). MORB has been ruled out previously, with the MORB normalized diagrams.

Wood's (1979) Th-Ta-Hf discrimination diagram allows further definition of tectonic settings for basalts. Figure 14 illustrates the Hembrillo basalts, which fall into the field of subduction zone related basalts (CPB). Data for the Casma group, central Chile (Atherton and others, 1985, and Lopez-Escobar, 1977) also plot in the CPB field. This gives further support to similarities between Cretaceous back-arc settings and the Hembrillo Canyon succession.

Felsic Volcanic Rocks

The rhyolitic rocks of the Hembrillo Canyon area are chemically indistinguishable from one another (Figs. 3, 4, 5, 6, and Table B-2, Appendix B), with variations only in magnitude of REE patterns (Fig. 15). Overall, REE patterns are enriched in light REE relative to heavy REE, similar to modern rhyolites in continental arc settings, rhyolites of the Calupuy and Casma groups, central Chile (Lopez-Escobar, 1977; Dostal, 1977) and rhyolites of the Sarmiento and Tortuga complexes of southern Chile (Saunders and others, 1979; Stern, 1980), as illustrated in Figure 16.

MORB normalized diagrams (Figs. 17 and 18) for Hembrillo rhyolites show similarities in overall patterns and magnitudes to continental margin arcs, and similarity in pattern to rhyolites from intracratonic rifts. These rhyolites are enriched in LIL elements versus HFS elements.

Tectonic settings of the Hembrillo rhyolites can be defined by the Rb-Hf-Ta

Figure 14
Th-Ta-Hf discrimination diagram (Wood, 1979).
Hembrillo basalts; open circles; Calupuy-Casma basalts,
filled circles; Tortuga and Sarmiento basalts, pluses.
N, N-type MORB; E, E-type MORB; WPB, within plate basalts

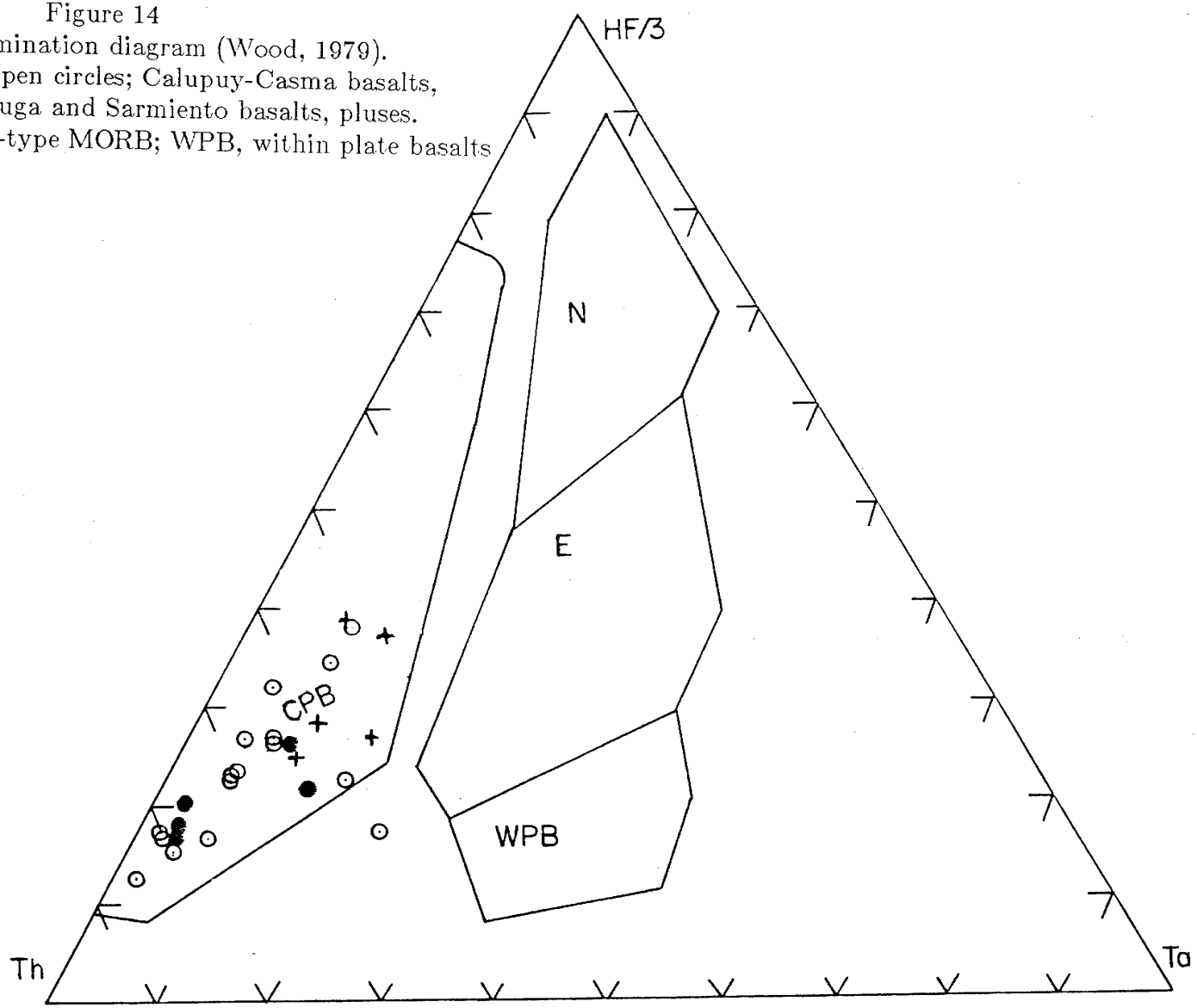

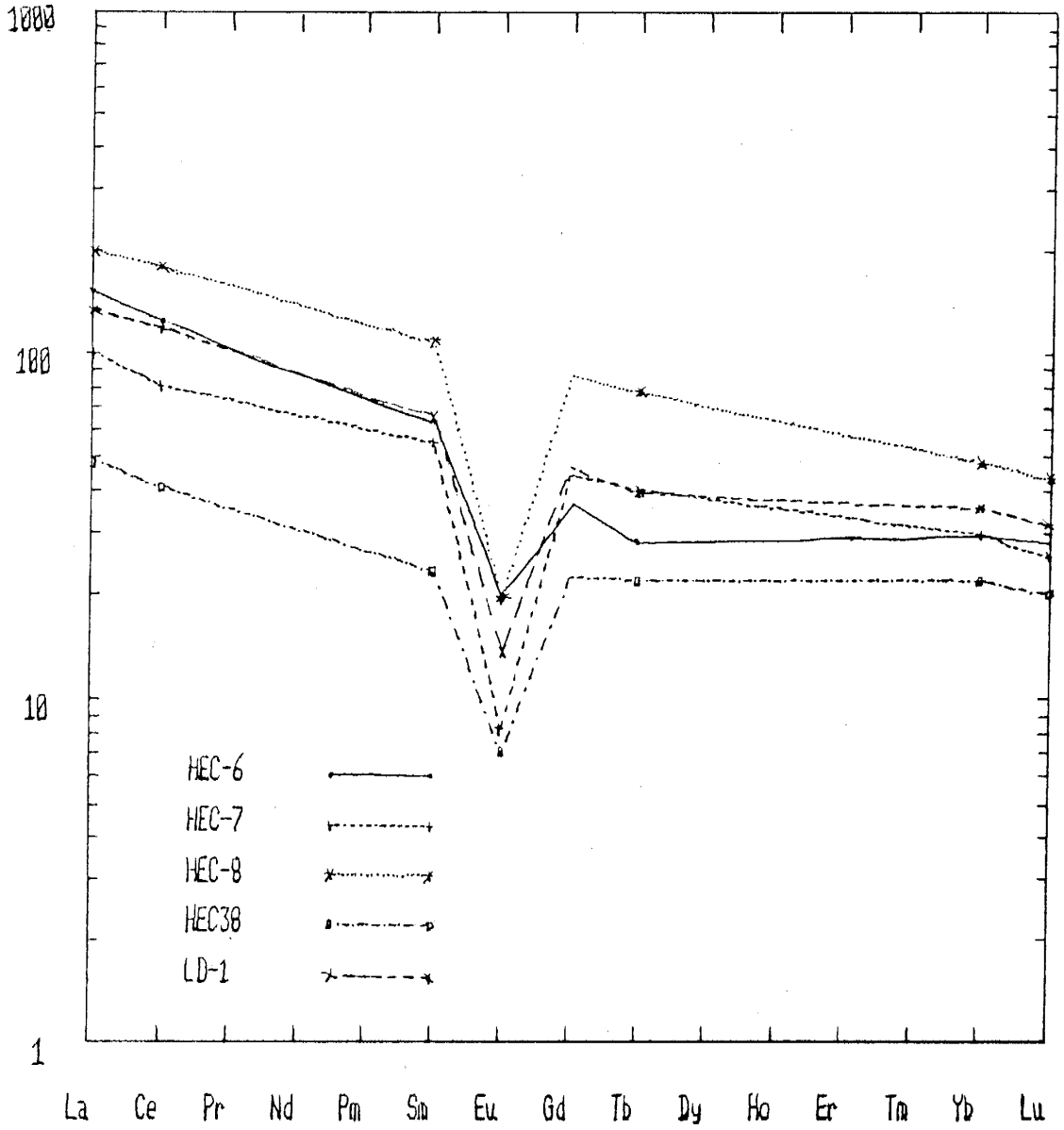

Figure 15
Chondrite normalized REE patterns for
Hembrillo Canyon rhyolites.

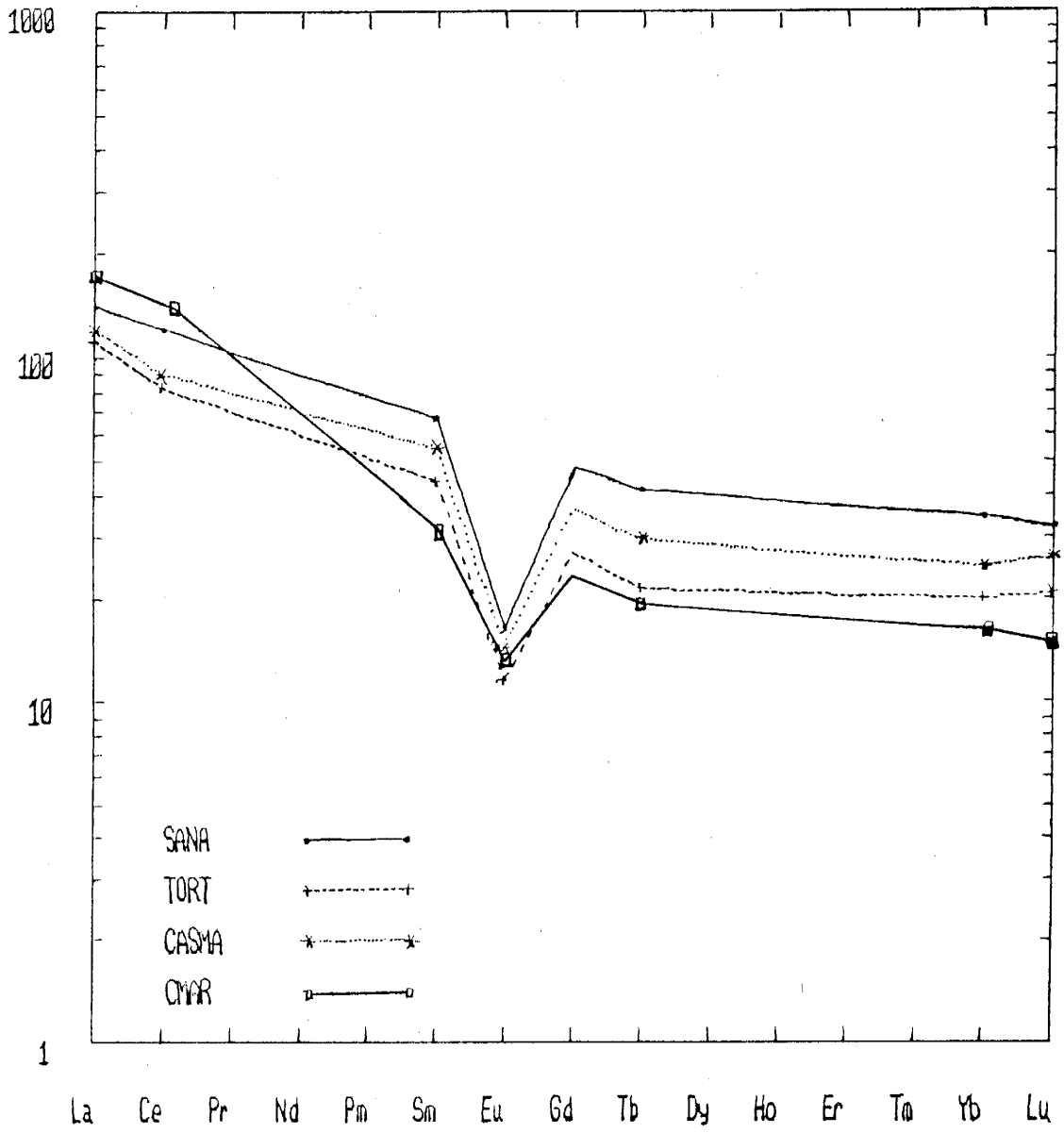

Figure 16
Chondrite normalized pattern comparing Hembrillo rhyolites (SANA) to modern continental arc rhyolites (CMAR); Calupuy-Casma group rhyolites (CASMA) and Tortuga-Sarmiento complex rhyolites (TORT).

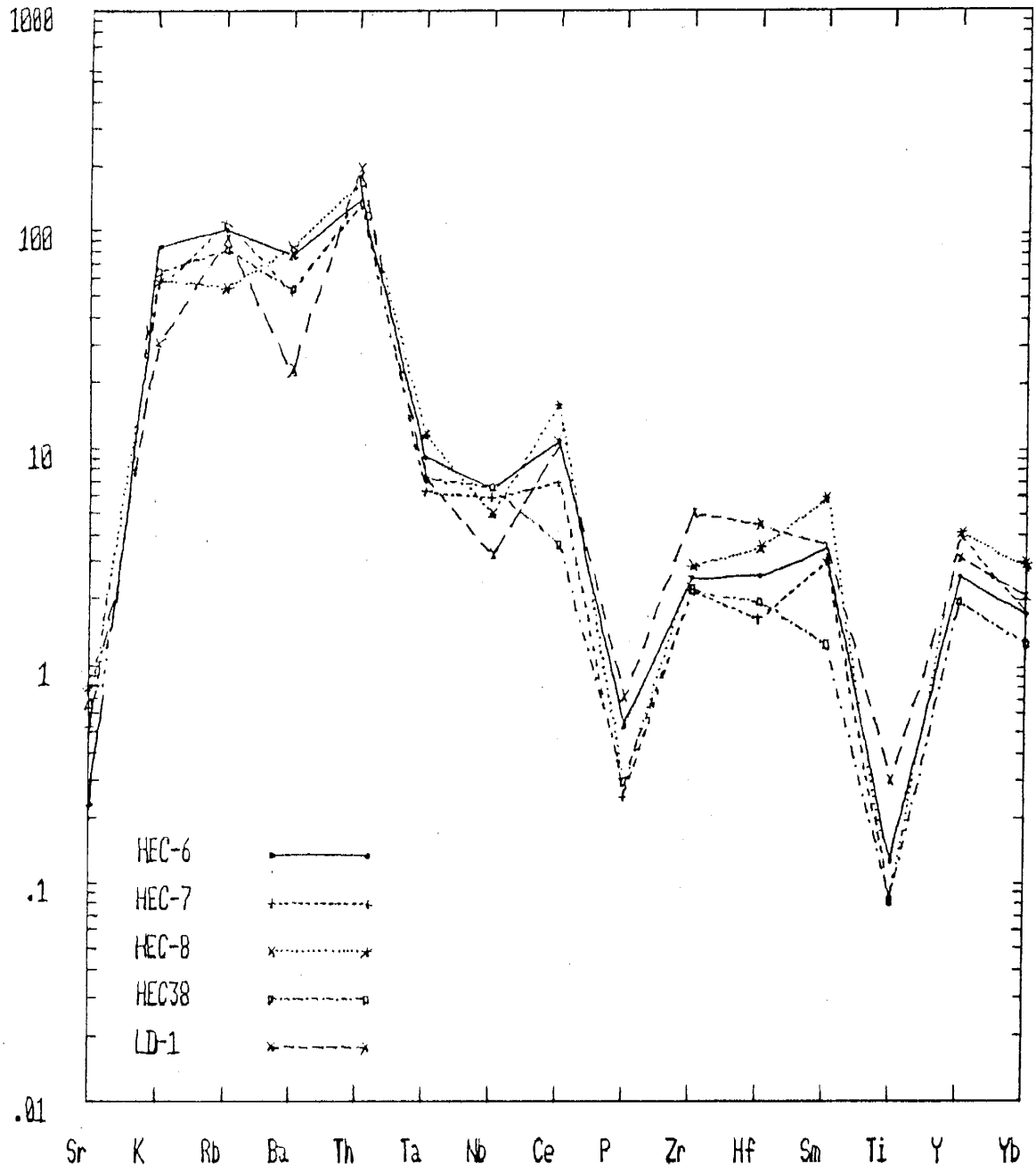

Figure 17
MORB normalized diagram for Hembrillo rhyolites.

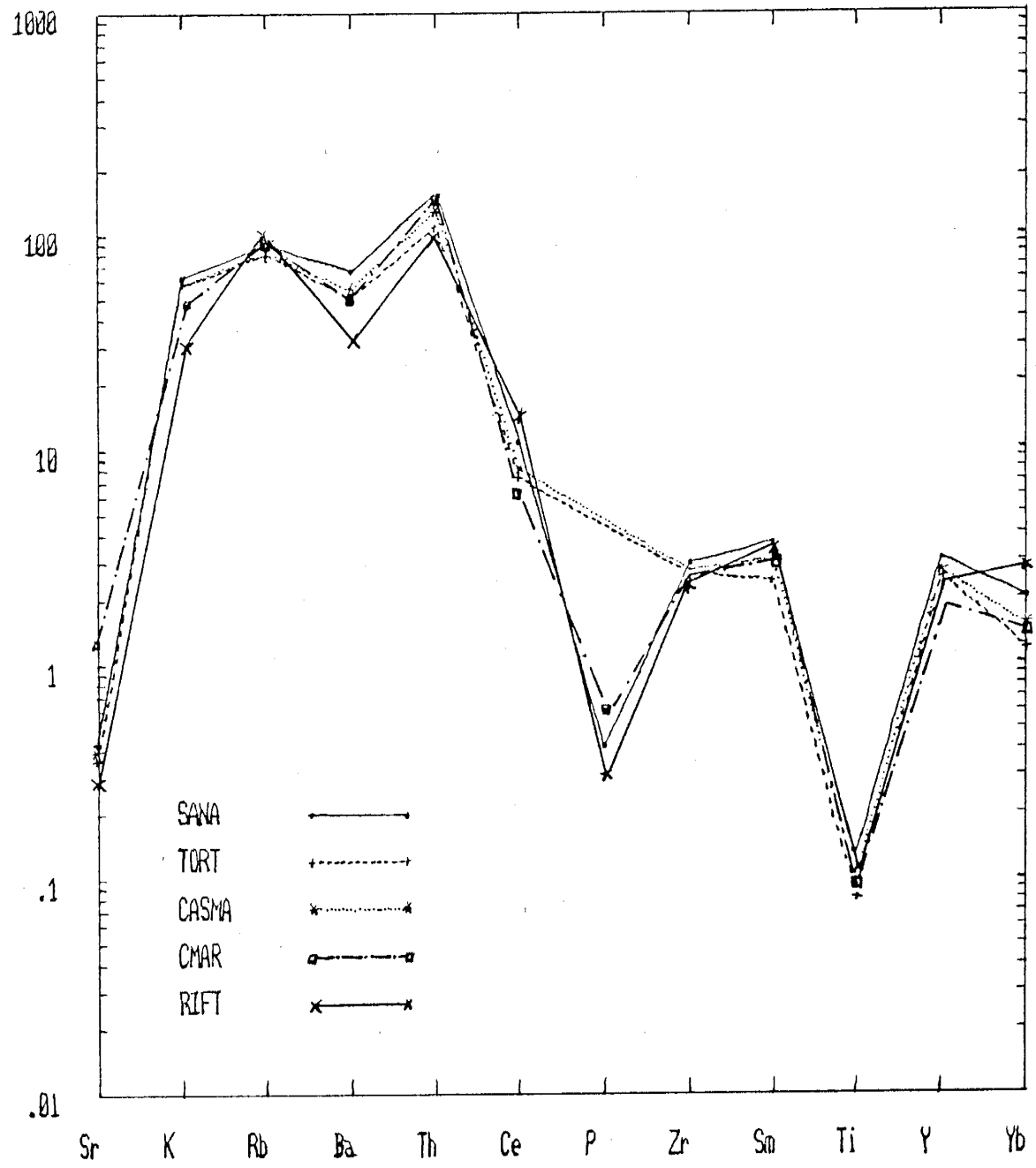

Figure 18
MORB normalized diagram for Hembrillo rhyolite average (SANA); Continental Margin Arc rhyolite average (CMAR); Intracratonic Rift rhyolites (RIFT); Casma-Calupuy groups (CASMA); and the Sarmiento-Tortuga Complex (TORT).

diagrams in Figures 19 and 20 (Harris and others, 1986). The fields in Figure 19 are divided into arc, within plate, syn-tectonic collisional (I) and post-tectonic collisional settings (II); those for Figure 20 are defined as arc, within plate, and ocean floor settings. The Hembrillo Canyon rhyolites fall within the arc field with the exception of one sample, HEC-6m, which falls in the within plate field.

The La/Yb-Yb diagram (Fig. 21; K.C. Condie, unpublished data) divides rhyolites into two fields: a volcanic arc field and a rift field, further establishing the Hembrillo Canyon succession as an arc-related supracrustal package.

Pearce's (1984) diagrams contrasting Rb versus Y and Nb, Rb versus Yb and Ta, and Ta versus Yb (Figs. 22, 23, and 24) allow rhyolites to be divided into four fields: volcanic arc, syn-collisional, within plate, and oceanic ridges. All of these diagrams suggest that the Hembrillo felsic volcanics formed in a subduction-related tectonic setting.

Summary

The volcanics of the Hembrillo Canyon succession are apparently of a subduction-related origin, and possibly formed in a narrow, juvenile back-arc basin. This interpretation is supported by element distribution, including MORB normalized diagrams, rare earth element distributions, and various tectonomagmatic diagrams. The Calupuy and Casma groups of central Chile and the Sarmiento and Tortuga complexes of southern Chile come from tectonic settings interpreted to be continental-arc-back arc basin in nature (Lopez-Escobar, 1977; Dostal, 1977). Element distributions in these Cretaceous rocks compare favorably with those of the Hembrillo volcanics.

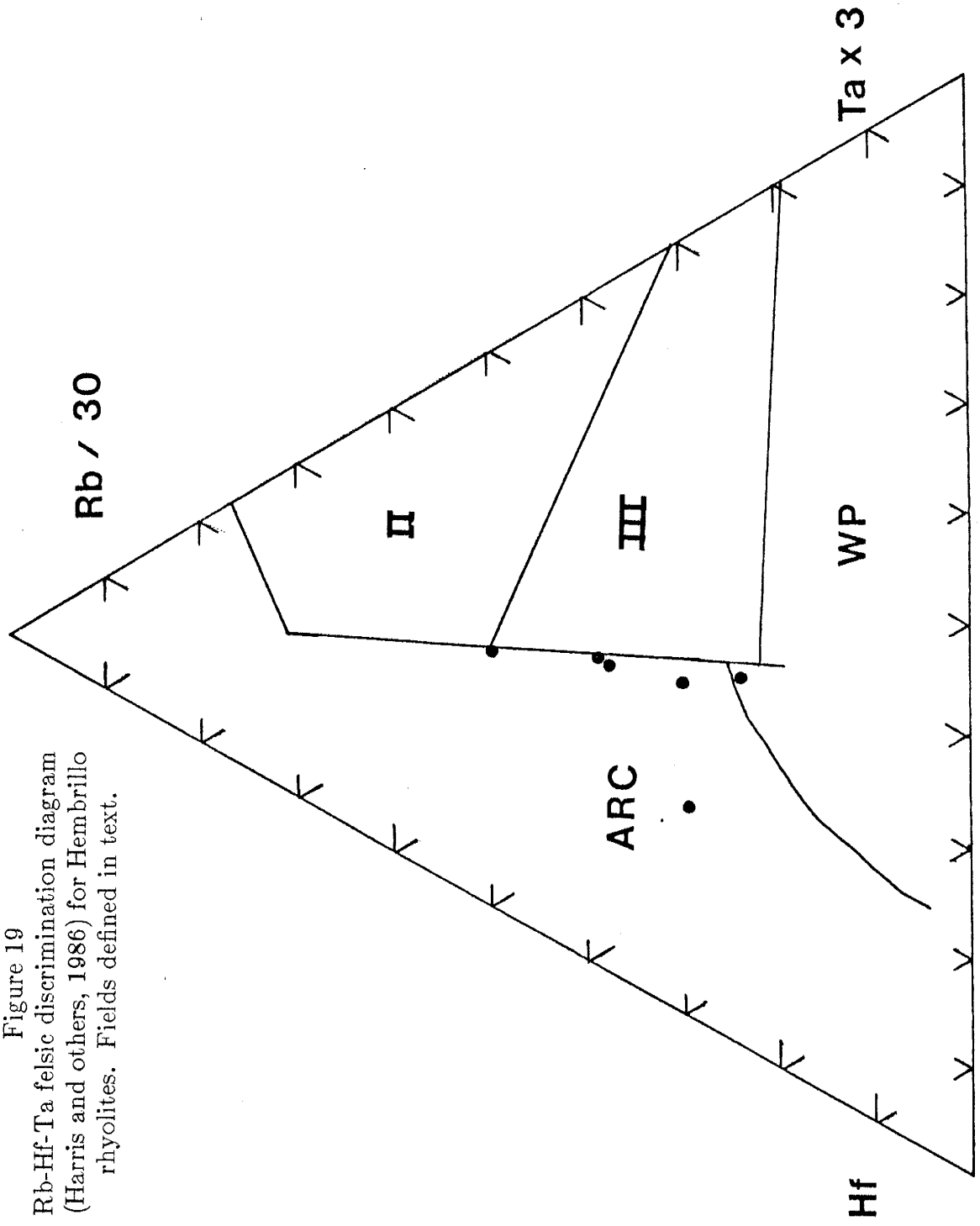

Figure 19
Rb-Hf-Ta felsic discrimination diagram (Harris and others, 1986) for Hembrillo rhyolites. Fields defined in text.

Figure 20
Rb-Hf-Ta felsic discrimination diagram
(Harris and other, 1986) for Hembrillo rhyolites.
Field defined in text.

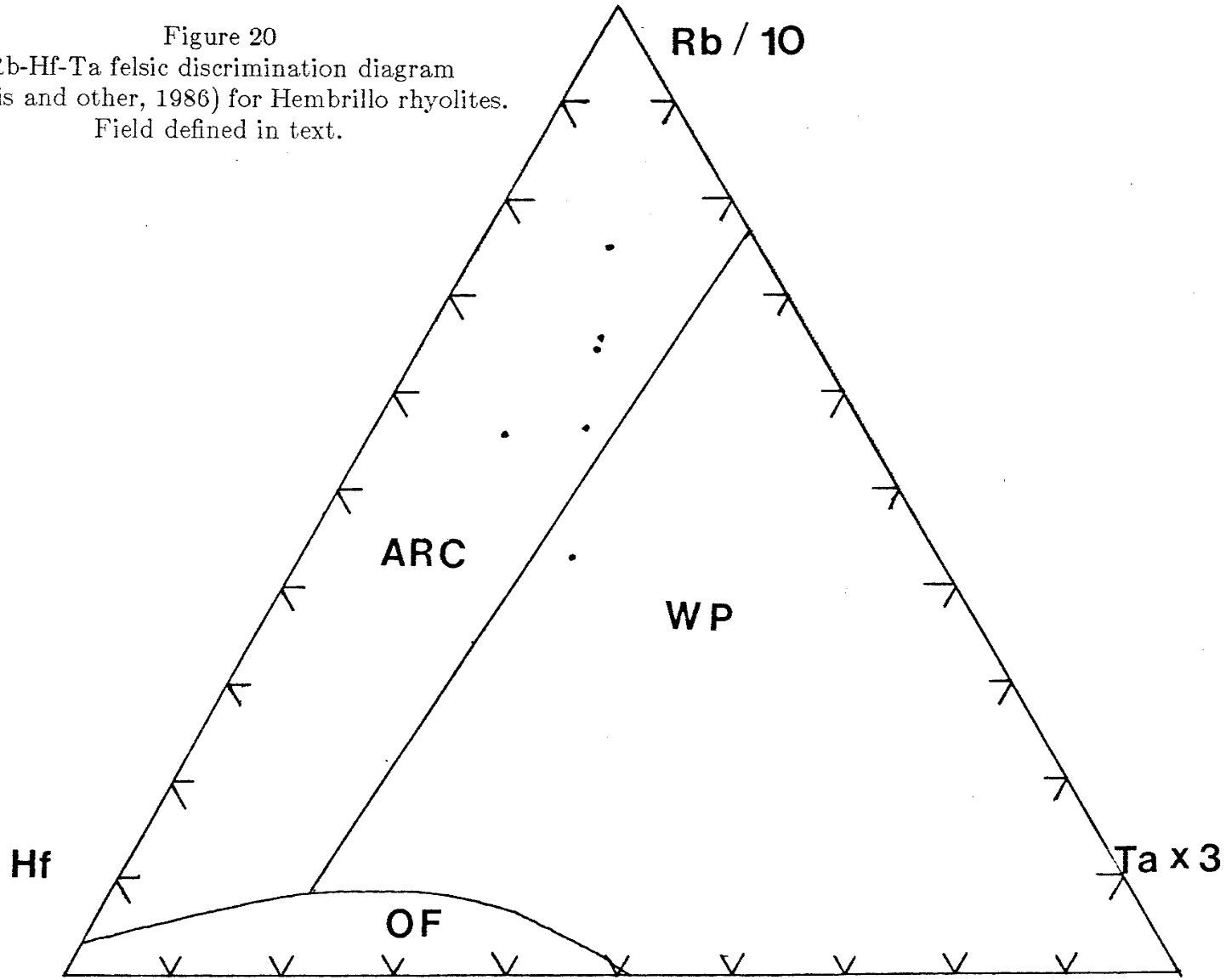

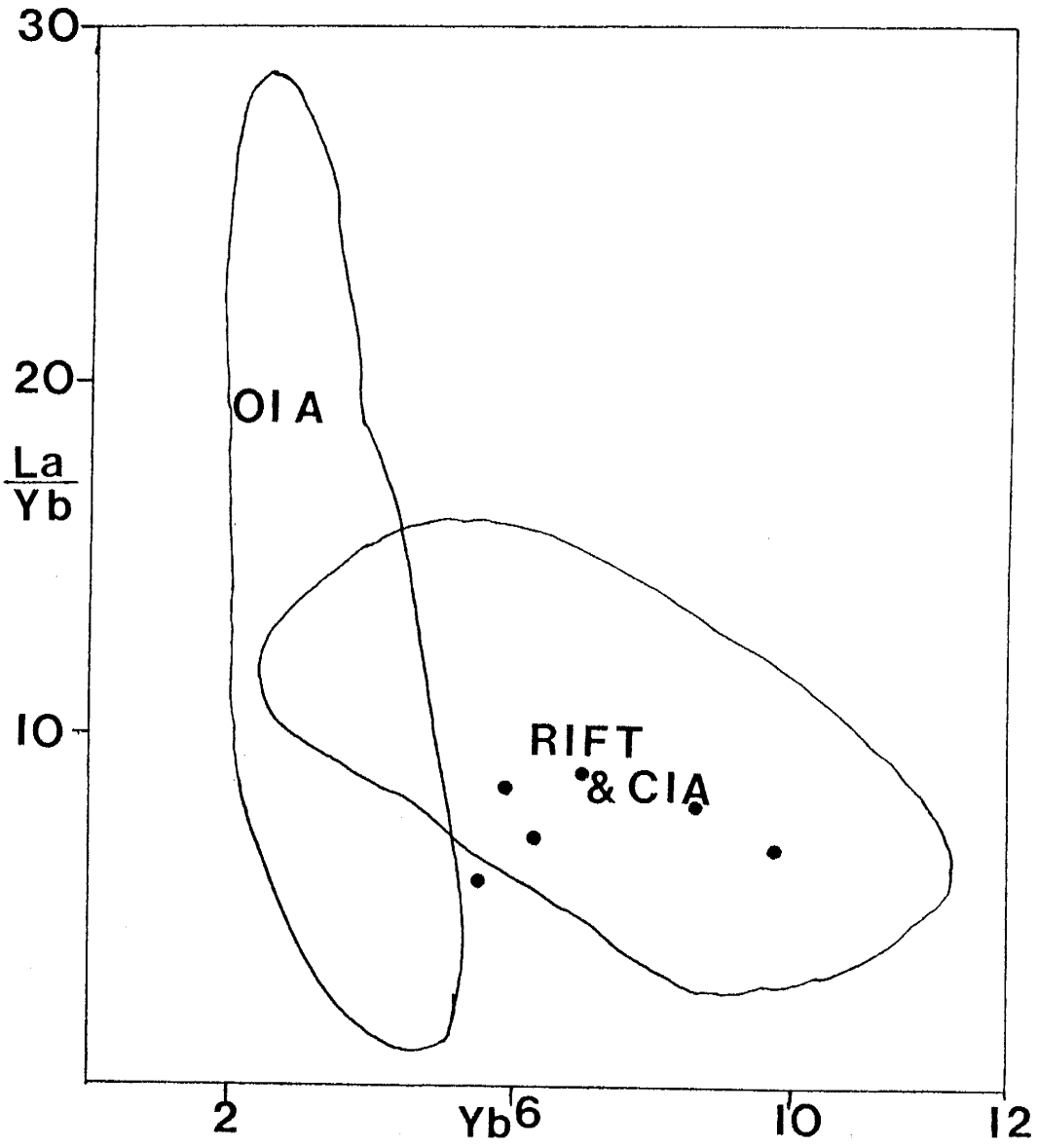

Figure 21
La/Yb-Yb tectonomagmatic diagram for felsic rocks. Fields from Condie (unpub. data). OIA = oceanic island arcs; RIFT and CIA = continental rift and continental island arc. See discussion in text.

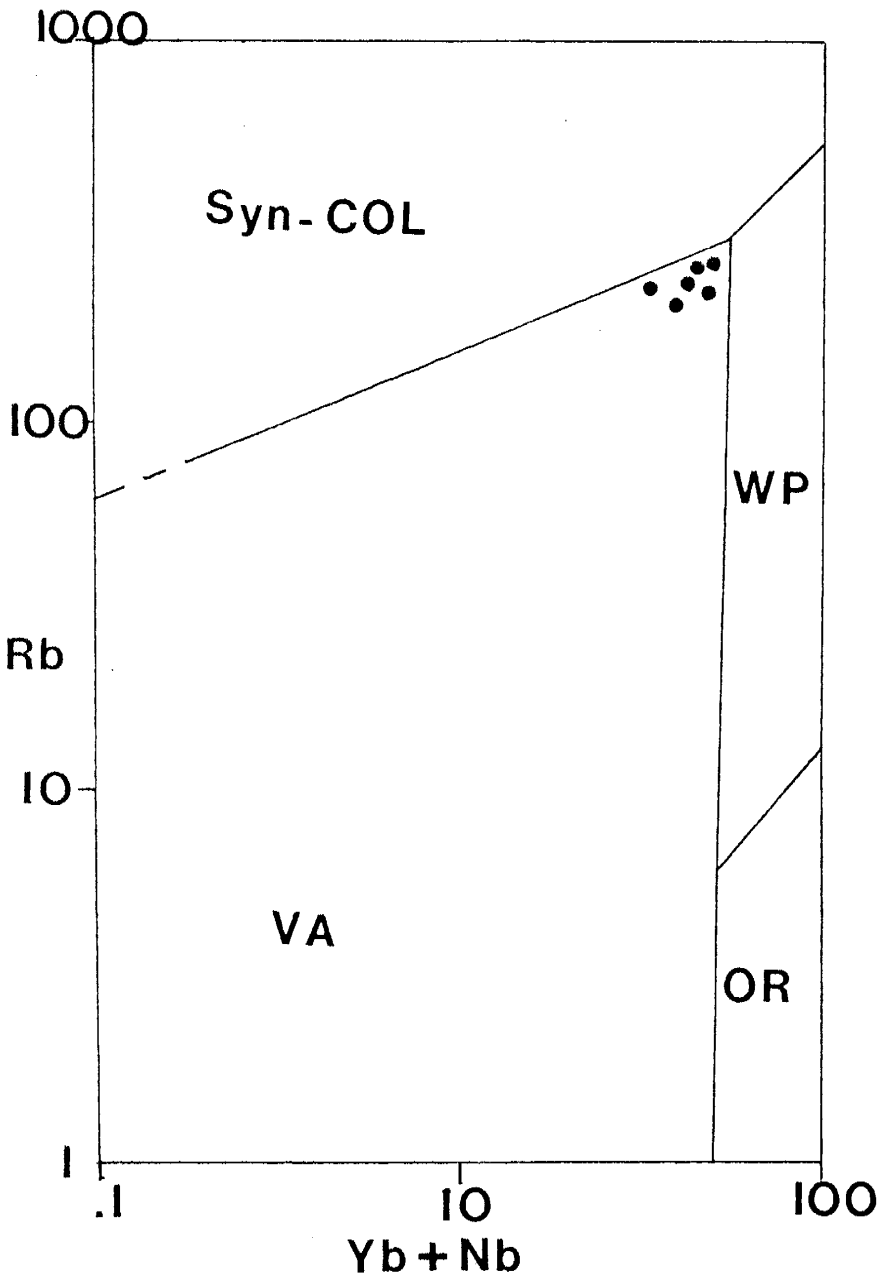

Figure 22
Rb-Y + Nb discrimination diagram (Pearce and others, 1984). Syn-col, syn-collisional felsics; WP, within plate (including continental margins); VA, volcanic arc; OR, oceanic ridge.

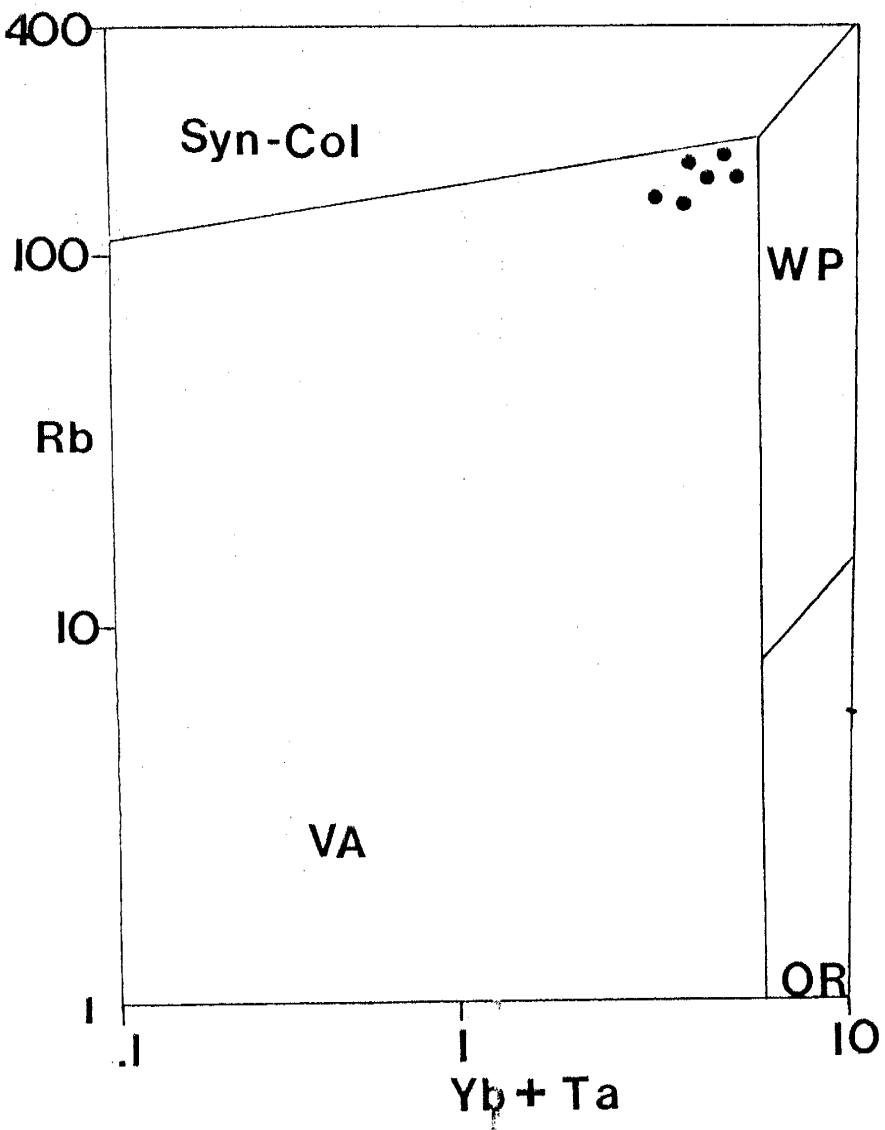

Figure 23
Rb-Yb + Ta discrimination diagram (Pearce and others, 1984) for Hembrillo felsic rocks. Fields as in Figure 23.

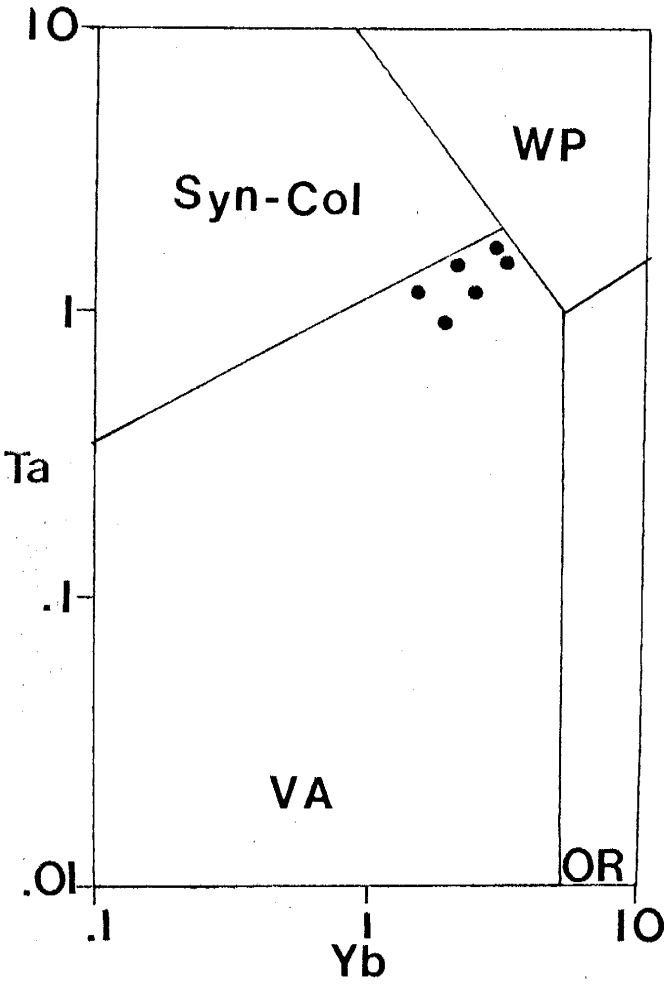

Figure 24
Ta-Yb discrimination diagram (Pearce and others, 1984) for Hembrillo felsic rocks. Fields as in Figure 23.

SEDIMENTARY ROCKS

Field Relations

The Hembrillo Canyon succession is dominated by terrigenous clastic sediments, which make up approximately 70% of the total lithologic package. Lithologies vary from coarse conglomerates with clasts up to 25 cm in size, to very fine-grained graywackes. Using Pettijohn et.al.'s (1972) classification scheme for terrigenous sediments (Fig. 25), the sediments in the Hembrillo Canyon succession are classified as quartz arenites, subarkoses, sublitharenites, conglomerates, quartzwackes, and graywackes. Most sediments fall in the quartz arenite and quartzwacke fields.

Forty percent of the sedimentary package consists of fine-grained quartz wackes and graywackes. Wackes commonly form slopes and saddles and vary in color from light gray to brown to light green. Occasionally, erosional contacts occur with larger clasts of underlying material forming a basal lag. This is well illustrated by a pebbly mudstone occurring near the unconformity on the north side of Hembrillo Canyon. Individual wacke units are generally 2 to 10 m thick, although those associated with other sandstones are on the order of 2 cm to 2 m thick.

Quartz wackes and graywackes are fine grained and poorly sorted containing irregularly shaped grains of broadly varying mineralogy. Based on this characterization for these fine-grained sediments, the term graywacke will be adopted for them as defined by Blatt and others (1980), Crook (1974), and Bhatia and Crook (1986). The graywackes of the Hembrillo Canyon succession are often

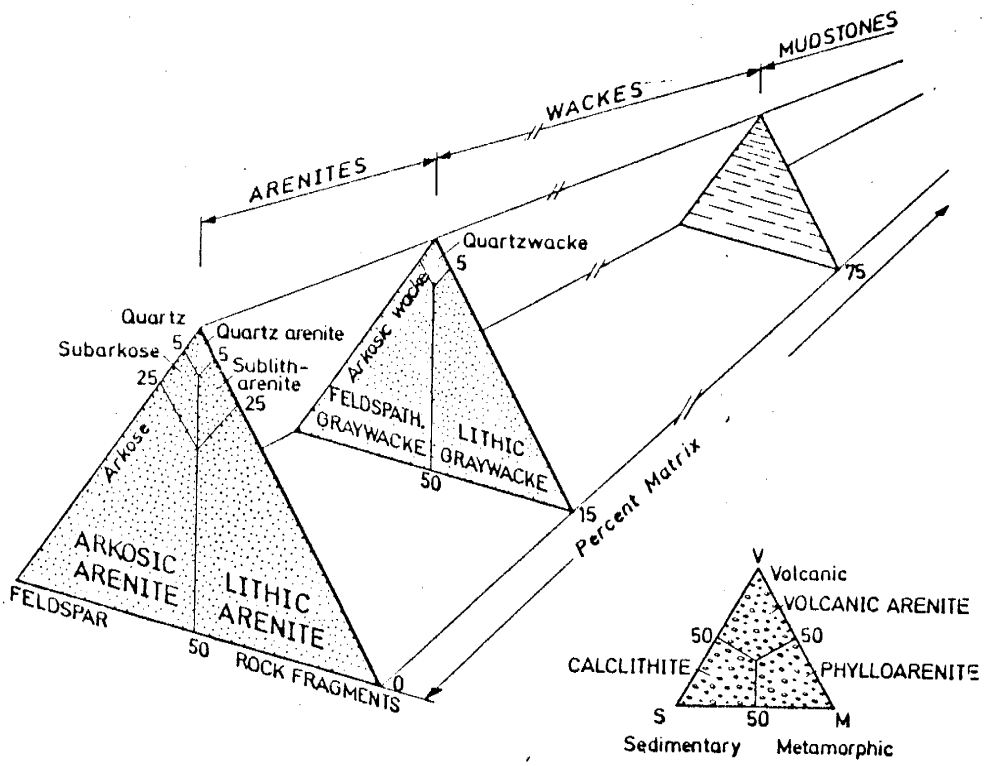

Figure 25
Classification of terrigenous sediments
(Pettijohn et.al. 1972).

parallel laminated. Large clasts (5-20 cm) often occur within these graywackes. These clasts are commonly imbricated, giving excellent data for paleocurrent directions (Appendix F, and Paleocurrent section).

Sand-to-shale ratios range from 1:10 to 1:1 in the graywackes. Sequences with a ratio of 1:10 commonly contain coarser interbeds of quartzose sandstones < 50 cm in thickness, with the graywacke units approximately 2 m thick. As the sand-to-shale ratio approaches 1:1, sand layers are 5 to 20 cm thick and graywacke layers are 1 to 15 m thick.

Approximately 60% of the sedimentary package consists of varying amounts of quartz arenite, subarkosic arenite, sublitharenite, and conglomerate. These rock types dominate most of the section south of Hembrillo Canyon, although a thick sequence of finely laminated, interbedded graywackes and sandstones occurs in this area as well.

Quartz arenites consist of > 95% quartz with minor amounts of lithic fragments and virtually no matrix. They are buff to white and are generally highly resistant to erosion, commonly forming cliffs and ridges of notable extent. Hematite staining occurs in joints and on some weathered surfaces, giving a red to orange color to some quartz arenites. These units exhibit low angle cross-bedding highlighted with hematite grains. Crossbeds observed in three dimensions allowed measurement of paleocurrent data (discussed later in text). Cross laminations are also observed, though not as commonly. Silicification has occurred in many of these units, obscuring some original textures. Those with original textures preserved show well rounded, moderate-to-well sorted, fine-to-coarse sized sand grains. The occurrence of low angle cross-bedding and cross laminae imply that

flow was in the upper part of the lower flow regime.

Arkoses comprise a small percentage of the sedimentary sequence and are of local importance. Arkoses are resistant cliff and ridge forming units with prominent outcrops. They weather red, orange, grey, and brown in color, primarily due to hematite and other iron oxide staining. No sedimentary structures are preserved other than graded bedding. These massive sandstones are generally very coarse and contain clasts of quartz arenite, graywacke, and other arkoses. A few very small clasts of granitic material were observed in Hembrillo Canyon, possibly indicating the source material for much of the sediments. Individual grains within the arkose include K-feldspar, quartz, and trace amounts of rutile, tourmaline and hematite. These arkoses contain less than 5% matrix. Contacts with other sediments are erosional, except for contacts with conglomerates which are gradational. Some arkoses occur as channel fill cut into underlying sediments. These commonly contain a basal lag of conglomeratic material. Particle sizes indicate that flow may have been in the upper flow regime.

Conglomerates occur as locally important horizons of small extent. Conglomerates vary in resistance to weathering. Well-cemented units form small cliffs and ridges, while poorly-cemented units form rubbly slopes. They weather buff to white in color, with staining from the hematite in the matrix. They commonly underlie arkoses, occurring as channel lag deposits cross cutting other sediments. Clasts consist dominantly of quartz arenite, arkosic arenite, lithic arenite and vein quartz fragments in a graywacke-like matrix. Clasts are randomly oriented and thus paleocurrent directions could not be determined. Grains are subangular to rounded and very poorly sorted, with grains sizes ranging from clay

size to cobble size or larger; beds are ungraded and exhibit no internal structures. Matrix comprises less than 15% of the rock, and consists of muscovite, sericite and quartz grains.

Sediments in the Hembrillo Canyon succession show remarkable similarities to turbidite deposits in a submarine fan system (Walker, 1978; Reading, 1980). Many units appear to be comparable to units of the Bouma idealized sequence (Bouma, 1962). Figure 26 compares Bouma's (1962) idealized columnar section and an idealized columnar section of sediments from Hembrillo Canyon. Finer-grained graywackes may be equivalent to T_D (fine-grained, parallel-laminated muds). Quartz wackes and graywackes with sand to silt ratios of approximately 1:1 may be equivalent to T_B. Cross-bedded sands and parallel-laminated sands are similar to T_C. Arkoses, coarse sandstones, and conglomerates which lack sedimentary structures appear equivalent to upper flow regime T_A sequences. T_{AB} sequences are common, as are T_{BC}. Less common are T_{ABD} and T_{CD} sequences, which may have been removed by prograding turbidite sequences.

Petrography

Twenty-six thin sections were petrographically analyzed. Of these, 20 are sandstones and 6 are of finer-grained graywackes.

Quartzose sandstones consist of $> 90\%$ quartz with $< 3\%$ matrix. Matrix is defined here as the fraction of material < 0.1 mm in size. Remaining constituents include heavy minerals (zircon, rutile, and magnetite) and muscovite/sericite. Grains are subrounded and moderately sorted. When plotted on the QFL diagram (Dickinson and Suczek, 1979; Fig. 27), these sandstones plot

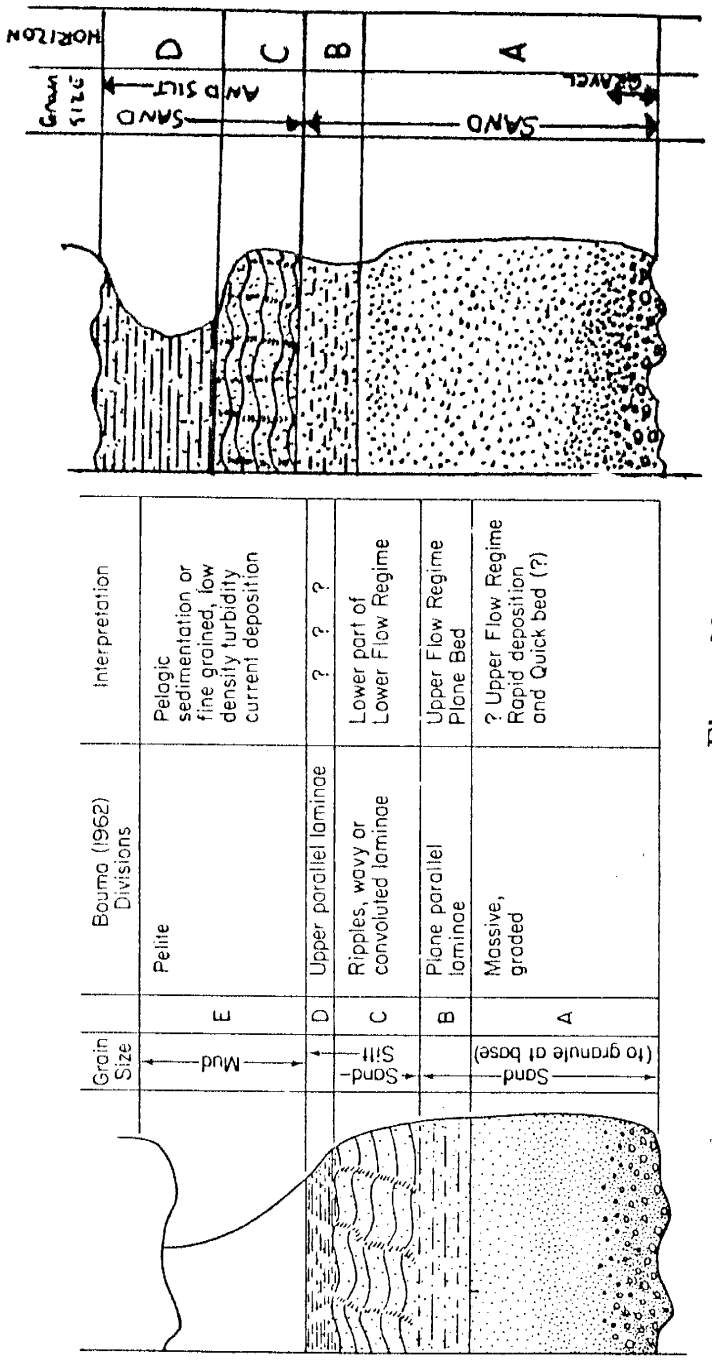

Figure 26
Idealized Bouma sequence (left) (Bouma, 1962) and
idealized turbidite sediments from Hembrillo Canyon (right).

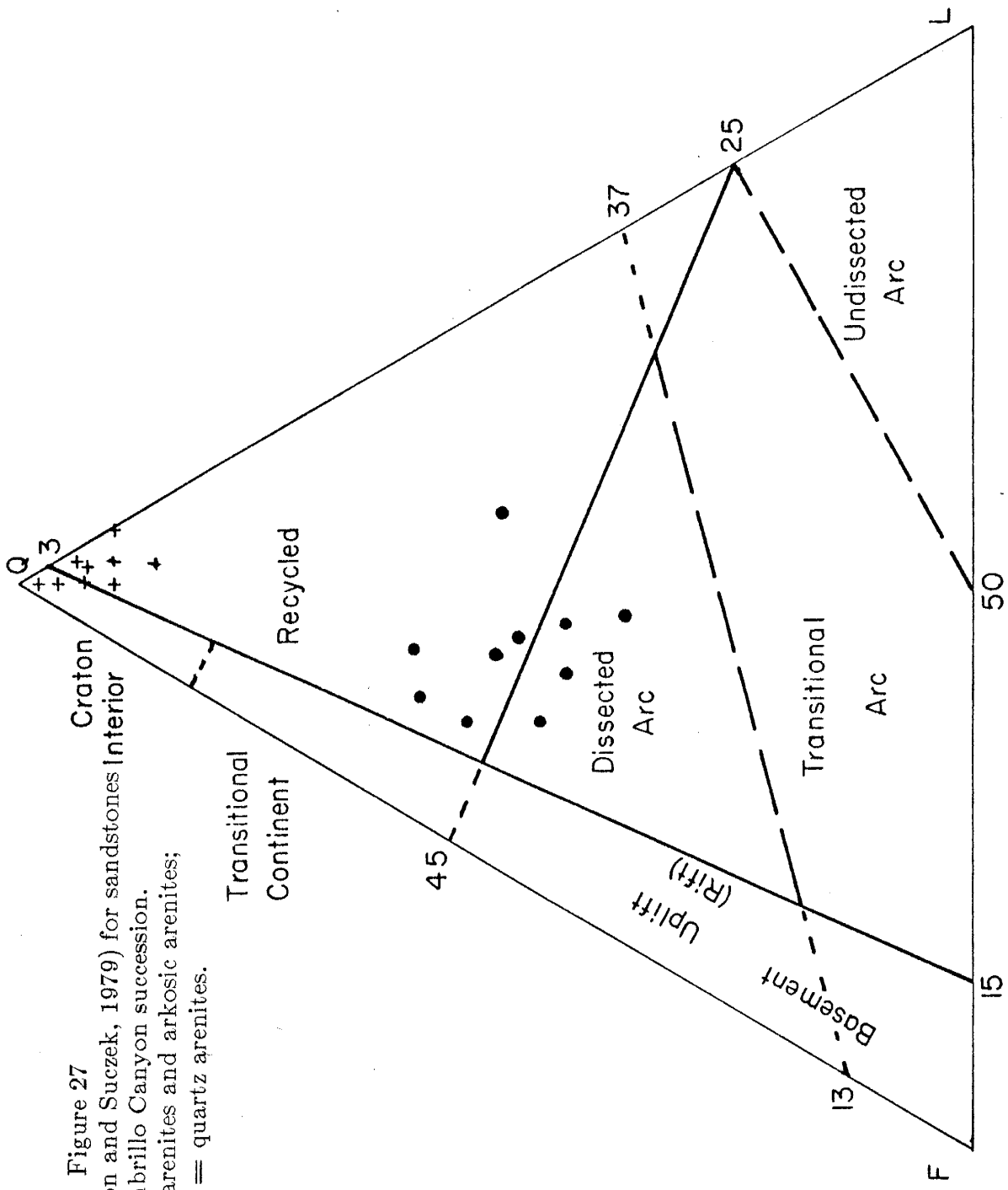

Figure 27
QFL diagram (Dickinson and Suczek, 1979) for sandstones from the Hembrillo Canyon succession.
Circles = lithic arenites and arkosic arenites;
plusses = quartz arenites.

in or near the recycled field, and generally exhibit northwest derived paleocurrent directions.

Sandstones loosely defined as arkoses contain greater amounts of feldspar and lithic fragments than quartz arenites. These units contain fine to coarse grained material consisting of 30 - 50% quartz, 25 - 30% K-feldspar, and 25 - 30% lithic fragments. Lithic fragments consist of granitic and volcanic fragments, quartzite and graywacke fragments, and other arkosic fragments. When plotted on the QFL diagram, these sands plot in the dissected arc field (Fig. 27), and commonly exhibit southeast derived paleocurrent directions.

Quartz wackes and graywackes are generally fine grained, commonly with silt to fine sand-sized grains. Sorting is poor, with angular to subrounded grains. Much of the matrix is too fine grained for petrographic analysis. Mineral constituents are quartz, K-feldspar, muscovite, sericite, and heavy minerals. Metamorphic deformation has imposed small-scale folds on these fine-grained sediments, which are emphasized by muscovite and sericite. Detailed analysis is difficult due to the fine-grained nature of the rock. Chemical analysis provides better insight to the origins of these rocks.

Geochemistry

Analyses for major, trace, and REE were made for 11 sandstones (quartz arenites and arkoses) and 7 quartz wackes and graywackes. The chemical compositions of sedimentary rocks contribute significantly to the interpretation of tectonic setting and evolution of the volcanic rocks from which the sediments are derived. Framework grain studies similar to those of Dickinson and Suczek (1979)

have shown the relationship between sandstone compositions and tectonic settings. However, framework grains in sandstones can be modified during burial metamorphism and thus cannot be used to infer tectonic settings (Bhatia and Crook, 1986).

Major element contents can provide important information as to provenance and tectonic regimes. Elements such as MnO, K_2O, P_2O_5, and Na_2O, however, are highly mobile and may not give accurate indications of provenance due to enrichment or depletion during metamorphism, ancient and modern weathering, diagenesis, and elemental adsorption during deposition. Hembrillo sediments, when plotted on Harker variation diagrams (Bhatia, 1983), are extremely scattered and give no indication of tectonic setting. Silicification of many sandstones has diluted the remaining elements, causing scatter to occur on such diagrams.

Another problem in determining provenance from the chemical composition of sandstones is the effect of heavy mineral constituents (Hubert, 1962). Heavy minerals, such as zircon, rutile, monazite, apatite, and allanite are highly resistive to weathering and may contribute significantly to the trace element and REE distribution of any given sediment, particularly in mature sandstones (Gromet and others, 1984; Hubert, 1962).

Copeland (1986) analyzed zircon separates from two sandstones to determine their zirconium contents. He assumed that all zirconium in the rock was contained in the zircon, and was thus able to calculate the contribution of zircon to individual element concentrations in the whole rock. Copeland concluded that 97% of the Hf and an enrichment in heavy REE (HREE) relative to light REE (LREE) was due to the zircon. Thus, the chemistry of any sediment may be

strongly affected by minor mineral phases.

Various discrimination diagrams for clastic sediments in terms of tectonic setting and provenance have been proposed by several authors (Taylor and McClennan, 1985; Bhatia and Crook, 1986; Cullers and others, 1974; Gromet and others, 1984). The use of REE discrimination diagrams for graywackes allows easy comparison between graywackes from various tectonic settings. The REE in Hembrillo quartz wackes and graywackes (Fig. 28) are enriched in LREE versus HREE and show varying negative Eu anomalies, indicating fractionation of plagioclase in the source rocks. When the average for Hembrillo graywackes is compared to the Post-Archean Australian Shale (PAAS) composite, the North American Shale Composite (NASC), and the European Shale Composite (ES) (Fig. 29), Hembrillo graywackes show similar patterns and magnitudes, although they are slightly enriched in HREE, possibly due to greater amounts of zircon in the sample. They are also slightly depleted in LREE relative to PAAS, NASC and ES, with larger negative Eu anomalies and lower LREE/HREE ratios.

Comparison of REE patterns between Hembrillo graywackes and graywackes of known tectonic settings (Fig. 30) may indicate a possible setting for the Hembrillo sediments. The Hembrillo pattern is similar to the pattern observed for continental island arc (CIA) - back-arc basins, and exhibits some similarities to active continental margins (ACM) and passive margins (PM).

Ti/Zr versus La/Sc diagram and the La/Y versus Sc/Cr diagrams (Bhatia and Crook, 1986; Figs. 31A and 31B), show excellent discrimination between OIA, CIA, ACM, and PM. Most Hembrillo graywackes fall in the CIA and ACM fields on the Ti/Zr - La/Sc diagrams, and in the CIA field on the La/Y - Sc/Cr di

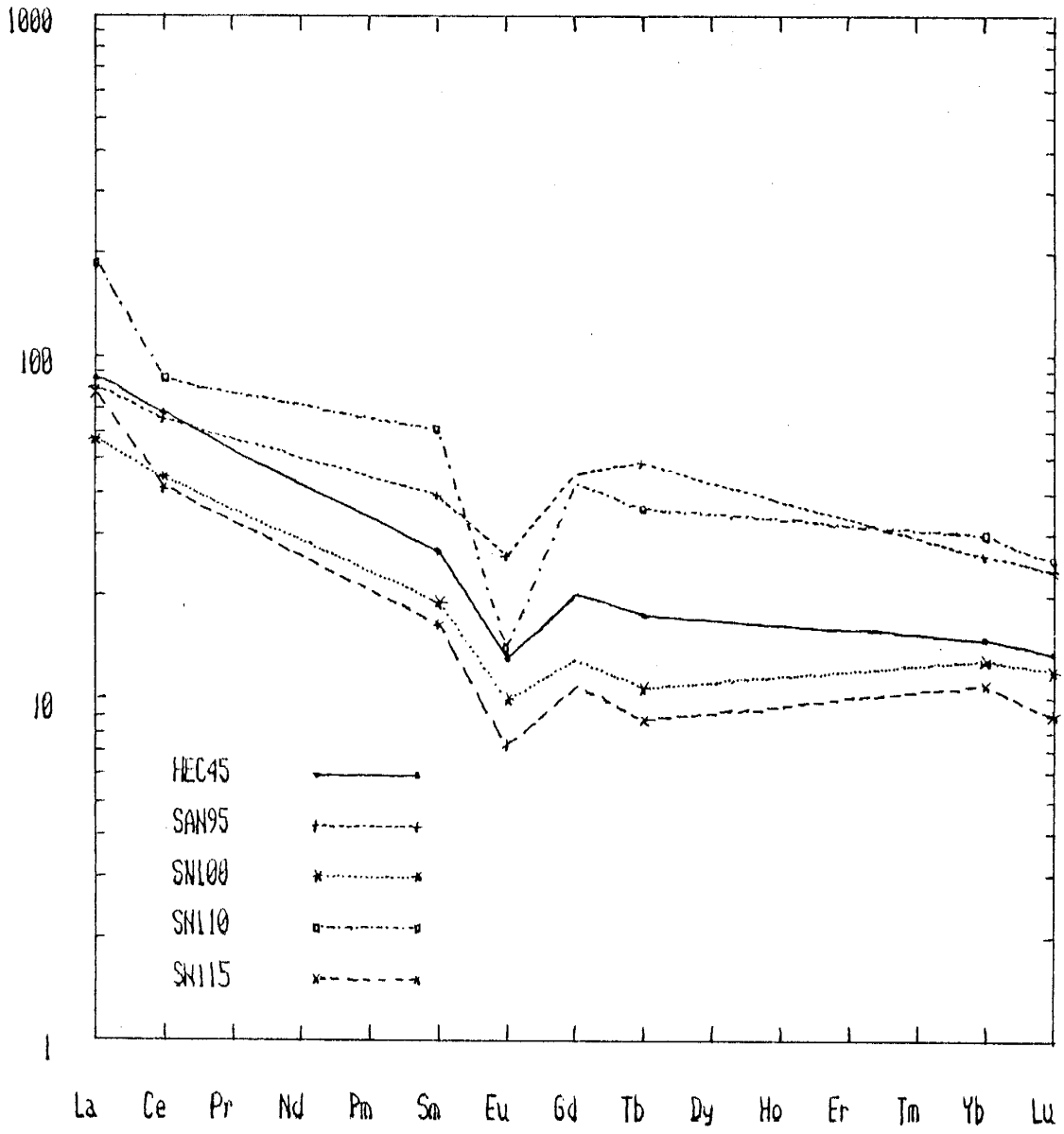

Figure 28
REE distribution for Hembrillo graywackes

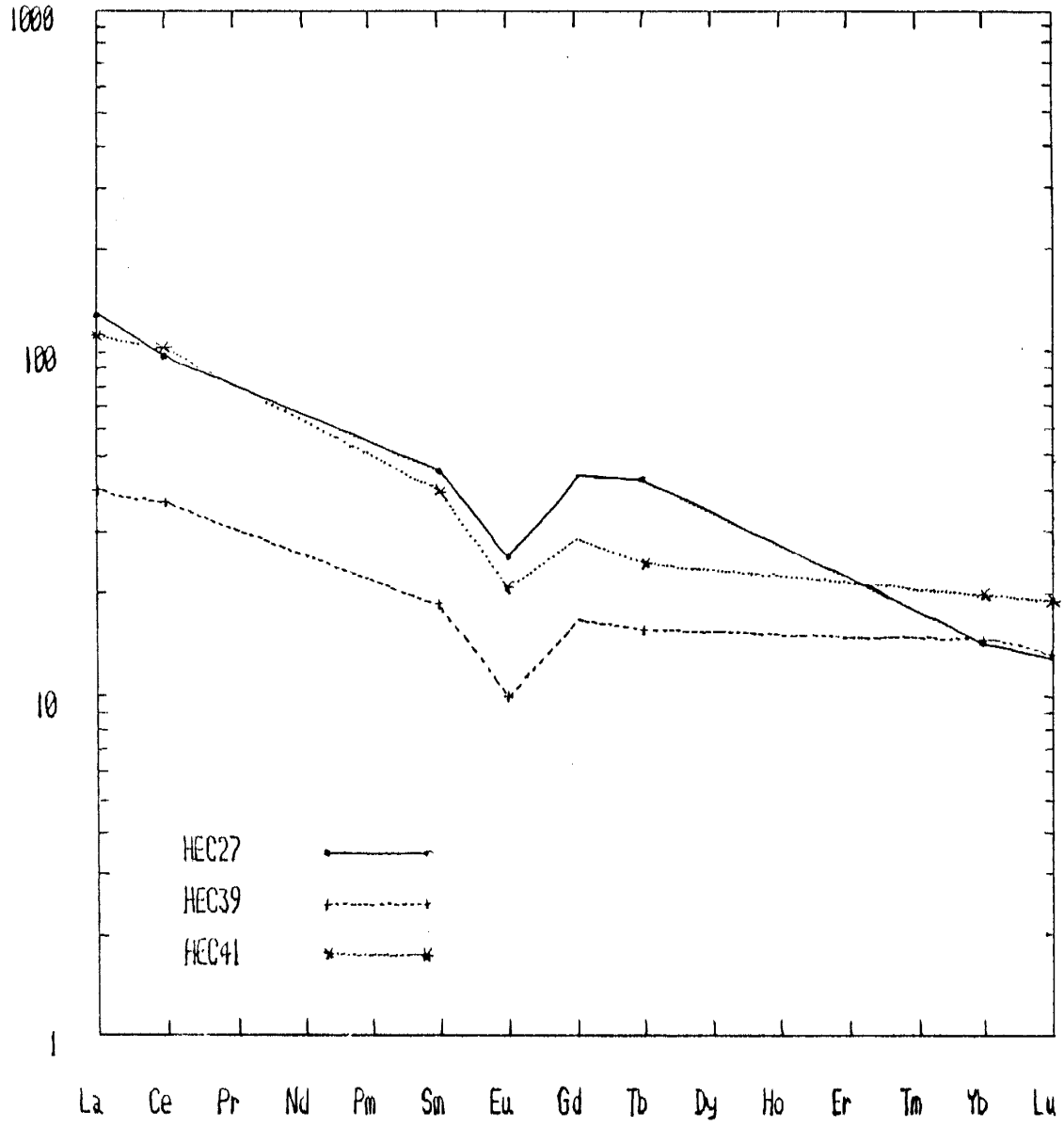

Figure 28 (continued)
REE distribution for Hembrillo graywackes

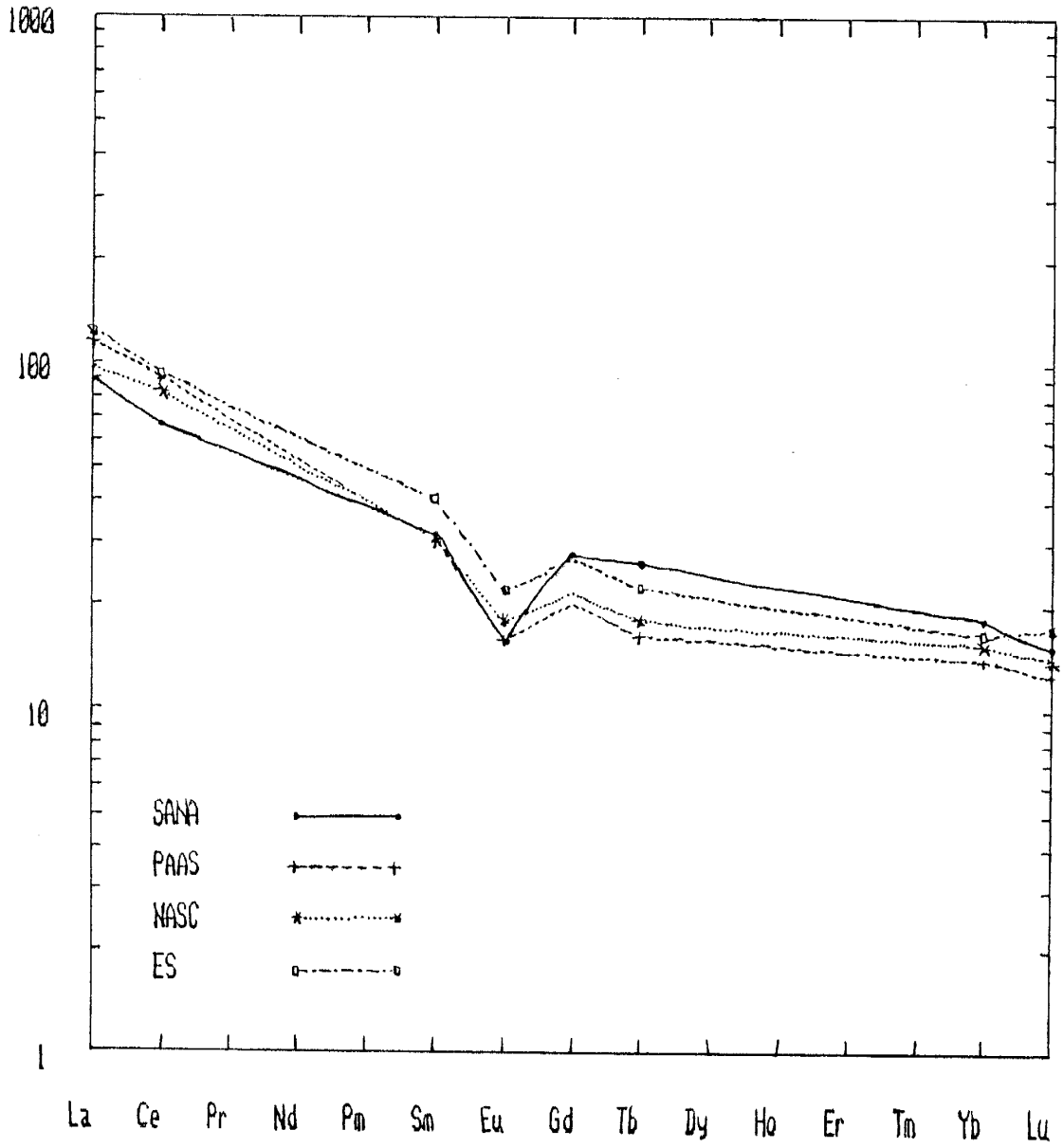

Figure 29
REE distribution for Hembrillo graywackes, PAAS, NASC, and ES. See text for discussion.

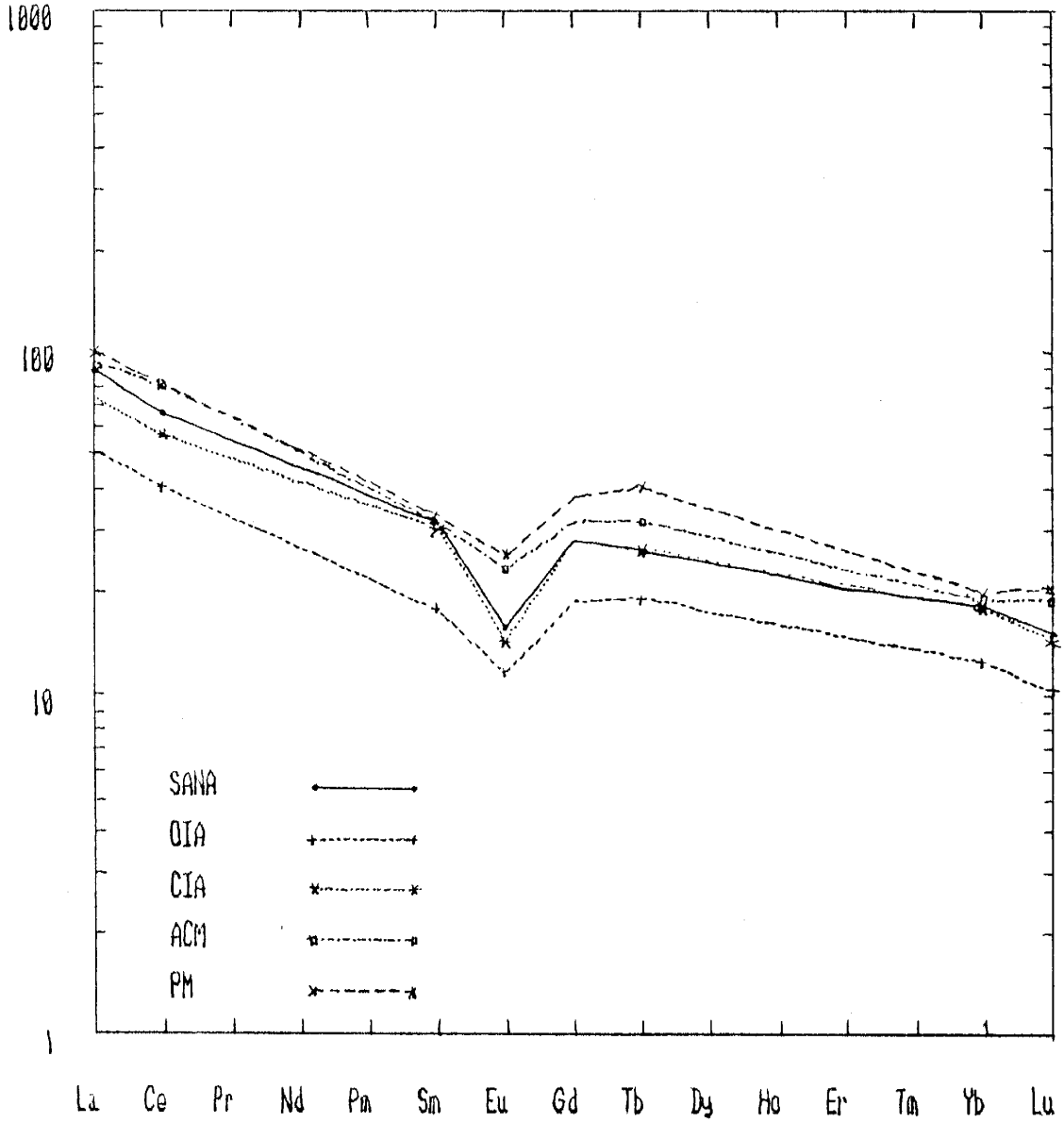

Figure 30
REE distribution for Hembrillo graywackes (SANA), and graywackes from various tectonic settings. OIA=oceanic island arc; CIA=continental island arc; ACM=active continental margins; PM=passive margin (Bhatia and Crook, 1986).

agram. ACM can be distinguished from CIA by higher La/Sc ratios.

The Th-Sc-Zr and Th-Co-Zr ternary diagrams (Bhatia and Crook, 1986; Figs. 32 and 33) also allow discrimination between graywackes of various tectonic provinces. Hembrillo graywackes fall in or near the CIA fields in both diagrams. These diagrams distinguish well between CIA and OIA, but not between PM and ACM (Bhatia and Crook, 1986).

Provenance of various sediments can be determined by the relative amounts of Th, Hf, and Co (Fig. 34) and La, Th, and Sc (Fig. 35). These diagrams, proposed by Taylor and McClennan (1985), allow comparison of graywackes to the composition of the present-day continental crust and thus their provenance. Taylor and McClennan's (1986) shale and subgraywacke field is equivalent to quartz wackes from this study, and the graywacke field is equivalent to graywackes as defined in this study. The Hembrillo graywacke data show two sources. One source is near the total crustal average (TC) in the graywacke field, where many mixed sediments occur (Taylor and McClennan, 1985). The second is apparently felsic in origin, probably similar to that of the sandstones. It is interesting to note that data in the graywacke field have paleocurrent directions from the southeast, while data in the subgraywacke field have paleocurrent directions from the northwest (see discussion in paleocurrent section).

Summary

The sedimentary package of the Hembrillo Canyon succession represents a diverse lithology, but one consistent with the concept of a narrow, juvenile, continental margin back-arc basin developed from the volcanic data. This concept is

supported by REE distributions and trace element discrimination diagrams. Sandstone sources are dominantly of felsic volcanic origin, probably derived from a cratonic source to the north of the basin as indicated by chemistry, petrography, and paleocurrent analysis.

Interbedded with these sands are quartz wackes which exhibit average crustal REE distributions and felsic volcanic sources. Paleocurrent data indicate that the source for these sediments also lies to the north. REE distributions indicate that these quartz wackes are similar to CIA graywackes, consistent with other data.

Graywackes contain paleocurrent directions from the south, but have virtually identical REE distributions as quartz wackes with opposite source directions. What distinguishes the graywackes from quartz wackes from the north are their trace element characteristics. Hembrillo graywackes show similarities to graywackes of mixed lithologies, such as sediments derived from the arc side of the back-arc basin, rather than the continental side.

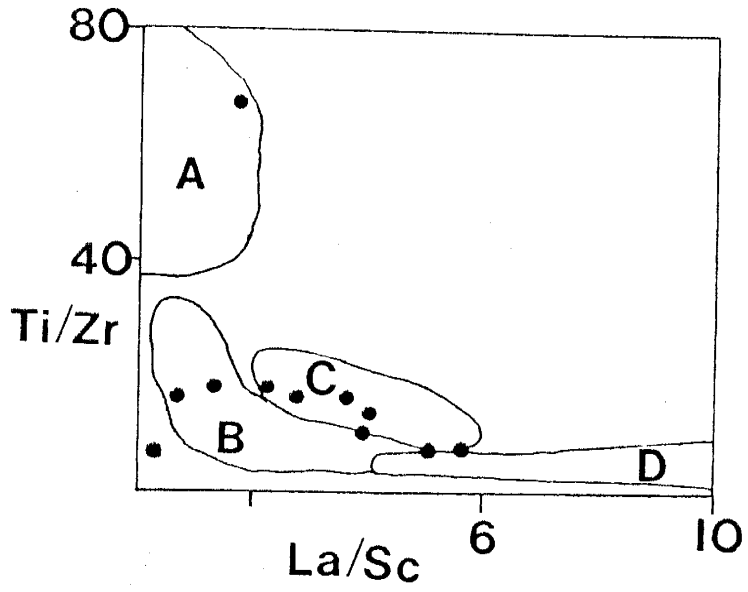

Figure 31A
Ti/Zr - La/Sc diagram for Hembrillo graywackes.
Fields as in Figure 31 (Bhatia and Crook, 1986).
A = oceanic island arc; B = continental island arc;
C = active continental margin; D = passive margin.

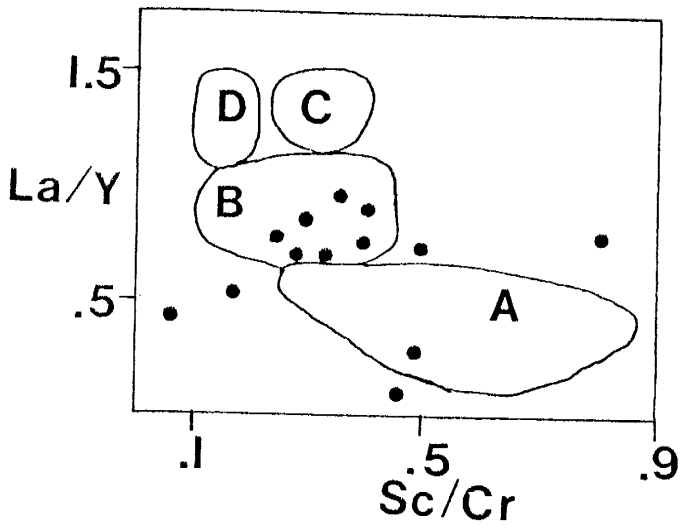

Figure 31B
La/Y - Sc/Cr diagram for Hembrillo graywackes.
Fields as above (Bhatia and Crook, 1986).

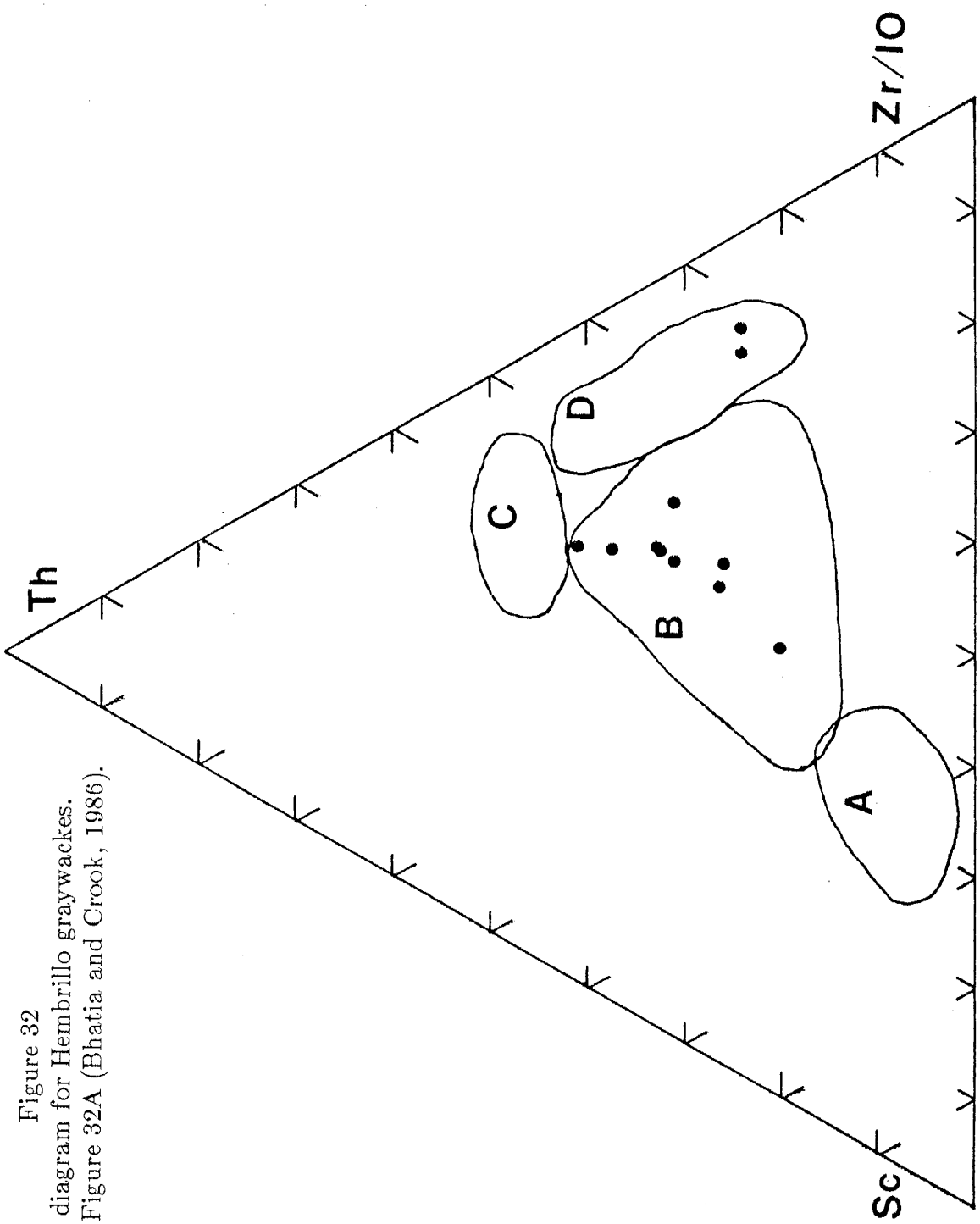

Figure 32
Th-Sc-Zr diagram for Hembrillo graywackes.
Fields as in Figure 32A (Bhatia and Crook, 1986).

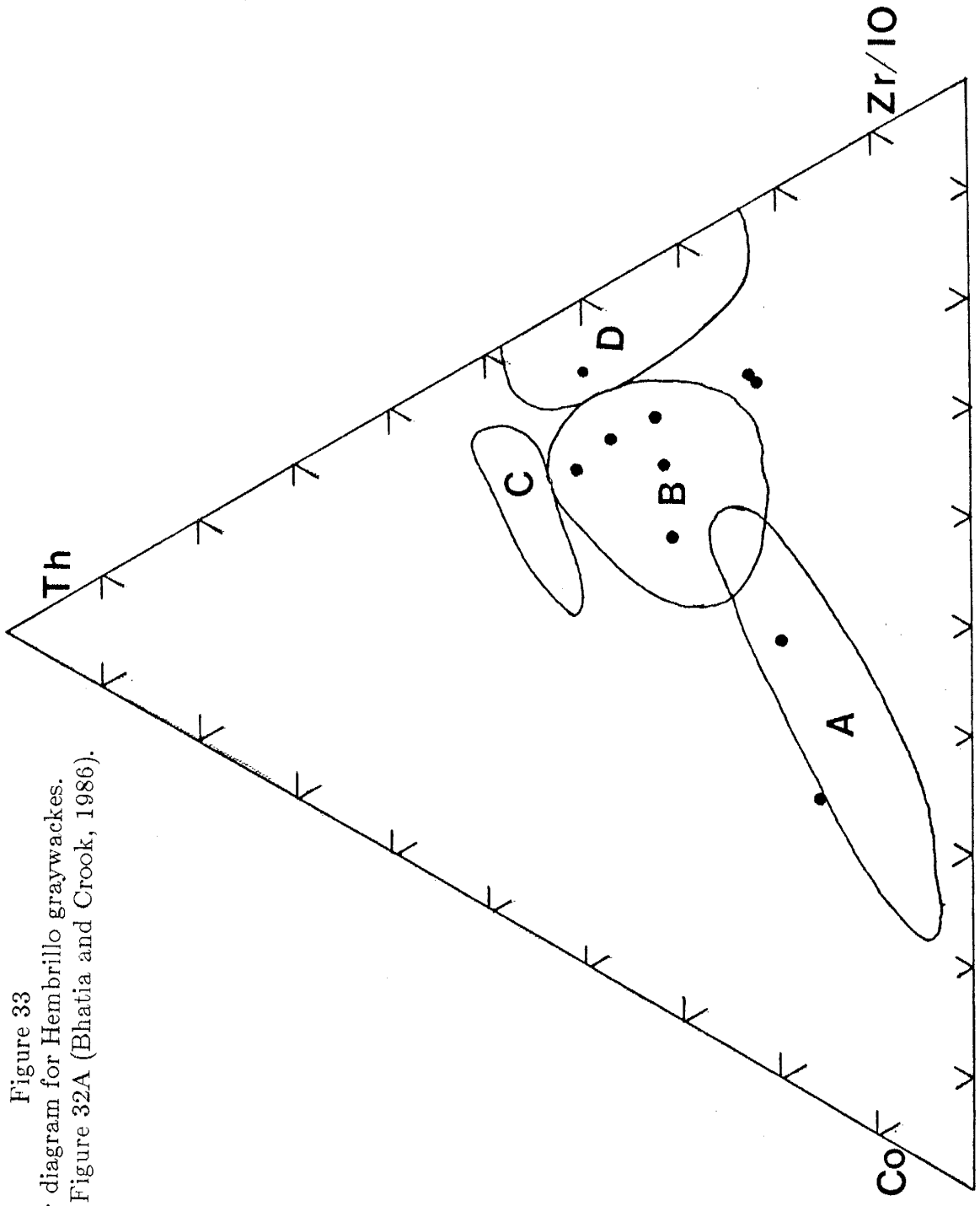

Figure 33
Th-Co-Zr diagram for Hembrillo graywackes.
Fields as in Figure 32A (Bhatia and Crook, 1986).

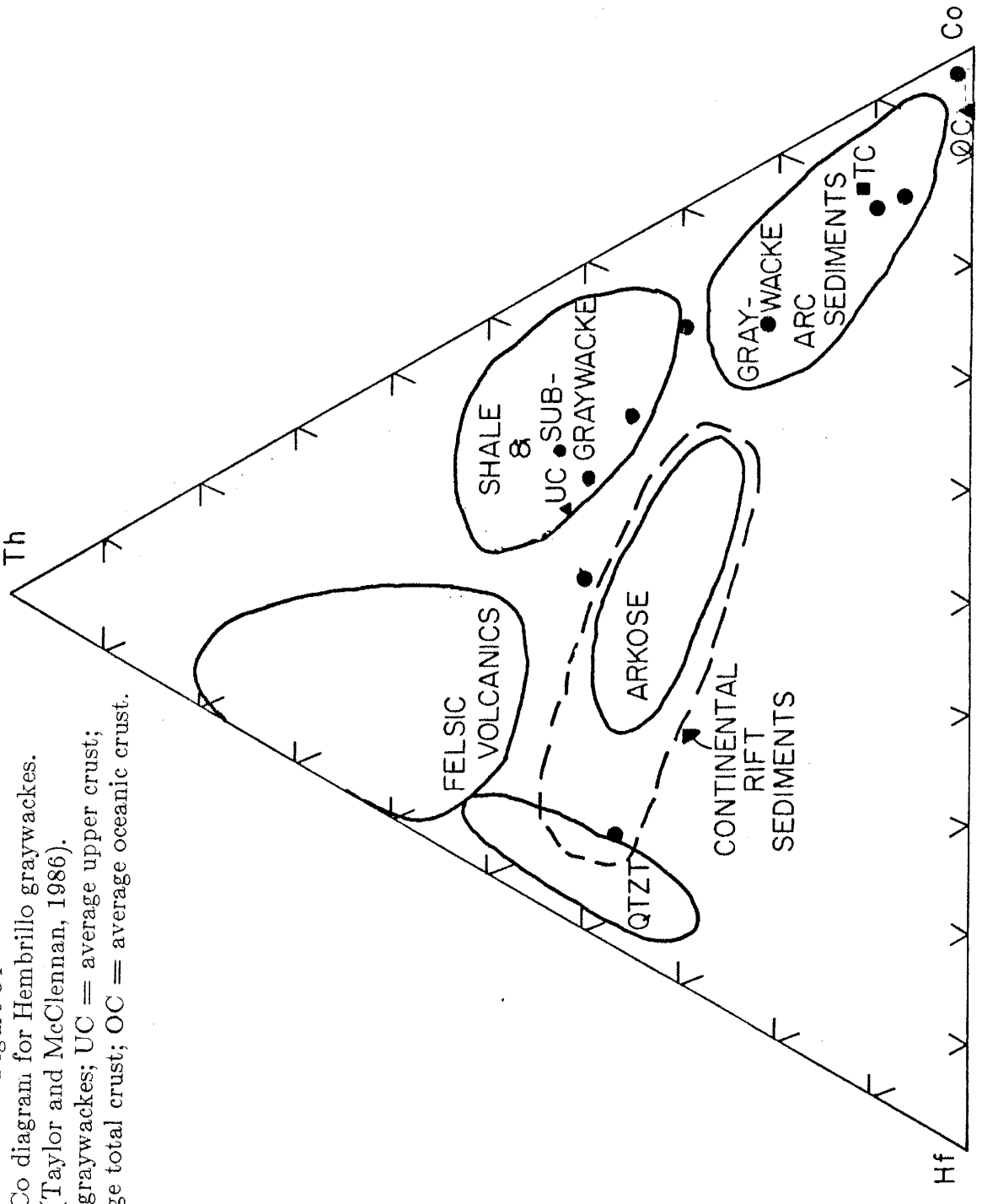

Figure 34
Th-Hf-Co diagram for Hembrillo graywackes.
(Taylor and McClennan, 1986).
Circle = graywackes; UC = average upper crust;
TC = average total crust; OC = average oceanic crust.

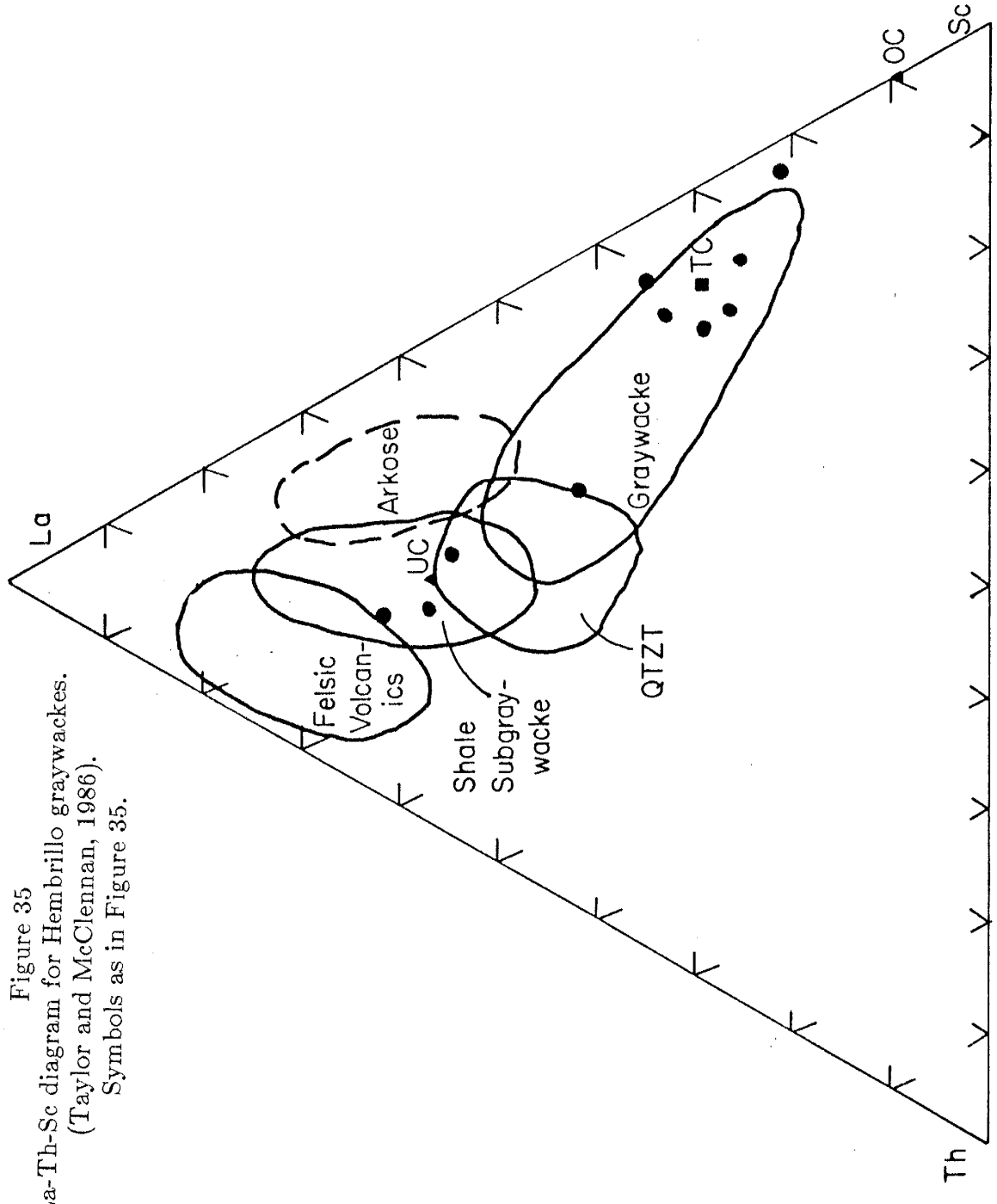

Figure 35
La-Th-Sc diagram for Hembrillo graywackes.
(Taylor and McClennan, 1986).
Symbols as in Figure 35.

PALEOCURRENT ANALYSIS

Paleocurrent analysis has provided over 200 paleocurrent directions. Data were taken from imbricated clasts in graywackes and sandstones, and from three-dimensional views of cross beds in sandstones. Figure 36 illustrates the method used for the structural reconstruction of paleocurrent data in the Hembrillo Canyon area. Structural reconstruction is performed by plotting the poles of the tilted bedding plane (P_1') and the tilted paleocurrent direction (P_2') on the stereographic Wulff net. Rotational axis R is parallel to the strike of the bedding plane, and is added as an aid to visualization. Line R-R is rotated to the N-S diameter of the net, where the pole P_1' is moved by its dip angle along the E-W diameter to the center of the net, point P_1. The bedding plane is now horizontal. The pole to the paleocurrent lineation P_2' moves by the same dip angle in the same direction, but along its small circle, to point P_2. From this new pole position, the great circle representing the restored cross bedding can now be drawn in (dashed arc) and its attitude read.

Each data point was rotated to the horizontal using the method previously described. It is presented in table F-1, Appendix F. A subset of the data from table F-1, where the younging direction of the associated beds is known, is plotted on the rose diagram in Figure 37. This well controlled subset of data indicates that there are two source directions. The data for this subset is listed in table F-2. It was reoriented in the same way as the example above, and is illustrated in Figure 38 for NW trending paleocurrents, and in Figure 39 for SE trending paleocurrents.

Paleocurrent data from the area was reoriented as previously described.

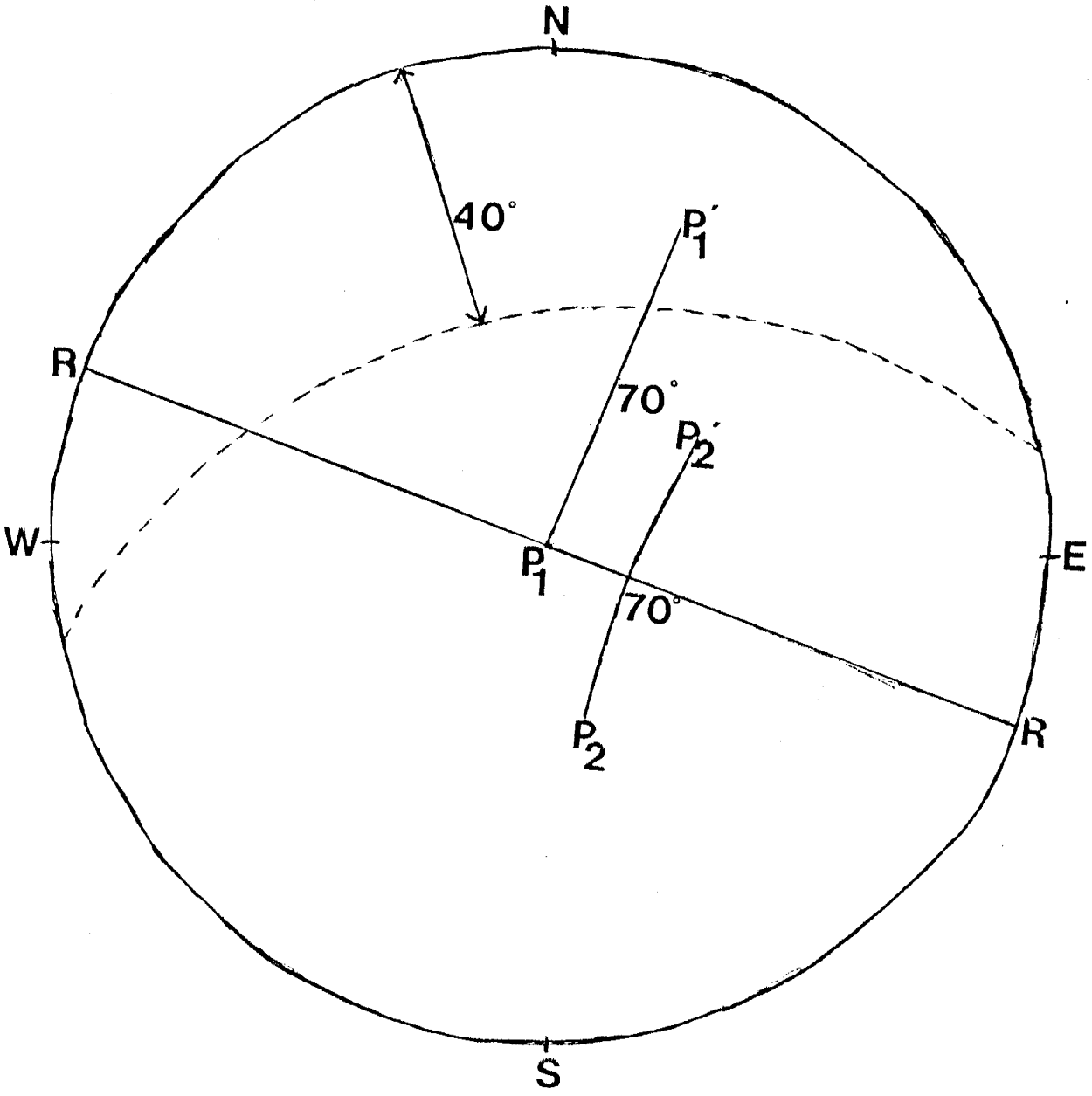

Figure 36
Illustration of structural reconstruction for
Hembrillo Canyon metasediments. P_1'=Tilted bedding;
P_1=Reoriented (Horizontal) Bedding; P_2'=tilted
Paleocurrent Trend; P_2=Reoriented Paleocurrent Trend.
R-R=Axis of Rotation. Dashed Line=Example of Reoriented Bedding.

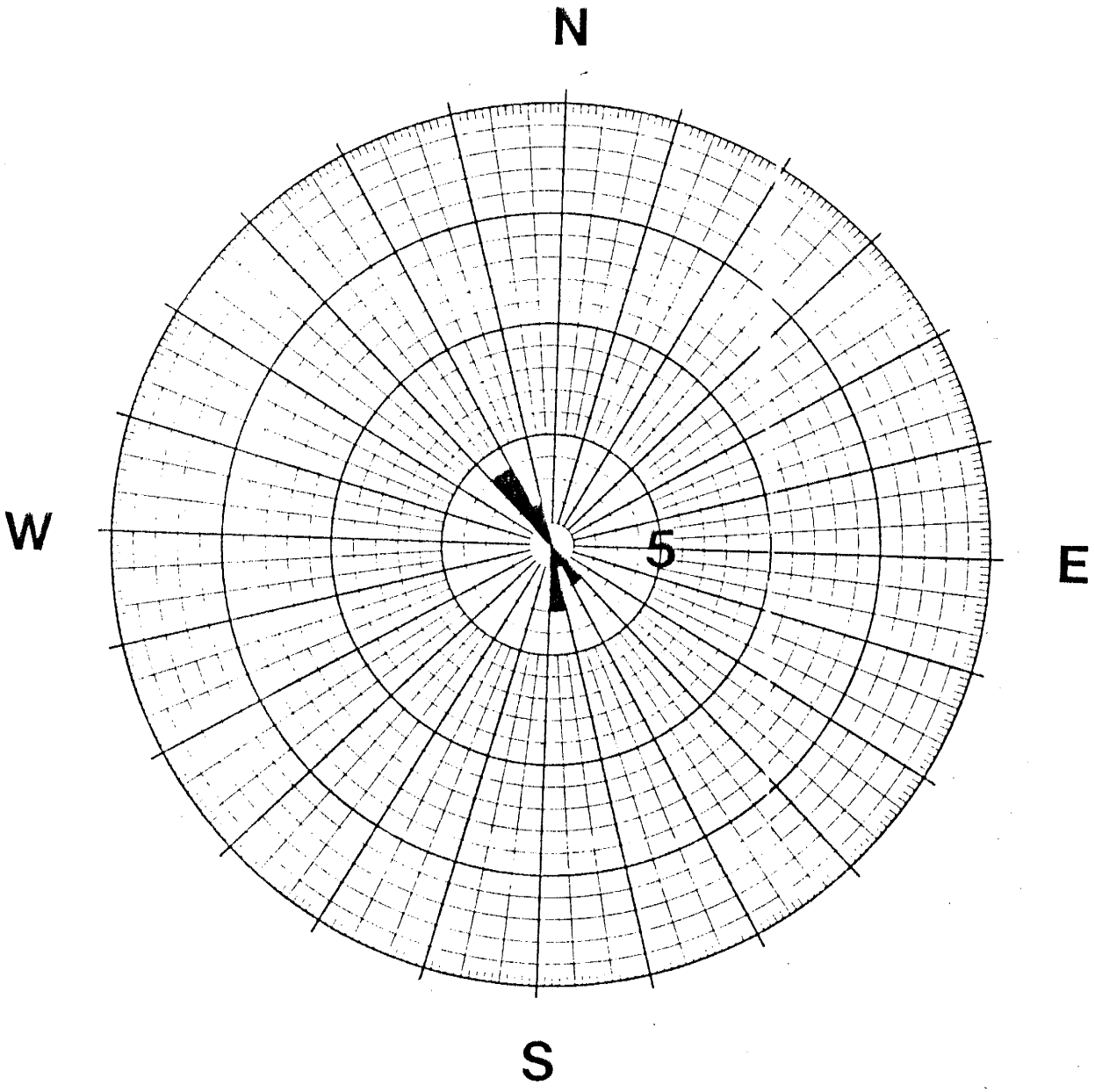

Figure 37
Rose diagram for data from Table F-1, Appendix F;
Younging Direction Established. N=12.

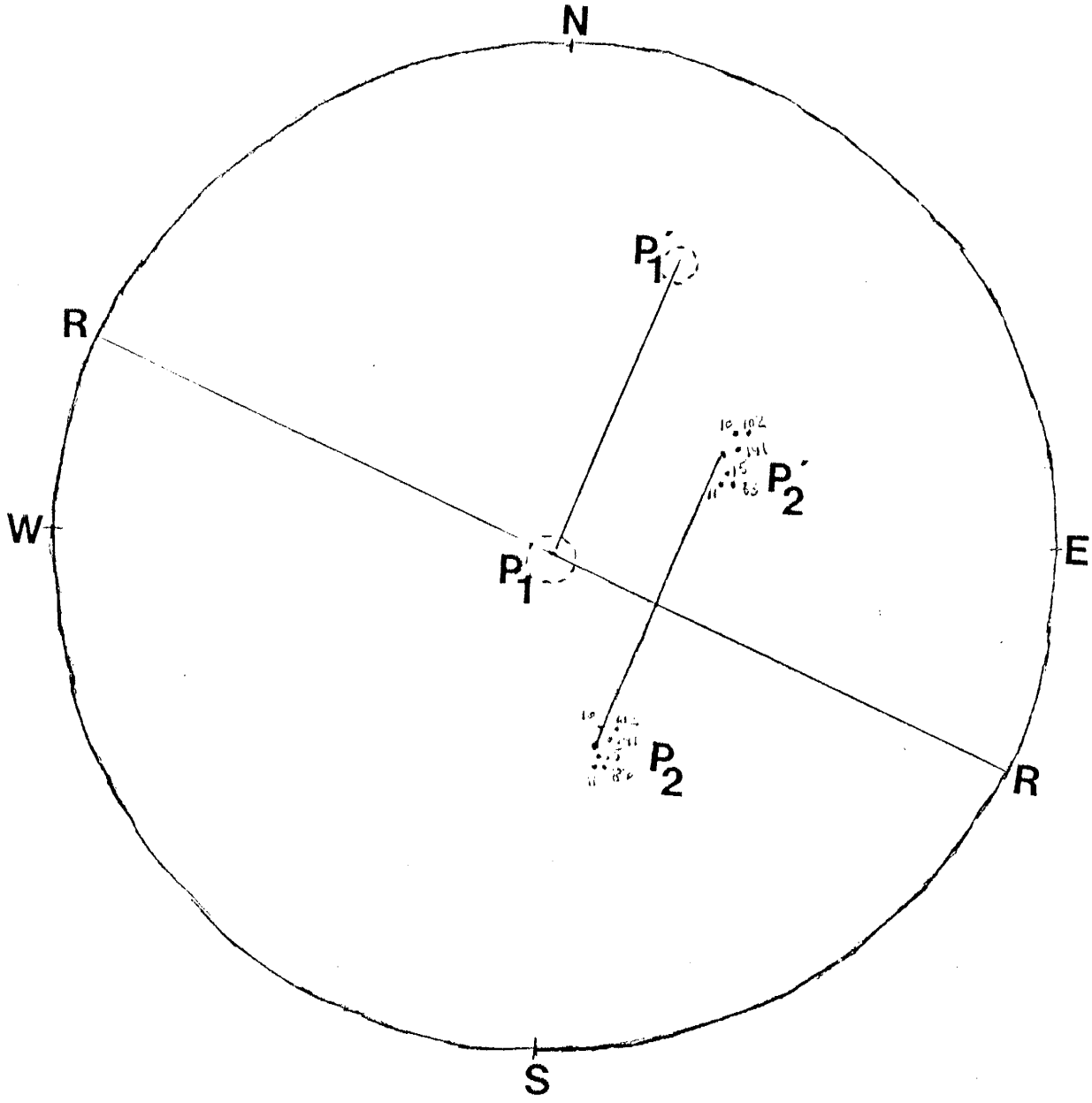

Figure 38
Structural reconstruction for data presented
in Figure 37 for NW trending currents.

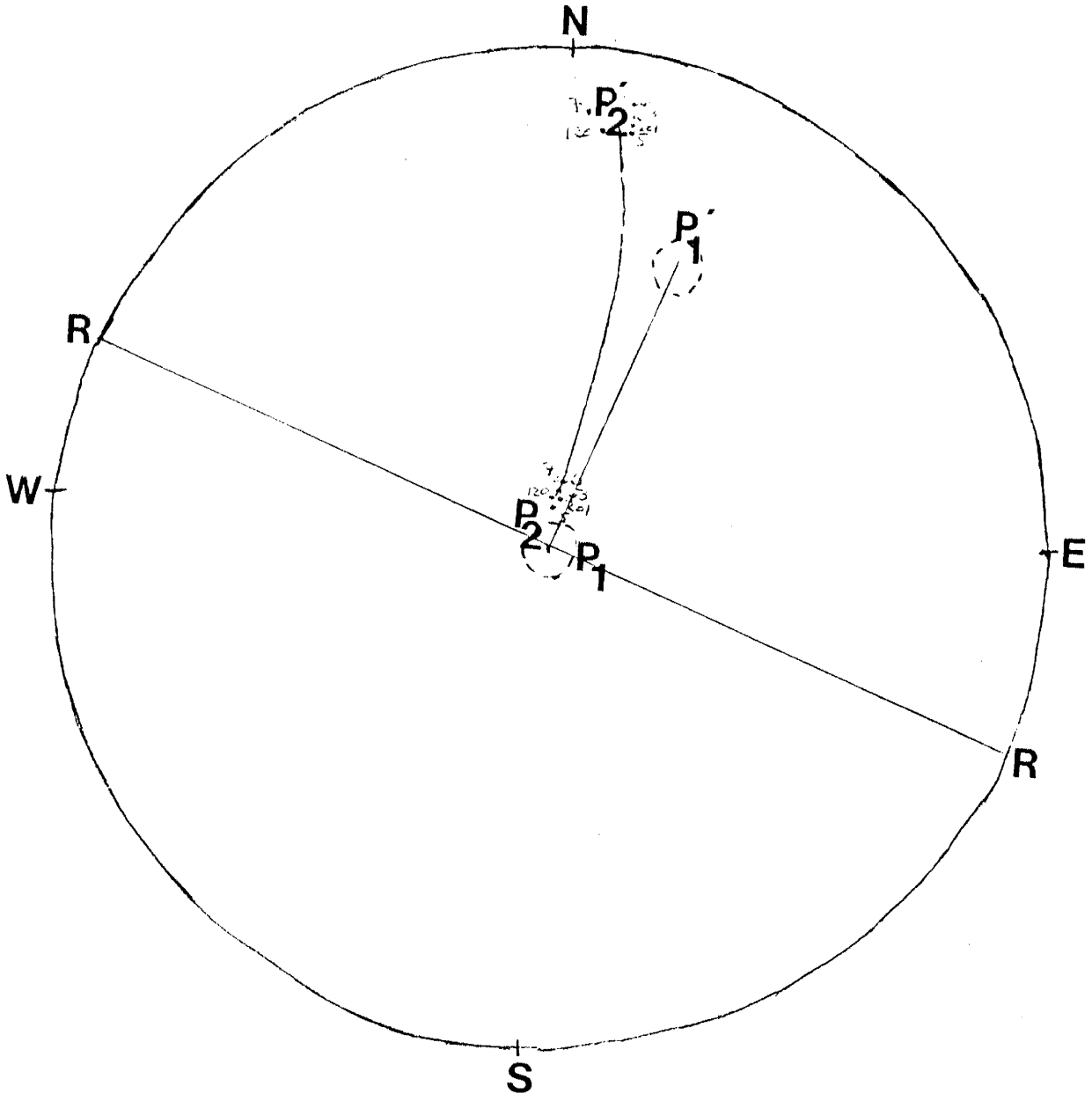

Figure 39
Structural reconstruction for data presented
in Figure 37 for SE trending currents.

This structural reorientation is illustrated in Figure 40 for NW trending paleocurrents, and in Figure 41 for SE trending paleocurrents. The resulting data is presented in Table F-1, Appendix F. A rose diagram for this data is presented in Figure 42. Although this data set has less control than the data for Figure 37, comparison with Figure 37 indicates that the data set is valid, and does represent the paleocurrent directions in the field area. The result from Figure 42 is two main flow directions: one to the northwest (approximately N 40 W) and one to the southeast (approximately S 30 E). The geologic map of the field area illustrates these opposing current directions (Plate 1). Comparison of paleocurrent data with the units they were derived from indicate that approximately 70% of all sandstones (mostly quartz arenites, quartz wackes and arkosic arenites) were derived from the northwest, while 30% of the sandstones (arkosic arenites, and lithic arenites) and 90% of the graywackes were derived from the southeast.

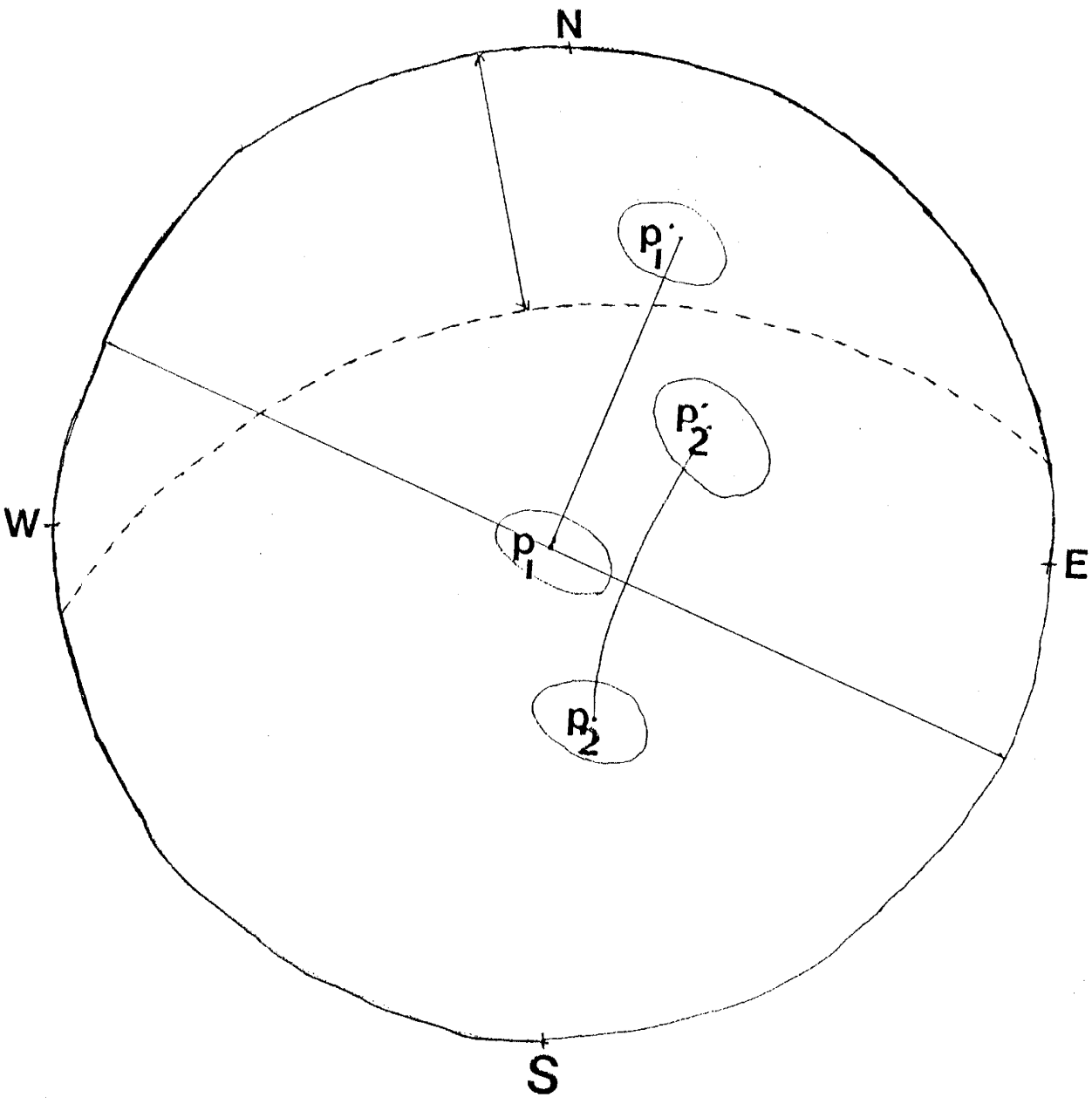

Figure 40
Structural reconstruction for all NW trending
paleocurrent data from Table F-1, Appendix F.

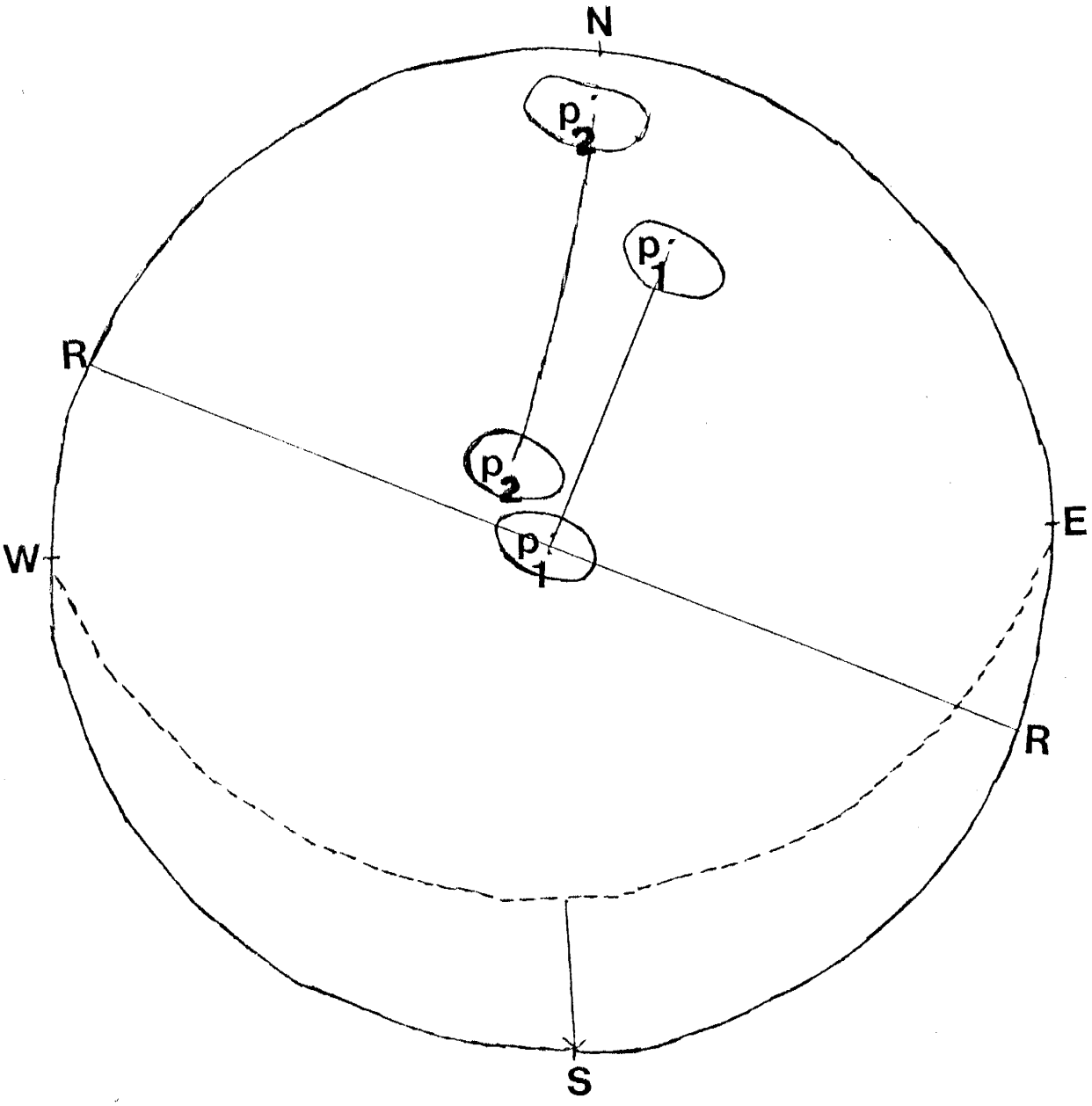

Figure 41
Structural reconstruction for all SE trending paleocurrent data from Table F-1, Appendix F.

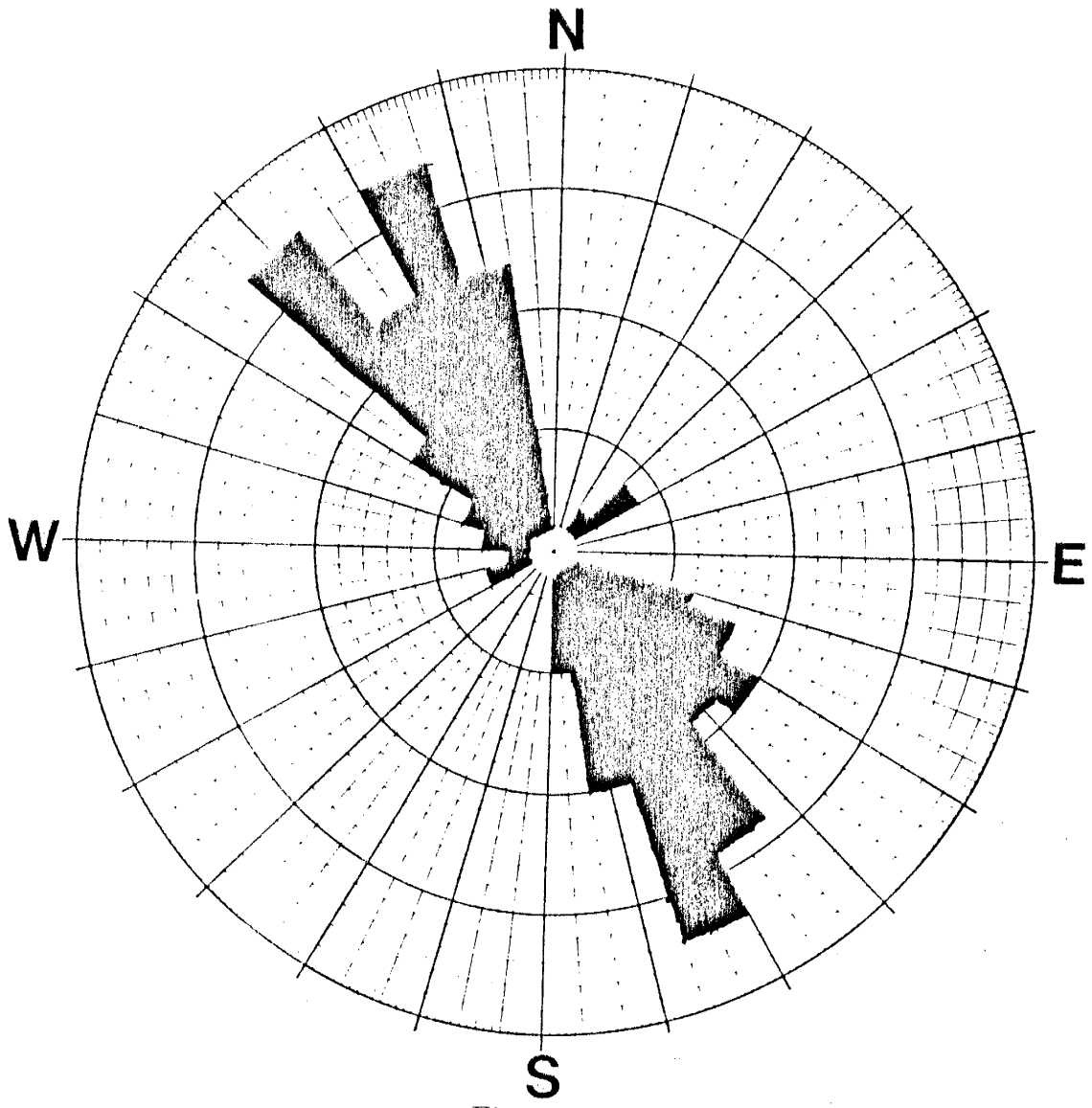

Figure 42
Rose diagram illustrating dual paleocurrent directions for all data, Table F-1, Appendix F.

METAMORPHISM

The Hembrillo Canyon succession is mildly deformed and metamorphosed to moderate grades (Condie, 1986). This is also characteristic of other Proterozoic terranes in the southwest U.S., such as the Dos Cabezas Mountains and other areas in southeastern Arizona (Bowling, 1987; Copeland, 1986; Copeland and Condie, 1986), and the Pedernal Hills, New Mexico (McKee, 1987). Rocks in each of these areas exhibit greenschist to lower amphibolite facies metamorphic grade. The Hembrillo Canyon succession has been metamorphosed to the upper greenschist facies. Two granitic intrusives, the Strawberry Peak and Mayberry Plutons (Plate 1), have locally metamorphosed the country rock to the amphibolite grade. Greenschist metamorphism is of the Barrovian type.

Difficulties were encountered in determining stable mineral associations during petrographic analysis of the study area samples. Retrograde reactions such as chloritization of biotite in basalts, sericitization of feldspars and other aluminum silicates in rhyolites and arkosites, and saussuritization of plagioclase in metagabbros obscure original mineral assemblages.

Characteristic mineral assemblages in these rocks are:

Greenschist Facies

Sedimentary and Felsic Rocks
- quartz-muscovite-chlorite
- quartz-muscovite-chloritoid
- quartz-muscovite-biotite-plagioclase
- quartz-biotite-K-feldspar-plagioclase
- quartz-muscovite-biotite-garnet

Mafic Rocks
- actinolitic hornblende-chlorite-epidote-plagioclase
- actinolitic hornblende-epidote

Amphibolite Facies

Sedimentary and Felsic Rocks
quartz-biotite-garnet-(plagioclase)

Mafic Rocks
green hornblende-chlorite-epidote-plagioclase

A summary of major metamorphic assemblages in rock types found in the San Andres Mountains as a function of increasing metamorphic grade is given in Table 1.

Twenty mafic rocks, six felsic rocks, twelve quartzose metasediments and nine schists and phyllites were chemically analyzed (Appendix B). Using these analyses, meta-volcanic rocks are plotted on an ACF diagram and sediments are plotted on an AKF diagram (Figs. 37A and B). Because total iron is analyzed as Fe_2O_3-T, adjustments were made for calculation of these diagrams by allotting three percent of the Fe_2O_3-T to magnetite in mafic rocks and one percent in silicate rocks (Winkler, 1979). The remainder was calculated as FeO and added to the MgO for calculation of the F value. In the AKF diagram, data points scatter, but all points fall within the subtriangle microcline-muscovite-biotite, which is the most common mineral assemblage found in the rocks. The ACF diagram illustrates the common assemblage epidote/zoisite-actinolite for mafic rocks in the greenschist facies. For mafic rocks from amphibolite facies terranes, the assemblage hornblende-plagioclase is most prevalent.

The chloritoid-staurolite-kyanite-sillimanite assemblage without andalusite indicates that the Hembrillo Canyon succession has undergone Barrovian facies series metamorphism (Myashiro, 1975). A stability diagram proposed by Condie and Budding (1979) for these and other Precambrian supracrustal rocks in New

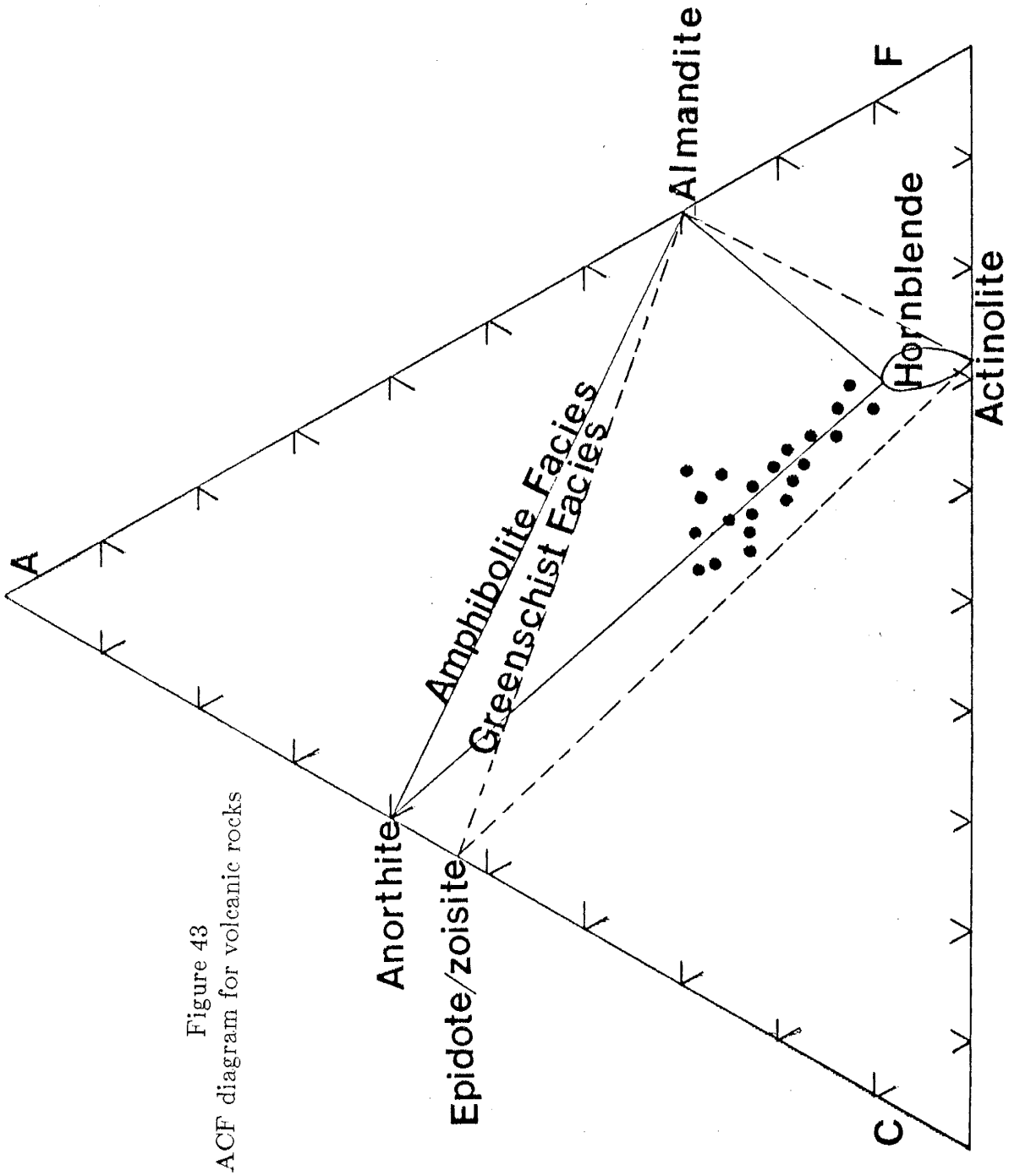

Figure 43
ACF diagram for volcanic rocks

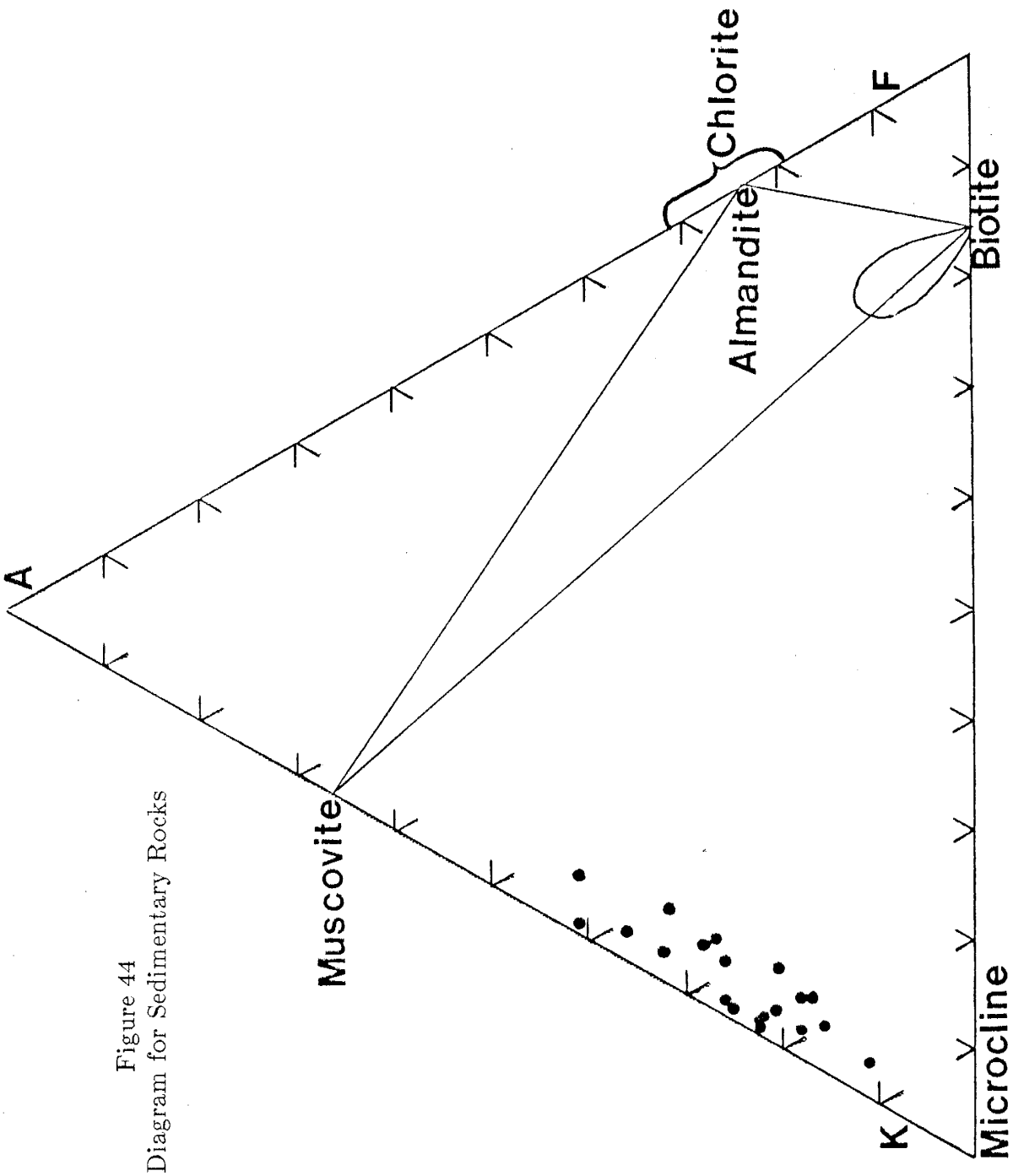

Figure 44
AKF Diagram for Sedimentary Rocks

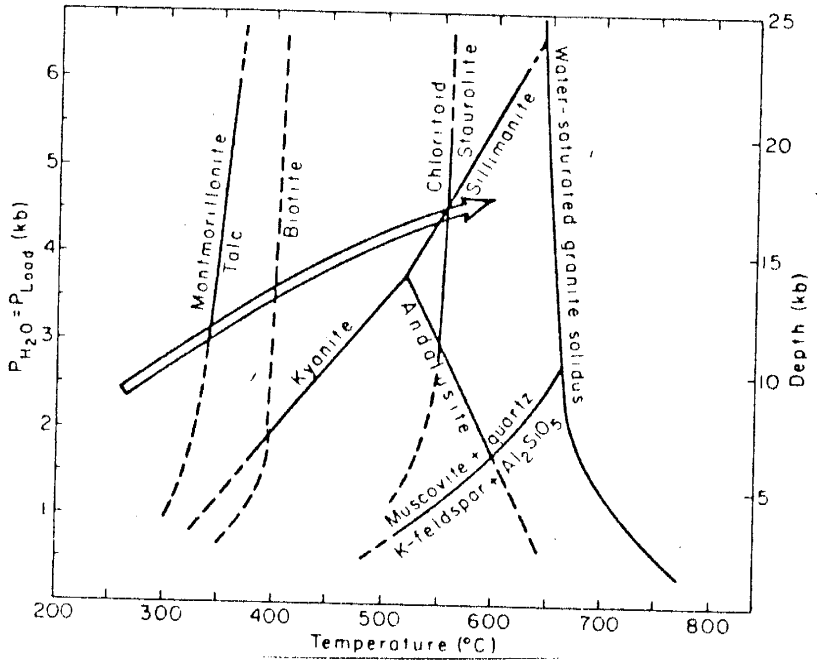

Figure 45
Stability diagram for Precambrian supracrustal in southern New Mexico rocks proposed by Condie and Budding (1979).

Mexico is illustrated in Figure 38. The probable path of metamorphism moves through the kyanite-sillimanite stability fields and crosses several other stability curves.

Of particular interest is an occurrence of a talc unit in Hembrillo Canyon. Thin section analysis reveals the unit is composed of greater than 95 percent talc with minor amounts of quartz and K-feldspar. Chemically, this unit is dominantly composed of silica and magnesium oxides (see Appendix B for chemical analyses). This is consistent with the petrographic data for this rock. Condie and Budding (1979) considered the possibility of this unit being derived from a siliceous dolomite by the reaction:

$$3 \text{ dolomite} + 4 \text{ quartz} + H_2O = \text{talc} + 3 \text{ calcite} + 3CO_2.$$

However, calcite is not observed in this unit, thus arguing against this possibility.

A second, more likely possibility suggested by Condie and Budding (1979), is that the talc is a metamorphic product of devitrification and hydration of a volcanic ash or tuff. Bentonites form as a result of alteration of a volcanic ash or tuff (Grim and Güven, 1978). Bentonites form from a wide range of volcanic parent rock compositions, but most commonly from latites, rhyolites, and dacites (Grim and Güven, 1978). Volcanic ashes containing less than 70 percent silica and 5 to 10 percent magnesia readily form bentonites. Interlamination of bentonites and shales occurs commonly in marine environments, where seawater can devitrify and hydrate volcanic debris (Grim and Güven, 1978). The talc unit in Hembrillo Canyon contains greater than 30 percent MgO and less than one percent alumina. This agrees well with the observations above. Metz and Winkler (1963) indicate that talc can form by the reaction:

$$\text{Mg rich - Montmorillonite} = \text{Talc} + H_2O$$

in a temperature-pressure regime of 275-300 ° C and 700-2000 bars with X_{CO_2} near zero.

Condie and Budding (1979) indicate that the Hembrillo Canyon area was metamorphosed to a maximum of 350 ° C at a probable depth of 5-8 km for burial metamorphism, and 600-650 ° C for contact metamorphism.

In a further attempt to quantify the pressure-temperature regime of the Hembrillo Canyon succession, the two-feldspar geothermometer is used. The Michel-Levy method was employed to determine plagioclase compositions. Visual estimates were made to determine the amount of albite exsolved in alkali feldspar (Kerr, 1969) (Table 2). The data in Table 2 are plotted on Stormer's (1975) calculated temperature curves for a pressure of 2 kb in Figure 39. Temperatures of approximately 350 ° C are estimated using this pressure scheme. A temperature of approximately 625 ° C is determined for rocks of the amphibolite grade. This compares favorably with other temperature estimates by Condie and Budding (1979) and with other data discussed in this paper.

To summarize, the Hembrillo Canyon succession has been metamorphosed to moderate degrees at approximately 350 ° C and a depth of about 5-8 km. This corresponds to a general metamorphic grade of greenschist facies of the Barrovian series. Local overprinting to amphibolite grade metamorphism has occurred along contacts with granitic plutons, elevating temperatures to approximately 625 ° C.

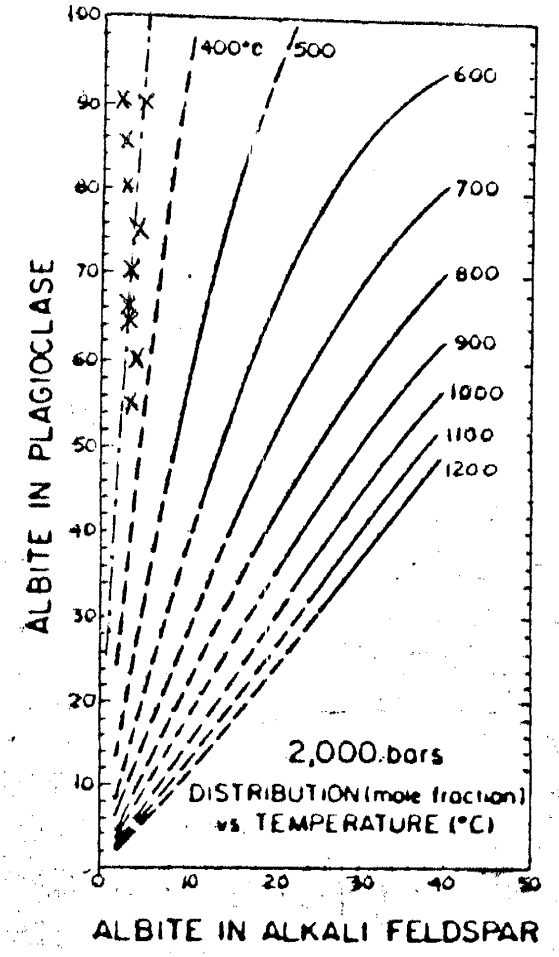

Figure 46
Data plotted on Stormer's (1975) calculated temperature curves for the two-feldspar thermometer data from Table 2.

TABLE 1

Progressive changes in metamorphic mineral assemblages in the Hembrillo Canyon succession, San Andres Mountains, New Mexico; —— = major phase; ---- = minor phase.

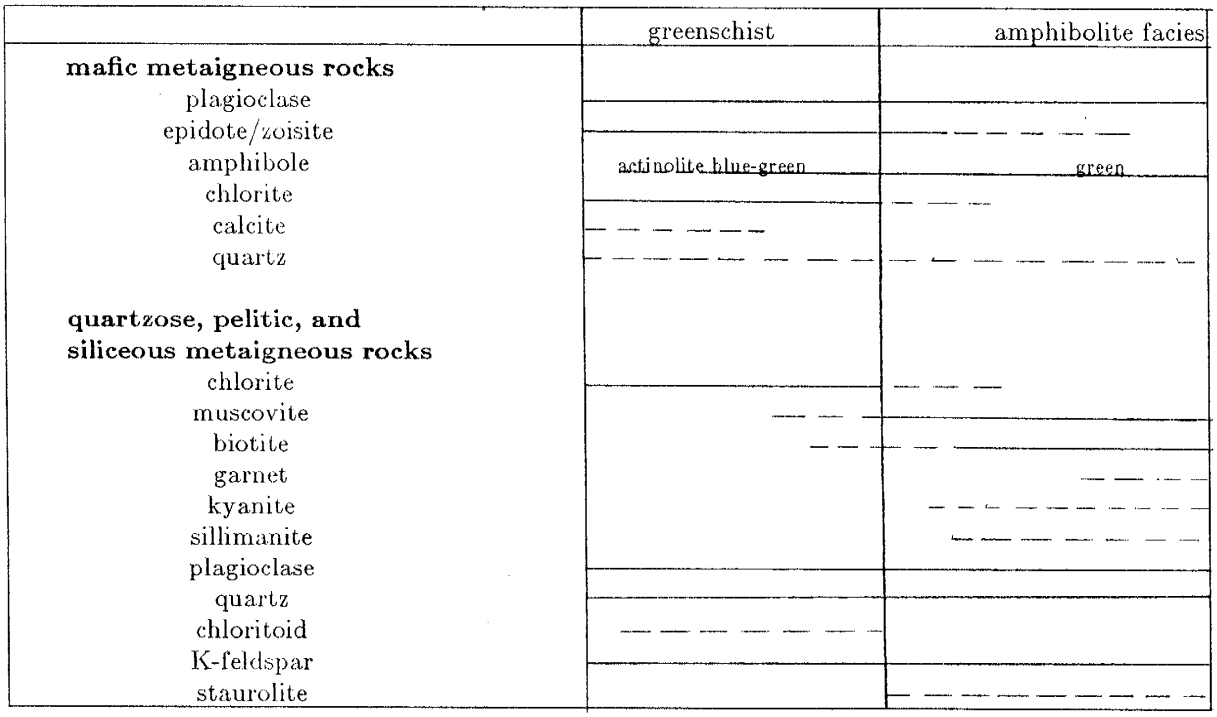

TABLE 2

Albite Content	
plagioclase	alkali feldspar
60%	5%
80%	2%
55%	5%
70%	5%
65%	5%
90%	2%
85%	4%
90%	5%
65%	5%
70%	5%
75%	7%

DISCUSSION AND CONCLUSIONS

From detailed chemical, petrographic, and field studies, a few general conclusions can be drawn for the Hembrillo Canyon succession. The data presented in previous sections indicate that these rocks formed in or near a magmatic arc environment (Figs. 7 thru 13, 19 thru 24). The volcanic rocks from this arc exhibit characteristics transitional between tholeiitic and calc-alkaline, with iron enrichment occurring in the tholeiites (Figs. 3, 4, and 5). Geochemical data for the volcanics indicate continental arc affinities, rather than those of an oceanic island arc (Figs. 14 and 19). Geochemistry of the graywackes in the succession are consistent with deposition of the sediments in a continental margin arc setting (Figs. 29 thru 34). These sediments are derived from both sides of the arc (Fig. 27 and Plate 1), which was most likely oriented east-west with the craton to the north and the arc to the south. Dual paleocurrent directions indicate that the sediments were probably formed in a back-arc basin in the form of density-flows and turbidity currents.

We can constrain the basin as being relatively narrow due to its high LIL/HFS ratios (Saunders and Tarney, 1984). Coalescing of turbidites may also indicate a narrow basin, because wide basins exhibit large amounts of basinal muds, which are not observed in the Hembrillo Canyon area.

Generalized data and conclusions can be confirmed by comparison with continental margin arc-back-arc basins. Volcanics from the Calupuy and Casma groups of central Chile and the Sarmiento and Tortuga complexes of southern Chile are from a Cretaceous subduction zone. This subduction zone was related

to a continental margin arc system with an associated back-arc basin (Lopez-Escobar, 1977; Dostal 1977; Saunders and others, 1979). These volcanic arc remnants contain sand-rich submarine fans and quartz wacke-graywacke turbidite sequences similar to those observed in the Hembrillo Canyon succession. Low Sc and Co contents of these sediments indicate a dominantly felsic volcanic origin for most sandstones and quartz wackes. Higher Sc and Co contents for remaining graywackes indicate an added mafic component. These data are consistent with paleocurrent analyses, indicating opposite source directions for these sediments and thus come from different sources.

PROPOSED MODEL

Emplacement and deposition of Hembrillo Canyon volcanics and sediments in a continental margin back-arc basin is consistent with most data in this thesis. Ta and Nb anomalies in basalts indicate that this arc system is significantly influenced by a subduction zone. The arc would be south or southeast of the Hembrillo Canyon area from paleocurrent data. The continental side of the arc would be to the north or northwest, with the basin striking approximately northeast-southwest.

An oceanic setting for the sediments seems most likely, due to sedimentary structures which are found below wave base. These sediments would have been transported from the craton by density flows and turbidity currents from both sides of the arc. This detritus was deposited in turbidites with well-developed Bouma sequences (Bouma, 1962).

Figure 40 illustrates diagrammatically the model proposed for the Hembrillo Canyon succession.

The Proterozoic of the southwestern United States is apparently a series of magmatic arcs which were accreted to the Archean craton (Condie, 1986). This arc accretion has evidently occurred throughout the Proterozoic and forms much of the continent seen today.

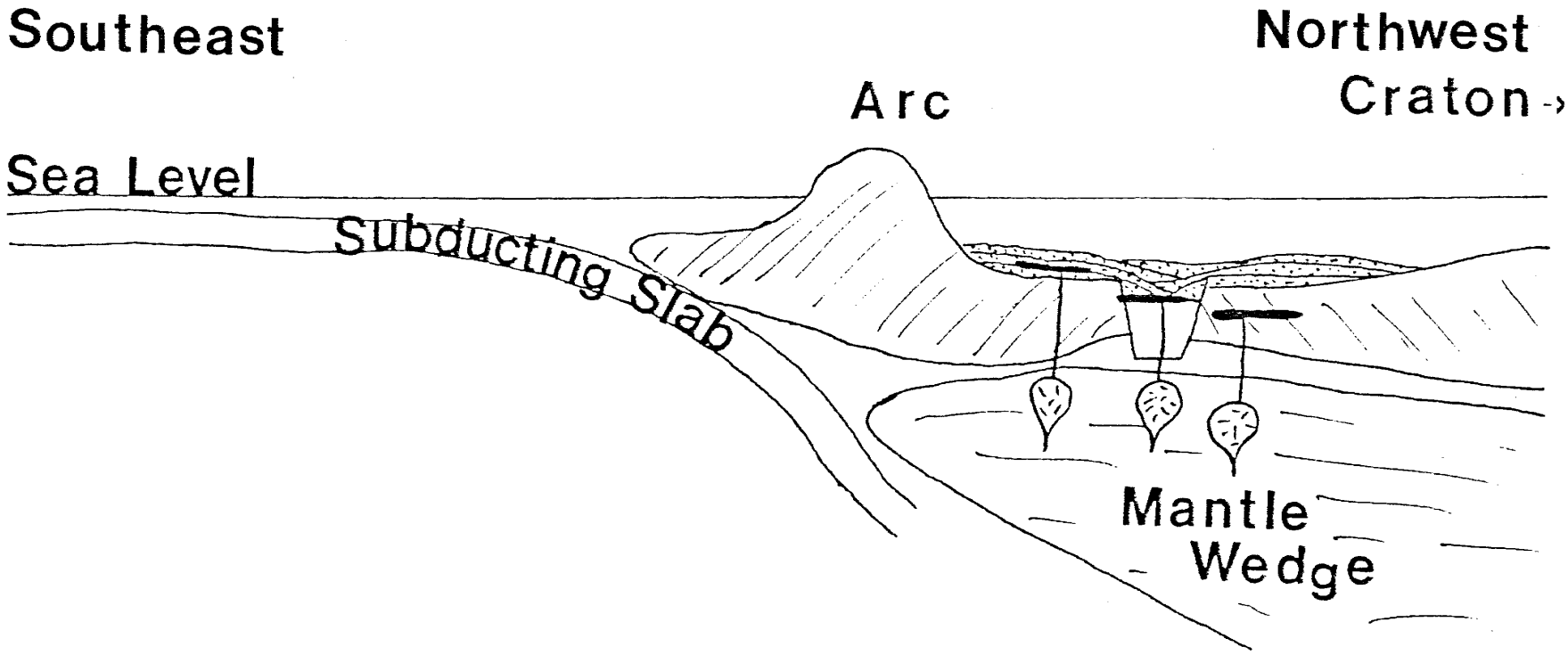

Figure 47
Schematic diagram for the proposed model for the origin of the Hembrillo Canyon succession.

REFERENCES

Aberg, G., Aguirre, L., Levi, B., and Nystrom, J.O., 1984, Spreading-subsidence and generation of ensialic marginal basins: An example from the early Cretaceous of central Chile. In: Kokelaar and Howells (Editors), *Marginal Basin Geology,* 322 pp.

Allegre, C.J., and Minster, J.F., 1978, Quantitative models of trace element behavior in magmatic processes. E.P.S.L., 38: 1-25.

Allen, P., 1985, The geochemistry of the amphibolite-granulite facies transition in central south India. NMIMT PhD thesis, 275 pp.

Asthana, D., and Leitch, E.C., 1985, Petroi Metabasalt: Alkaline within-plate mafic rocks from the Nambucca Slate Belt, northeastern New South Wales. Aust.J.E.S., 32: 261-277.

Atherton, M.P., et.al., 1985, The Mesozoic marginal basin of central Peru: A geochemical study of within-plate-edge volcanics. IN: Pitcher, W.S. and Atherton, M.P. (Editors), *Magmatism at a Plate Edge: The Peruvian Andes.* Wiley and Sons, pg. 58-67.

Bachman, G.O., and Harbour, R.L., 1970, Geologic map of the northern part of the San Andres Mountains, central New Mexico. USGS, Map I-600.

Bachman, G.O., and Myers, D.A., 1969, A study of the southern part of the San Andres Mountains, with emphasis on Paleozoic stratigraphy. USGS Bull., 1271-C.

Baker, P.E., Gonzalez-Ferran, O., and Rex, D.C., 1987, Geology and geochemistry of the Ojos del Salado volcanic region, Chile. J. Geol. Soc. London, 144: 85-96.

Bartholomew, D.S., and Tarney, J., 1984, Crustal extension in the Southern Andes. In: Kokelaar and Howells (Editors), *Marginal Basin Geology,* 322 pp.

Bhatia, M.R., 1983, Plate tectonics and geochemical compositions of sandstone. J. Geol., 91: 611-627.

Bhatia, M.R., and Crook, K.A.W., 1986, Trace element characteristics of graywackes and tectonic setting discrimination of sedimentary basins. Cont. Min. Petrol., 92: 181-193.

Blatt, H., Middleton, G., and Murray, R., 1980, *Origin of Sedimentary Rocks.* Prentice Hall, Englewood Cliffs, 728 pp.

Boardman, S.J., and Condie, K.C., 1986, Early Proterozoic bimodal volcanic rocks in central Colorado, U.S.A., Part II: Geochemistry, petrogenesis and tectonic setting. Precam. Res., 34: 37-68.

Bouma, A.H., 1962, *Sedimentology of Some Flysch Deposits.* Elsevier, Amsterdam, 108 pp.

Bowling, G.P., 1987, Geology and geochemistry of Early Proterozoic supracrustal rocks from the western Dos Cabezas Mountains, Cochise County, Arizona. NMIMT unpublished MS thesis, 126 pp.

Brophy, J.G., and Marsh, B.D., 1986, On the origin of high-alumina arc basalts and the mechanics of melt extraction. J. Petrol., 27: 763-789.

Bruhn, R.L., and Dalziel, I.W.D., 1977, Destruction of the early Cretaceous marginal basin in the Andes of Tierra Del Fuego. In: Talwani and Pitman (Editors), *Island Arcs, Deep Sea Trenches and Back-Arc Basins,* 420 pp.

Campbell, I.H., 1985, The difference between oceanic and continental tholeiites: A fluid dynamic explanation. Cont. Min. Petrol., 91: 37-43.

Cape, C.D., McGeary, S., and Thompson, G.A., 1983, Cenozoic normal faulting and shallow structure of the Rio Grande Rift near Socorro, New Mexico. GSA Bull., 94: 3-14.

Carey, S., and Sigurdsson, H., 1984, A model of volcanogenic sedimentation in marginal basins. In: Kokelaar and Howells (Editors), *Marginal Basin Geology,* 322 pp.

Condie, K.C., 1982, Early and middle Proterozoic supracrustal successions and their tectonic settings. Am. J. Sci., 282: 341-357.

Condie, K.C., 1982, Plate tectonic model for Proterozoic continental accretion in the southwestern United States. Geology, 10: 37-42.

Condie, K.C., 1986, Geochemistry and tectonic setting of early Proterozoic supracrustal rocks in the southerwestern United States. J. Geol., 94: 845-864.

Condie, K.C., and Budding, A.J., 1979, Geology and geochemistry of Precambrian rocks, central and south-central New Mexico. NMBM & MR, Memoir 35, 58 pp.

Condie, K.C., and DeMalas, J.P., 1985, The Pinal Schist: An early Proterozoic quartz wacke association in southeastern Arizona. Precam. Res., 27: 337-356.

Condie, K.C., Bowling, G.P., and Vance, R.K., 1985, Geochemistry and origin of

early Proterozoic supracrustal rocks, Dos Cabezas Mountains, southeastern Arizona. GSA Bull., 96: 655-662.

Copeland, P., 1986, Geochemistry and geology of the Pinal Schist, Cochise and Pima Counties, Arizona. NMIMT, MS thesis, 179 pp.

Crook, K.A., 1974, Lithologies and geotectonics: The significance of compositional variations in flysch arenites (graywackes). In: Dott, R.H. and Shaver, R.H. (Editors), *Modern and Ancient Geosynclinal Sedimentation,* SEPM Spec. Pub. 19, pp. 304-310.

Cullers, R.L., Chaudhuri, S., Kilbane, N., and Koch, R., 1979, Rare-earths in size fractions and sedimentary rocks of Pennsylvanian-Permian age from the mid-continent of the U.S.A. Geoc. Cosmo. Acta, 43: 1285-1301.

Cullers, R.L., Yeh, L., and Chaudhuri, S., 1974, Rare earth elements in Silurian pelitic schists from N.W. Maine. Geoc. Cosmo. Acta, 38: 389-400.

Denison, R.E., and Hetherington, E.A., Basement rocks in Far West Texas and south-central New Mexico. NMBM & MR, Circular #104, 16 pp.

Dickinson, W.R., 1970, Interpreting detrital modes of graywacke and arkose. J. Sed. Pet., 40: 695-707.

Dickinson, W.R., 1977, Tectono-stratigraphic evolution of subduction-controlled sedimentary assemblages. In: Talwani and Pitman (Editors), *Island Arcs, Deep Sea Trenches, and Back-Arc Basins,* 470 pp.

Dickinson, W.R., 1985, Interpreting provenance relations from detrital modes of sandstones. In: Zuffa, G.G. (Editor), *Provenance of Arenites,* pp. 333-361.

Dickinson, W.R., and Suczek, C.A., 1979, Plate tectonics and sandstone compositions. A.A.P.G. Bull., 63: 2164-2182.

Dickinson, W.R., et.al., 1983, Provenance of North American Phanerozoic sandstones in relation to tectonic setting. GSA Bull., 94: 222-235.

Dixon, T.H., and Batiza, R., 1979, Petrology and chemistry of recent lavas in the northern Marianas: Implications for the origin of island arc basalts. Cont. Min. Petrol., 70: 167-181.

Dixon, T.H., and Stern, R.J., 1983, Petrology, chemistry, and isotopic composition of submarine volcanoes in the southern Mariana arc. GSA Bull., 94: 1159-1172.

Dostal, J., et.al., 1977, Geochemistry and origin of volcanic rocks of the Andes. Cont. Min. Petrol., 63: 113-128.

Dott, R.H., and Shaver, R.H., 1974, *Modern and Ancient Geosynclinal Sedimentation.* SEPM Pub. 19, 380 pp.

Dott, R.H., et.al., 1982, Relationship of late Mesozoic and early Cenozoic sedimentation to the tectonic evolution of the southernmost Andes and Scotia arc. In: Craddock, C. (Editor), *Antarctic Geoscience,* University of Wisconsin Press, pp. 193-202.

Dunham, K.C., 1935, The geology of the Organ Mountains. NMSM, NMBM & MR Bull., 272 pp.

Ehlers, E.G., and Blatt, H., 1982, *Petrology: Igneous Sedimentary and Metamorphic.* W.H. Freeman and Co., 732 pp.

Engel, A.E.J., et.al., 1974, Crustal evolution and global tectonics: A petrogenetic view. GSA Bull., 85: 843-858.

Ewers, G.R., and Higgins, N.C., 1985, Geochemistry of the early Proterozoic metasedimentary rocks of the Alligator Rivers Region, Northern Territory, Australia. Precam. Res., 29: 331-357.

Farquharson, G.W., Hamer, R.D., and Ineson, J.R., 1984, Proximal volcaniclastic sedimentation in a Cretaceous back-arc basin, northern Antarctic Peninsula. In: Kokelaar and Howells (Editors), *Marginal Basin Geology,* 322 pp.

Fisher, R.V., 1984, Submarine volcaniclastic rocks. In: Kokelaar and Howells (Editors), *Marginal Basin Geology,* 322 pp.

Folk, R.L., 1980, *Petrology of sedimentary rocks.* Hemphill Publishing Co., 184 pp.

Furnes, H., Shimron, A.E., and Roberts, D., 1985, Geochemistry of Pan-African volcanic arc sequences in southeastern Sinai Peninsula and plate tectonic implications. Precam. Res., 29: 359-382.

Galan, E., Alvarez, A., and Esteban, M.A., 1986, Characterization and technical properties of a Mg-rich bentonites. Applied Clay Science, 1: 295-309.

Galloway, W.E., 1974, Deposition and alteration of sandstone in northeast Pacific arc-related basins: Implications for graywacke genesis. GSA Bull., 85: 379-390.

Gibson, I.L., and Jagam, P., 1980, Instrumental neutron activation analysis of rocks and minerals. In: Muecke, G.K. (Editor), *Short Course in Neutron Activation Analysis in the Geosciences.* Mineralogical Association of Canada, pp. 109-131.

Gordon, G.E., et.al., 1968, Instrumental neutron activation analysis of standard rocks with high resolution gamma-ray detectors. Geoc. Cosmo. Acta, 32: 369-396.

Govindaraju, K., (Editor), 1984, 1984 compilation of working values and sample description for 170 international reference samples of mainly silicate rocks and minerals. Geostandards Newsletter, v. 8, special issue.

Grim, R.E., and Güven, N., 1978, *Developments in Sedimentology No. 24; Bentonites.* Elsevier Scientific Publishing Co., New York, 256 pp.

Gromet, L.P., et.al., 1984, The "North American shale composite": Its compilation, major and trace element characteristics. Geoc. Cosmo. Acta, 48: 2469-2482.

Hart, S.R., et.al., 1970, Ancient and modern volcanic rocks: A trace element model. E.P.S.L., 10: 17-28.

Hawkesworth, C.J., et.al., 1977, A geochemical study of island-arc and back-arc tholeiites from the Scotia Sea. E.P.S.L., 36: 253-262.

Hodder, A.P.W., 1985, Depth of origin of basalts inferred from Ti/V ratios and a comparison with the K/s-4/d2/u/s0O-depth relationship for island-arc volcanics. Chem. Geol., 48: 3-16.

Holm, P.E., 1985, The geochemical fingerprints of different tectonomagmatic environments using hygromagmatophile element abundances of tholeiitic basalts and basaltic andesites. Chem. Geol., 51: 303-323.

Hubert, J.F., 1962, A zircon-tourmaline-rutile maturity index and the interdependence of the composition of heavy mineral assemblages with the gross composition and texture of sandstones. J. Sed. Pet., 32: 440-450.

Irvine,T.N., and Baragar, W.R.A., 1971, A guide to the chemical classification of the common volcanic rocks. CJES, 8: 523-548.

Jakes, P., and Gill, J., 1970, Rare earth elements and the island arc tholeiitic series. E.P.S.L., 9: 17-28.

Jakes, P., and White, A.J.R., 1972, Major and trace element abundance in volcanic rocks of orogenic areas. GSA Bull., 83: 29-39.

Jamieson, B.G., and Clarke, D.B., 1970, Potassium and associated elements in tholeiitic basalts. J. Petrol., 11: 183-204.

Jensey, L.S., 1976, A new cation plot for classifying subalkaline volcanic rocks. Ontario Division of Mines misc. paper66, 22 pp.

Kay, R.W., and Hubbard, N.J., 1978, Trace elements in ocean ridge basalts. E.P.S.L., 38: 95-116.

Kelley, V.C., 1955, Regional tectonics of south central New Mexico. NMGS Guidebook #6, pp. 96-104.

Kirwan, A.D., et.al., 1986, Time-dependent hydrodynamic models of turbidity currents analyzed with data from the Grand Banks and Orleansville events. J. Sed. Pet., 56: 279-386.

Klein, G.D., 1985, The control of depositional depth, tectonic uplift, and volcanism on sedimentation processes in the back-arc basins of the Western Pacific Ocean. J. Geol., 93: 1-25.

Kokelaar, B.P., et.al., 1984, The Ordovician marginal basin of Wales. In: Kokelaar and Howells (Editors), *Marginal Basin Geology,* 322 pp.

Kottlowski, et.al., 1956, Stratigraphic studies of the San Andres Mountains, New Mexico. NMBM & MR, Mem. 1, 14 pp.

Kottlowski, F.E., 1959, Sedimentary rocks of the San Andres Mountains. Roswell Geologic Society and Society of Economic Paleontologists and Mineralogists, Guidebook 12th Field Conference, pp. 256-277.

Kottlowski, F.E., 1955, Geology of the San Andres Mountains. NMGS Guidebook, #6, pp. 136-145.

Lee, D.E., et.al., 1977, Composition of calcium-poor quartzies of late Precambrian and Early Cambrian age from eastern White Pine County, Nevada. USGS Prof. Paper, 1158-B.

Leitch, E.C., 1984, Marginal basins of the SW Pacific and the preservation and recognition of their ancient analogues: A review. In: Kokelaar and Howells (Editors), *Marginal Basin Geology,* 322 pp.

Levin, R.I., and Rubin, D.S., 1980, *Applied Elementary Statistics.* Prentice-Hall Inc., Englewood Cliffs, pp. 86-109.

Loberg, B.E.H., 1980, A Proterozoic subduction zone in southern Sweden. E.P.S.L., 46: 287-294.

Loomis, T.P., 1986, Metamorphism of metapelites: Calculations of equilibrium assemblages and numerical simulations of the crystallization of garnet. J. Metamorphic Geol., 4: 201-229.

Lopez-Escobar, L., Frey, F.A., and Vergara, M., 1977, Andesites and high-alumina basalts from the central-south Chile High Andes: Geochemical evidence

bearing on their petrogenesis. Cont. Min. Petrol., 63: 199-228.

McCrink, T.P., 1982, Precambrian geology of the Taos range, Taos County, New Mexico. NMIMT MS thesis, 123 pp.

Meissner, and Rolf, 1986, *The Continental Crust: A Geophysical Approach.* Academic Press, Orlando, pp. 213-233, 368-379.

Meschede, Martin, 1986, A method of discriminating between different types of mid-ocean basalts and continental tholeiites with the Nb-Zr-Y diagram. Chem. Geol., 56: 207-218.

Metz, P.W., and Winkler, H.G.F., 1963, Experimentelle Gesteins-Metamorphose VII Die Bildung von Talk Aus Kieseligem Dolomit, Geoc. Cosmo. Acta, 27: 431-457.

Miller, R.G., and O'Nions, R.K., 1985, Source of Precambrian chemical and clastic sediments. Nature, 314: 325-329.

Mitchell, A.H., and Reading, H.G., 1971, Evolution of island arcs. J. Geol., 79: 253-284.

Miyashiro, A., 1975, *Metamorphism and Metamorphic Belts.* Unwin Brothers Ltd., Great Britain, 492 pp.

Muehlberger, W.R., Denison, R.E., and Lidiak, E.G., 1967, Basement rocks in the continental interior of United States. A.A.P.G. Bull., 51: 2351-2380.

Mullican, W.F., III, 1981, Stratigraphy and diagenisis of the San Andres Mountains, New Mexico. Texas Technological University, Lubbock, TX, MS thesis.

Mutti, E., and Ricci Lucchi, F., 1978, Turbidites of the northern Apennines: Introduction to facies analysis. Internat. Geology Rev., 20: 125-166.

Norrish, K., and Chappel, B.W., 1977, X-ray fluorescence. In: Zussman, J. (Editor), *Physical Methods in Determinitive Mineralogy.* Academic Press, pp. 235-262.

Norrish, K., and Hutton, J.T., 1969, An accurate x-ray spectrographic method for the analysis of a wide range of geological samples. Geoc. Cosmo. Acta, 33: 431-435.

Pearce, J.A., 1983, Role of sub-continental lithosphere in magma genesis at active continental margins. In: Hawkesworth, C.J. and Norry, M.J. (Editors), /flContinental Basalts and Mantle Xenoliths, Shiva Press, pp. 230-249.

Pearce, J.A., et.al., 1984, Characteristics and tectonic significance of supracrustal ophiolites. In: Kokelaar, B.P, and Howells, M.F. (Editors), /flMarginal Basin Geology, Geol. Soc. Lond-Spec. Pub. 16, pp. 77-94.

Pearce, J.A., and Cann, J.R., 1973, Tectonic setting of basic volcanic rocks determined by using trace element analysis. E.P.S.L., 19: 290-300.

Perfit, M.R., et.al., 1980, Chemical characteristics of island-arc basalts: implications for mantle sources. Chem. Geol., 30: 227-256.

Pharaoh, T.C., and Pearce, J.A., 1984, Geochemical evidence for the geotectonic setting of early Proterozoic metavolcanic sequences in Lapland. Precam. Res., 25: 283-308.

Pickering, K., et.al., 1986, Deep-water facies, processes and models: a review and classification scheme for modern and ancient sediments. Earth Sci. Rev., 23: 75-174.

Ringwood, A.E., 1977, Petrogenesis in island arc systems. In: Talwani and Pitman (Editors), *Island Arcs, Deep Sea Trenches and Back-Arc Basins,* 420 pp.

Robertson, J.M., and Moench, R.H., 1979, The Pecos greenstone belt: A Proterozoic volcano-sedimentary sequence in the southern Sangre de Cristo Mountains, New Mexico. NMGS Guidebook 30: 165-173.

Robinson, J.M., 1976, Annotated bibliography and mapping index of Precambrian of New Mexico. NMBM & MR Bull. 103, 90 pp.

Roser, B.P., and Korsch, R.J., 1986, Determination of tectonic setting of sandstone-mudstone suites using SiO_2 content and K_2O/Na_2O ratio. J. Geol., 94: 635-651.

Saunders, A.D., and Tarney, J., 1978, The geochemistry of basalts from a back-arc spreading centre in the East Scotia Sea. Geoc. Cosmo. Acta, 43: 555-572.

Saunders, A.D., and Tarney, J., 1984, Geochemical characteristics of basaltic volcanism within back-arc basins. In: Kokelaar and Howells (Editors), *Marginal Basin Geology,* 322 pp.

Saunders, A.D., et.al., 1979, Geochemistry of Mesozoic marginal basin floor igneous rocks from southern Chile. GSA Bull., 90: 237-238.

Sawyer, E.W., 1986, The influence of source rock type, chemical weathering and sorting on the geochemistry of clastic sediments from the Quetico Metasedimentary Belt, Superior Province, Canada. Chem. Geol., 55: 77-95.

Schwab, F.L., 1982, *Geosynclines: Concept and Place Within Plate Tectonics.* Hutchinson Ross Publishing Co., Stroudsburg, 411 pp.

Shanmugam, G., Damuth, J.E., and Moiola, R.J., 1985, Is the turbidite facies association scheme valid for interpreting ancient submarine fan environments? Geology, 13: 234-237.

Soegaard, K., and Eriksson, K.A., 1986, Transition from arc volcanism to stable-shelf and subsequent convergent-margin sedimentation in northern New Mexico from 1.76 Ga. J. Geol., 94: 47-66.

Stacey, J.S., and Hedlund, D.C., 1983, Lead-isotopic compositions of diverse igneous rocks and ore deposits from southwestern New Mexico and their implications for early Proterozoic crustal evolution in the western United States. GSA Bull., 94: 43-57.

Stattegger, K., 1987, Heavy minerals and provenance of sands: Modeling of lithological end members from river sands of northern Austria and from sandstones of the Austroalpine Gosau formation (late Cretaceous). J. Sed. Pet., No. 2, 57: 301-310.

Stern, C.R., 1980, Geochemistry of Chilean ophiolites: Evidence for the compositional evolution of the mantle source of back-arc basalts. J.G.R., 85: 955-966.

Stewart, J.H., and Poole, F.G., 1974, Lower Paleozoic and uppermost Precambrian Cordilleran miogeocline, Great Basin, western United States. In: Dickinson, W.R. (Editor), *Tectonics and Sedimentation.* SEPM Spec. Pub. No. 22.

Storey, B.C., and Macdonald, D.I.M., 1984, Processes of formation and filling of a Mesozoic back-arc basin on the island of South Georgia. In: Kokelaar and Howells (Editors), *Marginal Basin Geology,* 322 pp.

Stormer, J.C., Jr., 1965, A practical two feldspar thermometer. Am. Mineral., 55: 667-674.

Suarez, M., and Pettigrew, T.H., 1976, An Upper Mesozoic island-arc-back-arc system in the southern Andes and South Georgia. Geological Magazine, 113: 305-400.

Taylor, S.R., 1977, Island arc models and the composition of the continental crust. In: Talwani and Pitman (Editors), *Island Arcs, Deep Sea Trenches and Back-Arc Basins.* 420 pp.

Taylor, S.R., and McLennan, S.M., 1983, Geochemistry of Early Proterozoic sedimentary rocks and the Archean/Proterozoic boundary. In: Medaris, L.G.,

et.al. (Editors), *Proterozoic Geology: Selected Papers from an International Proterozoic Symposium.* GSA, Memoir 161, pp. 119-132.

Taylor, S.R., and McLennan, S.M., 1985, *The Continental Crust: Its Composition and Evolution.* Blackwell Scientific Publications, 312 pp.

Torres-Roldan, R.L., Poli, G., and Peccerillo, A., 1986, An Early Miocene arc-tholeiitic magmatic dike event from the Alboran Sea: Evidence for precollisional subduction and back-arc crustal extension in the westernmost Mediterranean. Geol. Rund., 75: 219-234.

Turner, F.J., 1981, *Metamorphic Petrology.* McGraw Hill, New York, 524 pp.

Vance, R.K., 1983, Investigations in the Precambrian rocks of the Dos Cabezas mountains, southeast Arizona. Unpublished manuscript.

Velbel, M.A., 1985, Mineralogically mature sandstones in accretionary prisms. J. Sed. Pet., 55: 685-690.

Walker, R.G., 1978, Deep-water sandstone facies and ancient submarine fans: Models for exploration for stratigraphic traps. AAPG Bull., 62: 932-966.

Ware, M.J., and Hiscott, R.N., 1985, Sedimentology of Proterozoic cratonic sheet sandstones of the eastern Canadian Shield: Sims Formation, Labrador, Canada. Precam. Res., 30: 1-26.

Waters, A.C., 1962, Basalt magma types and their tectonic associations: Pacific Northwest of the United States. Geophysical Mongraph, No. 6, pp. 158-170.

Weaver, S.D., et.al., 1979, A geochemical study of magmatism associated with the inital stages of back-arc spreading. Cont. Min. Petrol., 68: 151-169.

Wezel, F.C., 1986, *The Origin of Arcs.* Elsevier, Amsterdam, 567 pp.

Wildeman, T.R., and Haskin, L.A., 1973, Rare earths in Precambrian sediments. Geoc. Cosmo. Acta, 37: 419-438.

Wilkinson, J.F.G., 1986, Classification and average chemical compositions of common basalts and andesites. J. Petrol., 27: 31-62.

Wilson, G., and Cosgrove, J.W., *Introduction to Small-scale Geological Structures.* George Allen and Unwin Ltd., London, 128 pp.

Winchester, J.A., and Floyd, P.A., 1976, Geochemical magma type discrimination of different magma series and their differentiation products using immobile elements. Chem. Geol., 20: 325-343.

Winkler, H.G.F., 1979, *Petrogenisis of Metamorphic Rocks.* Springer-Verlag, New York, 348 pp.

Winn, R.D., and Dott, R.H., 1978, Submarine-fan turbidites and resedimented conglomerates in a Mesozic arc-rear marginal basin in southern South America. In: Stanley, D.J., and Kelling, G. (Editors), *Sedimentation in Submarine Canyons, Fans, and Trenches,* pp. 362-373.

Yamada, E., 1984, Subaqueous pyroclastic flows: their development and their deposits. In: Kokelaar and Howells (Editors), *Marginal Basin Geology,* 322 pp.

Young, S.W., 1976, Petrographic textures of detrital polycrystalline quartz as an aid to interpreting crystalline source rocks. J. Sed. Pet., 46: 595-603.

APPENDIX A: ACCESS TO STUDY AREA AND SAMPLE LOCATIONS.

Permission to enter the White Sands Missile Range must be obtained prior to entry into the study area. This is done through the Public Liaison's office of the U.S. Army. After permission is granted, a brief description of destination, dates of access, and purpose of visit must be given for scheduling. While on the range, continual consultation with the Military Police at range control is required before entry to and from the field area is allowed.

Major roads are well paved, providing access to within three to four miles of the area. Further access is provided by several unimproved roads initially made prior to militarization of public lands in the early 1950's. These roads provide good access to Hembrillo Canyon, Mayberry Canyon, Lost Man and Dead Man Canyons, and Sulfur Canyon. Access to other canyons is by one to four hour hikes in often rugged terrain. Access from Socorro through Stallion Range Center is approximately 100 miles. Access from Las Cruces via SMR gate on U.S. 70 is about 55 miles, and Range 10 is about 65 miles. All roads intersect or follow Range 7, which fronts the study area to the east. Continuous access time is difficult due to the number of missions and tests performed on the range. Access is generally limited to afternoon or morning stretches, rarely all-day, with the usual exceptions of weekends.

Sections of the following USGS 7 1/2 minute topographic quadrangle sheets accompany this Appendix: Gardner Peak, Hembrillo Canyon, and Strawberry Peak. Sample locations discussed in the text are plotted here.

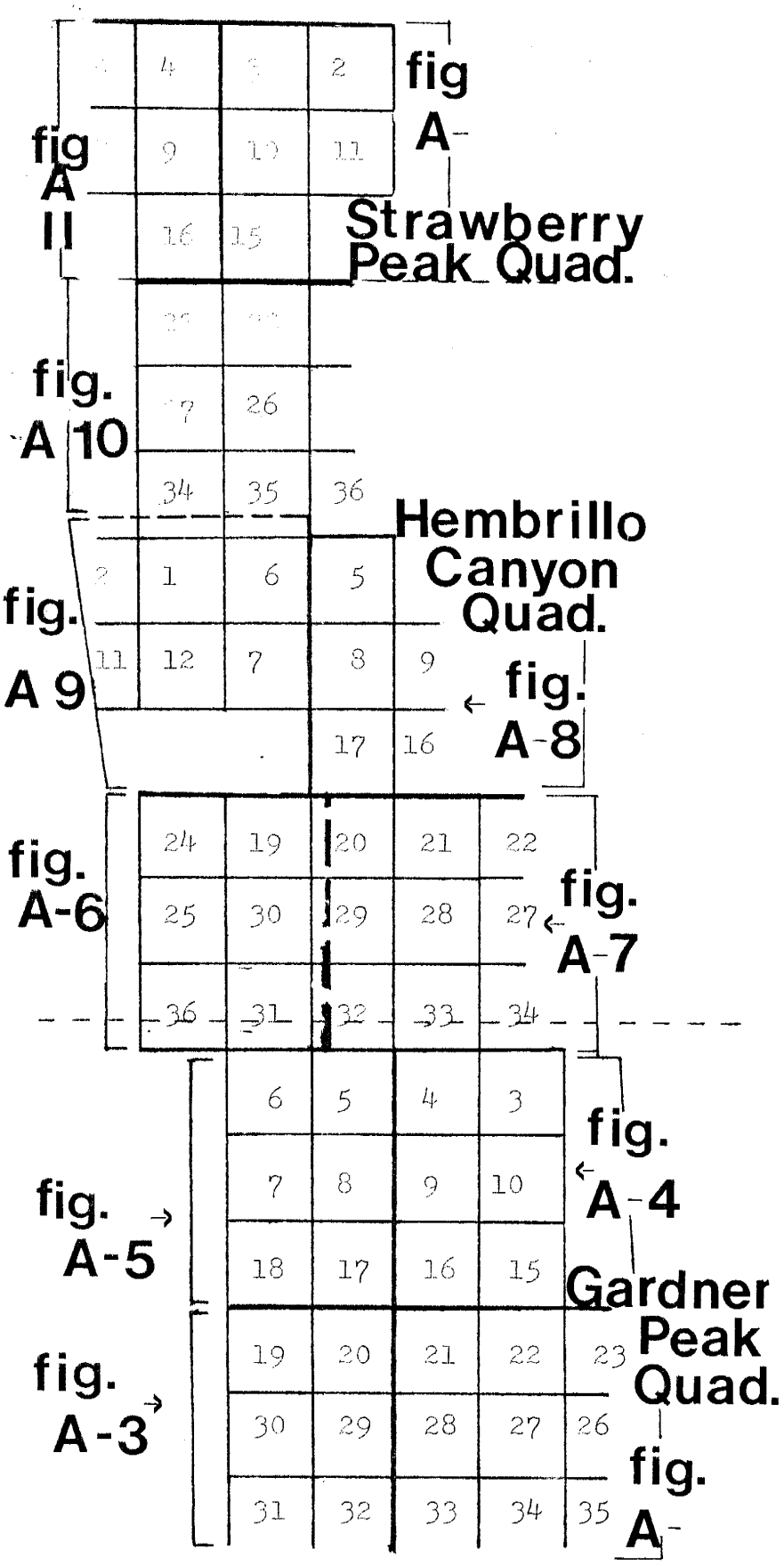

Figure A-1: Key to Sample Location Maps.

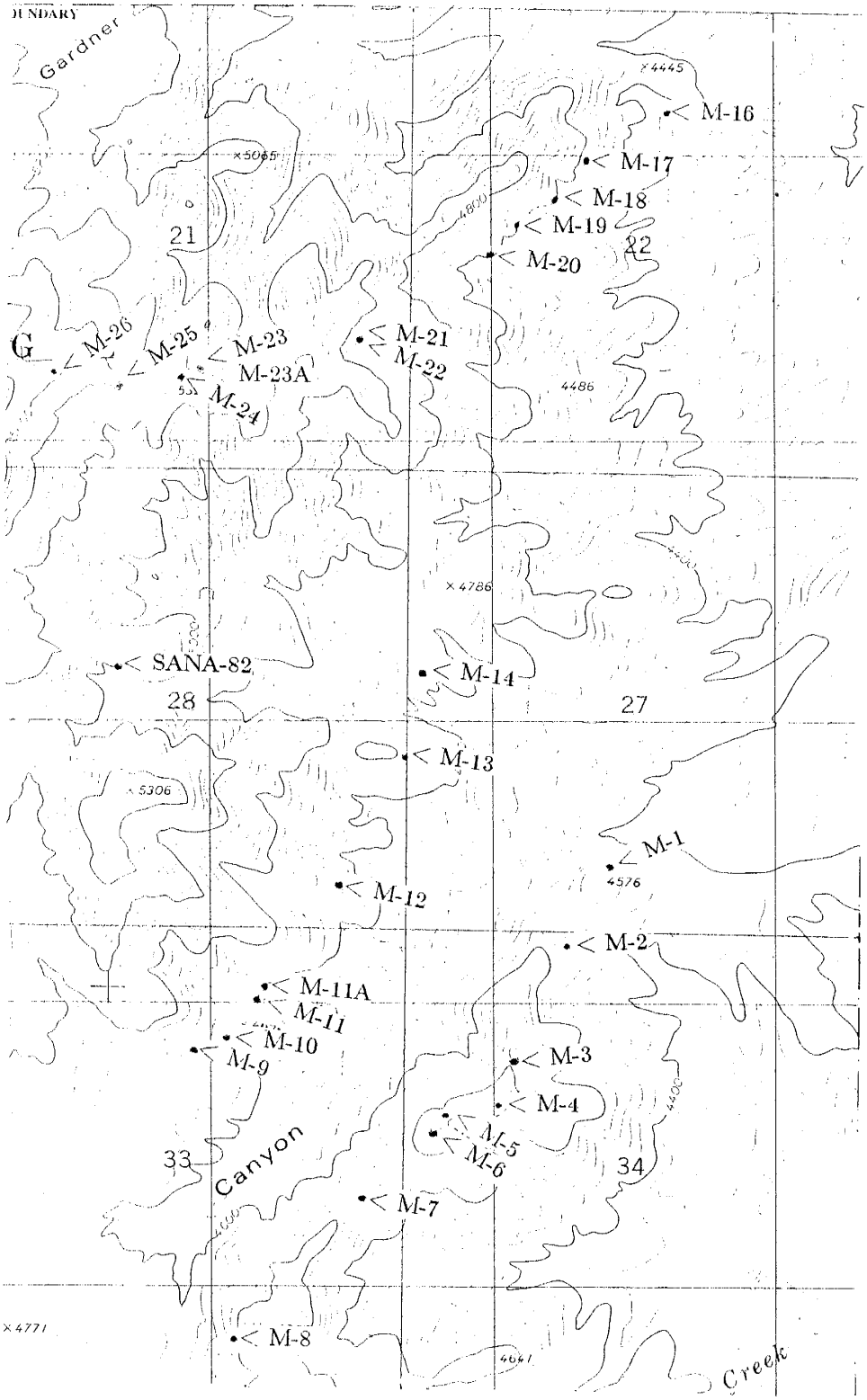

Figure A-2: Gardner Peak 7.5 Minute Quadrangle.

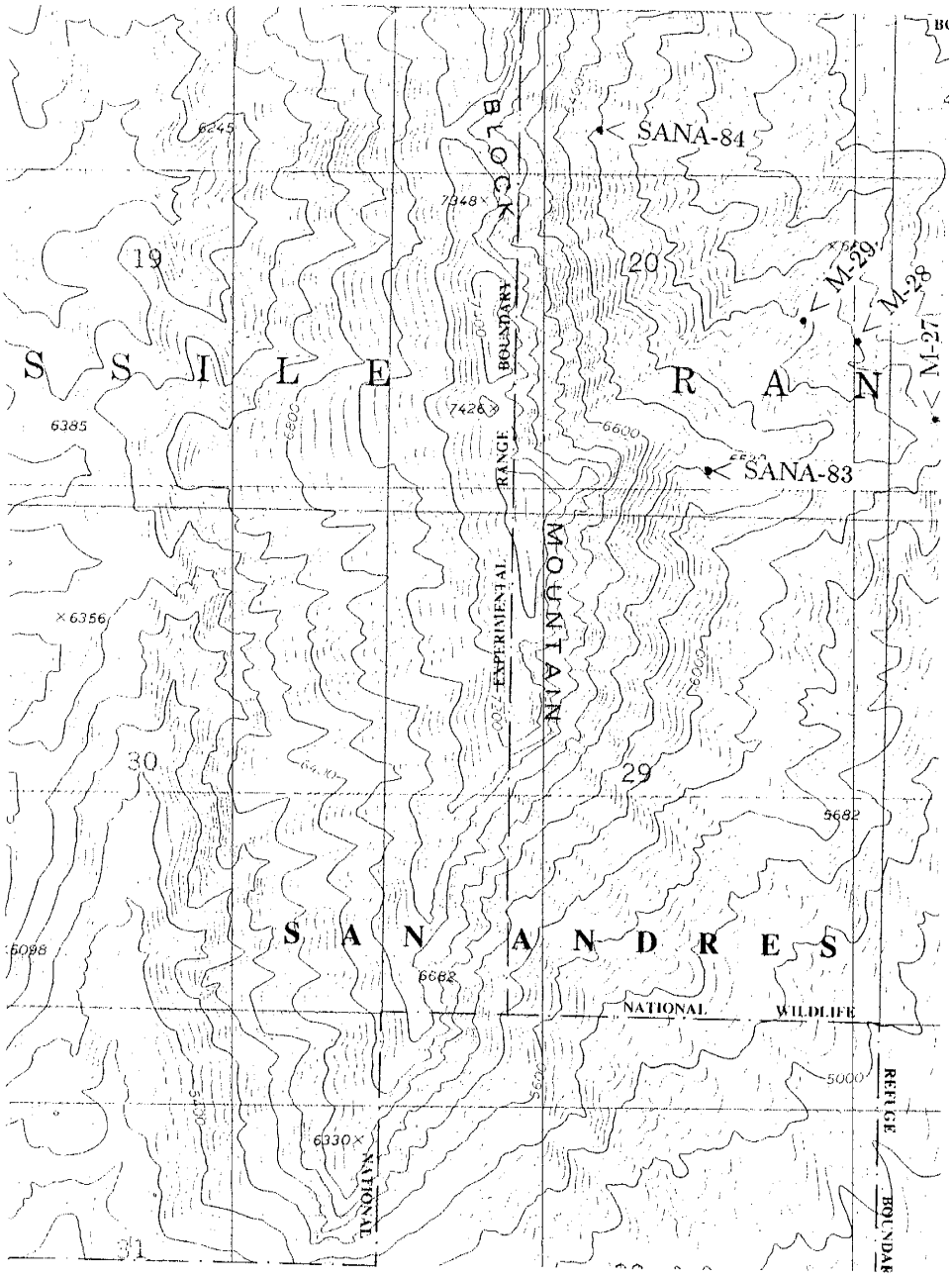

Figure A-3: Gardner Peak 7.5 Minute Quadrangle.

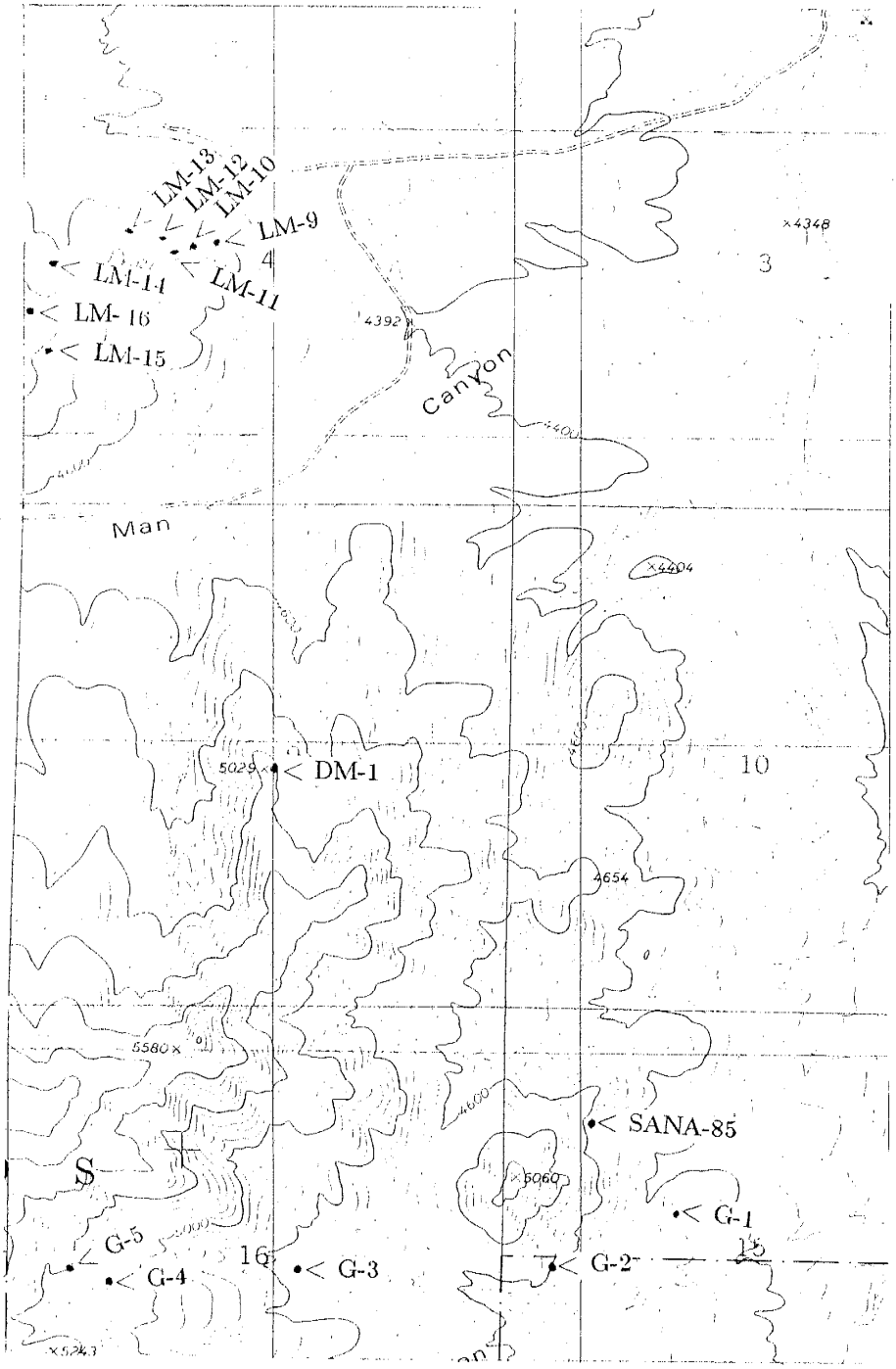

Figure A-4: Gardner Peak 7.5 Minute Quadrangle.

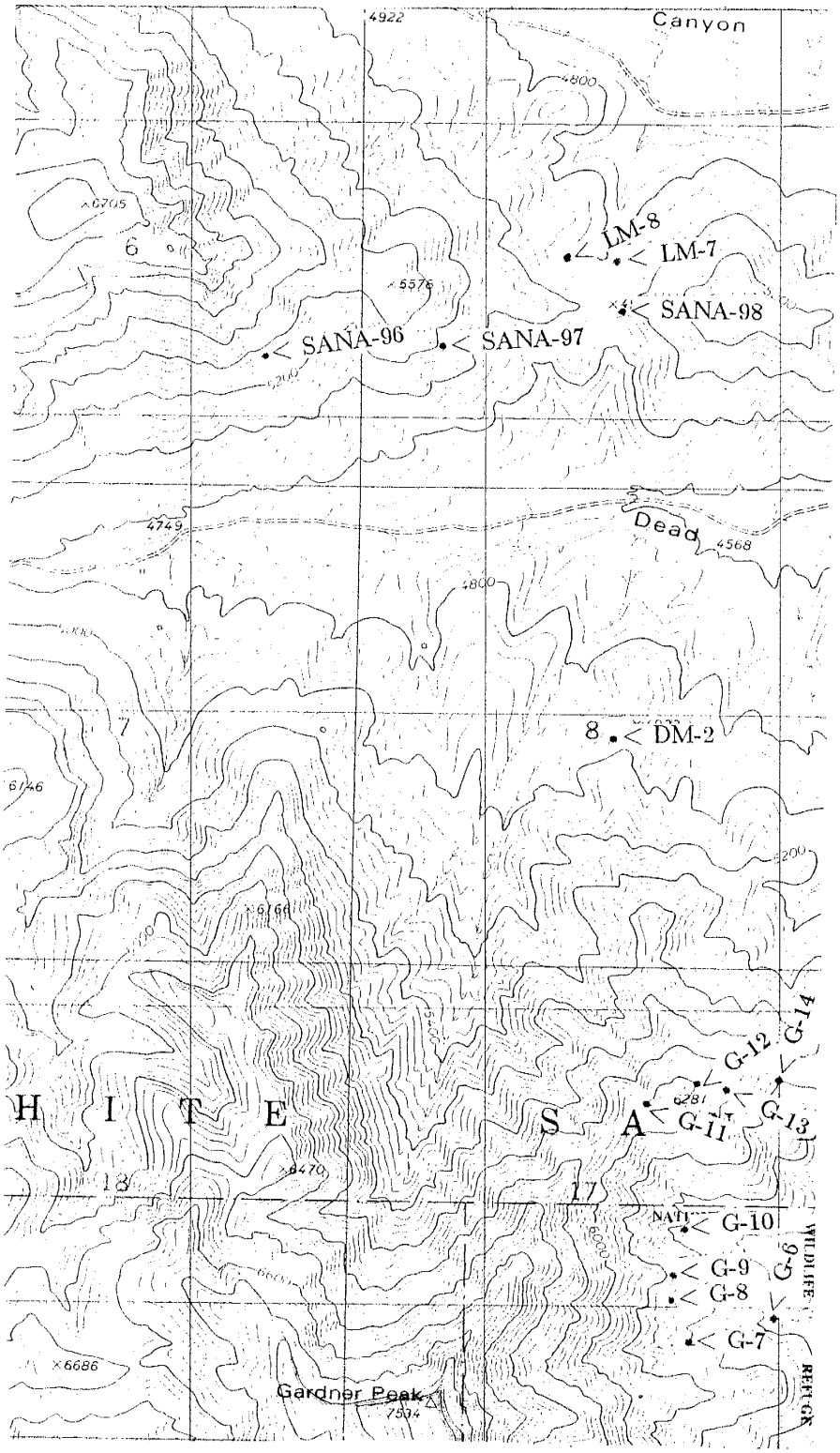

Figure A-5: Gardner Peak 7.5 Minute Quadrangle.

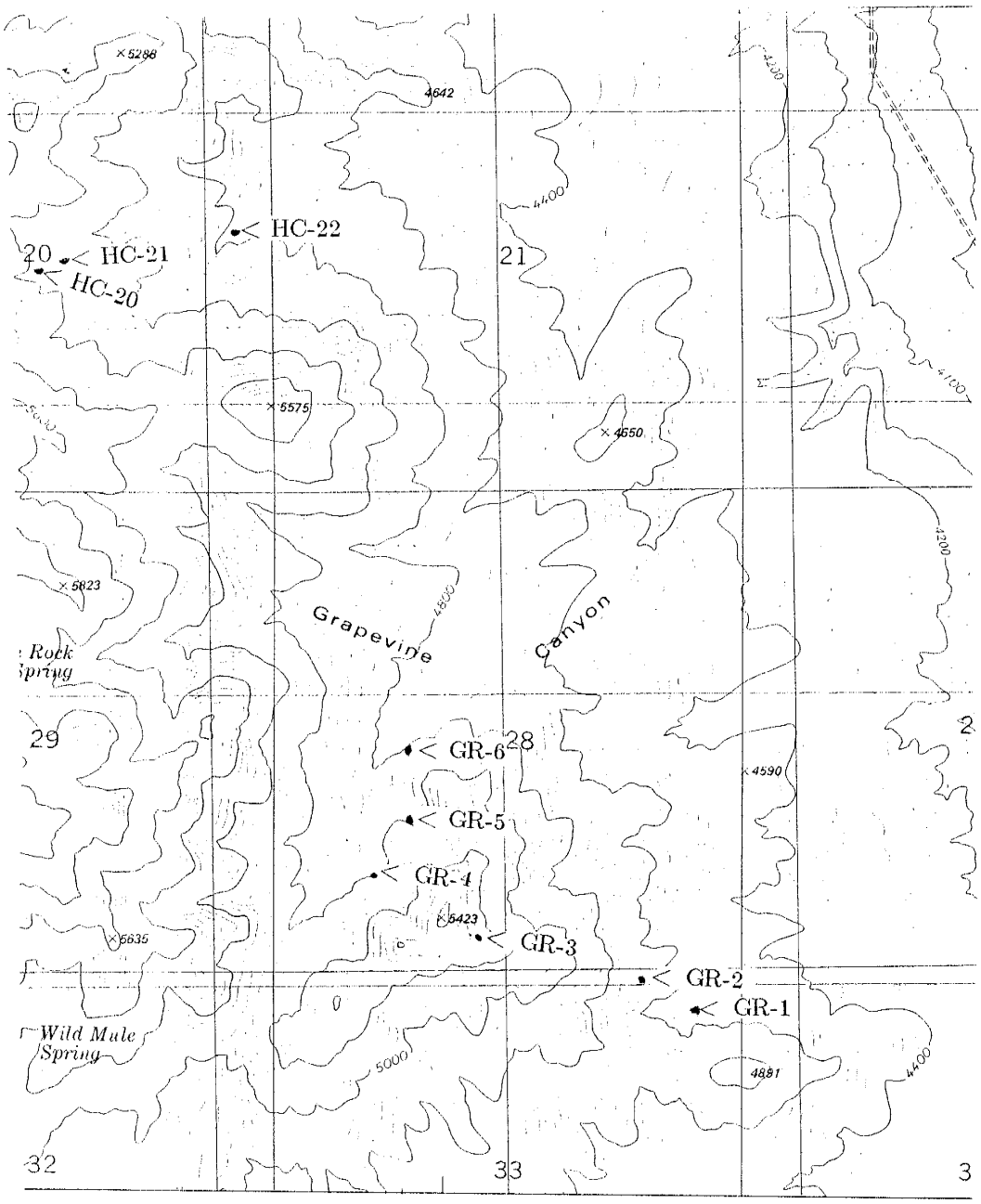

Figure A-6: Hembrillo Canyon 7.5 Minute Quadrangle.

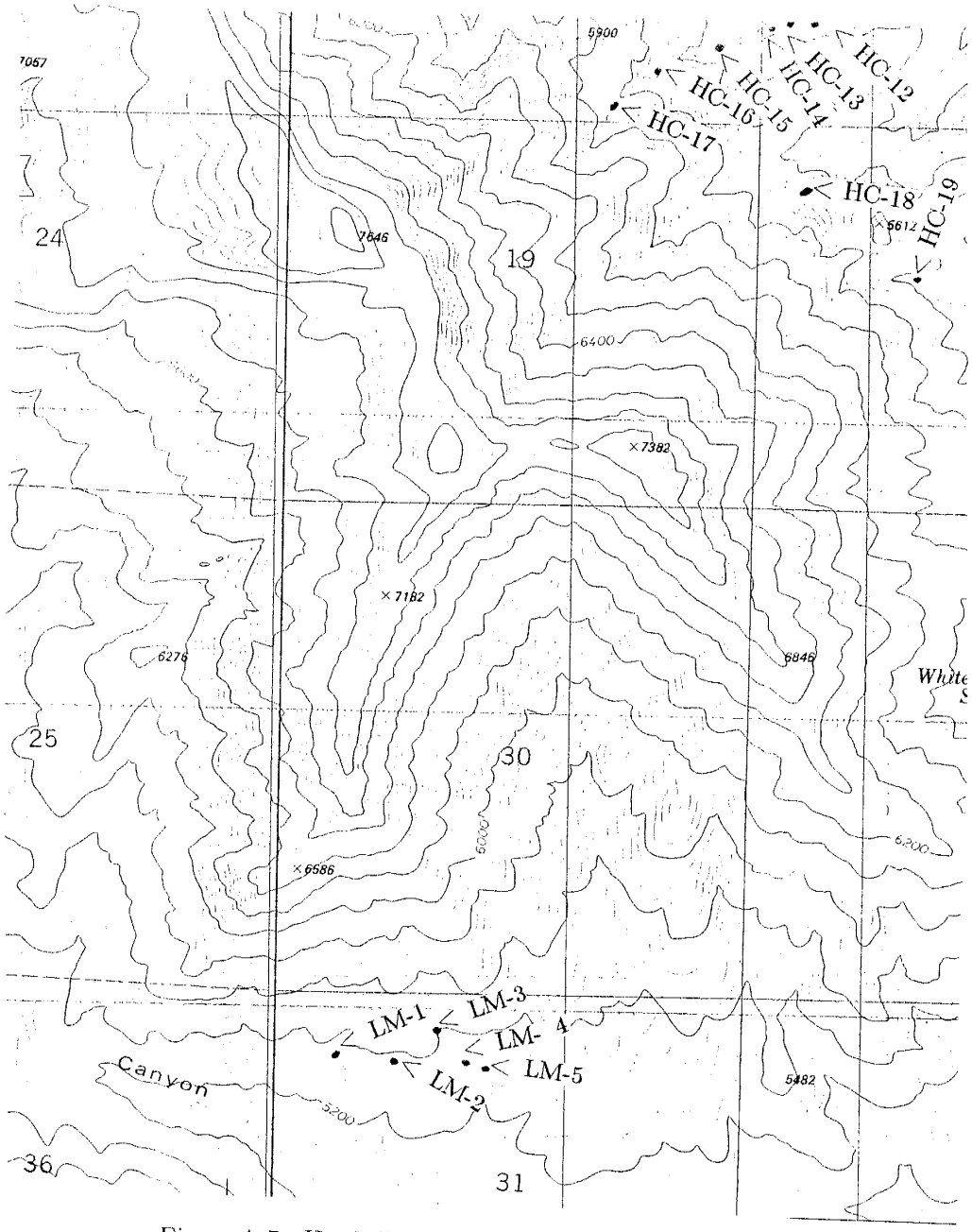

Figure A-7: Hembrillo Canyon 7.5 Minute Quadrangle.

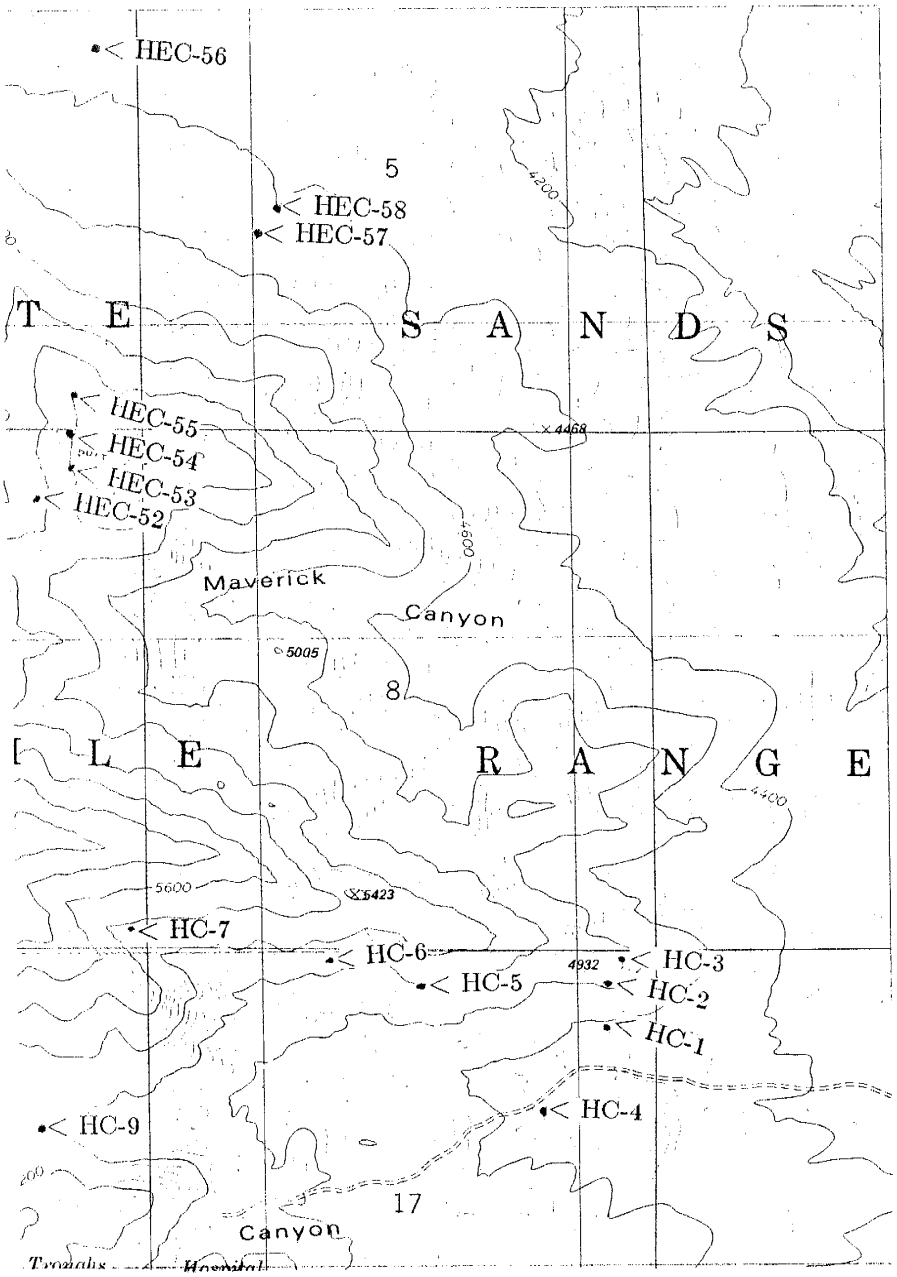

Figure A-8: Hembrillo Canyon 7.5 Minute Quadrangle.

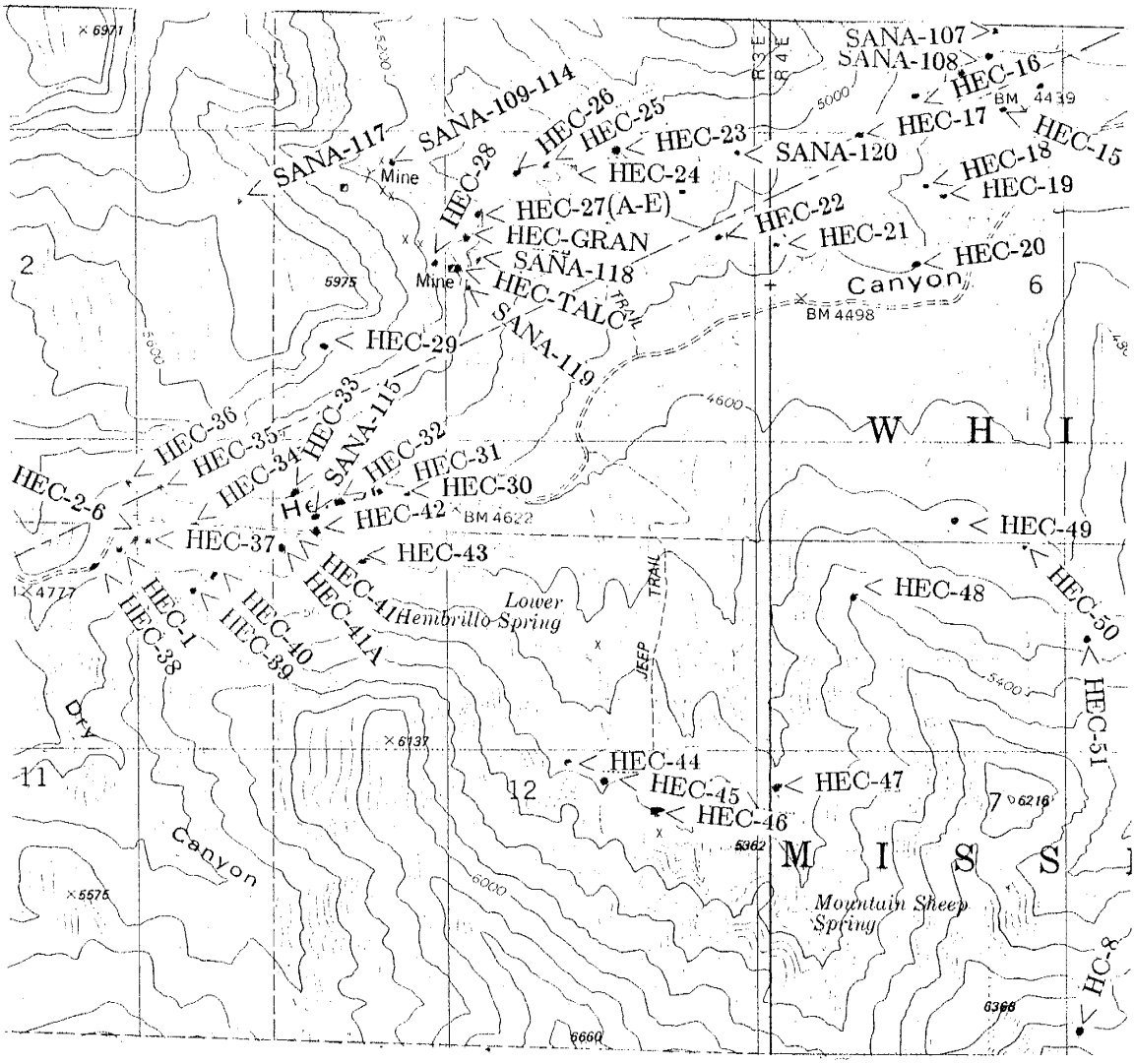

Figure A-9: Hembrillo Canyon 7.5 Minute Quadrangle.

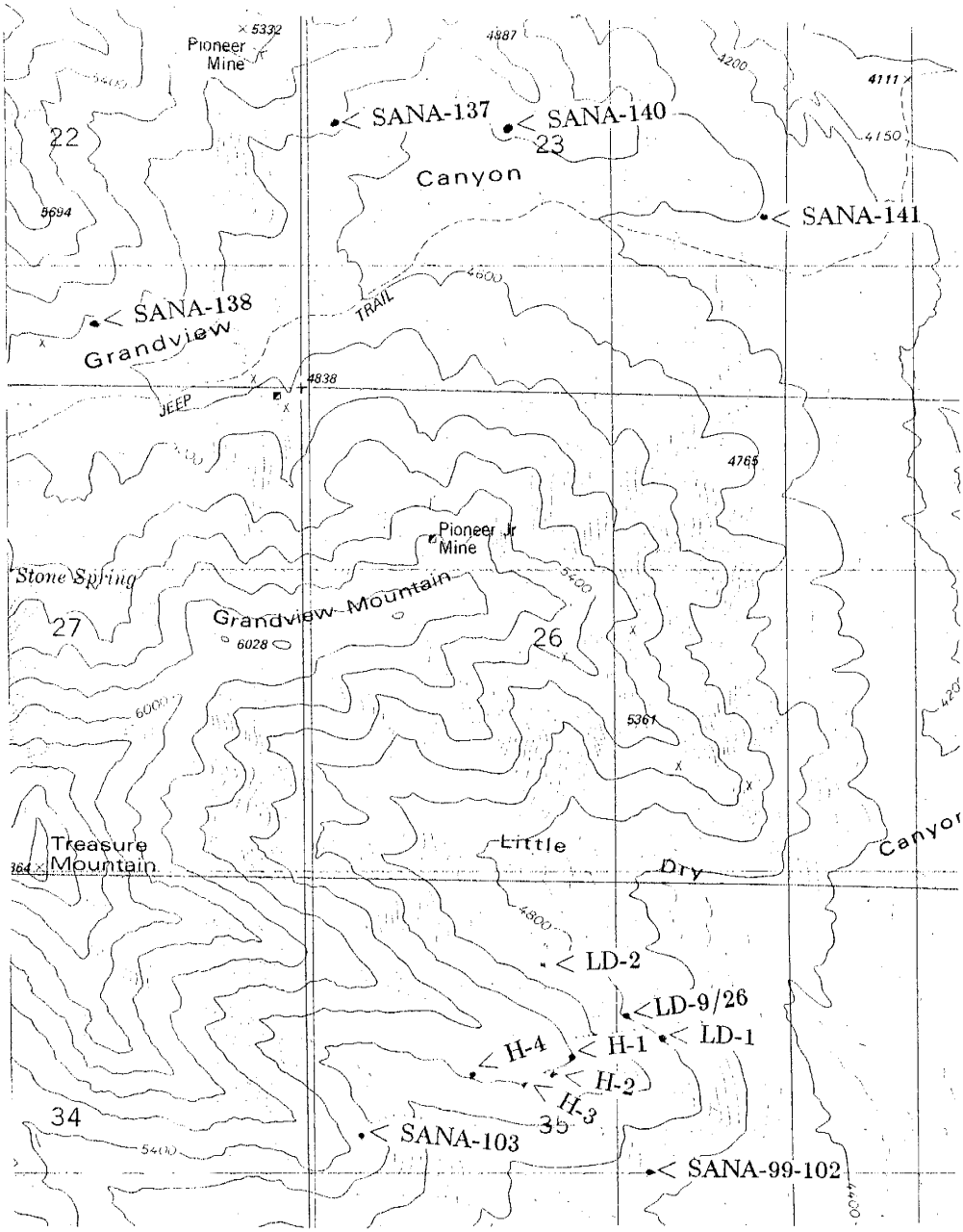

Figure A-10: Hembrillo Canyon 7.5 Minute Quadrangle.

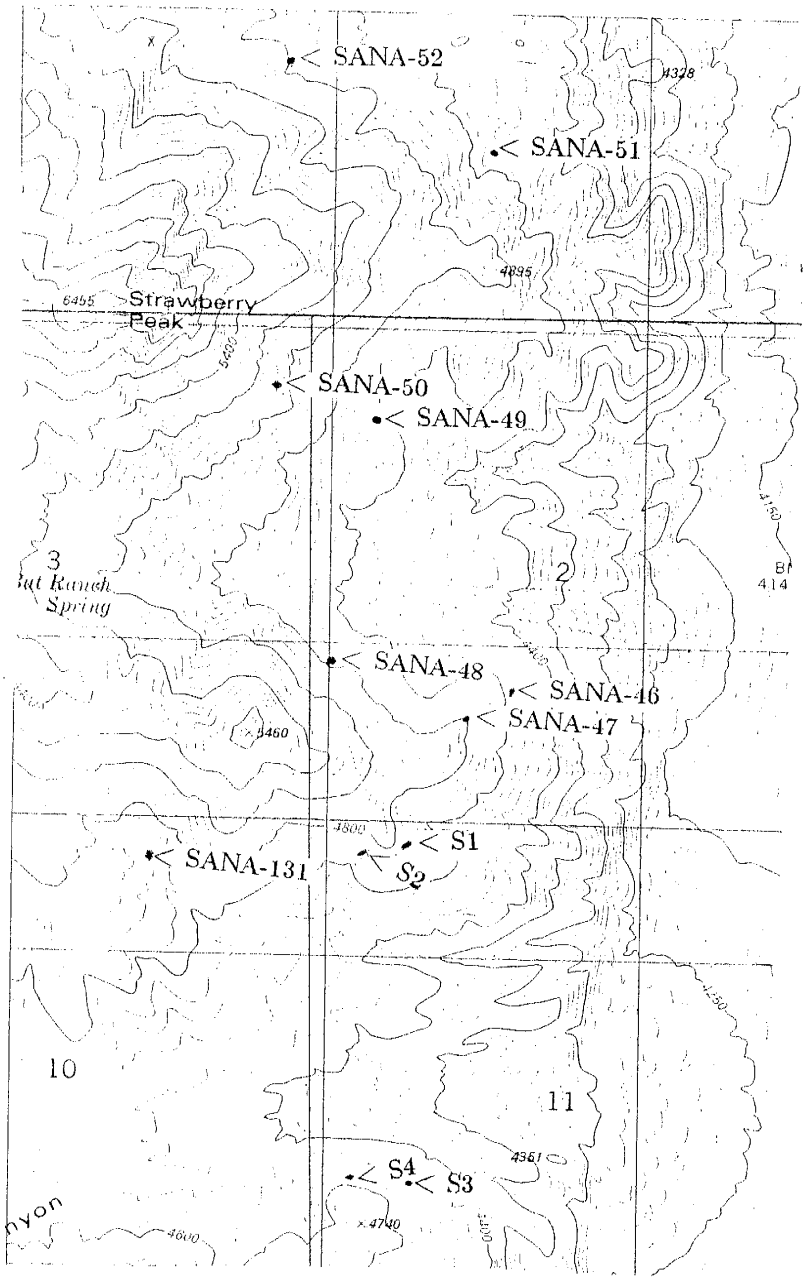

Figure A-11: Strawberry Peak 7.5 Minute Quadrangle.

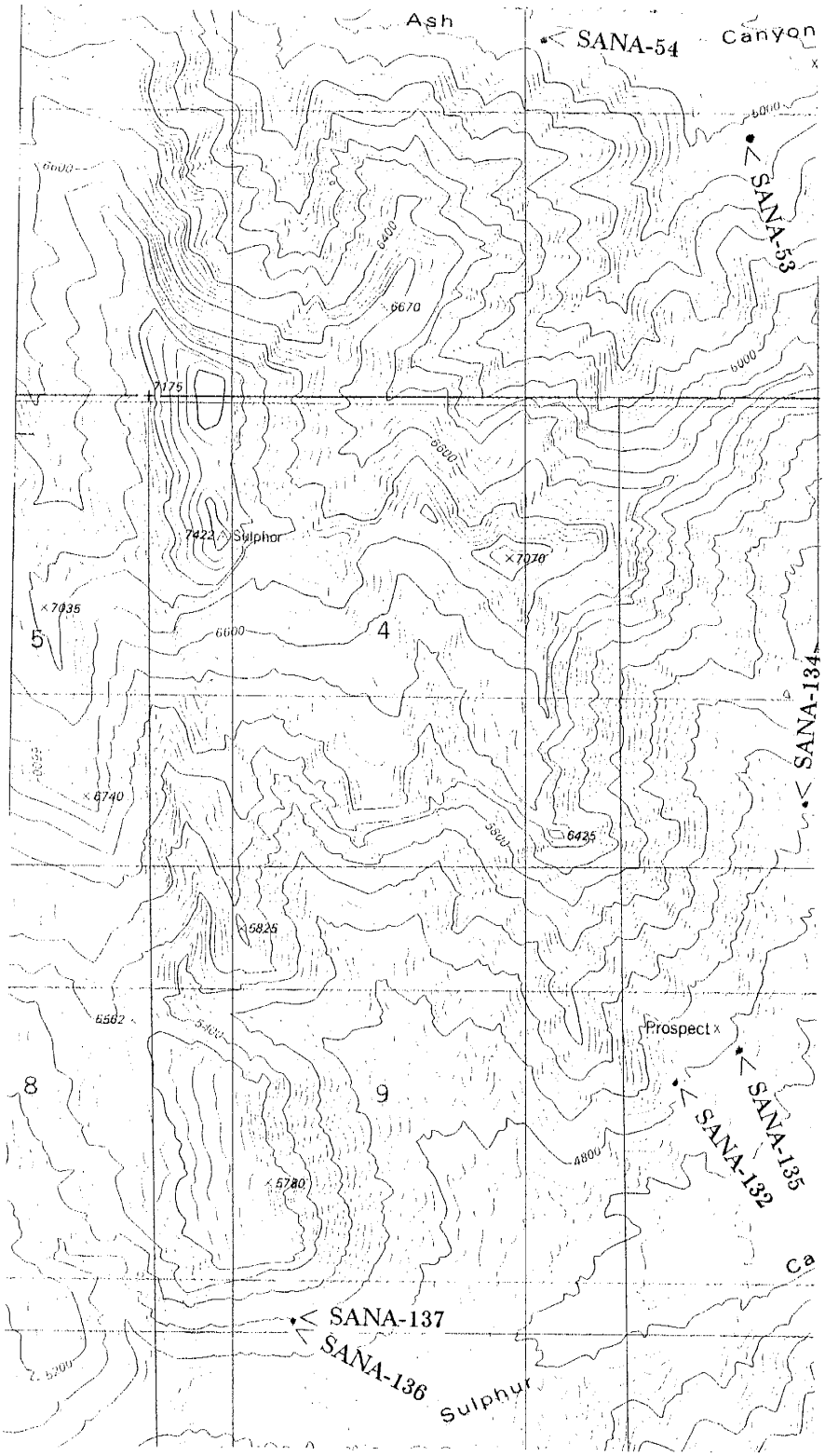

Figure A-12: Strawberry Peak 7.5 Minute Quadrangle.

APPENDIX B

Geochemical Data and CIPW Normative Minerals

EXPLANATION

$Fe_2O_{3_T}$: Total iron as Fe_2O_3

LOI: Loss on ignition

Major elements in %

Trace and rare earth elements in PPM

Mg number:

$(MgO/(MgO + (0.79*Fe_2O_{3_T})))*100$, molar proportions

CIA = Chemical index of alteration

$(Al_2O_3/(Al_2O_3 + K_2O + CaO + Na_2O))$, molar proportions

ERR = no value for calculation or division by zero for ratio calculation

Blank = not determined

TABLE B-1

Chemical Compositions of Mafic Metaigneous Rocks

SAMPLE	SANA-16	SANA-19	SANA-37	SANA-38	SANA-65
SiO_2	49.84	49.25	49.32	49.04	47.83
TiO_2	1.89	1.01	1.17	0.91	1.95
Al_2O_3	15.51	14.73	14.39	16.30	12.76
Fe_2O_3-T	14.99	12.53	12.99	10.81	16.82
MgO	6.39	7.88	7.07	7.72	6.11
CaO	7.49	9.76	11.16	11.04	9.07
Na_2O	2.79	2.58	2.54	2.66	1.85
K_2O	1.43	1.54	0.72	1.27	1.11
MnO	0.19	0.18	0.13	0.16	0.28
P_2O_5	0.15	0.17	0.21	0.07	0.20
LOI	1.6	1.2	0.13	1.2	1.1
TOTAL	102.25	100.83	99.83	101.19	99.08
Rb	98.9	72.8	17.6	78.5	75.8
Ba	136.0	124.5	105.0	163.8	140.0
Cs	1.1	0.8	0.5	2.7	1.2
Sr	199.1	221.6	230.4	261.5	116.8
Pb	7.8	17.2	19.7	18.2	10.9
Th	3.8	2.1	2.6	2.5	3.0
U	1.87	3.20	2.10	1.99	0.97
Sc	17.2	24.4	38.9	35.0	39.1
V	331.7	311.3	344.2	262.6	428.7
Cr	140.0	144.2	175.2	254.0	67.8
Co	36.7	24.5	40.8	45.4	41.5
Ni	138.5	59.0	46.0	147.0	42.0
Y	26.5	27.8	30.5	23.1	47.7
Zr	76.4	75.2	84.5	55.9	139.3
Nb	3.8	4.3	3.6	2.9	6.6
Hf	1.7	1.3	2.2	1.6	3.3
Ta	0.10	0.07	0.92	0.06	0.79
La	3.5	4.8	6.4	2.9	8.5
Ce	8.3	10.9	15.3	7.5	23.4
Sm	2.55	2.22	3.24	2.11	4.42
Eu	0.79	0.70	0.92	0.74	1.17
Tb	0.56	0.38	0.61	0.49	0.87
Yb	1.30	1.41	2.39	1.81	3.32
Lu	0.15	0.24	0.39	0.32	0.60
Mg Number	48.9	58.5	55.0	61.5	45.0

TABLE B-1 (continued)

Chemical Compositions of Mafic Metaigneous Rocks

SAMPLE	SANA-69	HEC-1	HEC-19	HEC-22	HEC-28
SiO_2	46.26	48.71	48.02	45.02	50.76
TiO_2	2.82	3.04	1.51	1.39	1.32
Al_2O_3	13.64	14.8	15.23	16.01	14.63
Fe_2O_3-T	19.83	20.26	12.48	13.00	10.45
MgO	5.68	5.27	6.98	7.29	7.57
CaO	8.59	0.66	9.57	6.55	5.52
Na_2O	2.54	0.11	2.56	2.15	4.97
K_2O	0.76	2.27	0.84	0.77	0.34
MnO	0.28	0.08	0.19	0.16	0.33
P_2O_5	0.37	0.36	0.21	0.17	0.17
LOI	0.40	7.84	0.10	7.13	2.89
TOTAL	101.18	103.40	97.69	99.64	98.95
Rb	31.5	173.6	41.0	32.7	7.9
Ba	100.5	180.0	692.5	218.7	
Cs	0.2	0.2	4.1	0.6	0.4
Sr	205.5	19.1	202.0	172.2	10.9
Pb	24.3	14.2	8.1	13.6	12.4
Th	2.9	6.3	2.3	2.0	3.1
U		3.38	0.46	1.81	1.18
Sc	46.1	50.0	40.2	19.2	32.3
V	507.5	389.7	315.0	229.1	227.4
Cr	117.5	92.5	255.0	44.9	439.0
Co	51.4	42.9	48.5	36.2	44.8
Ni	38.0	32.0	95.0	112.5	156.0
Y	58.9	41.3	36.6	34.0	31.9
Zr	208.1	227.9	121.5	125.1	121.4
Nb	7.6	11.3	4.3	6.8	6.3
Hf	5.3	5.9	3.5	2.4	3.0
Ta	0.47	0.54	0.19	0.24	0.26
La	13.3	25.1	8.5	6.5	7.5
Ce	16.3	58.5	19.4	15.3	17.5
Sm	7.32	8.83	4.64	3.39	3.75
Eu	2.19	1.94	1.31	0.96	0.93
Tb	1.59	1.09	0.92	0.60	0.69
Yb	4.77	4.04	3.35	2.39	3.07
Lu	0.73	0.70	0.61	0.40	0.44
Mg Number	39.2	36.9	55.7	55.8	61.9

TABLE B-1 (continued)

Chemical Compositions of Mafic Metaigneous Rocks

SAMPLE	HEC-32	HEC-33	HEC-34	HEC-35
SiO_2	45.77	48.23	44.59	42.31
TiO_2	2.65	1.81	1.5	3.27
Al_2O_3	13.91	15.34	15.55	13.94
Fe_2O_3-T	16.15	12.7	13.03	18.33
MgO	6.15	6.48	7.78	4.84
CaO	7.97	6.82	10.28	10.01
Na_2O	2.26	4.07	1.57	0.64
K_2O	0.06	0.42	0.48	1.95
MnO	0.23	0.25	0.19	0.28
P_2O_5	0.32	0.24	3.6	0.60
LOI	3.2	3.2	3.2	2.74
TOTAL	98.66	99.56	101.77	98.91
Rb	5.6	17.2	16.9	155.8
Ba	110.5		115.0	139.7
Cs	0.2	0.8	0.3	14.0
Sr	311.7	152.6	207.4	234.6
Pb	11.1	15.7	14.3	21.2
Th	2.2	2.2	2.3	6.6
U	1.89	1.23	0.48	2.44
Sc	39.0	23.4	41.6	27.4
V	445.2	231.6	324.4	328.3
Cr	116.2	189.8	148.2	26.8
Co	41.6	42.0	53.7	26.3
Ni	68.0	124.0	133.5	32.0
Y	50.4	36.1	30.0	82.2
Zr	198.0	151.9	100.9	392.7
Nb	9.5	6.3	4.5	12.9
Hf	5.2	2.7	2.7	4.3
Ta	0.48	0.26	0.18	0.58
La	15.4	7.4	7.4	15.3
Ce	42.6	18.1	18.1	38.7
Sm	6.97	3.98	3.71	6.78
Eu	1.92	0.84	1.13	1.50
Tb	1.32	0.72	0.73	1.42
Yb	4.48	2.4	2.80	4.02
Lu	0.70	0.34	0.39	0.57
Mg Number	46.1	53.4	57.3	37.2

TABLE B-1 (continued)

Chemical Compositions of Mafic Metaigneous Rocks

SAMPLE	HEC-37	HEC-40	G-5	M-27	LM-3
SiO_2	53.34	48.16	45.51	47.21	44.26
TiO_2	1.56	1.63	2.42	1.40	1.02
Al_2O_3	14.80	15.46	16.87	17.11	16.53
Fe_2O_3-T	15.59	11.85	13.48	12.63	11.96
MgO	4.69	6.21	5.61	6.23	8.38
CaO	2.56	8.20	6.24	8.79	8.58
Na_2O	3.90	4.00	3.77	2.83	2.06
K_2O	0.84	0.34	1.88	1.38	1.81
MnO	0.21	0.33	0.16	0.18	0.17
P_2O_5	0.17	0.24	0.42	0.15	0.09
LOI	3.34	2.75	0.9	0.4	1.2
TOTAL	101.01	99.17	97.26	98.30	96.07
Rb	36.6	11.2	59.5	81.0	88.0
Ba	223.3	68.3	520.4	195.5	145.7
Cs	4.0	0.2	0.8	1.8	2.5
Sr	62.0	191.1	455.5	203.5	244.5
Pb	10.6	14.7	7.2	10.6	11.6
Th	1.3	2.4	5.4	4.9	4.2
U	0.00	2.87	4.5	4.11	3.04
Sc	23.5	21.4	15.8	39.3	23.8
V	244.0	232.6	255.6	329.6	211.1
Cr	126.1	172.8	10.4	120.2	29.7
Co	34.6	36.1	36.2	47.0	63.5
Ni	90.0	126.5	41.0	65.5	120.0
Y	39.6	33.2	35.4	31.8	32.5
Zr	120.5	137.7	176.1	90.0	73.7
Nb	5.4	5.6	28.9	1.2	0.5
Hf	2.8	2.4	3.1	2.3	1.8
Ta	0.23	0.21	1.32	0.15	0.08
La	8.1	7.2	16.2	6.4	0.3
Ce	19.1	17.8	36.7	16.9	11.8
Sm	3.92	3.37	5.71	3.48	3.59
Eu	1.09	0.89	1.36	1.27	0.74
Tb	0.76	0.69	0.68	0.67	0.54
Yb	2.42	2.18	2.09	2.63	2.05
Lu	0.40	0.28	0.31	0.40	0.33
Mg Number	40.4	54.1	48.3	52.6	61.2

TABLE B-1 (continued)

Chemical Compositions of Mafic Metaigneous Rocks

SAMPLE	MEAN	STD. DEV.
SiO_2	47.50	2.48
TiO_2	1.77	0.69
Al_2O_3	15.13	1.08
Fe_2O_3-T	14.07	2.80
MgO	6.60	1.03
CaO	7.84	2.57
Na_2O	2.67	1.14
K_2O	1.02	0.62
MnO	0.21	0.07
P_2O_5	0.40	0.74
LOI	2.47	2.11
TOTAL	99.69	1.74
Rb	55.77	46.59
Ba	184.13	152.36
Cs	1.83	3.04
Sr	192.47	96.29
Pb	13.87	4.43
Th	3.28	1.43
U	1.99	1.25
Sc	31.18	9.91
V	309.05	81.03
Cr	148.77	101.57
Co	41.71	8.71
Ni	89.63	41.94
Y	37.82	13.25
Zr	139.15	74.25
Nb	6.86	5.85
Hf	2.96	1.25
Ta	0.37	0.32
La	8.89	5.50
Ce	22.48	12.82
Sm	4.35	1.78
Eu	1.17	0.42
Tb	0.79	0.32
Yb	2.75	0.95
Lu	0.43	0.16
Mg Number	51.45	8.06

TABLE B-1 (continued)

Ratios for Chemical Compositions of Mafic Metaigneous Rocks

SAMPLE	SANA-16	SANA-19	SANA-37	SANA-38	SANA-65
K_2O/Na_2O	0.51	0.60	0.28	0.48	0.60
Na_2O+K_2O	4.21	4.13	3.26	3.93	2.97
Al_2O_3/TiO_2	8.2	14.6	12.3	17.9	6.5
CaO/TiO_2	4.0	9.7	9.5	12.1	4.6
Zr/TiO_2	0.004	0.007	0.007	0.006	0.007
K/Rb	119.7	175.7	341.0	134.1	121.9
Ba/Sr	0.68	0.56	0.46	0.63	1.20
Rb/Sr	0.50	0.34	0.08	0.30	0.65
La/Yb	2.7	3.4	2.7	1.6	2.6
La/Sm	1.4	2.1	2.0	1.4	1.9
Sm/Eu	3.2	3.2	3.5	2.9	3.8
Ti/Zr	148.4	80.4	83.1	97.9	84.1
Zr/Nb	20.3	17.5	23.3	19.3	21.1
Nb/Y	0.14	0.15	0.12	0.13	0.14
Zr/Y	2.9	2.7	2.8	2.4	2.9
Nb/Ta	37.0	57.6	3.9	49.2	8.4
Nb/La	1.06	0.90	0.57	1.01	0.78
La/Ta	34.9	63.9	7.0	48.8	10.8
La/Th	0.9	2.3	2.5	1.2	2.8
Y/Tb	46.9	72.7	50.0	47.6	54.9
Th/Yb	2.90	1.50	1.07	1.38	0.91
Ta/Yb	0.08	0.05	0.39	0.03	0.24
Hf/Th	0.44	0.62	0.86	0.63	1.08
Ti/V	34.2	19.4	20.4	20.8	27.3
U/Pb	0.24	0.19	0.11	0.11	0.09
FeO-T/MgO	2.11	1.43	1.65	1.26	2.48
Sm/Yb	1.96	1.57	1.35	1.16	1.33

TABLE B-1 (continued)

Ratios for Chemical Compositions of Mafic Metaigneous Rocks

SAMPLE	SANA-69	HEC-1	HEC-19	HEC-22	HEC-28
K_2O/Na_2O	0.30	20.27	0.33	0.36	0.07
Na_2O+K_2O	3.31	2.38	3.40	2.91	6.31
Al_2O_3/TiO_2	4.8	4.9	10.1	11.5	11.1
CaO/TiO_2	3.1	0.2	6.3	4.7	4.2
Zr/TiO_2	0.01	0.01	0.01	0.01	0.01
K/Rb	201.3	108.5	170.0	193.9	360.8
Ba/Sr	0.49	9.42	3.43	1.27	18.71
Rb/Sr	0.15	9/09	0.20	0.19	0.73
La/Yb	2.8	6.2	2.5	2.7	2.4
La/Sm	1.8	2.8	1.8	1.9	2.0
Sm/Eu	3.3	4.6	3.5	3.5	4.0
Ti/Zr	81.2	80.0	74.6	66.6	65.2
Zr/Nb	27.4	20.2	28.1	18.3	19.3
Nb/Y	0.13	0.27	0.12	0.20	0.20
Zr/Y	3.5		5.5	3.3	3.7
Nb/Ta	16.1	21.0	22.4	28.9	24.5
Nb/La	0.57	0.45	0.51	1.05	0.84
La/Ta	28.1	46.8	44.0	27.4	29.1
La/Th	4.6	4.0	3.6	3.2	2.4
Y/Tb	37.0	37.8	39.7	56.9	46.4
Th/Yb	0.60	1.56	0.70	0.85	1.00
Ta/Yb	0.10	0.13	0.06	0.10	0.08
Hf/Th	1.85	0.93	1.48	1.21	0.97
Ti/V	33.3	46.8	28.8	36.4	34.8
U/Pb	0.00	0.24	0.06	0.13	0.10
FeO-T/MgO	3.14	3.46	1.61	1.60	1.24
Sm/Yb	1.53	2.19	1.39	1.42	1.22

TABLE B-1 (continued)

Ratios for Chemical Compositions of Mafic Metaigneous Rocks

SAMPLE	HEC-32	HEC-33	HEC-34	HEC-35	HEC-36
K_2O/Na_2O	0.02	0.10	0.31	3.03	0.07
Na_2O+K_2O	2.32	4.49	2.05	2.59	3.82
Al_2O_3/TiO_2	5.2	8.5	10.4	4.3	13.4
CaO/TiO_2	3.0	3.8	6.9	3.1	7.1
Zr/TiO_2	0.01	0.01	0.01	0.01	0.01
K/Rb	80.9	202.7	235.3	103.9	157.9
Ba/Sr	0.00	0.72	0.55	0.60	0.68
Rb/Sr	0.02	0.11	0.08	0.66	0.09
La/Yb	3.4	3.1	2.7	3.8	3.4
La/Sm	2.2	1.9	2.0	2.3	2.4
Sm/Eu	3.6	4.8	3.3	4.5	3.1
Ti/Zr	80.3	71.5	89.2	50.0	63.4
Zr/Nb	21.0	24.1	22.6	30.4	20.9
Nb/Y	0.19	0.17	0.15	0.16	0.19
Zr/Y	3.9	4.2	3.4	4.8	4.0
Nb/Ta	19.9	24.3	25.3	22.1	28.3
Nb/La	0.61	0.85	0.60	0.84	0.71
La/Ta	32.3	28.6	42.2	26.2	39.8
La/Th	7.1	3.4	3.2	2.3	2.0
Y/Tb	38.3	50.2	40.9	57.9	54.9
Th/Yb	0.48	0.92	0.82	1.63	1.68
Ta/Yb	0.11	0.11	0.06	0.15	0.09
Hf/Th	2.39	1.22	1.17	0.66	0.58
Ti/V	35.7	46.9	27.7	59.8	29.1
U/Pb	0.17	0.08	0.03	0.11	0.17
FeO-T/MgO	2.36	1.76	1.51	3.41	1.36
Sm/Yb	1.56	1.66	1.32	1.69	1.46

TABLE B-1 (continued)

Ratios for Chemical Compositions of Mafic Metaigneous Rocks

SAMPLE	HEC-37	HEC-40	G-5	M-27	LM-3
K_2O/Na_2O	0.22	0.09	0.50	0.49	0.88
Na_2O+K_2O	4.75	4.34	5.65	4.21	3.87
Al_2O_3/TiO_2	9.5	9.5	7.0	12.2	16.1
CaO/TiO_2	1.6	5.0	2.6	6.3	8.4
Zr/TiO_2	0.01	0.01	0.01	0.01	0.01
K/Rb	191.1	255.8	261.7	141.8	170.7
Ba/Sr	3.60	0.361.14	0.96	0.60	
Rb/Sr	0.59	0.06	0.13	0.40	0.36
La/Yb	3.3	3.3	7.8	2.4	0.2
La/Sm	2.1	2.1	2.8	1.8	0.1
Sm/Eu	3.6	3.8	4.2	2.7	4.8
Ti/Zr	77.6	70.9	82.5	93.5	83.4
Zr/Nb	22.5	24.5	6.1	75.6	144.4
Nb/Y	0.14	0.17	0.82	0.04	0.02
Zr/Y	3.0	4.2	5.0	2.8	2.3
Nb/Ta	23.6	26.7	21.9	7.8	6.2
Nb/La	0.66	0.78	1.78	0.19	1.53
La/Ta	35.5	34.2	12.3	42.0	4.0
La/Th	6.0	2.9	3.0	1.3	0.1
Y/Tb	51.9	48.2	51.9	47.5	59.9
Th/Yb	0.55	1.12	2.57	1.88	2.04
Ta/Yb	0.09	0.10	0.63	0.06	0.04
Hf/Th	2.11	0.99	0.58	0.46	0.43
Ti/V	38.3	41.9	56.9	25.5	29.1
U/Pb	0.00	0.19	0.63	0.39	0.26
FeO-T/MgO	2.99	1.72	2.16	1.82	1.28
Sm/Yb	1.62	1.54	2.73	1.32	1.75

TABLE B-1 (continued)

Ratios for Chemical Compositions of Mafic Metaigneous Rocks

SAMPLE	MEAN	STD. DEV.
K_2O/Na_2O0	1.47	4.36
Na_2O+K_2O	3.69	0.96
Al_2O_3/TiO_2	9.90	3.76
CaO/TiO_2	5.30	2.90
Zr/TiO_2	0.01	0.00
K/Rb	186.44	72.99
Ba/Sr	2.30	4.28
Rb/Sr	0.74	1.93
La/Yb	3.15	1.51
La/Sm	1.94	0.56
Sm/Eu	3.70	0.59
Ti/Zr	81.19	18.78
Zr/Nb	30.35	29.09
Nb/Y	0.18	0.16
Zr/Y	3.55	0.85
Nb/Ta	23.75	12.85
Nb/La	0.81	0.35
La/Ta	31.90	14.65
La/Th	2.95	1.61
Y/Tb	49.58	8.53
Th/Yb	1.31	0.65
Ta/Yb	0.13	0.14
Hf/Th	1.03	0.55
Ti/V	34.66	10.95
U/Pb	0.16	0.14
FeO-T/MgO	2.02	0.71
Sm/Yb	1.59	0.35

TABLE B-2

Chemical Compositions of Felsic Metaigneous Rocks

SAMPLE	HEC-6	HEC-6-M	HEC-7	HEC-8
SiO_2	74.28	73.81	76.22	74.01
TiO_2	0.19	0.151	0.13	0.12
Al_2O_3	14.68	14.77	11.34	12.69
Fe_2O_3-T	0.80	1.03	1.69	1.50
MgO	0.32	0.33	0.43	0.49
CaO	0.25	0.25	0.73	0.56
Na_2O	0.17	0.23	0.31	0.48
K_2O	12.67	12.62	8.29	8.90
MnO			0.02	0.01
P_2O_5	0.07	0.07	0.03	0.04
LOI	1.17	1.17	0.6	0.48
TOTAL	104.29	104.42	99.79	99.27
Rb	203.0	200.6	219.2	109.8
Ba	1552.5	2155.0	1042.5	1697.5
Cs	0.7	1.0	0.6	0.97
Sr	28.8	31.7	77.3	70.7
Pb	14.4	13.7	23.2	24.1
Th	28.6	30.3	29.0	33.7
U	3.28	2.64	6.81	6.35
Sc	6.4	9.5	5.2	10.7
V	13.8	11.6	6.1	10.5
Cr	3.3	5.6		2.75
Co	1.5	2.3	1.3	2.5
Ni	2.0	5.0		
Y	76.7	71.7	118.8	122.9
Zr	226.6	233.9	200.4	260.3
Nb	22.8	22.1	20.6	17.6
Hf	6.2	8.9	3.9	8.3
Ta	1.67	2.24	1.13	2.08
La	50.4	70.6	33.5	66.0
Ce	109.9	160.6	70.8	159.3
Sm	11.50	16.18	9.96	19.62
Eu	1.38	2.13	0.57	1.35
Tb	1.32	1.87	1.89	3.66
Yb	5.89	8.58	5.95	9.68
Lu	0.96	1.46	0.87	1.47
Mg Number	33.6	41.74	36.43	42.30

TABLE B-2 (continued)

Chemical Compositions of Felsic Metaigneous Rocks

SAMPLE	HEC-38	LD-1	LD-926	MEAN	STD. DEV.
SiO_2	75.51	75.19	72.01	74.84	0.87
TiO_2	0.12	0.45	0.68	0.19	0.12
Al_2O_3	11.60	12.79	14.6	12.98	1.34
Fe_2O_3-T	2.59	2.77	3.61	1.73	0.73
MgO	0.37	0.61	1.05	0.38	0.18
CaO	0.14	0.84	0.15	0.46	0.27
Na_2O	0.09	3.67	0.92	0.82	1.28
K_2O	9.54	4.54	4.53	9.43	2.77
MnO		0.01	0.05	0.01	0.01
P_2O_5	0.04	0.09	0.04	0.05	0.02
LOI	0.5	0.2	2.05	0.69	0.36
TOTAL	100.5	101.14	99.68	101.57	7.94
Rb	164.6	184.5	246.0	180.28	35.79
Ba	1090.0	452.0	669.3	1331.58	544.11
Cs	0.5	2.1	9.5	0.97	0.53
Sr	30.9	64.0	50.56	20.48	
Pb	18.5	24.9	10.0	19.80	4.53
Th	26.3	39.2	13.0	31.18	4.23
U	5.28	8.14		5.42	1.94
Sc	3.1	5.8	10.4	6.78	2.57
V	14.9	18.5		12.56	3.85
Cr	0.5	7.9	40.3	4.01	2.53
Co	0.92	3.15	6.69	1.95	0.77
Ni		1.3	11.0	2.77	1.60
Y	58.9	95.1		90.65	23.86
Zr	200.4	450.0	230.0	261.94	86.58
Nb	23.2	11.3		19.58	4.15
Hf	4.7	10.8	8.1	7.14	2.43
Ta	1.31	1.33	1.1	1.63	0.41
La	16.1	44.6	26.8	46.86	18.58
Ce	36.1	104.7	61.1	106.88	44.65
Sm	4.20	11.88	5.4	12.22	4.84
Eu	0.49	0.94	0.98	1.14	0.56
Tb	1.03	1.86	1.1	1.94	0.83
Yb	4.35	7.07	4.2	6.92	1.78
Lu	0.68	1.08	0.63	1.09	0.29
Mg Number	24.2	33.0	30.98	11.84	

TABLE B-2 (continued)

Ratios of Chemical Compositions of Felsic Metaigneous Rocks

SAMPLE	HEC-6	HEC-6-M	HEC-7	HEC-8
K_2O/Na_2O	76.30	55.84	26.56	18.75
Na_2O+K_2O	12.83	12.85	8.60	9.38
Al_2O_3/TiO_2	78.90	97.79	89.29	103.98
CaO/TiO_2	1.33	1.63	5.75	4.62
Zr/TiO_2	0.12	0.15	0.16	0.21
K/Rb	517.73	522.19	313.75	673.38
Ba/Sr	53.83	68.07	13.49	24.01
Rb/Sr	7.04	6.34	2.84	1.55
La/Yb	8.56	8.23	5.63	6.82
La/Sm	4.38	4.36	3.36	3.36
Sm/Eu	8.31	7.58	17.35	14.57
Ti/Zr	4.92	3.87	3.80	2.81
Zr/Nb	9.95	10.61	9.75	14.83
Nb/Y	0.30	0.31	0.17	0.14
Zr/Y	2.96	3.26	1.69	2.12
Nb/Ta	13.63	9.84	18.19	8.43
Nb/La	0.45	0.31	0.61	0.27
La/Ta	30.19	31.53	29.62	31.66
La/Th	1.76	2.33	1.15	1.95
Y/Tb	58.20	38.38	62.90	33.60
Th/Yb	4.85	3.53	4.88	3.49
Ta/Yb	0.28	0.26	0.19	0.22
Hf/Th	0.22	0.29	0.13	0.25
Ti/V	80.87	78.10	124.92	69.71
U/Pb	0.23	0.19	0.29	0.26
FeO-T/MgO	22.61	2.82	3.53	2.76
Sm/Yb	1.95	1.89	1.67	2.03

TABLE B-2 (continued)

Ratios of Chemical Compositions of Felsic Metaigneous Rocks

SAMPLE	HEC-38	LD-1	MEAN	STD. DEV.
K_2O/Na_2O	109.64	1.24	48.05	36.89
Na_2O+K_2O	9.63	8.21	10.25	1.89
Al_2O_3/TiO_2	93.58	28.73	82.04	25.05
CaO/TiO_2	1.11	1.89	2.72	1.79
Zr/TiO_2	0.16	0.10	0.15	0.04
K/Rb	481.01	204.19	452.04	152.54
Ba/Sr	35.33	7.06	33.63	21.61
Rb/Sr	5.34	2.88	4.33	2.02
La/Yb	3.70	6.31	6.54	1.63
La/Sm	3.84	3.75	3.84	0.42
Sm/Eu	8.62	12.65	11.51	3.62
Ti/Zr	3.71	5.93	4.18	1.00
Zr/Nb	8.63	39.82	15.60	11.01
Nb/Y	0.39	0.12	0.24	0.10
Zr/Y	3.40	4.73	3.03	0.98
Nb/Ta	17.78	8.50	12.73	4.10
Nb/La	1.44	0.25	0.56	0.41
La/Ta	12.34	33.55	28.15	7.18
La/Th	0.61	1.14	1.49	0.58
Y/Tb	57.15	51.14	50.23	10.72
Th/Yb	6.04	5.54	4.72	0.95
Ta/Yb	0.30	0.19	0.24	0.04
Hf/Th	0.18	0.28	0.22	0.06
Ti/V	49.93	144.64	91.36	32.75
U/Pb	0.29	0.33	0.26	0.04
FeO-T/MgO	6.33	4.11	7.03	7.07
Sm/Yb	0.96	1.68	1.70	0.35

TABLE B-3

Chemical Compositions of Quartzose Metasedimentary Rocks

SAMPLE	HEC-9	HEC-10	HEC-11A	HEC-12	HEC-13
SiO_2	91.68	82.50	97.34	89.46	95.74
TiO_2	0.41	0.54	0.08	0.29	0.05
Al_2O_3	6.81	7.81	2.60	5.20	1.66
Fe_2O_3-T	2.27	3.49	0.29	1.97	1.06
MgO	0.35	0.77	0.04	0.44	0.35
CaO	0.10	0.12	0.03	0.09	0.03
Na_2O	0.69	0.85	0.11	0.42	0.03
K_2O	1.97	1.99	0.72	1.40	0.39
MnO	0.02	0.02			
P_2O_5	0.04	0.06	0.03	0.07	0.04
LOI	0.98	1.4	0.70	0.9	0.01
TOTAL	105.32	99.56	99.94	100.26	99.34
Rb	87.6	81.5	28.0	66.2	11.9
Ba	300.5	696.1	232.1	208.5	261.3
Cs	5.5	4.1	1.0	6.3	0.7
Sr	37.3	37.1	5.8	17.2	5.3
Pb	22.7	29.2	15.6	23.0	14.3
Th	10.1	21.9	2.4	6.5	1.7
U	2.66	3.54	1.42	2.76	1.02
Sc	10.6	5.3	0.8	2.9	0.6
V	34.0	54.4	1.7		1.4
Cr	29.9	46.4	2.5	17.2	9.8
Co	16.0	9.5	0.4	4.4	1.3
Ni	5.0	7.0	0.2	7.3	3.0
Y	30.8	57.8	18.3	26.0	16.5
Zr	285.0	736.2	51.1	175.9	47.5
Nb	6.2	6.1	0.4	5.2	0.4
Hf	5.2	6.6	1.0	4.2	0.8
Ta	1.01	0.86	0.13	0.45	0.10
La	22.3	29.1	5.6	13.4	6.8
Ce	56.8	74.2	16.5	37.3	17.7
Sm	4.38	6.09	1.39	2.61	1.68
Eu	0.91	0.92	0.23	0.41	0.24
Tb	0.66	0.97	0.37	0.44	0.25
Yb	2.84	4.13	0.88	1.80	0.68
Lu	0.45	0.49	0.12	0.30	0.10
CIA	66.32	67.39	72.07	68.73	76.47

TABLE B-3 (continued)

Chemical Compositions of Quartzose Metasedimentary Rocks

SAMPLE	HEC-14	HEC-16	HEC-17	HEC-21	HEC-30
SiO_2	98.11	90.70	97.90	97.74	94.27
TiO2	0.06	0.09	0.04	0.06	0.21
Al_2O3	1.03	4.90	0.62	1.08	2.76
Fe_2O_3-T	0.54	1.64	1.27	0.31	1.92
MgO	0.05	0.40	0.01	0.04	0.18
CaO	0.13	0.03	0.03	0.02	0.05
Na_2O	0.08		0.06	0.02	
K_2O	0.17	2.16	0.14	0.30	0.65
MnO			0.01		0.04
P_2O_5	0.03	0.04	0.03	0.02	0.04
LOI	0.21	0.7	0.26	0.41	0.65
TOTAL	100.39	100.65	100.35	100.00	100.76
Rb	0.9	86.7	6.4	5.5	29.0
Ba	253.3	546.4	234.0	247.5	244.3
Cs	0.3	3.6	0.4	0.1	0.4
Sr	4.8	18.1	3.1	2.4	5.5
Pb	17.6	13.9	5.9	17.3	20.5
Th	1.9	6.1	0.9	2.4	6.5
U	1.68	1.36	2.16	2.28	1.07
Sc	0.4	1.7	0.3	0.3	2.2
V	0.7	23.7			10.8
Cr	2.1	6.8	5.9	2.1	8.4
Co	0.6	1.8	0.3	0.3	4.0
Ni		3.6	0.8	1.9	0.7
Y	12.2	22.3	21.2	10.6	18.1
Zr	33.5	62.9	19.1	46.2	199.7
Nb		1.7			1.3
Hf	0.8	1.4	0.5	0.8	5.6
Ta	0.08	0.26	0.04	0.10	0.26
La	4.9	11.0	1.7	4.4	7.8
Ce	13.9	29.8	4.4	10.0	25.5
Sm	1.02	2.47	0.62	0.90	1.79
Eu	0.18	0.46	0.18	0.13	0.45
Tb	0.19	0.38	0.41	0.15	0.33
Yb	0.49	1.17	1.10	0.50	1.29
Lu	0.08	0.20	0.15	0.08	0.24
CIA	65.34	67.14	67.90	74.01	77.74

TABLE B-3 (continued)

Chemical Compositions of Quartzose Metasedimentary Rocks

SAMPLE	HEC-47	HEC-48	M-12	MEAN	STD. DEV.
SiO_2	93.47	99.37	84.79	93.28	5.18
TiO_2	0.14	0.06	0.14	0.15	0.14
Al_2O3	2.72	1.18	7.95	3.29	2.48
Fe_2O_3-T	1.69	0.31	1.47	1.33	0.89
MgO	0.26	0.02	0.35	0.24	0.22
CaO	0.09	0.04	0.47	0.09	0.12
Na_2O	0.52	0.08	2.02	0.35	0.56
K_2O	0.26	0.23	2.59	0.92	0.85
MnO	0.01			0.01	0.01
P_2O_5	0.04	0.04	0.05	0.04	0.01
LOI	0.86	0.71	0.2	0.58	0.37
TOTAL	100.05	102.05	100.03	100.28	0.66
Rb	7.5	2.8	88.5	34.57	34.07
BaO	258.0	79.7	566.1	335.60	158.70
Cs7	0.7	0.3	2.3	1.69	1.90
Sr	5.0	4.1	37.6	12.91	12.10
Pb	17.8	13.1	21.5	17.46	5.58
Th	5.0	2.6	10.2	5.68	5.56
U	1.57	0.56	1.93	1.78	0.79
Sc	1.5	0.7	2.5	1.60	1.41
V	5.2	6.0	10.2	10.37	15.45
Cr	8.8	2.4	7.8	10.02	11.73
Co	2.4	0.3	3.5	2.40	2.59
Ni	4.2	1.3	3.3	2.78	2.36
Y	13.5	12.2	31.9	21.72	12.41
Zr	180.5	45.8	279.1	156.46	192.37
Nb	1.7			1.68	2.10
Hf	4.8	1.5	3.1	2.59	2.08
Ta	0.24	0.12	0.43	0.26	0.22
La	8.0	14.0	18.1	10.41	7.20
Ce	22.9	34.9	48.5	27.94	18.36
Sm	1.96	2.43	3.64	2.22	1.42
Eu	0.37	0.45	0.86	0.41	0.24
Tb	0.32	0.30	0.57	0.39	0.21
Yb	1.12	0.79	1.88	1.32	0.95
Lu	0.17	0.13	0.32	0.21	0.16
CIA	67.67	72.43	53.26	69.18	6.11

TABLE B-3 (continued)

Ratios for Chemical Compositions of Quartzose Metasedimentary Rocks

SAMPLE	HEC-10	HEC-11A	HEC-12	HEC-13	HEC-14
K_2O/Na_2O	2.33	6.29	3.34	15.60	2.20
SiO_2/Al_2O_3	10.56	36.61	17.21	57.71	95.72
Th/U	6.20	1.65	2.36	1.67	1.15
K/Rb	202.99	212.69	175.78	272.02	1521.67
Rb/Sr	2.20	4.87	3.85	2.25	0.19
Ba/Rb	8.54	8.30	3.15	21.96	281.44
Ba/Sr	18.75	40.37	12.12	49.30	53.21
Th/Sc	4.14	2.94	2.24	2.83	4.82
La/Sc	5.50	7.03	4.62	11.33	12.25
Zr/Y	12.74	2.79	6.77	2.88	2.74
Ti/Zr	4.42	9.74	9.82	6.56	10.38
Zr/Nb	119.90	134.45	33.83	118.75	ERR
La/Yb	7.05	6.37	7.44	10.00	9.98
La/Th	1.33	2.39	2.06	4.00	2.54
Ni/Co	0.74	0.51	1.66	2.31	0.00
Cr/V	0.85	1.45	ERR	7.00	3.23
V/Ni	7.77	8.65	0.00	0.47	ERR
Cr/Zr	0.06	0.05	0.10	0.21	0.06
Co/Th	0.43	0.17	0.68	0.76	0.33
Eu/Eu*	0.45	0.45	0.47	0.44	0.51

TABLE B-3 (continued)

Ratios for Chemical Compositions of Quartzose Metasedimentary Rocks

SAMPLE	HEC-16	HEC-17	HEC-21	HEC-30	HEC-47
K_2O/Na_2O	ERR	2.30	20.13	ERR	0.50
SiO_2/Al_2O_3	18.53	157.65	90.17	34.12	34.39
Th/U	4.49	0.41	1.07	6.09	3.15
K/Rb	207.12	178.97	456.58	185.24	291.50
Rb/Sr	4.80	2.07	2.34	5.24	0.53
Ba/Rb	6.30	36.56	45.08	8.43	34.58
Ba/Sr	30.27	75.73	105.32	44.18	18.35
Th/Sc	3.57	3.18	7.67	2.96	3.30
La/Sc	6.44	5.97	13.93	3.54	5.36
Zr/Y	2.82	0.90	4.35	11.04	13.41
Ti/Zr	8.10	10.99	8.30	6.27	4.62
Zr/Nb	37.92	ERR	ERR	152.44	105.57
La/Yb	9.39	1.52	8.91	6.04	7.20
La/Th	1.80	1.88	1.82	1.19	1.63
Ni/Co	1.97	2.96	6.74	0.18	1.73
Cr/V	0.29	ERR	ERR	0.78	1.68
V/Ni	6.59	0.00	0.00	15.44	1.25
Cr/Zr	0.11	0.31	0.05	0.04	0.05
Co/Th	0.30	0.30	0.12	0.61	0.49
Eu/Eu*	0.57	1.66	0.43	0.73	0.56

TABLE B-3 (continued)

Ratios for Chemical Compositions of Quartzose Metasedimentary Rocks

SAMPLE	HEC-48	M-12	MEAN	STD. DEV.
K_2O/Na_2O	2.91	1.28	ERR	ERR
SiO_2/Al_2O_3	84.21	10.66	53.96	42.99
Th/U	4.66	5.28	3.18	1.99
K/Rb	688.22	242.62	386.28	370.97
Rb/Sr	0.69	2.35	2.61	1.66
Ba/Rb	99.54	6.40	46.69	75.45
Ba/Sr	68.72	15.06	44.28	27.14
Th/Sc	3.53	4.08	3.77	1.35
La/Sc	18.90	7.24	8.51	4.40
Zr/Y	3.74	8.75	6.08	4.17
Ti/Zr	7.99	3.05	7.52	2.45
Zr/Nb	ERR	ERR	ERR	ERR
La/Yb	17.78	9.63	8.44	3.62
La/Th	5.36	1.77	2.31	1.15
Ni/Co	5.20	0.94	2.08	1.96
Cr/V	0.40	0.76	ERR	ERR
V/Ni	4.58	3.09	ERR	ERR
Cr/Zr	0.05	0.03	0.09	0.08
Co/Th	0.10	0.34	0.39	0.21
Eu/Eu*	0.60	0.72	0.63	0.33

TABLE B-4

Chemical Compositions of Quartz Wackes

SAMPLE	HEC-39	HEC-41	HEC-45	SANA-100
SiO_2	69.37	71.50	65.27	81.2
TiO_2	0.68	0.58	0.61	0.27
Al_2O_3	15.73	14.16	17.27	10.2
Fe_2O_3-T	6.67	3.59	5.41	2.31
MgO	1.69	0.90	1.28	0.51
CaO	0.39	0.86	0.65	0.56
Na_2O	0.16	1.70	1.43	2.37
K_2O	7.95	4.06	3.75	2.01
MnO	0.01	0.06	0.10	0.02
P_2O_5	0.15	0.09	0.10	0.04
LOI	2.44	2.21	4.8	1.2
TOTAL	105.22	99.71	100.67	100.68
Rb	155.0	195.7	188.6	84.0
Ba	510.8	906.9	538.5	453.0
Cs	2.0	5.3	5.5	4.3
Sr	5.0	57.0	49.8	51.0
Pb	5.6	13.0	17.4	20.0
Th	14.5	15.7	22.1	19.5
U	4.46	2.85	4.42	2.30
Sc	16.9	10.4	10.6	14.7
V		149.0		123.0
Cr	35.4	30.9	37.2	29.0
Co	7.6	6.5	9.6	7.7
Ni	11.0	3.0	8.0	
Y	51.3	54.6	43.0	26.0
Zr	236.5	243.2	210.5	261.0
Nb	12.9	11.6	14.4	11.0
Hf	4.7	6.6	5.2	6.7
Ta	0.87	0.90	1.01	0.85
La	13.1	37.3	28.6	19.0
Ce	32.1	90.4	75.2	39.0
Sm	3.36	7.25	4.91	3.50
Eu	0.69	1.44	0.90	0.68
Tb	0.74	1.15	0.83	0.51
Yb	2.96	3.97	2.97	2.60
Lu	0.45	0.64	0.46	0.41
CIA	62.15	61.79	69.45	58.98

TABLE B-4 (continued)

Chemical Compositions of Quartz Wackes

SAMPLE	SANA-110	MEAN	STD. DEV.
SiO_2	67.9	71.05	5.47
TiO_2	0.54	0.54	0.14
Al_2O_3	17.7	15.01	2.71
Fe_2O_3-T	4.03	4.40	1.50
MgO	0.96	1.07	0.40
CaO	0.45	0.58	0.16
Na_2O	2.51	1.63	0.84
K_2O	3.94	4.34	1.95
MnO	0.07	0.05	0.03
P_2O_5	0.05	0.08	0.04
LOI	2.32	2.59	1.19
TOTAL	100.48	101.35	1.97
Rb	201.0	164.86	43.49
Ba	1536.0	789.04	406.19
Cs	7.1	4.85	1.68
Sr	45.0	41.55	18.67
Pb	14.0	13.99	4.89
Th	22.0	18.77	3.14
U	5.10	3.83	1.06
Sc	16.0	13.72	2.72
V	144.0	138.67	11.26
Cr	44.0	35.30	5.26
Co	8.4	7.07	2.18
Ni		7.33	3.30
Y	64.0	47.78	12.80
Zr	289.0	248.05	26.11
Nb	19.0	13.78	2.86
Hf	8.0	6.24	1.17
Ta	1.60	1.05	0.28
La	61.0	31.78	16.79
Ce	76.0	62.53	22.79
Sm	11.00	6.00	2.86
Eu	0.98	0.94	0.28
Tb	1.70	0.99	0.41
Yb	6.00	3.70	1.24
Lu	0.86	0.56	0.17
CIA	65.77	63.63	3.62

TABLE B-4 (continued)

Ratios of Chemical Compositions of Quartz Wackes

SAMPLE	HEC-39	HEC-41	HEC-45	SANA-100
K_2O/Na_2O	50.29	2.38	2.62	0.85
SiO_2/Al_2O_3	4.41	5.05	3.78	7.96
Th/U	3.26	5.51	5.00	8.48
K/Rb	425.50	172.02	165.18	198.61
Rb/Sr	31.00	3.43	3.79	1.65
Ba/Rb	3.30	4.63	2.86	5.39
Ba/Sr	102.16	15.91	10.82	8.88
Th/Sc	0.86	1.51	2.08	1.33
La/Sc	0.77	3.59	2.69	1.29
Zr/Y	4.61	4.45	4.89	10.04
Ti/Zr	17.24	14.25	17.34	6.20
Zr/Nb	18.32	20.97	14.63	23.73
La/Yb	4.41	9.40	9.60	7.31
La/Th	0.90	2.38	1.29	0.97
Ni/Co	1.69	0.31	1.04	
Cr/V	ERR	0.21	ERR	0.24
V/Ni		49.67		ERR
Cr/Zr	0.15	0.13	0.18	0.11
Co/Th	0.45	0.61	0.35	0.16
Eu/Eu*	0.57	0.60	0.55	0.6

TABLE B-4 (continued)

Ratios of Chemical Compositions of Quartz Wackes

SAMPLE	SANA-110	MEAN	STD. DEV.
K_2O/Na_2O	1.57	11.54	19.38
SiO_2/Al_2O_3	3.84	5.01	1.55
Th/U	4.31	5.31	1.75
K/Rb	162.70	224.80	101.15
Rb/Sr	4.47	8.87	11.11
Ba/Rb	7.64	4.76	1.70
Ba/Sr	34.13	34.38	35.04
Th/Sc	1.38	1.43	0.39
La/Sc	3.81	2.43	1.21
Zr/Y	4.52	5.70	2.17
Ti/Zr	11.20	13.25	4.18
Zr/Nb	15.21	18.57	3.44
La/Yb	10.17	8.18	2.12
La/Th	2.77	1.66	0.77
Ni/Co		0.61	0.66
Cr/V	0.31	ERR	ERR
V/Ni	ERR	ERR	ERR
Cr/Zr	0.15	0.14	0.02
Co/Th	0.38	0.39	0.15
Eu/Eu*	0.27	0.52	0.12

TABLE B-5

Chemical Compositions of Graywackes

SAMPLE	HEC-27	SANA-95	SANA-115	MEAN	STD. DEV.
SiO_2	64.99	51.4	57.0	57.80	5.57
TiO_2	0.57	2.88	0.23	1.23	1.18
Al_2O_3	17.39	12.3	15.6	15.10	2.11
Fe_2O_3-T	4.88	18.2	6.73	9.94	5.89
MgO	1.72	6.77	2.82	3.77	2.17
CaO	0.28	0.59	7.37	2.75	3.27
Na_2O	1.29	0.16	2.21	1.22	0.84
K_2O	3.74	2.81	1.09	2.55	1.10
MnO	0.06	0.07	0.08	0.07	0.01
P_2O_5	0.09	0.44	0.03	0.19	0.18
LOI	3.7	4.28	5.63	4.54	0.81
TOTAL	98.71	99.90	98.79	99.14	0.54
Rb	190.4	139.0	133.0	154.13	25.75
Ba	607.5	450.0	2996.0	1351.17	1164.85
Cs	5.3	2.5	2.3	3.36	1.40
Sr	59.9	11.0	349.0	139.97	149.15
Pb	21.1	14.0	11.0	15.35	4.22
Th	20.1	14.5	10.8	15.14	3.83
U	3.17	2.20	0.35	1.91	1.17
Sc	11.8	16.0	21.0	16.27	3.76
V	169.3	423.0	173.0	255.10	118.73
Cr	39.5	19.0	46.0	34.83	11.51
Co	7.6	53.0	23.0	27.87	18.85
Ni		16.0		5.33	5.33
Y	50.5	68.0	59.3	59.26	7.16
Zr	218.9	252.0	218.0	229.64	15.81
Nb	15.4	14.0	13.9	14.42	0.66
Hf	6.1	6.5	6.8	6.47	0.29
Ta	1.20	0.67		0.62	0.49
La	42.4	27.0	5.8	25.05	14.99
Ce	86.3	58.0	11.0	51.77	31.06
Sm	8.16	7.10	1.40	5.55	2.97
Eu	1.76	1.80	0.50	1.35	0.60
Tb	2.46	2.30	0.28	1.68	0.99
Yb	2.87	5.20	2.78	3.62	1.12
Lu	0.44	0.80	0.13	0.46	0.27
CIA	72.23	73.75	46.13	64.04	12.68

TABLE B-5 (continued)

Ratios of Chemical Compositions of Graywackes

SAMPLE	HEC-27	SANA-95	SANA-115	MEAN	STD. DEV.
K_2O/Na_2O	2.89	17.56	0.49	6.98	7.54
SiO_2/Al_2O_3	3.74	4.18	3.65	3.86	0.23
Th/U	6.34	6.59	30.86	14.60	11.50
K/Rb	163.18	167.79	68.02	133.00	45.98
Rb/Sr	3.18	12.64	0.38	5.40	5.24
Ba/Rb	3.19	3.24	22.53	9.65	9.10
Ba/Sr	10.14	40.91	8.58	19.88	14.88
Th/Sc	1.70	0.91	0.51	1.04	0.50
La/Sc	3.59	1.69	0.28	1.85	1.36
Zr/Y	4.34	3.71	3.68	3.91	0.31
Ti/Zr	15.66	68.52	6.33	30.17	27.38
Zr/Nb	14.26	18.00	15.68	15.98	1.54
La/Yb	14.76	5.19	2.09	7.34	5.39
La/Th	2.11	1.86	0.54	1.50	0.69
Ni/Co		0.30		0.10	0.14
Cr/V	0.23	0.04	0.27	0.18	0.10
V/Ni	ERR	26.44	ERR	ERR	ERR
Cr/Zr	0.18	0.08	0.1	0.16	0.06
Co/Th	0.38	3.66	2.13	2.05	1.34
Eu/Eu*	0.61	0.75	1.02	0.79	0.17

TABLE B-6

Chemical Compositions of Talc Unit

SAMPLE	TALC
SiO_2	63.41
TiO_2	0.02
Al_2O_3	0.16
Fe_2O_3-T	0.793
MgO	30.9
CaO	0.03
Na_2O	0.44
K_2O	0.0
MnO	0.09
P_2O_5	0.01
LOI	4.7
TOTAL	100.51
Rb	1.0
Ba	6.0
Cs	0.1
Sr	
Pb	
Th	0.03
U	
Sc	0.25
V	
Cr	0.77
Co	0.35
Ni	
Y	
Zr	
Nb	
Hf	0.02
Ta	0.01
La	
Ce	0.03
Sm	0.03
Eu	0.01
Tb	0.02
Yb	0.03
Lu	
Mg Number	

TABLE B-7

CIPW Normative Minerals (Weight %)

Mafic Metaigneous Rocks

MINERAL	SANA-16	SANA-19	SANA-37	SANA-38	SANA-65
Orthoclase	8.5	9.2	4.3	7.6	6.8
Albite	23.7	22.2	21.8	22.4	16.2
Anorthite	25.7	24.4	26.1	29.0	24.0
Diopside	8.7	19.3	23.5	20.9	17.5
Hypersthene	22.1	5.8	12.3		24.1
Olivine	2.4	13.2	5.4	14.5	
Magnetite	4.9	3.7	3.9	3.5	5.2
Ilmenite	3.6	1.9	2.3	1.8	3.8
Apatite	0.4	0.4	0.5	0.2	0.5
Nepheline				0.2	
Quartz					1.8
Corundum					

MINERAL	SANA-69	HEC-1	HEC-19	HEC-22	HEC-28
Orthoclase	4.6	14.3	5.1	4.9	2.1
Albite	21.7	1.0	22.4	19.9	44.1
Anorthite	23.7	1.0	28.5	34.3	17.4
Diopside	14.0		15.7		8.2
Hypersthene	18.1	32.4	16.3	31.6	9.9
Olivine	5.4		4.0	1.3	10.9
Magnetite	6.3	7.0	4.5	4.6	4.3
Ilmenite	5.4	6.1	3.0	2.9	2.6
Apatite	0.9	0.9	0.5	0.4	0.4
Nepheline					
Quartz		24.7			
Corundum		12.6		0.2	

TABLE B-7 (continued)

Mafic Metaigneous Rocks

MINERAL	HEC-32	HEC-33	HEC-34	HEC-35	HEC-36
Orthoclase	0.4	2.6	2.9	12.2	1.6
Albite	20.3	36.1	13.6	5.7	32.4
Anorthite	29.3	23.4	28.2	31.0	26.3
Diopside	8.5	8.5		14.3	12.1
Hypersthene	25.3	11.3	32.1	19.9	6.2
Olivine		8.9			14.8
Magnetite	6.4	5.0	4.5	7.3	4.1
Ilmenite	5.3	3.6	2.9	6.6	2.3
Apatite	0.8	0.6	8.5	1.5	0.4
Nepheline					
Quartz	3.7		4.8	1.6	
Corundum			2.4		

MINERAL	HEC-37	HEC-40	G-5	M-27	LM-3
Orthoclase	5.2	2.1	11.6	8.4	11.4
Albite	34.3	35.4	30.1	24.7	17.3
Anorthite	12.0	24.3	24.7	30.8	32.5
Diopside		13.6	4.0	10.8	9.9
Hypersthene	28.7	6.0		4.4	
Olivine		10.0	16.0	13.5	22.0
Magnetite	4.6	4.7	6.0	4.3	3.9
Ilmenite	3.1	3.2	4.8	2.8	2.1
Apatite	0.4	0.6	1.0	0.4	0.2
Nepheline			1.8		0.7
Quartz	8.4				
Corundum	3.4				

TABLE B-7 (continued)

Felsic Metaigneous Rocks

MINERAL	HEC-6	HEC-6M	HEC-7	HEC-8	HEC-38	LD-1
Quartz	23.7	22.6	40.9	35.8	37.8	33.8
Corundum	0.4	0.4	0.6	1.3	1.0	0.5
Orthoclase	72.6	72.2	49.4	53.3	56.4	26.6
Albite	1.4	1.9	2.7	4.1	0.7	30.8
Anorthite	0.8	0.8	3.5	2.6	0.5	3.6
Hypersthene	0.1	0.8	1.1	1.2	1.0	1.5
Hematite	0.8	1.0	1.6	1.5		1.2
Rutile	0.	0.2	0.1	0.1		
Apatite	0.1	0.2	0.1	0.1	0.8	0.2
Ilmenite			0.2	0.02	0.2	0.8
Magnetite					2.4	1.1

APPENDIX C: PETROGRAPHIC DESCRIPTIONS

Mafic Volcanic Rocks

HEC-40 Hembrillo Canyon

Amphibolite Probable Protolith: Basalt

Plagioclase (approximately 40%): laths 0.1 to 0.3 mm long, alteration to sericite common, twinning observed in most well-preserved crystals. Epidote (approximately 10%): occurs as amygdule filling with quartz and in veins. Euhedral to subhedral crystals 0.01 to 0.5 mm long. Quartz (approximately 10%): occurs as amygdule and vein filling. Crystals are <0.03 mm in length. Chlorite (approximately 5%): green crystals 0.5 to 2 mm long with green pleochroism. Actinolite (approximately 15%): green acicular crystals 0.8 to 1.5 mm long. Occurs with chlorite. Opaques (approximately 5%): disseminated, anhedral crystals 0.01 to 0.1 mm in size.

HEC-41 Hembrillo Canyon

Fine-grained Amphibolite Probable Protolith: Basalt

Plagioclase (approximately 40%): small laths 0.05 to 0.1 mm long, well preserved. Hornblende (approximately 30%): subhedral to anhedral crystals 0.2 to 1 mm long, blue-green color. Quartz (approximately 10%): anhedral crystals 0.05 to 0.2 mm in diameter, undulose extinction. Epidote/clinozoisite (approximately 10%): subhedral to euhedral crystals 0.05 to 0.1 mm in length. Chlorite (approximately 10%): irregular anhedral crystals < 0.1 mm long. Opaques (TR): euhedral to anhedral crystals 0.1 to 0.5 mm in diameter.

HEC-42 Sulfur Canyon

Slightly Foliated

Amphibolite Probable Protolith: Gabbro

Plagioclase (approximately 60%): occurs as laths (approximately 30%) 0.05 to 0.1 mm long which exhibit foliation, and as subhedral crystals (approximately 70%) 0.05 to 0.3 mm long. Partially altered to sericite. Chlorite ? (approximately 30%): occurs as fine-grained groundmass < 0.1 mm in length. Hornblende (approximately 5%): blue-green to green colored, subhedral crystals 0.2 to 0.5 mm in diameter. Opaques (approximately 5%): anhedral to euhedral crystals 0.1 to 0.5 mm in diameter. Secondary minerals (TR): quartz and calcite as vein and amygdule fillings.

HEC-43

Amphibolite Probable Protolith: Basalt

Plagioclase (approximately 65%): acicular and laths 0.1 to 1 mm long, slightly altered to sericite. Actinolite (approximately 10%): acicular needles 0.05 to 0.5 mm long in radiating bundles, blue to blue-green. Epidote (approximately 15%): occurs as amygdule fillings and as radiating crystals 0.05 to 0.5 mm long. Quartz (approximately 10%): anhedral crystals 0.05 to 0.1 mm in diameter, and as vein and amygdule filling with epidote. Opaques (approximately 5%): anhedral crystals 0.05 to 1 mm in diameter.

Felsic Volcanic Rocks

HEC-6 Hembrillo Canyon, at unconformity

Rhyolite

K-feldspar (approximately 75%): large crystals 0.1 to 4 mm in diameter anhedral to subhedral crystals, albite, Carlsbad and microcline twinning common, indistinct borders with matrix. Quartz (approximately 20%): anhedral to subhedral grains 0.1 to 0.8 mm in diameter, sutured borders with K-feldspar. Poly- and monocrystalline varieties are both common. Matrix (approximately 5%): quartz, K-feldspar, and sericite in crystals < 0.01 mm in size. Much of the matrix stains for K-feldspar. Opaques (TR): anhedral crystals 0.01 to 0.05 mm in diameter. Accessory minerals (TR): zircon.

HEC-7 Hembrillo Canyon

Rhyolite

K-feldspar (approximately 70%): large crystals 0.1 to 3 mm in diameter intergrown with plagioclase in perthite and antiperthite. Crystals are commonly twinned following carlsbad and albite laws. Quartz (approximately 10%): poly- and monocrystalline grains 0.1 to 0.5 mm in diameter with sutured borders. Undulatory extinction. Plagioclase (approximately 5%): subhedral crystals 0.05 to 0.1 mm long with reaction rims. Matrix (approximately 10%): K-feldspars, quartz, and sericite. Opaques (approximately 5%): anhedral crystals 0.05 to 0.1 mm. Accessory minerals (TR): zircon, euhedral crystals 0.01 to 0.05 mm long.

HEC-8 Hembrillo Canyon

Rhyolite

K-feldspar (approximately 75%): large crystals 0.1 to 3 mm in diameter showing carlsbad, albite, and tartan twinning. Some alteration to sausserite occurs around

crystal edges. Anhedral to subhedral. Quartz (approximately 15%): subhedral crystals 0.01 to 0.5 mm in diameter with undulose extinction and sutured borders. Plagioclase (approximately 10%): long, thin crystals reminiscent of relict fiamme, 0.2 to 2 mm long, poikilitically enclose fine-grained quartz crystals and opaques. Opaques (TR): small euhedral crystals 0.01 to 0.05 mm long, commonly poikilitically enclosed by plagioclase. Zircon (TR): small subhedral to euhedral crystals 0.01 to 0.05 mm in diameter.

HEC-38 Hembrillo Canyon

Rhyolite

K-feldspar (approximately 60%): subhedral crystals 0.05 to 2.5 mm in diameter intergrown with quartz and poikilitically enclosing quartz, zircon, and opaques. Carlsbad and albite twins are common. Alteration along some crystal edges to sausserite. Lineated by crystal orientation in some cases. Quartz (approximately 35%): small anhedral crystals 0.05 to 0.3 mm in diameter, often poikilitically enclosed by K-feldspar. Opaques (approximately 5%): probably hematite, 0.01 to 0.1 mm diameter, anhedral to subhedral.

LD-1 Little Dry Canyon

Rhyolite

Quartz (approximately 50%): linear crystals 0.05 to 0.5 mm long, undulatory extinction subhedral. Plagioclase (approximately 25%): 0.01 mm to > 1 cm long, lineated, apparently relict fiamme, well-preserved anhedral to subhedral, graded by crystal size. Some sericitization, but most crystals well preserved. Distinct, sharp boundaries with adjacent crystals. K-feldspar (approximately 10%): small,

mostly in matrix material < 0.01 to 0.05 mm long. Matrix (approximately 10%): fine grained, contains mostly K-feldspar and quartz. Accessory minerals: zircon and sphene, 0.01 to 0.1 mm long, subhedral to euhedral, poikilitically enclosed in plagioclase.

Sedimentary Rocks

HEC-9 Hembrillo Canyon

Quartzite Probable Protolith: Quartz Arenite

Quartz (approximately 90%): rounded to subangular grains, concavo/convex contacts, undulose, dominantly monocrystalline (approximately 90%) with minor polycrystalline grains (approximately 10%). Grains are 0.05 to 3 mm in diameter. Muscovite (approximately 5%): thin, elongate crystal, probably recrystallized matrix material. 0.1 to 0.3 mm long. Occurs in interstices between quartz grains. Matrix (approximately 5%): consists of K-feldspar (retains staining) and fine-grained quartz and biotite < 0.01 mm.

Folk (1980) name: supermature, coarse grained, quartz arenite.

HEC-11A Hembrillo Canyon

Quartzite Probable Protolith: Quartz Arenite

Quartz (approximately 90%): subrounded to rounded equant grains 0.05 to 2 mm in diameter, average 0.8 mm, well sorted, concavo/convex contacts, monocrystalline, undulose. K-feldspar (approximately 5%): subangular, subequant grains 0.01 to 0.3 mm in length with Carlsbad twins. Muscovite (approximately 5%): elongate grains, 0.1 to 0.2 mm long, probably recrystallized matrix. Cement:

quartz rims surround many grains, but is < 5% (TR) of total rock.

Folk (1980) name: supermature, coarse grained, quartz cemented, quartz arenite.

HEC-14 Hembrillo Canyon

Quartzite Probable Protolith: Quartz Arenite

Quartz (approximately 98%): rounded to well-rounded equant grains 0.1 to 1 mm in diameter, average 0.8 mm. Well sorted, sutured grain-to-grain contacts dominant. Monocrystalline, undulose. Muscovite (approximately 2%): small grains 0.01 to 0.1 mm long. Bent around undeformed quartz grains. Probably recrystallized matrix. Cement: some quartz overgrowths.

Folk (1980) name: supermature, coarse grained, quartz cemented, quartz arenite.

HEC-16 Hembrillo Canyon

Quartzite Probable Protolith: Quartz Arenite

Quartz (approximately 90%): rounded equant grains 0.3 to 1.0 mm in diameter, undulose with sutured contacts and quartz overgrowths. Well sorted. Muscovite (approximately 5%): occurs between quartz grains and associated with biotite. Elongate grains 0.05 to 0.1 mm long. Biotite (TR): small grains, 0.05 mm long. Occurs with muscovite. K-feldspar (TR): very small grains, rounded, < 0.05 mm long.

Folk (1980) name: supermature, coarse grained, quartz cemented, quartz arenite.

HEC-21 Hembrillo Canyon

Quartzite Probable Protolith: Quartz Arenite

Quartz (approximately 95%): rounded, equant grains 0.4 to 1 mm in diameter,

monocrystalline, undulose with sutured and concavo/convex contacts and quartz overgrowths. Muscovite (approximately 3%): occurs between quartz grains as elongate, 0.1 to 0.2 mm long grains, possibly as recrystallized matrix. Opaques (approximately 2%): 0.05 to 0.1 mm in diameter, probably hematite. Occurs in thin bands, perhaps emphasizing bedding.

Folk (1980) name: supermature, coarse grained, quartz cemented, quartz arenite.

HEC-30 Hembrillo Canyon

Quartzite Probable Protolith: Quartz Arenite

Quartz (approximately 95%): well rounded, very equant grains, 0.5 to 0.8 mm in size, monocrystalline, undulose, silica overgrowths, concavo/convex and line contacts. Well sorted. Muscovite (approximately 5%): probably recrystallized matrix. Grains 0.01 to 0.05 mm long. Zircon (TR): subrounded with quartz overgrowths, 0.05 to 0.1 mm long. Opaques (TR): probably hematite highlighting crossbeds. 0.05 to 0.1 mm long.

Folk (1980) name: supermature, coarse grained, quartz cemented, quartz arenite.

HEC-41 Hembrillo Canyon

Foliated

Biotite-Chlorite-Schist Probable Protolith: Graywacke

Quartz (approximately 60%): subrounded, subequant grains, monocrystalline and polycrystalline grains. Undulose, matrix supported. 0.01 to 0.1 mm in diameter. Muscovite (approximately 15%): elongate, 0.01 to 0.2 mm long, crenulated, accentuates foliation trend, parallel bands. Matrix (approximately 20%): fine grained, consisting of K-feldspar, quartz, and muscovite. Biotite (approximately

5%): randomly oriented grains in matrix, 0.01 to 0.05 mm long.

Folk (1980) name: arkosic wacke.

HEC-47 Hembrillo Canyon

Quartzite Probable Protolith: Quartz Arenite

Quartz (approximately 93%): well rounded, equant grains 0.1 to 0.7 mm in diameter, undulose with concavo/convex contacts and quartz overgrowths. Monocrystalline grains. Well sorted. Muscovite (approximately 7%): elongate, 0.05 to 0.1 mm long. Probably recrystallized matrix material. K-feldspar (TR): equant grains 0.01 to 0.05 mm long. Occur with muscovite. Zircon (TR): equant grains 0.01 to 0.05 mm long. Overgrown with quartz.

Folk (1980) name: supermature, coarse grained, quartz cemented, quartz arenite.

HEC-48 Hembrillo Canyon

Quartzite Probable Protolith: Quartz Arenite

Quartz (approximately 98%): well-rounded, very equant grains 0.2 to 0.5 mm in diameter, average 0.3 mm. Undulose with concavo/convex contacts and some sutured contacts. Monocrystalline grains with silica cement. Muscovite (approximately 2%): elongate, 0.05 to 0.1 mm long.

Folk (1980) name: supermature, medium grained, quartz cemented, quartz arenite.

SANA-117 Hembrillo Canyon

Arkosite Probable Protolith: Arkosic Arenite

Quartz (approximately 70%): subangular to subrounded, subequant grains, 0.1 to

0.5 mm in diameter, monocrystalline, undulose with point and line contacts. Rock fragments (approximately 10%): angular to subangular, subequant grains 0.05 to 0.5 mm. Grains are of indeterminable composition, although trace amounts of muscovite, sericite, K-feldspar, and sausserite in the grains might indicate that these rock fragments are of felsic volcanic origin. K-feldspar (approximately 15%): subangular to subrounded grains, subequant 0.01 to 0.5 mm long. Carlsbad and albite twins common. Alteration to sausserite prevalent. Matrix (approximately 5%): contains K-feldspar (stained), quartz and white micas.

Folk (1980) name: submature, medium grained arkosic arenite.

SANA-136 Sulfur Canyon

Arkosite Probable Protolith: Arkosic Arenite

Quartz (approximately 85%): subangular to subrounded, subequant grains, 0.1 to 0.25 mm, monocrystalline, undulose with concavo/convex and line contacts. K-feldspar (approximately 10%): subangular, subequant grains 0.05 to 0.3 mm long. Carlsbad, albite, and microcline twinning occur. Matrix (approximately 5%): contains muscovite, K-feldspar, quartz, and opaques. Heavy minerals (TR): rutile and zircon, 0.05 to 0.1 mm long.

Folk (1980) name: submature, fine grained subarkosic arenite.

LM-4 Lost-Man Canyon

Arkosite Probable Protolith: Lithic Arenite

Quartz (approximately 80%): subrounded to rounded, subequant grains 0.5 to 1 mm in diameter.

APPENDIX D: ANALYTICAL PROCEDURES

Sample Preparation

Fresh hand specimens taken in the field were crushed in a jaw crusher to 2-4 cm. Reduction to coarse powder (30 mesh or smaller) was made by using a high speed rotary ceramic disc grinder. An automatic agate mortar and pestle was used to reduce the coarse powder to $\leq$ 200 mesh. Three separations were then made, one each for XRF major and trace elements, and INAA.

Instrumental Neutron Activation Analysis (INAA)

Trace elements Cs, Ba, Sc, Hf, Ta, Cr, Co, Zn, U, and 8 REE were analyzed by INAA. Rock powders at $\leq$ 200 mesh (approximately 0.3 g) were sealed in polyethylene vials and irradiated at the annual core research reactor at the Sandia National Laboratories, Albuquerque, NM.

INAA involves inducing radioactivity in the elements of interest in the sample by bombardment with neutrons and selectively measuring the intensities of the induced radioactivities which are directly proportional to the amounts of the elements in the sample (Muecke, 1980).

Quality of INAA data is determined by intensity, stability, and homogeneity of the thermal neutron flux. The Sandia reactor has moderate intensity and homogeneity with a thermal neutron flux of about 5×10^{11} cm^{-2} sec^{-1} (Phillip Kyle, pers. comm.). Minor variations in flux stability have little effect on final results if samples are compared to reference standards that have been simultaneously irradiated with the samples (Muecke, 1980). Reference standards used were NBS-1633A and BCR-1. Check standards used were BCR-1, ANG, AGV-1, DTS-1, BE-N,

and G-2.

Irradiation time also plays an important role in INAA. Longer irradiation times allow more atoms to be bombarded by neutrons, and gives a more precise indication of actual element concentrations. The Sandia irradiation time is relatively short (approximately 10000 seconds), compared to other reactors (the University of Missouri reactor irradiates for approximately 40 hours), and the resulting data may not be as good as is possible.

Counts were made at 7 and 40 days, using a liquid nitrogen cooled, coaxial intrinsic detector. Data was channelled and analyzed with a nuclear data 6600 multichannel analyzer and a LSI-11 computer. Analytical methods are well described in Gibson and Jagam (1980) and Allen (1985).

Data precision and accuracy can be found in appendix E, and can be generalized as $\leq 2\sigma$ (95% certainty) and $< 1\%$ C.V.

X-Ray Flourescence (XRF)

Analyses for the major elements Si, Ti, Al, Fe, Mn, Mg, Ca, Na, K, and P, and the trace elements Ba, U, Cr, Ni, Y, Rb, Sr, Nb, Zr, Th, and Pb were performed by XRF. Rock powders at $\leq$ 200 mesh (approximately 8 g) were pressed with 8 drops of polyvinal alcohol and a boric acid backing (to insure infinite thickness at 10 tons per square inch).

Analysis was performed on an automated Rigaku 3064 XRF spectrometer with associated PDP-11 computer and in-house software at the New Mexico Bureau of Mines and Mineral Resources. Analytical peaks measured were k-alpha peaks with a vacuum X-ray path used for all elements listed above except for Rb, Sr, Y, Nb, Zr, Th, and Pb which used an air X-ray path. Coefficients of variance

and standard deviations are calculated in Appendix E.

Ten rock standards (AGV-1, BCR-1, BLCR, GSP-1, HI-31, JB-1, JG-1, LOSP, PCC-1, and SY-1) were used for construction of calibration curves. All are USGS rock standards, with the exceptions of BLCR, HI-31, and LOSP which are in-house standards. Standards run with unknowns for precision and accuracy are discussed and tabulated in Appendix E.

The raw counting data were processed through the PDP-11 computer and in-house software. Matrix effects for the major elements were removed by multiple linear regresssion of the standards used to construct the calibration curves. Mass absorption coefficients for each sample were calculated at the specific wave length for each element.

APPENDIX E: ANALYTICAL PRECISION AND ACCURACY

INAA

For the procedures outlined in Appendix D, Tables E-3 through E-5 represent data for the calculation of the precision and accuracy of representative rock standards.

For INAA, it was found that the elements W, Ni, Br, Sb, U, and Th showed a σ greater than 2 (95% certainty) and are thus not good elements to analyze by INAA. These elements are better analyzed by XRF. Good to excellent data occurs with the elements Sc, Rb, Cs, Ce, Nd, Sm, Eu, Tb, Yb, Lu, Hf, and Ta. Coefficients of variance (C.V.) for these elements are $\leq 1.0\%$ and within 2σ of published values.

Precision for elements with low C.V. values is within 2σ of the mean, particularly for samples BCR-1, AN-G, AGV-1, DTS-1, BE-N, and NIM-P. Good reproducibility (accuracy) occurs for most elements described above, although Eu is commonly below accepted data values. Rb is commonly higher than published data. Other elements scatter both above and below published values, indicating errors incurred during sample preparation, irradiation irregularities, and software inaccuracy during counting procedures. Scatter of these elements is generally within 2σ, and are thus acceptable data for use in this thesis.

XRF

Precision is excellent for data occuring with the major elements (Si, Ti, Al, Fe, Mn, Mg, Ca, Na, K, and P), and many trace elements (Ba, V, Cr, Y, Nb, Zr, Rb, and Th). Coefficients of variance and standard deviations for these elements

are generally $< 1\%$ and within 2σ, respectively. Some elements, notably U, Pb, Ni, and Sr, are greater than 1% C.V. and 2σ, but were analytically more accurate than INAA.

Reproducibility occurs with most elements described above. However, silica is often high, particularly for samples $> 75\%$ silica. This is probably due to the lack of high silica standards to calculate a calibration curve. Most elements within 1% C.V. and 2σ scatter both above and below published values, indicating error in sampling, crushing, pellet or fused disk making, or counting irregularities. Because scatter is within 1% C.V. and 2σ, these data are acceptable for use in this thesis.

Equations used for calculation of coefficient of variance (C.V.), mean, and

$$\bar{x} = \frac{\sum x}{N}$$

$$\sigma = \sqrt{\frac{\sum x^2}{N} - \mu^2}$$

$$C.V. = \frac{\sigma}{\mu}(100)$$

$\bar{x}$ = mean

x = individual data point

N = total number of elements in the population

σ = standard deviation

Although the standard deviation (σ) is an absolute measure of dispersion expressing variation in the same units as the original data, the coefficient

of variance (C.V.) is a more relative measure that indicates the magnitude of the deviation relative to the magnitude of the mean. C.V. expresses σ as a percentage of the mean and is a better indicator of relative magnitudes of deviation (Levin and Rubin, 1980).

TABLE E-1

Number of Analyses for Seven Rock Standards by INAA

Element	BCR-1	G-2	AN-G	AGV-1	DTS-1	BE-N	NIM-P
Na_2	20	12	10	10	10	6	6
K		6					
CaO	20		10	10		6	6
FeO	20	12	10	10	10	6	6
Sc	20	12	10	10	10	6	6
Cr	20	12	10	10	10	6	6
Co	20	12	10	10	10	6	6
Zn	20	12	10	10	10	6	6
Ni	20	12	10		10	6	6
Br		12	10			6	
Rb	20	12	10	10		6	
Sr	20	12	10	10		6	
Zr	20	12	10	10		6	
Sb	20	12	10	10	10	6	6
Cs	20	12	10	10	10	6	6
Ba	20	12	10	10	10	6	6
U	20	12	10	10	10	6	6
La	20	12	10	10	10	6	6
Ce	20	12	10	10	10	6	6
Nd	20	12	10	10	10	6	6
Sm	20	12	10	10		6	6
Eu	20	12	10	10	10	6	6
Tb	20	12	10	10		6	6
Yb	20	12	10	10	10	6	6
Lu	20	12	10	10		6	6
Hf	20	12	10	10		6	6
Ta	20	12	10	10		6	6
Th	20	12	10	10		6	6
W		12					

TABLE E-2

Number of Analyses for Five Rock Standards by XRF

ELEMENT	G-2	AGV-1	BCR-1	BE-N	AN-G
SiO_2	8	8	12	6	10
TiO_2	8	8	12	6	10
Al_2O_3	8	8	12	6	10
Fe_2O_3	8	8	12	6	10
MnO	8	8	12	6	10
MgO	8	8	12	6	10
CaO	8	8	12	6	10
Na_2O	8	8	12	6	10
K_2O	8	8	12	6	10
P_2O_5	8	8	12	6	10
Ba	10	6	10	6	4
Ti	10	6	10	6	4
V	10	6	10	6	4
Cr	10	6	10	6	4
Ni	10	6	10	6	4
Y	8	8	10	4	4
Sr	8	8	10	4	4
Nb	8	8	10	4	4
Zr	8	8	10	4	4
U	8	8	10	4	4
Rb	8	8	10	4	4
Th	8	8	10	4	4
Pb	8	8	10	4	4

Duplicate samples run for LOSP, HI-31, and BLCR
(in-house standards, analyzed 6, 6, and 8 times, respectively).

TABLE E-3

Mean Values and Coefficients of Variance for Rock Standards Using INAA

BCR-1				
ELEMENT	MEAN	CV (%)	PUBLISHED	% ERROR
Na_2O	3.27±0.02	0.61	3.3	0.91
Sc	31.99±0.04	0.13	33	3.06
Cr	10.12±0.29	2.9	15	32.5
FeO	12.25±0.001		13.41	8.69
Co	37.57±0.06	0.15	36	4.36
Zn	143.2±0.4	0.28	125	14.6
Ni	50±12.5	25	10	400.0
Rb	50.53±0.225	0.45	47	7.51
Sr	331.2±17.6	5.3	330	0.36
Sb	0.58±0.03	5.2	0.6	3.33
Cs	0.81±.002	0.19	0.96	15.6
Ba	642.7±15.2	2.4	6.78	678
U	1.51±0.085	5.6	1.7	11.2
La	24.4±0.1	0.41	27	9.63
Ce	52.63±0.68	1.3	53	0.70
Nd	28.99±0.71	2.5	26	11.5
Sm	6.74±0.01	0.15	6.5	3.69
Eu	1.92±0.01	0.52	2	4.00
Tb	1.06±0.00	0.0	1.0	6.00
Yb	3.54±0.16	4.5	3.4	4.12
Lu	0.51±0.011	2.1	0.5	1.80
Hf	5.13±0.03	0.59	5	2.60
Ta	0.75±0.005	0.67	0.8	6.86
Th	5.74±0.02	0.35	6.1	5.90

TABLE E-3 (continued)

Mean Values and Coefficients of Variance for Rock Standards Using INAA

G-2				
ELEMENT	MEAN	CV (%)	PUBLISHED	% ERROR
Na_2O	4.36±0.21	4.82	4.06	7.39
K_2O	4.84±0.79	16.2	4.46	8.41
Sc	3.51±0.015	0.43	3.5	0.14
Cr	6.42±0.417	6.5	8	19.8
FeO	2.93±0.355	12.1	2.69	8.92
Co	4.39±0.05	1.14	5	12.2
Zn	64.22±2.69	4.2	84	23.5
Br	0.33±0.02	4.6	0.3	10.0
Rb	170.2±2.75	1.62	170	0.12
Sr	528.6±32.4	6.1	480	10.1
Sb	0.04±0.0033	9.1	0.06	39.5
Cs	1.33±0.025	1.9	1.4	5.00
Ba	1834.05±3.45	0.2	1900	3.47
U	1.84±0.075	4.1	2.1	12.4
La	70.91±8.01	11.3	92	22.9
Ce	158.2±14.7	9.3	160	1.13
Nd	60.6±0.125	0.21	58	4.48
Sm	7.33±0.31	4.2	7.2	1.81
Eu	1.42±0.005	0.35	1.4	1.07
Tb	0.49±0.022	4.4	0.5	2.20
Yb	0.68±0.037	5.5	0.86	21.3
Zr	328.3±10	3.1	300	9.43
Lu	0.12±0.007	6.1	0.1	15.0
Hf	8.73±0.02	0.23	8	9.13
Ta	0.77±0.041	5.3	0.8	3.63
W	0.14±0.0142	100	0.1	42.0
Th	24.38±0.025	0.1	25	2.48
Ni	13.35±3.85	28.8	3.5	287

TABLE E-3 (continued)

Mean Values and Coefficients of Variance for Rock Standards Using INAA

AN-G				
ELEMENT	MEAN	CV (%)	PUBLISHED	% ERROR
Na_2O	1.63±0.007	0.44	1.63	0.06
CaO	19.3±0.4	2.1	15.92	21.2
Sc	9.82±0.02	0.02	10	1.8
Cr	46.9±0.17	0.36	50	6.2
FeO	3.00±0.007	0.23	2.24	33.8
Co	24.8±0.03	0.1	25	0.80
Zn	21.9±2.41	11.0	20	9.5
Ni	30±13.3	44.4	35	14.3
Br	2.91±0.16	5.4		
Rb	1.5±0.02	10.0	1	50.0
Sr	49.3±6.7	13.5	76	35.1
Zr			15	
Sb	0.081±0.09	11.6		
Cs	0.06±0.011	18.1		
Ba	31.8±2.42	7.6	34	6.47
U	0.06±0.008	14.6		
La	2.16±0.07	0.31	2	8.0
Ce	5.25±0.21	3.97	4.7	11.7
Nd	2.27±0.017	0.73	2	13.5
Sm	0.72±0.003	0.47	0.7	2.14
Eu	0.33±0.01	3.3	0.37	10.8
Tb	0.17±0.78	4.6	0.2	15.0
Yb	0.78±0.007	0.93	0.85	8.24
Lu	0.12±0.001	1.2	0.12	3.33
Hf	0.25±0.023	8.9	0.38	33.4
Ta	0.14±0.004	3.1	0.2	30.0
Th	0.04±0.0063	16.5		

TABLE E-3 (continued)

Mean Values and Coefficients of Variance for Rock Standards Using INAA

AGV-1				
ELEMENT	MEAN	CV (%)	PUBLISHED	% ERROR
Na_2O	4.24±0.018	0.42	4.32	1.85
CaO	4.97±0.3	6.04	4.94	0.61
Sc	11.7±0.073	0.19	12.5	6.4
Cr	9.39±0.45	4.8	10	6.1
FeO	6.1±0.007	0.12	2.03	66.7
Co	15.42±0.043	0.28	16	3.63
Zn	88.9±0.92	1.03	86	3.37
Ni			15	
Br			0.5	
Rb	66.25±0.5	0.76	67	1.12
Sr	666±36	541	660	0.91
Zr	241.7±14	5.8	230	5.09
Sb	4.24±0.027	0.64	4.3	1.40
Cs	1.24±0.008	0.67	1.3	4.62
Ba	1158.4±12	1.04	1200	3.47
U	1.8±0.085	4.7	1.95	7.69
La	37.05±0.15	0.4	36	2.92
Ce	69.7±0.32	0.45	71	1.83
Nd	31.9±0.45	1.4	37	13.8
Sm	5.88±0.013	0.2	5.9	0.34
Eu	1.58±0.01	0.63	1.6	1.25
Tb	0.66±0.008	1.2	0.7	5.71
Yb	1.7±0.017	1.01	1.9	10.5
Lu	0.25±0.002	0.59	0.3	15.7
Hf	5.35±0.046	0.86	5	7.00
Ta	0.84±0.009	1.1	1.4	400
Th	6.03±0.002	0.03	6.4	5.78

TABLE E-3 (continued)

Mean Values and Coefficients of Variance for Rock Standards Using INAA

DTS-1				
ELEMENT	MEAN	CV (%)	PUBLISHED	% ERROR
Na_2O	0.02±0.0001	0.56	0.01	80.0
CaO			0.14	
Sc	3.37±0.012	0.35	3.8	11.3
Cr	4238.3±20.9	0.49	4200	0.91
FeO	7.93±0.015	0.19	8.7	8.85
Co	139.7±0.19	0.14	135	3.48
Zn	46.9±1.2	2.5	46	1.96
Ni	3066.7±2333	7.6	2300	3.33
Br			0.2	
Rb			0.05	
Sr			0.4	
Zr			10	
Sb	0.34±0.018	5.1	0.5	31.4
Cs	0.01±0.002	23.6	0.01	50.0
Ba	28±4.5	16.1	5	460
U	0.07±0.018	26.9		1530
La	0.05±0.009	19.6	0.04	15.0
Ce	0.06±0.22	361	0.06	
Nd	1.22±0.35	28.7		
Sm				
Eu	0.01±0.002	28.6		600.0
Tb				
Yb	0.07±0.016	23.9	0.01	580.0
Lu				
Hf			0.01	
Ta				
Th			0.01	

TABLE E-3 (continued)

Mean Values and Coefficients of Variance for Rock Standards Using INAA

BE-N				
ELEMENT	MEAN	CV (%)	PUBLISHED	% ERROR
Na_2O	3.22±0.015	0.5	3.20	0.63
CaO	15.1±0.17	1.1	13.94	8.32
Sc	22.4±0.04	0.18	22	1.82
Cr	369.2±0.75	0.2	360	2.56
FeO	11.82±0.02	0.15	12.9	8.37
Co	63.1±0.12	0.19	61	3.44
Zn	123.5±1.2	0.95	120	2.92
Ni	280±18.3	6.6	270	3.70
Br				
Rb	48.75±0.67	1.4	47	3.72
Sr	1566.7±65	4.15	1350	16.1
Zr	295±30	10.2	270	9.26
Sb	0.19±0.008	3.95		
Cs	0.61±0.012	1.9	0.8	23.8
Ba	1005.8±7.5	0.75	1050	4.21
U	2.44±0.13	5.2	2.4	1.67
La	79.9±0.25	0.31	82	2.56
Ce	152.9±0.51	0.33	150	1.93
Nd	65.2±1.1	1.7	70	6.86
Sm	12.45±0.018	0.15	12	3.75
Eu	3.58±0.013	0.35	3.6	0.56
Tb	1.34±0.009	0.68	1.3	3.08
Yb	1.98±0.076	3.8	1.8	10.0
Lu	0.28±0.002	0.6	0.24	16.7
Hf	5.94±0.063	1.1	5.4	10.0
Ta	5.81±0.026	0.45	5.5	3.64
Th	10.21±0.03	0.26	11	7.18

TABLE E-3 (continued)

Mean Values and Coefficients of Variance for Rock Standards Using INAA

NIM-P				
ELEMENT	MEAN	CV (%)	PUBLISHED	% ERROR
Na_2O	0.37±0.003	0.9	0.37	0.81
K_2O			0.09	
CaO	2.73±0.1	3.8	2.66	2.63
Sc	28.34±0.05	0.18	29	2.28
Cr	22490.8±1095.8	4.5	24000	6.29
FeO	11.82±0.023	0.19	16.96	30.3
Co	112.3±0.11	0.10	110	2.09
Zn	122.6±1.58	1.3	100	22.6
Ni	313.3±31.7	10.1	560	44.1
Rb			5	
Sr			32	
Zr			30	
Sb	0.07±0.008	11.4	0.8	90.9
Cs	0.14±0.009	6.3		
Ba	39.3±3.33	8.5	46	14.6
U	0.39±0.06	15.4	0.4	2.5
La	1.95±0.005	0.26	2	91.7
Ce	4.13±1	24.2	50	
Nd	1.49±0.8	53.7		
Sm	0.81±0.012	1.5		
Eu	0.12±0.009	7.1	0.2	40.5
Tb	0.27±0.03	12.4		
Yb	1.15±0.1	8.8	0.6	91.7
Lu	0.07±0.004	5.7		
Hf	0.28±0.19	6.9		
Ta	0.09±0.014	15.6		
Th	0.77±0.02	2.8	1	23.0

TABLE E-4

Mean Values and Coefficients of Variance for Rock Standards Using XRF

G-2				
ELEMENT	MEAN	CV (%)	PUBLISHED	% ERROR
SiO_2	69.21±0.20	0.29	69.04	0.24
TiO_2	0.48±0.01	2.07	0.49	2.24
Al_2O_3	15.19±0.69	4.54	15.14	0.34
Fe_2O_3	2.70±0.11	4.07	2.68	0.78
MnO	0.04±0.001	2.78	0.03	5.88
MgO	0.86±0.01	1.17	0.76	12.76
CaO	1.90±0.008	0.42	1.97	3.7
Na_2O	4.45±0.03	0.67	4.07	9.34
K_2O	4.35±0.05	1.15	4.49	3.12
P_2O_5	0.14±0.005	3.62	0.14	1.43
Ba	1869.1±28.2	1.51	1880	0.58
V	31.7±0.04	0.13	36	11.94
Cr	7.1±0.07	0.89	9	12.22
Ni	5.1±0.02	0.39	5	2.00
Y	11.52±0.45	3.91	11.4	1.05
Sr	463.94±17.3	3.73	478	2.94
Nb	13.93±0.07	0.50	13	7.15
Zr	295.96±7.9	2.67	300	1.35
U	3.10±0.01	0.32	2.04	51.96
Rb	164.89±4.99	3.03	170	3.01
Th	25.57±0.68	2.66	24.6	3.94
Pb	34.42±0.41	1.19	31	11.03

TABLE E-4 (continued)

Mean Values and Coefficients of Variance for Rock Standards Using XRF

AGV-1				
ELEMENT	MEAN	CV (%)	PUBLISHED	% ERROR
SiO_2	59.52±0.02	0.03	59.25	0.45
TiO_2	1.05±0.001	0.09	1.06	1.13
Al_2O_3	17.08±0.03	0.18	17.15	7.2
Fe_2O_3	6.58±0.007	0.10	6.76	2.65
MnO	0.08±0.001	1.20	0.10	15.6
MgO	1.51±0.002	0.13	1.53	1.05
CaO	4.89±0.03	0.61	4.94	0.97
Na_2O	4.42±0.03	0.68	4.25	4.0
K_2O	2.83±0.07	2.47	2.90	2.21
P_2O_5	0.47±0.001	0.21	0.48	0.90
Ba	1218±18.7	1.54	1220	0.16
V	121.3±1.7	1.4	123	1.38
Cr	11.21±0.01	0.09	12	6.58
Ni	16.1±0.09	0.56	17	5.29
Y	22.2±0.07	0.32	21	5.71
Sr	627.1±2.1	0.33	660	4.98
Nb	14.35±0.03	0.21	15	4.33
Zr	238.5±8.1	3.39	225	6.0
U	2.81±0.40	14.24	1.89	48.68
Rb	65.7±0.07	0.11	67	1.9
Th	6.62±0.02	0.30	6.5	1.85
Pb	34.9±0.40	1.15	36	3.06

TABLE E-4 (continued)

Mean Values and Coefficients of Variance for Rock Standards Using XRF

BCR-1				
ELEMENT	MEAN	CV (%)	PUBLISHED	% ERROR
SiO_2	54.54±0.5	0.92	54.35	0.35
TiO_2	2.22±0.01	0.45	2.22	0.40
Al_2O_3	13.49±0.01	0.07	13.63	1.04
Fe_2O_3	12.64±0.03	2.37	13.46	6.07
MnO	0.34±0.001	0.29	0.18	87.91
Mg0	3.58±0.03	0.84	3.45	3.62
CaO	6.93±0.07	1.01	6.95	3.3
Na_2O	3.75±0.02	0.53	3.27	14.71
K_2O	1.67±0.01	0.59	1.69	1.07
P_2O_5	0.36±0.003	0.84	0.37	3.24
Ba	670.1±7.1	1.06	678	1.17
V	400.7±2.2	0.55	404	0.82
Cr	14.9±0.04	0.27	16	6.88
Ni	12.25±0.03	0.25	13	5.77
Y	37.19±0.001	0.24	39	4.64
Sr	330.35±1.05	0.32	330	0.12
Nb	13.54±0.01	0.07	14	3.29
Zr	188.43±1.4	0.74	191	1.35
U	3.12±0.01	0.32	1.72	81.40
Rb	52.99±0.5	0.94	47	12.75
Th	3.18±0.02	0.28	6.04	18.87
Pb	18.08±0.09	0.50	13.6	32.94

TABLE E-4 (continued)

Mean Values and Coefficients of Variance for Rock Standards Using XRF

BE-N				
ELEMENT	MEAN	CV (%)	PUBLISHED	% ERROR
SiO_2	38.38±0.03	0.08	38.2	0.47
TiO_2	2.64±0.03	1.03	2.61	1.15
Al_2O_3	10.00±0.014	0.14	10.07	0.70
Fe_2O_3	12.28±0.022	0.18	12.84	4.36
MnO	0.18±0.0025	1.39	0.20	10.0
MgO	13.10±0.11	0.87	13.15	0.38
CaO	13.91±0.06	0.40	13.87	0.29
Na_2O	3.30±0.032	0.97	3.18	3.77
K_2O	1.36±0.003	0.22	1.39	2.16
P_2O_5	1.01±0.0005	0.05	1.05	3.81
Ba	1020.1±2.3	0.23	1025	0.48
V	235.1±1.11	0.47	235	0.04
Cr	362.1±6.2	0.48	360	0.58
Ni	255.3±3.3	1.29	267	4.38
Y	28.8±0.07	0.24	30	4.0
Sr	1290.1±7.9	0.61	1370	5.83
Nb	88.79±4.2	4.73	100	11.21
Zr	263.2±5.1	1.94	265	0.68
U	2.51±0.03	1.20	2.4	4.58
Rb	43.2±0.07	0.16	47	8.09
Th	10.1±0.05	0.50	11	8.2
Pb	2.1±0.03	1.43	4	47.5

TABLE E-4 (continued)

Mean Values and Coefficients of Variance for Rock Standards Using XRF

AN-G				
ELEMENT	MEAN	CV (%)	PUBLISHED	% ERROR
SiO_2	45.2±0.05	0.11	46.3	2.38
TiO_2	0.12±0.009	7.5	0.22	45.45
Al_2O_3	28.8±0.06	0.21	29.8	3.36
Fe_2O_3	3.24±0.003	0.09	3.36	3.57
MnO	0.06±0.001	1.67	0.04	50.0
Mg0	1.6±0.009	0.56	1.8	11.11
CaO	14.7±0.02	0.14	15.9	7.55
Na_2O	1.72±0.007	0.41	1.63	5.52
K_2O	0.11±0.002	1.82	0.13	15.38
P_2O_5	0.05±0.009	18.0	0.01	400.0
Ba	32.1±0.07	0.22	34	5.59
V	68.8±0.04	0.06	70	1.71
Cr	48.2±0.02	0.04	50	3.6
Ni	33.9±0.01	0.03	35	3.14
Y	9.42±0.05	0.53	8	17.75
Sr	74.97±0.07	0.9	76	1.36
Nb	3.12±0.02	0.64	2	56.0
Zr	13.68±0.02	0.15	15	8.8
U	2.37±0.005	0.21		
Rb	2.43±0.7	28.8	1	143.0
Th	4.84±0.005	0.10		
Pb	13.86±0.9	6.5	12	15.50

TABLE E-4 (continued)

Mean Values and Coefficients of Variance for In-House Standards Using XRF

BLCR				
ELEMENT	MEAN	CV (%)	PUBLISHED	% ERROR
SiO_2	55.76±0.2	0.36	55.65	0.20
TiO_2	0.83±0.003	0.36	0.87	4.60
Al_2O_3	16.89±0.01	0.06	16.97	0.47
Fe_2O_3	7.22±0.01	0.14	7.43	2.83
MnO	0.12±0.001	0.83	0.13	7.7
MgO	6.02±0.009	0.15	5.86	2.73
CaO	7.79±0.01	0.13	7.9	1.39
Na_2O	3.79±0.01	0.26	3.72	1.88
K_2O	1.39±0.003	0.22	1.45	4.14
P_2O_5	0.17±0.001	0.61	0.16	3.13
Ba	368.1±7.9	2.15	375	1.84
V	2.0±1.7	85.0		
Cr	149.3±2.4	1.61	160	6.69
Ni	99.7±0.7	0.70	103	3.20
Y	31.96±0.9	2.82	30.7	4.10
Sr	223.92±7.2	3.22	231	3.07
Nb	4.64±0.07	15.09	7.2	35.55
Zr	172.76±2.1	1.21	173	0.14
U	2.05±0.007	0.34	1.5	36.67
Rb	37.56±0.02	0.05	38	1.16
Th	3.44±0.004	0.12	4.1	16.10
Pb	11.58±0.1	0.86	5.8	99.66

TABLE E-4 (continued)

Mean Values and Coefficients of Variance for In-House Standards Using XRF

LOSP				
ELEMENT	MEAN	CV (%)	PUBLISHED	% ERROR
SiO_2	74.3±0.01	0.14	76.01	2.25
TiO_2	0.23±0.002	0.87	0.19	21.1
Al_2O_3	11.94±0.03	0.25	12.03	0.75
Fe_2O_3	2.01±0.05	2.49	2.20	8.68
MnO	0.15±0.007	4.67	0.08	87.50
MgO	0.30±0.009	3.0	0.10	200.00
CaO	0.74±0.004	0.54	0.65	13.85
Na_2O	3.28±0.01	0.31	3.75	12.53
K_2O	4.61±0.01	0.22	4.77	3.35
P_2O_5	0.09±0.007	7.78	0.02	350.00
Ba	931.1±8.7	0.93	970	4.01
V	24.3±0.01	0.04		
Cr	2.1±0.02	0.95	2.5	16.00
Ni	7.35±0.09	1.23	12	38.75
Y	115.50±1.12	0.97	117	1.28
Sr	38.78±0.07	0.18	41	5.42
Nb	21.13±0.06	0.28	26	18.7
Zr	278.30±0.7	0.25	290	4.03
U	3.4±0.13	3.80	4.8	29.17
Rb	182.3±0.12	0.07	184	0.92
Th	19.29±0.002	0.01	19.7	2.08
Pb	37.47±0.02	0.05	29	29.21

TABLE E-4 (continued)

Mean Values and Coefficients of Variance for In-House Standards Using XRF

HI-31				
ELEMENT	MEAN	CV (%)	PUBLISHED	% ERROR
SiO_2	58.23±0.1	0.17	59.46	2.07
TiO_2	0.66±0.002	0.30	0.81	18.52
Al_2O_3	16.31±0.01	0.06	17.02	4.17
Fe_2O_3	8.02±0.02	0.25	7.07	13.44
MnO	0.17±0.001	0.59	0.11	54.54
MgO	2.66±0.01	0.38	2.81	5.33
CaO	5.95±0.02	0.34	6.32	5.85
Na_2O	2.83±0.01	0.35	3.12	9.30
K_2O	2.58±0.001	0.04	2.53	1.98
P_2O_5	0.44±0.001	0.23	0.38	15.79
Ba	811.39±10.3	1.27	795	2.06
V	131.37±8.07	614		
Cr	36.4±0.01	0.03	38	4.21
Ni	17.37±0.01	0.06	14	24.10
Y	30.30±0.03	0.10	32	5.3
Sr	689.26±9.1	1.32	705	2.23
Nb	12.28±0.08	0.65	14	12.29
Zr	180.01±1.37	0.76	184	2.17
U	1.73±0.04	2.3	0.7	147.14
Rb	55.93±0.1	0.18	58	3.57
Th	5.02±0.02	0.40	6.6	23.94
Pb	12.75±0.05	0.40	4.5	183.33

TABLE E-4 (continued)

Duplicate Sample

Mean Values and Coefficients of Variance Using XRF

HEC-6 n=6			
ELEMENT	MEAN	STD. DEV.	CV (%)
SiO_2	74.05	0.02	0.03
TiO_2	0.17	0.02	11.76
Al_2O_3	14.72	0.05	0.31
Fe_2O_3	0.92	0.12	13.1
MnO			
MgO	0.33	0.01	1.36
CaO	0.25	0.00	0.81
Na_2O	0.20	0.03	15.0
K_2O	12.65	0.02	0.16
P_2O_5	0.07	0.003	4.55
Ba	1853.8	301.25	16.25
V	12.7	1.4	11.02
Cr	4.45	1.15	20.54
Ni	3.50	1.50	42.86
Y	74.20	2.5	3.37
Sr	30.25	1.45	4.79
Nb	22.45	0.35	1.56
Zr	7.55	1.35	17.88
U	2.96	0.32	10.81
Rb	201.8	1.2	0.60
Th	29.45	0.85	2.89
Pb	14.05	0.35	2.49

APPENDIX F

Paleocurrent Data

EXPLANATION

Sample Number = location of raw paleocurrent data on geologic map (plate 1).

Lithologies:

Q = Quartz Arenite
LA = Lithic Arenite
A = Arkosic Arenite
QW = Quartz Wacke
GW = Graywacke

X = Lineation from Cross Bed
IC = Lineation from Imbricated Clast

TABLE F-1

Site #	Lithology	Data Type	Orientation	
			Trend	Plunge
1	Q	X	N 70 W	30
2	LA	IC	N 40 W	20
3	LA	IC	N 48 W	12
4	LA	IC	N 42 W	18
5	A	X	N 45 W	16
6	A	X	N 40 W	11
7	A	X	N 29 W	14
8	A	X	N 33 W	22
9	Q	X	S 20 E	24
10	GW	IC	S 41 E	13
11	GW	IC	S 13 E	17
12	Q	X	N 28 W	18
13	LA	X	N 40 W	18
14	QW	IC	N 40 W	28
15	LA	X	S 12 E	10
16	LA	X	S 48 E	14
17	LA	X	S 20 E	16
18	Q	X	S 10 E	22
19	Q	X	S 25 E	24
20	Q	X	S 25 E	23
21	QW	IC	N 18 W	29
22	QW	IC	N 40 W	32
23	QW	IC	N 45 W	16
24	QW	IC	N 40 W	12
25	QW	IC	N 15 W	11
26	QW	IC	N 28 W	17
27	QW	IC	N 30 W	20
28	GW	IC	N 32 W	18
29	GW	IC	N 18 W	19
30	GW	IC	N 48 W	24
31	GW	IC	S 40 E	30
32	QW	IC	S 5 E	6
33	Q	X	S 25 E	22
34	GW	IC	S 30 E	23
35	A	IC	N 10 W	22
36	A	X	N 15 W	18
37	A	X	N 22 W	24
38	A	X	N 28 W	13
39	A	X	N 40 W	15
40	A	X	N 28 W	17

TABLE F-1 (continued)

Site #	Lithology	Data Type	Orientation	
			Trend	Plunge
41	A	X	N 30 W	18
42	A	X	N 12 W	24
43	A	X	N 48 W	26
44	A	X	N 21 W	25
45	A	X	N 16 W	13
46	GW	IC	N 48 W	12
47	QW	IC	N 65 W	29
48	QW	IC	N 40 W	16
49	QW	IC	S 41 E	14
50	QW	IC	S 17 E	12
51	QW	IC	S 22 E	13
52	QW	IC	S 30 E	19
53	QW	IC	N 48 W	18
54	QW	IC	N 21 W	21
55	QW	IC	N 40 W	24
56	QW	IC	N 35 W	23
57	QW	IC	N 26 W	18
58	Q	X	N 30 W	17
59	Q	X	S 22 E	20
60	GW	IC	S 40 E	21
61	GW	IC	S 60 E	28
62	GW	IC	S 17 E	17
63	Q	X	N 40 W	22
64	Q	X	N 28 W	28
65	Q	X	N 37 W	10
66	Q	X	N 36 W	15
67	Q	X	N 28 W	21
68	LA	X	N 70 W	22
69	LA	X	N 60 W	24
70	LA	X	N 25 W	27
71	A	IC	N 40 W	21
72	A	IC	N 41 W	23
73	A	IC	N 44 W	25
74	A	IC	N 39 W	27
75	A	IC	N 26 W	29
76	A	IC	N 60 W	31
77	A	IC	N 58 W	33
78	A	IC	S 14 E	12
79	A	IC	N 50 W	16
80	A	IC	N 40 W	18

TABLE F-1 (continued)

Site #	Lithology	Data Type	Orientation	
			Trend	Plunge
81	A	IC	N 42 W	22
82	A	IC	N 38 W	23
83	Q	IC	S 12 E	17
84	Q	IC	N 10 W	16
85	Q	IC	N 15 W	15
86	Q	IC	N 70 W	14
87	Q	IC	N 48 W	21
88	Q	IC	N 45 W	25
89	Q	IC	N 46 W	17
90	Q	IC	N 55 W	19
91	GW	IC	S 15 E	25
92	GW	IC	S 22 E	24
93	GW	IC	S 33 E	22
94	GW	IC	S 41 E	14
95	GW	IC	S 28 E	21
96	Q	X	N 30 W	14
97	Q	X	N 15 E	28
98	Q	X	N 21 W	15
99	GW	IC	S 23 E	12
100	LA	X	S 34 E	32
101	LA	X	S 15 E	16
102	LA	X	S 43 E	17
103	Q	X	N 25 W	27
104	Q	X	N 45 W	25
105	Q	X	N 28 W	30
106	Q	X	N 23 W	13
107	Q	X	N 24 W	23
108	Q	X	N 34 W	14
109	Q	X	N 45 W	18
110	Q	X	N 34 W	24
111	Q	X	N 45 W	12
112	Q	X	N 49 W	23
113	Q	X	N 34 W	12
114	Q	X	N 28 W	28
115	LA	X	S 23 E	29
116	LA	X	N 34 W	23
117	LA	X	N 24 W	26
118	A	IC	N 43 W	14
119	A	IC	N 23 W	26
120	A	IC	N 24 W	30

TABLE F-1 (continued)

Site #	Lithology	Data Type	Orientation	
			Trend	Plunge
121	A	IC	S 12 E	24
122	LA	X	N 26 W	16
123	LA	X	N 36 W	18
124	LA	X	N 24 W	24
125	LA	X	N 34 W	26
126	LA	X	N 28 W	29
127	LA	X	N 17 W	23
128	LA	X	N 34 W	29
129	LA	X	N 28 W	24
130	A	IC	N 27 W	30
131	A	IC	N 25 W	21
132	A	IC	N 46 W	22
133	A	IC	N 66 W	18
134	A	IC	N 40 W	12
135	A	IC	N 39 W	15
136	LA	X	S 23 E	12
137	LA	IC	S 26 E	23
138	LA	IC	S 15 W	30
139	LA	IC	S 27 E	28
140	GW	IC	S 34 E	23
141	GW	IC	S 14 E	26
142	QW	IC	N 34 W	23
143	QW	IC	N 23 W	29
144	QW	IC	N 46 W	12
145	GW	IC	S 24 E	17
146	GW	IC	S 38 E	28
147	GW	IC	S 12 E	11
148	QW	IC	S 27 E	28
149	GW	IC	S 14 E	23
150	GW	IC	S 27 E	24
151	GW	IC	S 23 E	27
152	GW	IC	S 11 E	17
153	GW	IC	S 19 E	23
154	GW	IC	S 34 E	14
155	GW	IC	S 45 E	28
156	GW	IC	S 29 E	29
157	GW	IC	S 35 E	11
158	GW	IC	S 17 E	16
159	GW	IC	S 35 E	27
160	GW	IC	S 45 E	19

TABLE F-1 (continued)

Site #	Lithology	Data Type	Orientation	
			Trend	Plunge
161	GW	IC	S 38 E	23
162	GW	IC	S 58 E	27
163	GW	IC	S 23 E	15
164	QW	IC	N 21 W	17
165	GW	IC	S 23 E	28
166	GW	IC	S 28 E	18
167	GW	IC	S 34 E	21
168	GW	IC	S 28 E	27
169	GW	IC	S 17 E	13
170	GW	IC	S 35 E	17
171	GW	IC	S 29 E	28
172	GW	IC	S 48 E	11
173	GW	IC	S 60 E	10
174	GW	IC	S 29 E	5
175	GW	IC	S 39 E	16
176	GW	IC	S 54 E	28
177	GW	IC	S 35 E	12
178	GW	IC	S 40 E	24
179	QW	IC	N 23 W	18
180	QW	IC	S 37 E	29
181	QW	IC	N 47 W	12
182	QW	IC	N 55 W	17
183	QW	IC	N 22 W	19
184	QW	IC	N 44 W	22
185	Q	X	N 28 W	23
186	Q	X	N 57 W	22
187	QW	IC	N 61 W	28
188	QW	IC	N 38 W	13
189	QW	IC	N 45 W	12
190	QW	IC	N 47 W	18
191	GW	IC	S 34 E	23
192	GW	IC	S 23 E	12
193	GW	IC	S 37 E	27
194	GW	IC	S 26 E	13
195	GW	IC	S 45 E	19
196	GW	IC	S 55 E	27
197	GW	IC	S 47 E	12
198	Q	X	N 46 W	28
199	Q	X	N 47 W	11
200	Q	X	N 55 W	21
201	Q	X	N 45 W	27
202	Q	X	N 23 W	12

TABLE F-2

Paleocurrent Subset: Younging Directions to the NE

Site #	Lithology	Data Type	Orientation	
			Trend	Plunge
5	A	X	N 45 W	16
6	A	X	N 40 W	11
7	A	X	N 29 W	14
10	GW	IC	S 41 E	13
11	GW	IC	S 13 E	17
15	LA	X	S 12 E	10
63	Q	X	N 40 W	22
83	Q	IC	S 12 E	17
102	LA	X	S 43 E	17
120	A	IC	N 24 W	30
191	GW	IC	S 34 E	23
201	Q	X	N 45 W	27

This thesis is accepted on behalf of the faculty of the Institute by the following committee:

Advisor

April 30, 1987
Date

Summary for the San Andreas Sediments

Directed Study Project
By : Jim Crichton
May 1, 1992

Sediments from the Hembrillo Canyon succession, San Andreas Mountains, New Mexico, consist of quartz arenites, quartz wackes, and graywackes. Paleocurrent data indicates that the quartz arenites and quartz wackes were derived from northerly sources (cratonic) whereas the graywackes were derived from southerly sources (island arcs). Geochemically, the quartz arenites and quartz wackes show similar distributions on various trace-element diagrams, whereas the graywackes are more heterogeneous. Two graywackes (samples HEC 27 and SANA 95) typically plot within the quartz arenite and quartz wacke field on most trace-element diagrams, whereas sample SANA 115 is distinctly different. The purpose of this study is to determine if the geochemistry of the graywackes would indicate an island-arc source, whereas the geochemistry of the quartz arenites and quartz wackes would indicate a cratonic source. No conclusions could be drawn due to the small number of graywacke samples (three) and their heterogeneous nature.

A strong inverse correlation is observed for the quartz arenites and quartz wackes on a Al_2O_3 versus SiO_2 diagram (Fig. 1) which suggests a quartz dilution effect. Two graywacke samples deviate from this trend toward the basalt endmember. This may indicate they contain an island-arc component.

Graphs of both La and Yb versus Al_2O_3 show positive correlations for the quartz arenites (Figs. 2-3). This correlation may be a result of quartz dilution or it may suggest these elements are contained mainly within clay

minerals. The distribution of the quartz wackes and graywackes are more scattered with several samples plotting near the basalt endmember. Again, this may indicate these samples have a large island-arc component.

On a Eu/Eu* versus $(La/Yb)_n$ diagram (Fig. 4), the quartz arenites, quartz wackes, and two graywacke samples form a relatively tight grouping. The Eu/Eu* ratio of these samples is similar to that of cratonic sediments ranging from about 0.40 to 0.73. The $(La/Yb)_n$ ratios of these samples range from about 2 to 6, which is lower than average Phanerozoic shales (La_n/Yb_n = 8.3). One graywacke, again, plots near the basalt endmember.

A positive correlation is seen for all samples between Th/Sc and La/Sc (Fig. 5). A possible mixing line is present between the granite and basalt endmembers. The graywackes and the quartz wackes plot closer to the basalt endmember than due the quartz arenites which plot closer to the granite endmember. This may indicate these sediments represent mixing between an island-arc source and a cratonic source. However, quartz arenites and quartzites (from many different ages and locations) tend to have higher La/Sc and Th/Sc ratios than do associated pelites. Therefore, these ratios may not reflect sediment provenance.

Fig.1

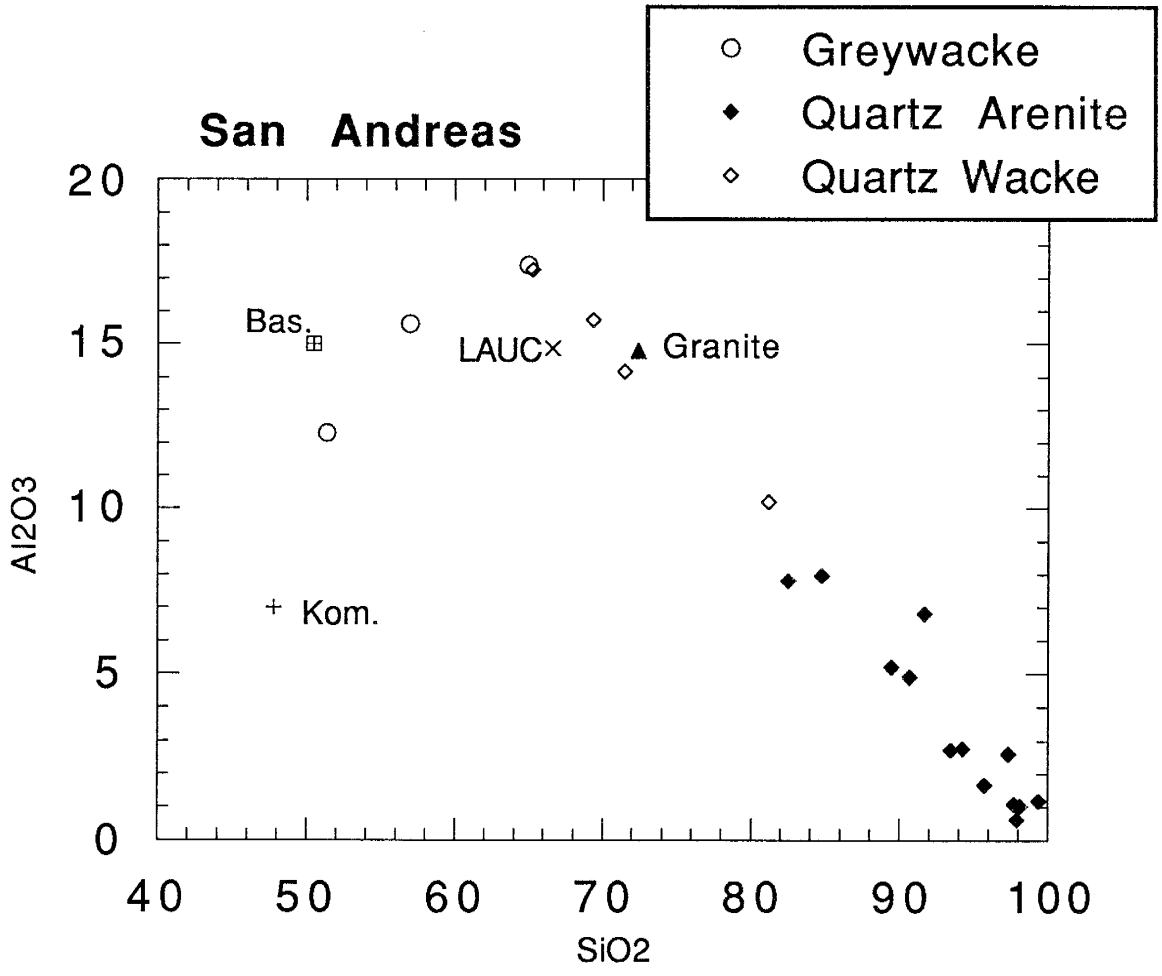
San Andreas
Greywacke
Quartz Arenite
Quartz Wacke
Bas.
LAUC
Granite
Kom.
Al2O3
SiO2
0
5
10
15
20
40
50
60
70
80
90
100

Fig. 2

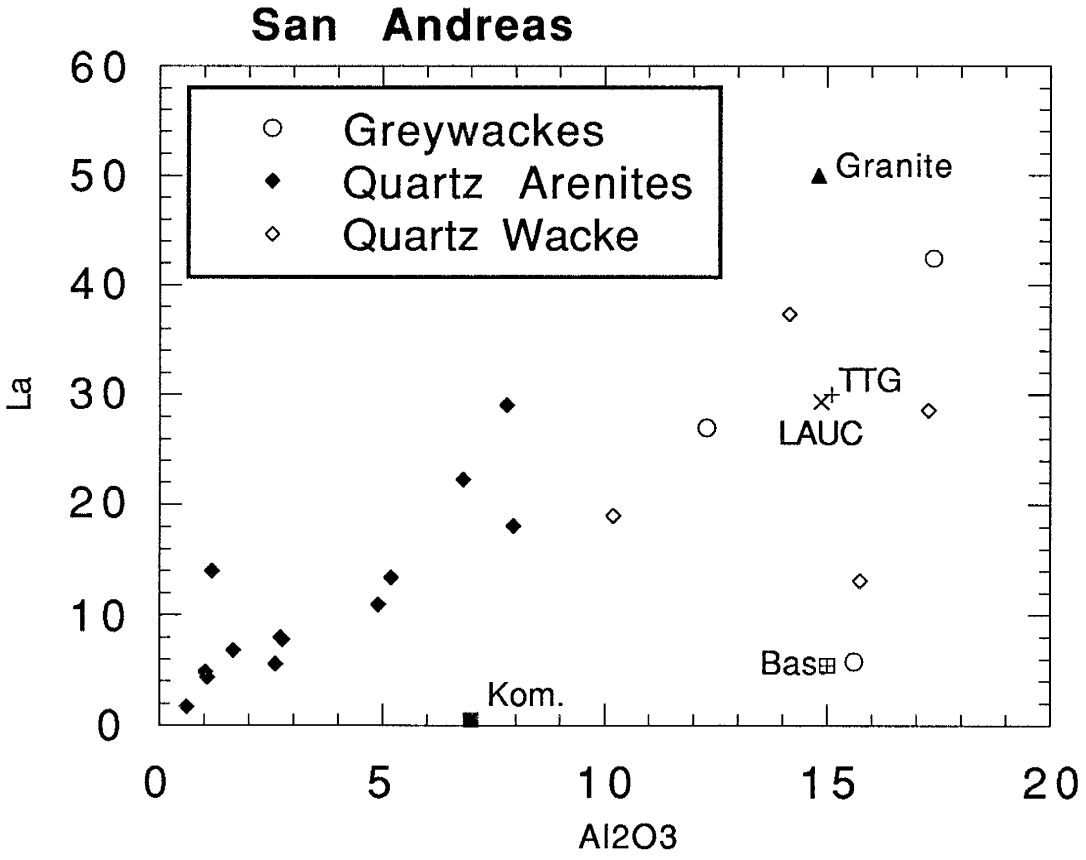
San Andreas
Greywackes
Quartz Arenites
Quartz Wacke
Granite
TTG
LAUC
Bas
Kom.
La
Al2O3
0
10
20
30
40
50
60
0
5
10
15
20

Fig. 3

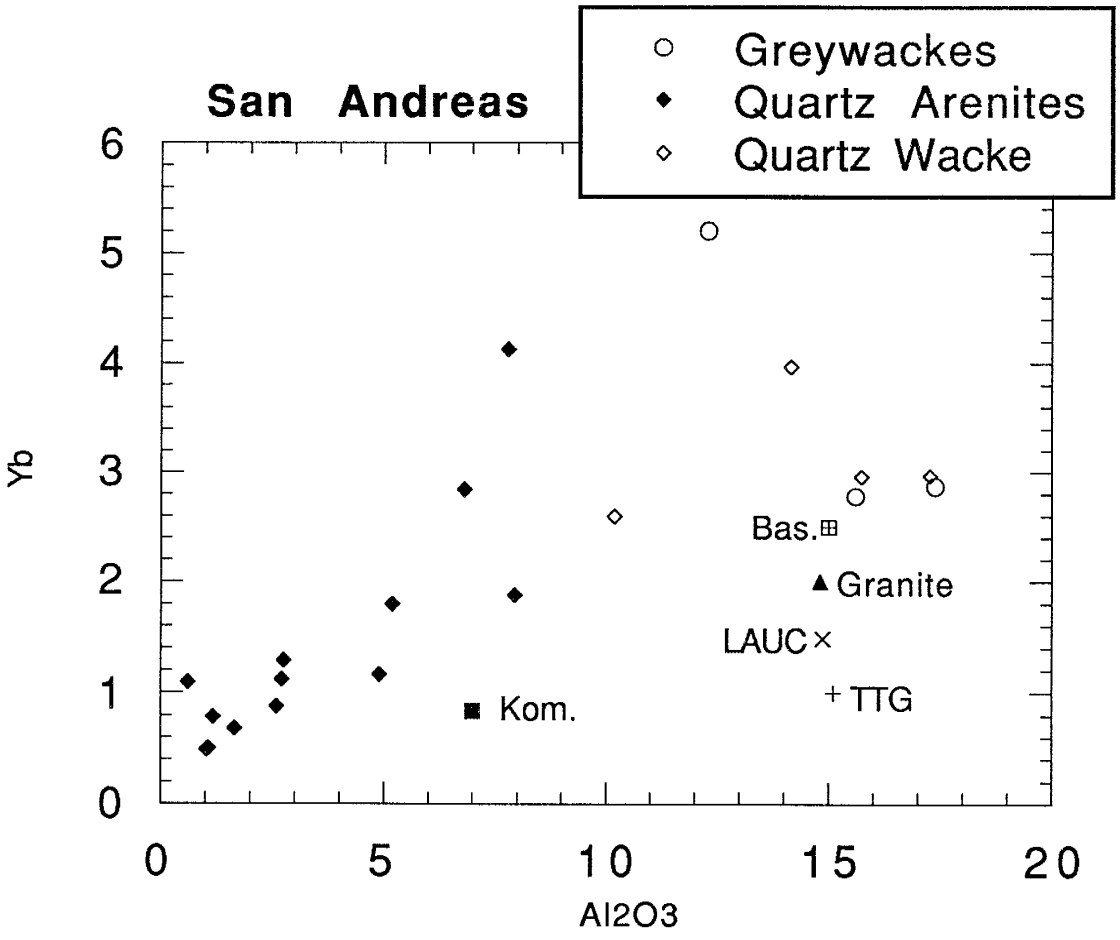
San Andreas
Greywackes
Quartz Arenites
Quartz Wacke
Yb
0
1
2
3
4
5
6
0
5
10
15
20
Al2O3
Bas.
Granite
LAUC
TTG
Kom.

Fig. 4

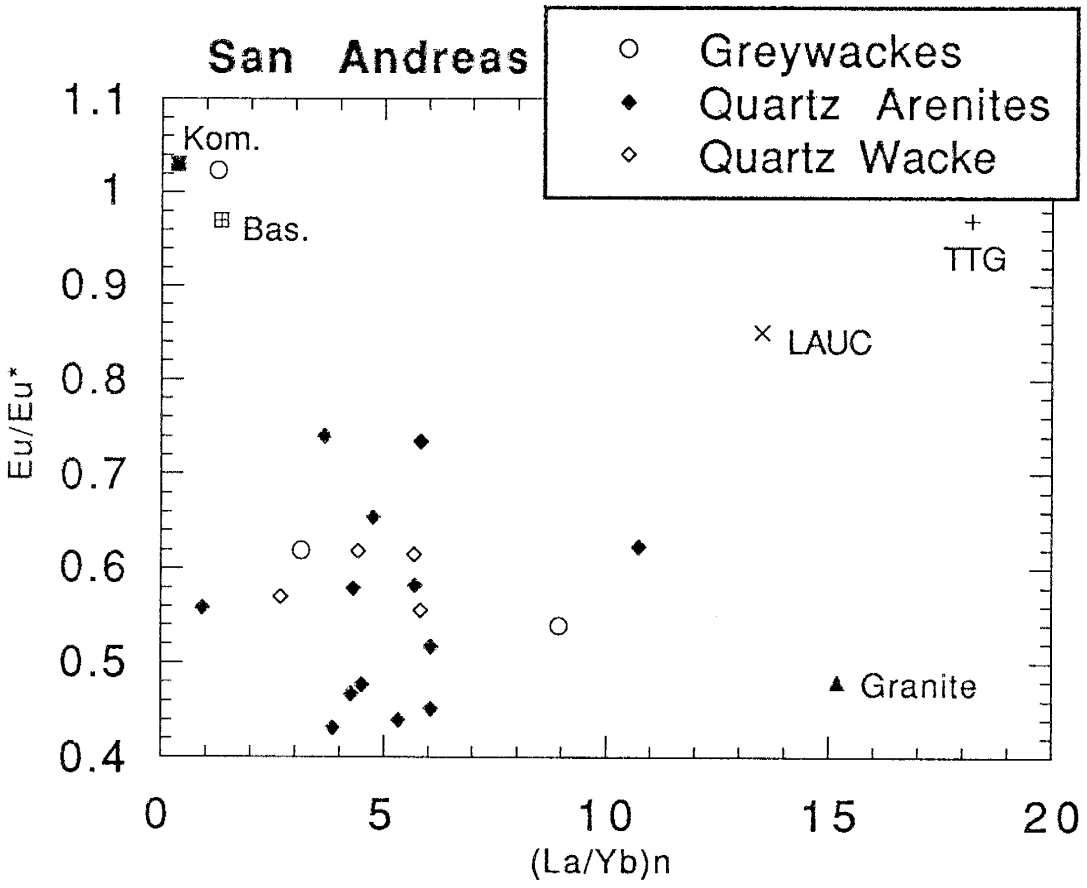
San Andreas
Greywackes
Quartz Arenites
Quartz Wacke
Kom.
Bas.
TTG
LAUC
Granite
Eu/Eu*
1.1
1
0.9
0.8
0.7
0.6
0.5
0.4
0
5
10
15
20
(La/Yb)n

Fig 5

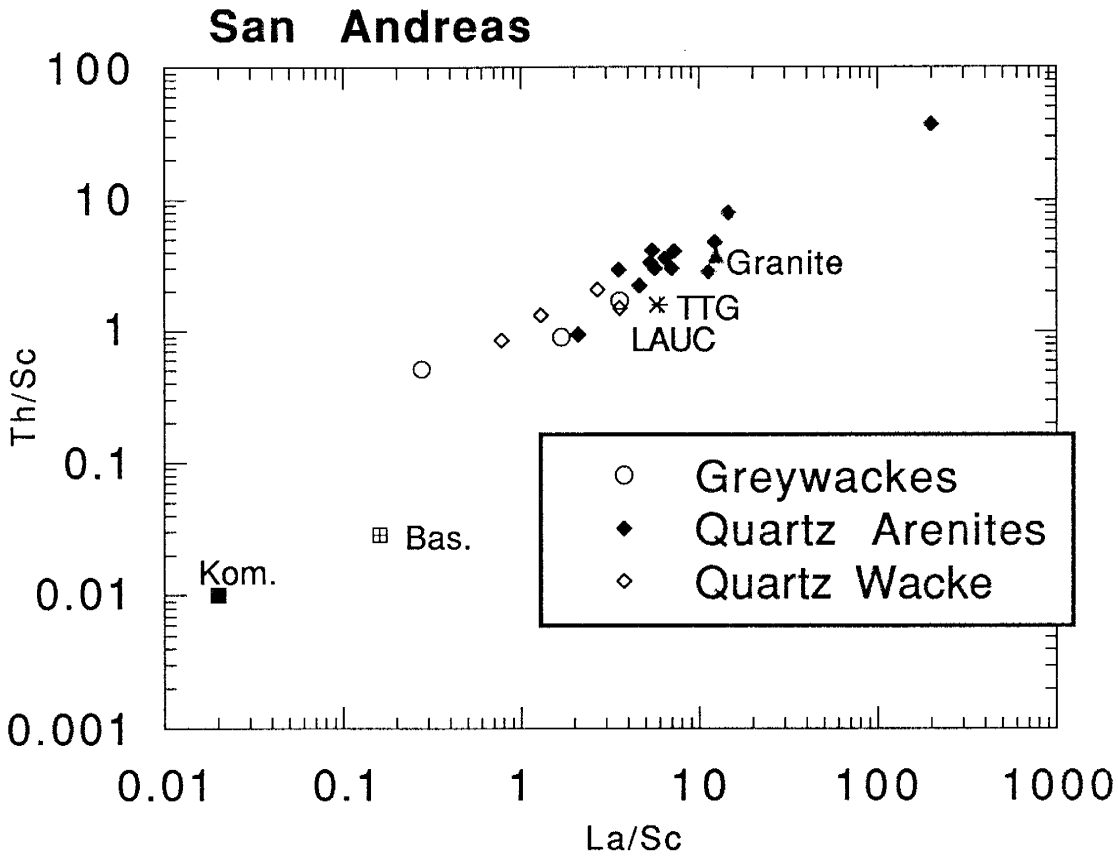
San Andreas
100
10
1
0.1
0.01
0.001
Th/Sc
0.01
0.1
1
10
100
1000
La/Sc
Granite
TTG
LAUC
Bas.
Kom.
Greywackes
Quartz Arenites
Quartz Wacke

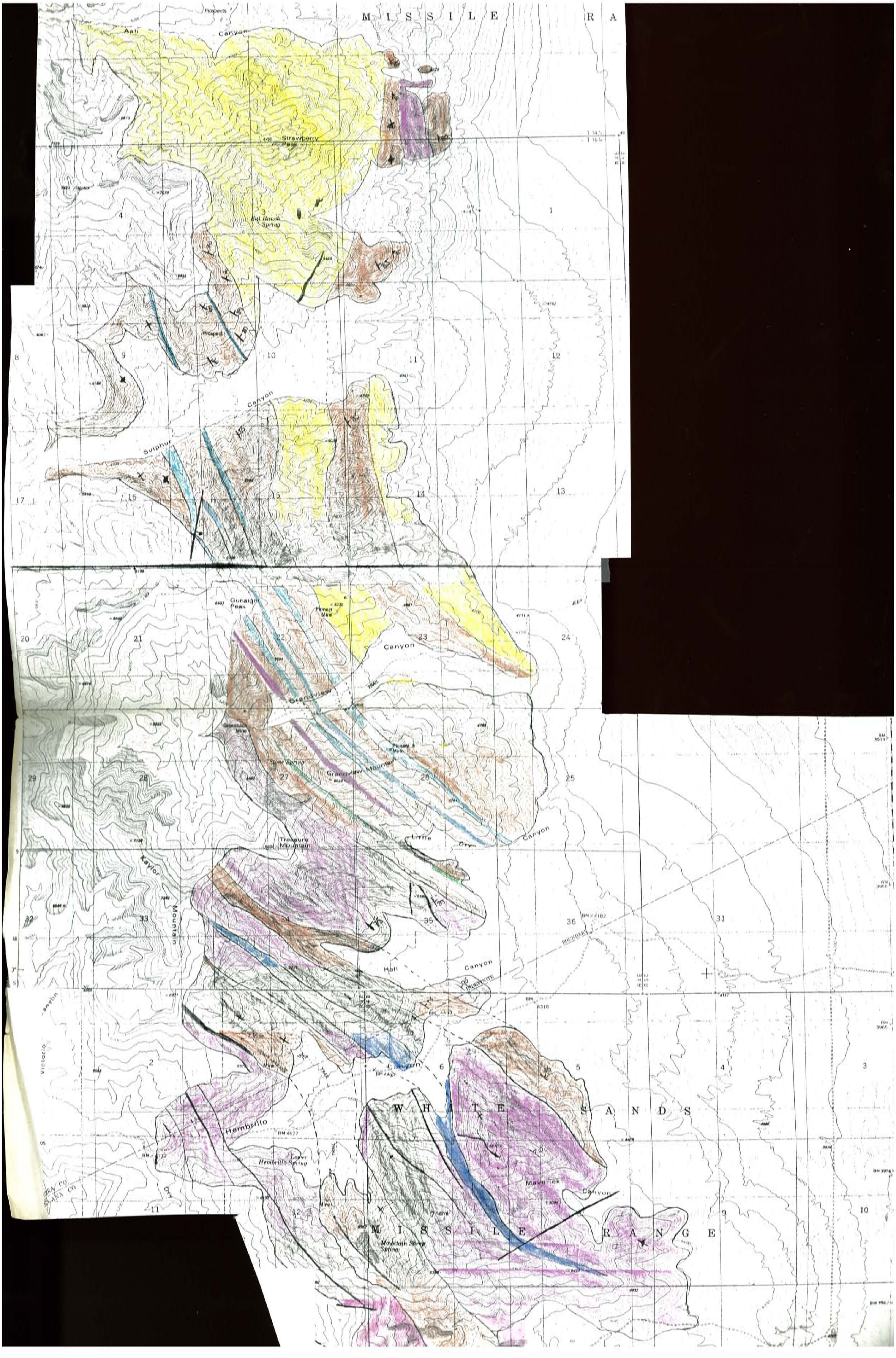
MISSILE RANGE
Ash Canyon
Prospects
Strawberry Peak
Bat Ranch Spring
Prospect
Sulphur Canyon
Gunsight Peak
Pioneer Mine
Canyon
Grandview
Grandview Mountain
Little Dry Canyon
Treasure Mountain
Kaylor Mountain
Hall Canyon
Victorio Canyon
Hembrillo
Lower Hembrillo Spring
Dry
WHITE SANDS
MISSILE RANGE
Maverick Canyon
Mountain Sheep Spring
BOUNDARY

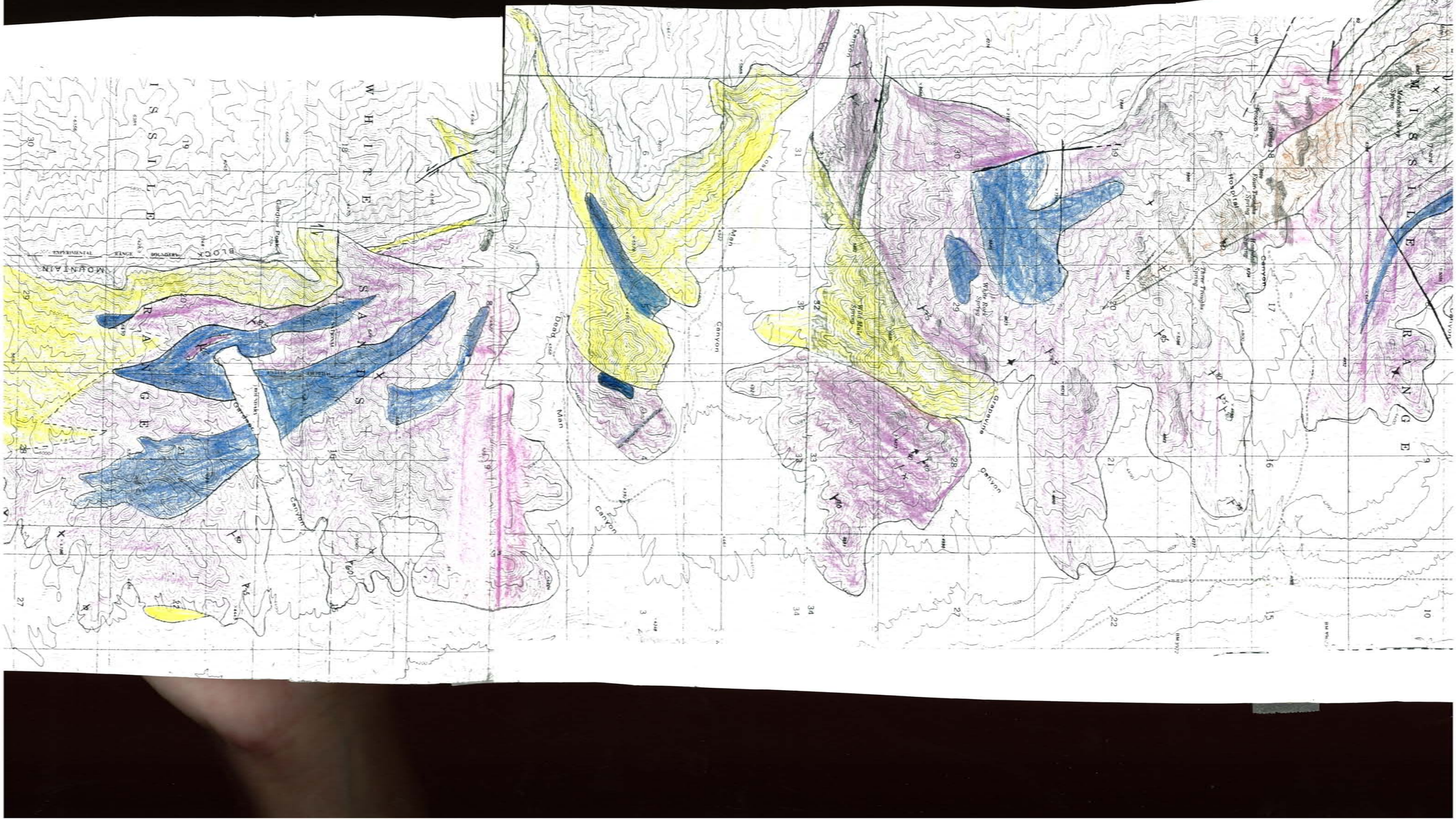
WHITE SANDS RANGE
Gardner Peak
Gardner Canyon
Dark Canyon
Main Canyon
Wild Rose Spring
Three Troughs Spring
Hospital Canyon
Grapevine Canyon
Pool
EXPERIMENTAL RANGE BOUNDARY
BLOCK MOUNTAIN

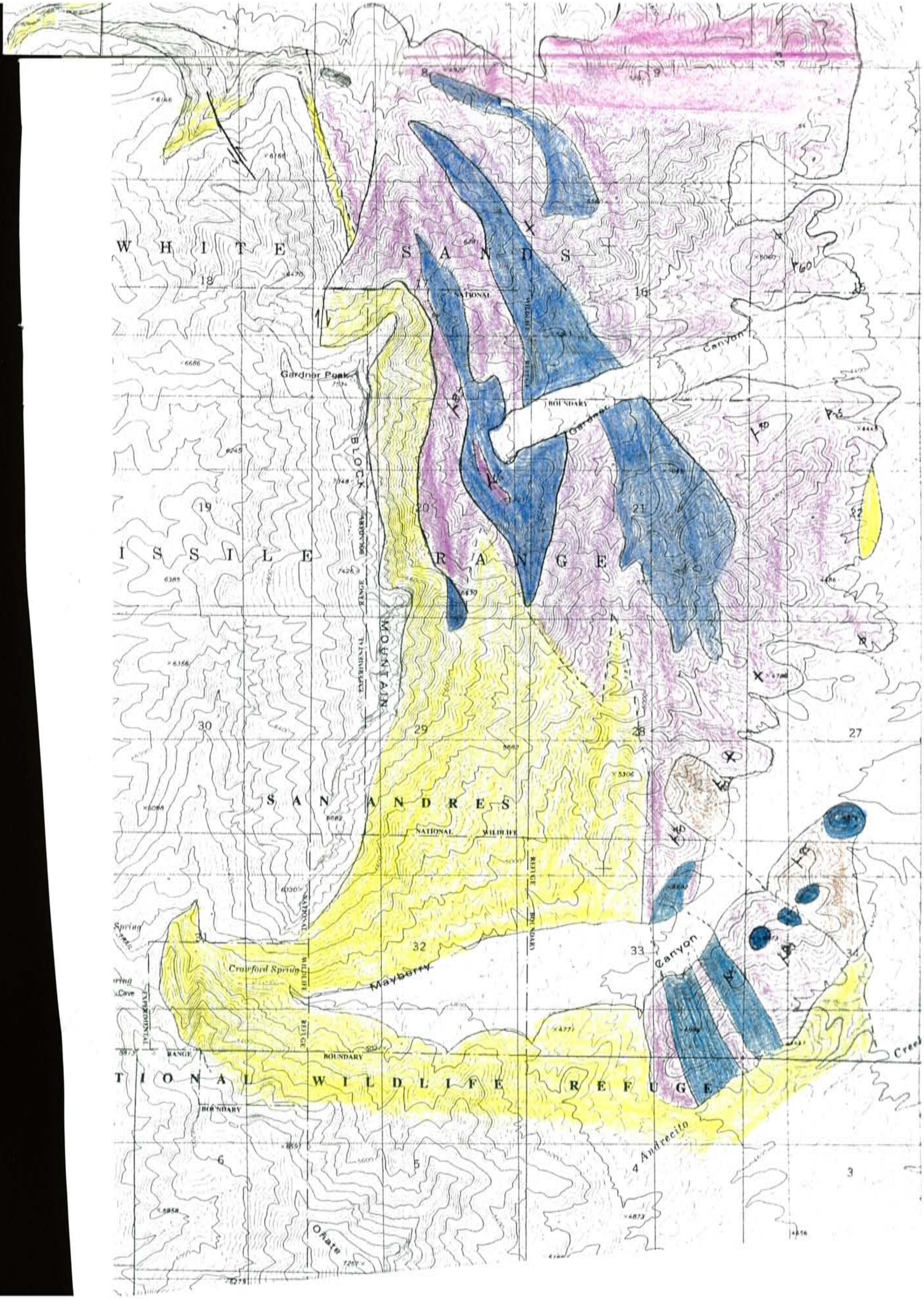
WHITE SANDS MISSILE RANGE
SAN ANDRES NATIONAL WILDLIFE REFUGE
BLOCK MOUNTAIN
Gardner Peak
Gardner Canyon
Crawford Spring
Mayberry Canyon
Andrecito Creek
Oñate
EXPERIMENTAL RANGE BOUNDARY
NATIONAL WILDLIFE REFUGE BOUNDARY